

MICRORNA-455 IN CARTILAGE AND SKELETAL DEVELOPMENT

PAIGE PADDY



THESIS SUBMITTED FOR THE DEGREE OF DOCTOR OF PHILOSOPHY

University of East Anglia
School of Biological Sciences
Norwich, United Kingdom

2021

This copy of the thesis has been supplied on condition that anyone who consults it is understood to recognise that its copyright rests with the author and that use of any information derived there-from must be in accordance with current UK Copyright Law. In addition, any quotation or extract must include full attribution.

DEDICATION

I would like to dedicate this thesis to my family

My parents

Nicola Paddy & Darran Paddy

My brothers

Callum Paddy & Tommy Paddy

For their ever-present love, support and friendship in all things great and small

In a year to appreciate everything we have most of all

“I do not know what I may appear to the world; but to myself I seem to have been only like a boy playing on the seashore, and diverting myself in now and then finding a smoother pebble or a prettier shell than ordinary, whilst the great ocean of truth lay all undiscovered before me.”

– Isaac Newton

Acknowledgements

Firstly, I would like to thank my primary supervisor Professor Ian Clark, for all of his support and guidance during my PhD. I thank him for the opportunity to develop as a researcher, and for sharing his endless stream of knowledge. I will be forever grateful.

I would like to thank all of the Clark lab members, especially Dr Tracey Swingler and Dr Rose Davidson, for their invaluable expertise and time, it would have been impossible without them. Thanks to my fellow PhD students Perry and Liz for making the duration of my PhD enjoyable, and a special thanks to Liz for help with MSC culture.

I would also like to thank my secondary supervisor Professor Tamas Dalmay, for his suggestions and support in my project. A massive thank you to Dr Simon Moxon, for the RNA-seq analysis and advice on anything bioinformatics, I am truly grateful. Thank you to Dr Geoff Mok for his help on all things chick embryo, and to Professor Andrea Munsterberg and the Munsterberg lab for allowing me to perform the chick embryo experiments with them.

I am thankful to the Biomedical Research Centre staff for all support and training, and to the DMU staff for anything mouse related. Thanks to Dr Yoanna Ariosa-Morejon at The Kennedy Institute of Rheumatology in Oxford for the microdissection training, and Noman Chaudhry for advice on the CRISPR/ Cas9 protocol.

My funding body, The Dunhill Medical Trust, a huge thank you for funding the project, and for supporting us during the Covid-19 pandemic. Thank you for the continued support provided by them and our collaborator in Newcastle, Professor David Young.

Finally, for emotional support during my PhD years, thank you to my friends and family, for keeping me sane and supporting me in all possible ways. Thank you to my parents for always encouraging me in everything that I do, and to my brothers and partner for making sure that I always have a smile on my face.

Abstract

microRNAs (miRNAs) are a family of short endogenous non-coding RNAs with a sequence length of 19 to 23 nucleotides, functioning as post-transcriptional regulators of gene expression. During skeletal development, several miRNAs have been identified as important regulators of osteochondral genes. For example, miR-455 is located in an intron of the COL27A1 gene and has been implicated in cartilage physiology and pathology. The aim of this research was to define a role for miR-455-3p in cartilage and skeletal development, identifying regulatory function and novel mRNA targets.

The expression of miR-455-3p increases during chondrogenesis, and overexpression of miR-455-3p prior to differentiation results in a downregulation of chondrogenic marker genes. This suggests that although miR-455-3p is required during chondrogenesis, an upregulation of miR-455-3p results in a dysregulation of the differentiation process. Analysis of RNA-seq data from miR-455 null mouse articular cartilage and SW1353 cells inhibiting miR-455-3p supports this finding, demonstrating that differentially expressed genes in response to reduced miR-455 expression were associated with skeletal system development.

Overexpression of miR-455-3p in the developing chick limb bud also inhibits limb development. Microinjection of miR-455-3p into the limb bud of chick embryos resulted in a smaller limb bud size and delayed development phenotype. RNA-seq data revealed that differentially expressed genes were involved in mitochondrial dysfunction and a disruption to the cell cycle. The majority of these genes are not miR-455-3p predicted targets, however, they have a common promoter sequence for CREB1 suggesting regulation by the transcription factor. In the chick limb bud, CREB1 is downregulated by miR-455-3p and further analysis identified CREB1 as a direct target of miR-455-3p.

To conclude, this research indicates that miR-455-3p has a role in chondrogenesis, regulating the expression of CREB1, and possibly influencing chondrocyte proliferation. Within skeletal development, the impact of miR-455-3p demonstrates a significant regulatory mechanism to explore further.

Access Condition and Agreement

Each deposit in UEA Digital Repository is protected by copyright and other intellectual property rights, and duplication or sale of all or part of any of the Data Collections is not permitted, except that material may be duplicated by you for your research use or for educational purposes in electronic or print form. You must obtain permission from the copyright holder, usually the author, for any other use. Exceptions only apply where a deposit may be explicitly provided under a stated licence, such as a Creative Commons licence or Open Government licence.

Electronic or print copies may not be offered, whether for sale or otherwise to anyone, unless explicitly stated under a Creative Commons or Open Government license. Unauthorised reproduction, editing or reformatting for resale purposes is explicitly prohibited (except where approved by the copyright holder themselves) and UEA reserves the right to take immediate 'take down' action on behalf of the copyright and/or rights holder if this Access condition of the UEA Digital Repository is breached. Any material in this database has been supplied on the understanding that it is copyright material and that no quotation from the material may be published without proper acknowledgement.

Table of Contents

| | |
|---|-----------|
| Acknowledgements | 3 |
| Abstract | 4 |
| List of Figures | 9 |
| List of Tables | 12 |
| List of Appendices | 13 |
| 1. INTRODUCTION | 15 |
| 1.1. Mesenchymal stem cell differentiation | 15 |
| 1.1.1. Mesenchymal stem cells | 15 |
| 1.1.2. Chondrogenesis | 17 |
| 1.1.3. Osteogenesis..... | 18 |
| 1.1.4. Stem cells and regenerative medicine | 19 |
| 1.2. Skeletal development | 20 |
| 1.2.1. Anatomical features of vertebrate limb development | 21 |
| 1.2.2. Gene regulatory networks | 23 |
| 1.2.3. Model organisms for studying vertebrate limb development | 28 |
| 1.2.4. Impact on disease | 28 |
| 1.3. The synovial joint | 29 |
| 1.3.1. Development and structure..... | 29 |
| 1.3.2. Endochondral ossification..... | 31 |
| 1.3.3. Growth plate cartilage | 33 |
| 1.3.4. Articular cartilage..... | 33 |
| 1.4. Pathophysiology of Osteoarthritis | 36 |
| 1.4.1. Osteoarthritis phenotype..... | 36 |
| 1.4.2. Cartilage changes and Osteoarthritis..... | 38 |
| 1.4.3. Gene expression in Osteoarthritis | 39 |
| 1.5. microRNAs | 41 |
| 1.5.1. Biogenesis and mechanism..... | 41 |
| 1.5.2. microRNAs in skeletal development | 44 |
| 1.5.3. microRNAs during chondrogenesis..... | 45 |
| 1.5.4. Cartilage specific microRNA expression..... | 47 |
| 1.6. microRNAs and Osteoarthritis | 48 |
| 1.6.1. Differential expression of microRNAs in cartilage | 48 |
| 1.6.2. Implicated roles for microRNAs in Osteoarthritis | 52 |
| 1.6.3. microRNAs as biomarkers of Osteoarthritis..... | 54 |
| 1.6.4. Therapeutic use of microRNAs in Osteoarthritis | 55 |
| 1.7. microRNA-455 | 56 |
| 1.7.1. microRNA-455 expression in cartilage | 56 |
| 1.7.2. microRNA-455 null mouse model | 57 |
| 1.7.3. microRNA-455 during mesenchymal stem cell differentiation..... | 60 |
| 1.7.4. microRNA-455 in disease | 61 |
| 1.8. Identification of microRNA target genes | 61 |
| 1.8.1. microRNAs and their targets..... | 61 |
| 1.8.2. Methods for identifying microRNA targets..... | 63 |
| 1.8.3. CRISPR/Cas genome editing and microRNAs | 65 |
| 1.8.3.1. CRISPR/Cas9 gene editing system | 65 |
| 1.8.4. microRNAs and the future..... | 68 |

| | | |
|-------------|---|-----------|
| 1.9. | Hypothesis and Aims..... | 70 |
| 2. | MATERIALS & METHODS..... | 72 |
| 2.1. | microRNA-455 during MSC differentiation | 72 |
| 2.1.1. | Cell lines and cell culture | 72 |
| 2.1.1.1. | Mesenchymal stem cells | 72 |
| 2.1.2. | Transfection using Lipofectamine 3000..... | 72 |
| 2.1.3. | MSC differentiation..... | 73 |
| 2.1.3.1. | Adipogenesis | 73 |
| 2.1.3.2. | Chondrogenesis | 74 |
| 2.1.3.3. | Osteogenesis | 74 |
| 2.1.4. | Quantitative Real Time Polymerase Chain Reaction (RT-qPCR)..... | 74 |
| 2.1.4.1. | Cells to cDNA | 74 |
| 2.1.4.2. | miRCURY LNA miRNA PCR | 75 |
| 2.1.4.3. | Taqman Real Time PCR mRNA..... | 75 |
| 2.1.4.4. | SYBR Green Real Time PCR miRNA | 76 |
| 2.1.4.5. | Statistical analysis..... | 77 |
| 2.1.5. | Cell staining..... | 77 |
| 2.1.5.1. | Alizarin Red staining | 77 |
| 2.2. | Mouse cartilage microRNA-455 knockout..... | 77 |
| 2.2.1. | Mouse WT and KO lines..... | 77 |
| 2.2.2. | Cartilage microdissection..... | 77 |
| 2.2.3. | Cell lines and cell culture | 78 |
| 2.2.3.1. | SW1353 cell line | 78 |
| 2.2.4. | Lipofectamine 3000 transfection | 78 |
| 2.2.5. | Total RNA isolation from cultured cells | 78 |
| 2.2.5.1. | Trizol RNA extraction..... | 78 |
| 2.2.5.2. | TURBO DNase treatment..... | 79 |
| 2.2.5.3. | Qiagen RNeasy Mini kit | 79 |
| 2.2.6. | Total RNA extraction from cartilage tissue | 80 |
| 2.2.6.1. | Mouse articular cartilage..... | 80 |
| 2.2.6.2. | mirVana™ miRNA Isolation kit..... | 80 |
| 2.2.7. | Electrophoresis for RNA integrity | 80 |
| 2.2.7.1. | Gel electrophoresis..... | 80 |
| 2.2.7.2. | Bio-Rad Experion Automated Electrophoresis system | 81 |
| 2.2.8. | Quantitative Real Time Polymerase Chain Reaction (RT-qPCR)..... | 81 |
| 2.2.8.1. | SuperScript II Reverse Transcription | 81 |
| 2.2.8.2. | miRCURY LNA miRNA PCR | 82 |
| 2.2.8.3. | Taqman Real Time PCR mRNA..... | 82 |
| 2.2.8.4. | SYBR Green Real Time PCR miRNA | 82 |
| 2.2.8.5. | Statistical analysis..... | 82 |
| 2.2.9. | mRNA-seq Novogene & Bioinformatic analysis | 82 |
| 2.3. | Limb bud development and microRNA-455 | 83 |
| 2.3.1. | Model organism | 83 |
| 2.3.2. | Microinjection into chick limb bud | 83 |
| 2.3.3. | Embryo harvest and limb bud dissection..... | 85 |
| 2.3.4. | RNA extraction from chick limb bud | 85 |
| 2.3.4.1. | Qiagen RNeasy Micro kit | 85 |
| 2.3.5. | Quantitative Real Time Polymerase Chain Reaction (RT-qPCR)..... | 85 |
| 2.3.5.1. | SuperScript II Reverse Transcription | 85 |
| 2.3.5.2. | miRCURY LNA miRNA PCR | 85 |
| 2.3.5.3. | SYBR Green Real Time PCR mRNA..... | 86 |
| 2.3.5.4. | SYBR Green Real Time PCR miRNA | 86 |
| 2.3.5.5. | Statistical analysis..... | 86 |
| 2.3.6. | mRNA-seq Novogene | 86 |

| | |
|--|------------|
| 2.4. Identifying microRNA-455 targets | 87 |
| 2.4.1. Cell lines and cell culture | 87 |
| 2.4.1.1. SW1353 cell line | 87 |
| 2.4.1.2. DF1 cell line | 87 |
| 2.4.2. 3'UTR Luciferase Reporter Assay | 87 |
| 2.4.2.1. Transformation of 3'UTR into SW1353 cells..... | 87 |
| 2.4.2.2. Luciferase Reporter Assay | 87 |
| 2.4.3. microRNA-target interactions by CRISPR/Cas9 genome engineering | 88 |
| 2.4.3.1. miR-CRISPR sgRNA design | 88 |
| 2.4.3.2. HDR-mediated MRE replacement ssODN design | 88 |
| 2.4.3.3. pX330 backbone vector | 89 |
| 2.4.3.4. sgRNA cloning into pX330 vector | 89 |
| 2.4.3.4.1. pX330 digest | 89 |
| 2.4.3.4.2. Gel purification of digested pX330 | 90 |
| 2.4.3.4.3. Oligo annealing and phosphorylation | 90 |
| 2.4.3.4.4. Ligation into pX330 vector | 90 |
| 2.4.3.4.5. Transformation | 91 |
| 2.4.3.4.6. Isolation of plasmid DNA | 91 |
| 2.4.3.5. HDR-mediated MRE engineering into SW1353 cell line | 92 |
| 2.4.3.6. DNA/RNA extraction from MRE engineered cells | 92 |
| 2.4.3.6.1. Qiagen Allprep DNA/RNA mini kit..... | 92 |
| 2.4.3.6.2. ExoSAP-IT Cleanup | 93 |
| 2.4.3.7. Quantitative Real Time Polymerase Chain Reaction (RT-qPCR) | 93 |
| 2.4.3.7.1. Qiagen QuantiTect RT kit | 93 |
| 2.4.3.7.2. SYBR Green Real-Time PCR | 93 |
| 2.4.3.7.3. Statistical analysis | 94 |
| 2.4.3.7.4. MRE-score calculation..... | 95 |
| 3. The role of microRNA-455-3p during mesenchymal stem cell differentiation | 97 |
| 3.1. Introduction | 97 |
| 3.2. Results | 97 |
| 3.2.1. microRNA-455-3p expression during hMSC differentiation | 97 |
| 3.2.2. A complex role for microRNA-455-3p during osteogenesis..... | 99 |
| 3.2.3. Overexpression of microRNA-455-3p suppresses chondrogenesis | 101 |
| 3.1. Discussion | 109 |
| 4. Functions of microRNA-455-3p in cartilage..... | 111 |
| 4.1. Introduction | 111 |
| 4.2. Results | 111 |
| 4.2.1. Mouse cartilage microdissection | 111 |
| 4.2.2. miR-455 null cartilage mRNA-seq | 113 |
| 4.2.3. mRNA-seq overexpressing and inhibiting miR-455 in SW1353 cells..... | 119 |
| 4.2.4. Downregulating miR-455 results in skeletal system development phenotype | 119 |
| 4.3. Discussion | 123 |
| 5. Limb bud development and microRNA-455-3p..... | 125 |
| 5.1. Introduction | 125 |
| 5.2. Results | 125 |
| 5.2.1. Overexpression of miR-455 inhibits chick limb bud formation..... | 125 |
| 5.2.2. Dysregulation of development-related signalling pathway genes..... | 128 |
| 5.2.3. Disruption to cell cycle and abnormal mitochondria | 138 |
| 5.2.4. miR-455-3p targets the transcription factor CREB1..... | 138 |
| 5.2.5. CREB1 siRNA phenocopies miR-455-3p in chondrogenesis | 143 |

| | | |
|---------------|---|------------|
| 5.2.6. | CREB1 siRNA phenocopies miR-455-3p in hMSC's..... | 145 |
| 5.2.7. | Skeletal tissues and CREB1..... | 148 |
| 5.3. | Discussion | 153 |
| 6. | <i>Identifying microRNA-455-3p targets.....</i> | 156 |
| 6.1. | Introduction | 156 |
| 6.1.1. | Assessing microRNA-455 activity by CRISPR-mediated HDR..... | 156 |
| 6.2. | Results | 159 |
| 6.2.1. | Optimization and protocol development in SW1353 cells | 159 |
| 6.2.2. | Validating RNA-seq data and identifying novel miR-455-3p targets..... | 160 |
| 6.1. | Discussion | 166 |
| 1. | <i>Discussion</i> | 168 |
| 1.1. | microRNA-455-3p in cartilage and skeletal development..... | 168 |
| 1.2. | CREB1 | 170 |
| 1.3. | CREB1 in chondrogenesis and endochondral ossification..... | 170 |
| 1.4. | CREB1 and endochondral disease | 173 |
| 1.5. | CREB1/ miR-455-3p interaction in chondrocytes | 174 |
| 1.5.1. | miR-455-3p/CREB1, DRP1 and the cell cycle..... | 174 |
| 1.5.2. | miR-455-3p/CREB1, HIF1a and mitochondrial dysfunction | 176 |
| 1.6. | miR-455-3p predicted targets | 177 |
| 1.6.1. | PRELP | 177 |
| 1.6.2. | Collagen VI | 178 |
| 1.7. | Future directions..... | 179 |
| 1.7.1. | Growth plate phenotype in miR-455 null | 180 |
| 1.7.2. | The role of miR-455-3p/CREB1 in chondrogenesis | 181 |
| 1.7.3. | Identification of miR-455-3p/CREB1 targets..... | 182 |
| 1.8. | Final conclusions | 182 |
| | <i>Bibliography.....</i> | 185 |
| | <i>Appendices.....</i> | 208 |

List of Figures

- Figure 1.1.** Mesenchymal stem cell differentiation
- Figure 1.2.** The developing limb bud
- Figure 1.3.** Coordination of limb development by crosstalk of pathways
- Figure 1.4.** Limb bud development signal integration and feedback control
- Figure 1.5.** The synovial joint structure
- Figure 1.6.** Endochondral ossification
- Figure 1.7.** Growth plate structure
- Figure 1.8.** Osteoarthritis joint phenotype
- Figure 1.9.** MicroRNA biogenesis
- Figure 1.10.** Roles of microRNAs in Osteoarthritis
- Figure 1.11.** microRNA-455 expression in the developing embryo
- Figure 1.12.** microRNA-455 null mouse model
- Figure 1.13.** CRISPR/Cas9
- Figure 1.14.** The future of microRNAs
- Figure 2.1.** Chick limb bud microinjection
- Figure 2.2.** MRE score calculation
- Figure 3.1.** Expression of miR-455-3p during hMSC differentiation
- Figure 3.2.** Osteogenesis differentiation assay
- Figure 3.3.** Osteogenic marker gene expression during hMSC osteogenesis assay (mimic)
- Figure 3.4.** Osteogenic marker gene expression during hMSC osteogenesis assay (inhibitor)
- Figure 3.5.** Alizarin red staining of hMSCs during osteogenic differentiation
- Figure 3.6.** Chondrogenesis differentiation assay
- Figure 3.7.** Chondrogenic marker gene expression during hMSC chondrogenesis assay (mimic)
- Figure 3.8.** Chondrogenic marker gene expression during hMSC chondrogenesis assay (inhibitor)
- Figure 4.1.** Mouse cartilage microdissection
- Figure 4.2.** miR-455 null cartilage RNA-seq data analysis
- Figure 4.3.** miR-455 null cartilage RNA-seq data ($q \leq 0.05$)

Figure 4.4. miR-455 null cartilage RNA-seq data ($p \leq 0.05$)

Figure 4.5. RNA-seq data showing upregulated genes ($p \leq 0.05$) in miR-455 null articular cartilage

Figure 4.6. RNA-seq data showing genes ($q \leq 0.1$) in SW1353 cells transfected with miR-455 mimic and inhibitor

Figure 4.7. Combining RNA-seq data from SW1353 cells +/- miR-455 ($q \leq 0.1$) and miR-455 KO cartilage ($p \leq 0.05$)

Figure 5.1. Microinjection of miR-455-3p mimic and antagomir into the developing chick limb bud

Figure 5.2. Overexpression of miR-455-3p inhibits chick limb bud formation

Figure 5.3. RNA-seq data from chick limb bud overexpressing miR-455-3p

Figure 5.4. Dysregulation of development-related signalling pathway genes ($p \leq 0.05$) in limb buds overexpressing miR-455-3p

Figure 5.5. Combining development-related signalling pathways

Figure 5.6. Heat map of differentially expressed genes ($p \leq 0.05$) identified by GO analysis associated with the cell cycle

Figure 5.7. Heat map of differentially expressed genes ($p \leq 0.05$) identified by GO analysis associated with abnormal mitochondria

Figure 5.8. miR-455-3p targets CREB1

Figure 5.9. CREB1 during chondrogenesis

Figure 5.10. CREB1 siRNA phenocopies miR-455-3p in hMSC chondrogenesis

Figure 5.11. CREB1 siRNA phenocopies miR-455-3p in hMSCs: mitochondrial gene expression

Figure 5.12. CREB1 siRNA phenocopies miR-455-3p in hMSCs: cell cycle gene expression

Figure 5.13. CREB1 siRNA phenocopies miR-455-3p in hMSCs

Figure 5.14. CREB1 expression across skeletal samples

Figure 5.15. Comparison of CREB1 and DRP1 expression

Figure 5.16. Comparison of CREB1 and HIF1a expression

Figure 6.1. CRISPR-mediated HDR and MRE activity protocol

Figure 6.2. Optimization and development of protocol in SW1353 cells

Figure 6.3. Validation of RNA-seq data

Figure 6.4. PRELP expression across cartilage samples

Figure 6.5. Identifying PRELP as a target of miR-455-3p

Figure 7.1. Inhibiting CREB1 in chondrocytes

Figure 7.2. miR-455-3p/ CREB1 schematic in chondrocytes

List of Tables

Table 2.1. miRCURY LNA miR-455-3p mimic, inhibitor, and controls

Table 2.2. Adipogenic culture medium and adipogenic maintenance medium final concentration and volume

Table 2.3. Chondrogenic culture medium concentration and volume.

Table 2.4. Taqman qPCR reagents and volumes

Table 2.5. SYBR green qPCR reagents and volumes for detecting microRNA

Table 2.6. SYBR green qPCR reagents and volumes for detecting mRNA

Table 2.7. pX330 primer and sequence

Table 2.8. Combinations of template and primers for microRNA-target interactions by CRISPR/Cas9 genome engineering qPCR

Table 2.9. qPCR reagents for microRNA-target interactions by CRISPR/Cas9 genome engineering

Table 4.1. Table of significantly ($q \leq 0.05$) upregulated genes in miR-455 KO cartilage samples with enrichment for biological processes

Table 4.2. Table of significantly ($p \leq 0.05$) upregulated genes in miR-455 KO cartilage samples with enrichment for endochondral-related human phenotype ontologies

Table 4.3. Table of gene ontology for common genes combining RNA-seq data from SW1353 cells +/- miR-455 ($q \leq 0.1$) and miR-455 KO cartilage ($p \leq 0.05$)

Table 5.1. RNA-seq data from chick limb bud overexpressing miR-455-3p.

Table 5.2. RNA-seq data showing disruption to cell cycle

Table 5.3. RNA-seq data showing abnormal mitochondria and metabolism

Table 5.4. Downregulated genes ($p \leq 0.05$) identified by GO analysis associated with the cell cycle in limb buds overexpressing miR-455-3p

List of Appendices

Appendix 1. Osteogenic marker genes, 2802f hMSC donor line

Appendix 2. Osteogenic marker genes, 2454e hMSC donor line

Appendix 3. Osteogenic marker genes, 071598a hMSC donor line

Appendix 4. Chondrogenic marker genes, 2802f hMSC donor line

Appendix 5. Chondrogenic marker genes, 2454e hMSC donor line

Appendix 6. Chondrogenic marker genes, 071598a hMSC donor line

Appendix 7. RNA-seq data from WT and miR-455 KO mouse articular cartilage

Appendix 8. Collagen expression in WT and miR-455 KO mouse articular cartilage

Appendix 9. RNA-seq and qPCR data from WT and miR-455 KO mouse articular cartilage

Appendix 10. RNA-seq and qPCR data from WT and miR-455 KO mouse articular cartilage

Appendix 11. RNA-seq and qPCR data from chick limb buds injected with AM-Scr control, miR-455 mimic, and miR-455 AM

Appendix 12. RNA-seq and qPCR data from chick limb buds injected with AM-Scr control, miR-455 mimic, and miR-455 AM

Appendix 13. Chick primers

Appendix 14. Mouse primers

Appendix 15. Human primers

Appendix 16. CRISPR/Cas9 genome engineering qPCR design

Appendix 17. CRISPR/Cas9 genome engineering sgRNA design

Appendix 18. CRISPR/Cas9 genome engineering ssODN design

Chapter 1

Introduction

1. INTRODUCTION

The processes of ageing, injury, and disease result in the loss of functional cells. Adult stem cells such as mesenchymal stem cells play a key role in replacing these cells and are an important focus of research with the potential for clinical application, for example chondrocytes in cartilage. Understanding the mechanisms that control differentiation and proliferation can translate into regenerative medicine, creating cells to replace diseased or degenerating tissues such as Osteoarthritis. The purpose of this thesis is to explore the role of microRNA-455 during skeletal development and cartilage tissue. From the process of chondrogenesis in mesenchymal stem cells, to the analysis of the developing limb tissue, and adult cartilage from a developed synovial joint.

1.1. Mesenchymal stem cell differentiation

1.1.1. Mesenchymal stem cells

Mesenchymal stem cells (MSCs) are adult stem cells which can be isolated from the bone marrow compartment of humans and animals. Human MSCs can be described as non-haematopoietic, multipotent stem cells and have the capacity to proliferate, giving rise to daughter cells (1). MSCs exhibit the ability to self-renew and the potential to differentiate into several different mesodermal lineages. These include chondrogenic (cartilage), osteogenic (bone), adipogenic (fat), myogenic (muscle), tenogenic (tendon), and stromal (marrow stroma) lineages (Figure 1.1) (2). As MSCs contribute to the regeneration of mesenchymal tissues, they are considered an extremely promising tool for cell based gene therapy in musculoskeletal repair (3).

Besides bone marrow derived MSCs, cells have also been isolated from tissues of the joint such as synovium, periosteum, and synovial fluid for cartilage repair (4–6). Of these, MSCs derived from synovium have been shown as a cell type with highly proliferative capacity and chondrogenic potential (4). Importantly, synovium MSCs can be easily harvested from the joint, for example during clinical examination of the joint (7). Human MSCs also modify the host immune environment by secreting certain cytokines and immune relevant receptors which makes them distinct from other stem cells (8). This

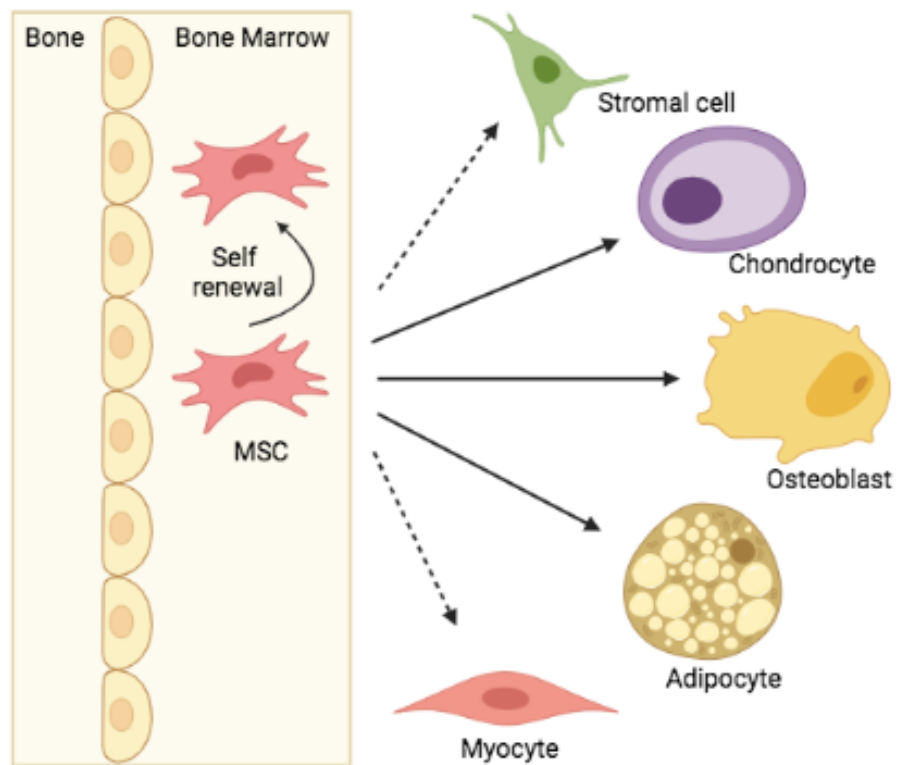


Figure 1.1: Mesenchymal stem cell differentiation. Mesenchymal stem cells have the ability to self-renew and differentiation into mesodermal lineages. Solid arrows indicate differentiation into chondrocyte, osteoblast and adipocyte lineages. Adapted from A. Uccelli et al. (358).

immunomodulatory property is another factor supporting MSCs in cell replacement therapy.

Characteristic features of MSCs include retaining their ability to expand for long periods of time, they are easy to isolate, and have the capacity to differentiate *in vitro* into fibroblasts or chondrogenic, osteogenic, and adipogenic lineages under appropriate culture conditions (9). These properties make MSCs accessible to study *in vitro* and MSC derived chondrocytes are suitable for regenerative medicine application, due to the fact that they are easy to isolate and manipulate (5). The identification of MSCs include adherence properties, cell surface antigen expression, and haematopoietic marker absence (7). It is important to understand the underlying mechanisms in which MSCs are regulated and modulated, in order to translate to cell therapy and clinical applications.

1.1.2. Chondrogenesis

The process of chondrogenesis involves mesenchymal cell condensation followed by chondroprogenitor cell differentiation. However, endochondral ossification also follows chondrogenesis where hypertrophic cartilage is replaced by bone. In this process, chondrocytes undergo proliferation, terminal differentiation to chondrocyte hypertrophy, and apoptosis (10). Endochondral ossification occurs during limb development, where, at the ends of bones, resting chondrocytes form cartilage. During embryonic development, chondrocytes are derived from mesenchymal progenitor cells, and form the cartilage templates for future cartilage and bone (11).

Chondrogenesis regulators include fibroblast growth factors (FGFs), insulin-like growth factors (IGFs), transforming growth factor β (TGF- β) members, and Wnt signalling pathway members (12). During embryogenesis, cell proliferation, differentiation and apoptosis are regulated by TGF- β members. Of the isoforms, TGF- β 3 has the highest chondrogenic cell differentiation potential (13).

Sox9 was identified as the first transcription factor essential for the differentiation of chondrocytes and formation of cartilage (14). The signalling molecule SHH upregulates Sox9 expression through the induction of Bapx1. A positive feedback loop is formed

between Bapx1 and Sox9 in cooperation with BMPs (bone morphogenic proteins), and this influences chondrogenic factor expression (15). There are other Sox family members involved in chondrogenesis, although Sox9 and Runt-related transcription factor 2 (Runx2) are the principal regulators. Runx2 is involved in cell hypertrophic maturation, whilst Sox9 leads to articular cartilage formation, and both are expressed from mesenchymal condensation to terminal chondrocyte hypertrophy during the entire chondrogenic process (7). Expression of early cartilage marker genes are activated by Sox9 for cell survival (16), for example type II collagen alpha I gene (Col2a1).

The signalling polypeptides BMPs are involved in many biological responses such as proliferation, differentiation, cell growth and apoptosis. BMP-2 is commonly found in bone and cartilage, stimulating cellular condensation with BMP-7 (7). Early chondrogenesis is induced by BMP-4 through mediating Runx2, and the synthesis of type II collagen, aggrecan, and extracellular matrix (ECM) proteins are also stimulated by BMP-4. As well as promoting chondrogenesis, BMPs can also stimulate endochondral ossification (17). Determining the regulatory mechanisms behind chondrogenesis and cartilage development will create a better understanding of musculoskeletal pathologies, and develop new approaches for treating cartilage disease (18).

Chondrogenesis is a complex process whereby much more research is needed to understand the regulatory steps in which stem cells are directed towards chondrocytes. During skeletal development, BMP-7 is a crucial factor, playing an important protective role with its ability to repair cartilage damage (19). BMP-14, -13, and -12, known as the cartilage derived morphogenetic proteins (CDMP-1, -2, -3), also play a role in the maintenance and regeneration of articular cartilage. During early limb development these proteins are responsible for cartilaginous tissue, and during later development the formation of the articular joint cavity (20).

1.1.3. Osteogenesis

Through endochondral ossification, chondrocytes are replaced with bone by osteoblasts and osteoclasts. In the commitment of mesenchymal cells to the osteoblastic lineage, RUNX2, SP7 and Wnt signalling play an essential role during osteoblast differentiation

(21). Following osteoblastic lineage commitment, bone matrix proteins are expressed by osteoblasts at varying levels, dependant on cell maturation. From preosteoblasts to immature osteoblasts, Col1a1 expression is upregulated. Immature osteoblasts express Spp1 and Ibsp, and osteoblasts which have matured express Bglap (22). The mature osteoblasts will express Dmp1 when they embed into the bone matrix and become osteocytes (23).

The Runx2 transcription factor is essential for the commitment of MSCs to the osteoblast lineage. The major role of Runx2 begins in the late stage of chondrocyte differentiation and terminal hypertrophic chondrocytes, regulating Col10a1 expression. Bone matrix protein genes are upregulated during osteoblast differentiation by Runx2, including Col1a1, Col1a2, spp1, and Bglap, and activate many promoters (22). Despite this, the overexpression of Runx2 inhibits osteoblast maturation, reducing both Col1a1 and Bglap expression. Research has demonstrated that during the development of bone, osteoblast differentiation is induced by Runx2 increasing immature osteoblasts to form immature bone. The level of Runx2 is then downregulated to enable differentiation into mature osteoblasts and therefore mature bone (22). Another master regulator of osteogenesis is the transcription factor Osterix (24).

Signalling pathways such as Wnt, BMP, and FGF (fibroblast growth factor) provide signals executed by Runx2, and Osterix is responsible for commitment to mature osteoblasts (24). Such signalling pathways are essential during osteogenesis. For example, in combination with BMP-7 (osteogenic protein-1 [OP-1]), BMP-1, -2 and -3 enhance the formation of bone through osteoblast production and control the remodelling of ECM proteins dependant on matrix metalloproteinases (MMPs) activity (7). An increased expression of type I collagen and osteocalcin results from increased BMP-1 expression (25). During both development and adulthood, BMP-6 is a regulator of MSC differentiation into osteoblasts, possibly by upregulation by the ECF-like factor (26).

1.1.4. Stem cells and regenerative medicine

Adult stem cells such as MSCs play a key role in replacing functional cells which have been lost due to the process of ageing, injury and disease and are an important focus of

research. In addition to adult stem cells, pluripotent stem cells can be isolated from the early embryo, or induced by reprogramming adult cells, and can differentiate into many cell types. Repairing cartilage by stem-cell based tissue engineering has its challenges. For example, the inability of chondrocytes to lay down a new matrix with properties formed during development is an aspect of investigation (10). Therefore, more effective strategies for promoting cartilage repair and preventing damage may result from understanding the mechanisms of cartilage remodelling during development and comparing with disease states. Numerous orthopaedic disorders, including articular cartilage defects, are hopeful of treatments using stem cells in future regenerative medicine (7).

An advantage of using MSCs for cell therapies is that they can be expanded *ex vivo* to high numbers making them an abundant cell source in contrast to mature chondrocytes (7). Disadvantages of MSCs include the low bone marrow MSC percentage, difficulty obtaining a pure population, and controlling differentiation precisely (27). Further research is required before regenerative medicine can be applied in clinical practice through the use of stem cells, either adult or pluripotent (7). A more efficient control of these processes, including chondrogenesis, will be achieved by a better understanding of the molecular mechanisms underlying MSC differentiation, and may lead to essential progression in regenerative orthopaedic research.

1.2. Skeletal development

By manipulating and analysing skeletal development and particularly the development of limb buds, there have been significant advances in the understanding of molecular and cellular mechanisms. During embryogenesis, these mechanisms are involved in processes such as epithelial-mesenchymal transitions, feedback signalling, embryo patterning, and growth (28). Studying the formation of cartilage, bones, and joints during development can provide essential information for cartilage and bone tissue regeneration and engineering, to enhance our understanding of clinical conditions caused by abnormal skeletal development and ageing. As a result of this, and the power of embryogenesis, new treatments may evolve.

1.2.1. Anatomical features of vertebrate limb development

The study of development is essential to understanding disease. An important paradigm for organogenesis during embryo development is the developing limb bud. This developmental process proceeds through cell proliferation, differentiation, and patterning which involves signal transduction mechanisms and spatially and temporally regulated gene expression.

Somatopleural cells in the lateral plate mesoderm (LPM) accumulate and appear as outgrowths resulting in limb buds at specific positions along the flank of the embryo. During early limb bud formation, the small limb bud consists of an outer layer of epithelial cells and an inner core of mesenchymal cells (29). Prior to the initiation of limb bud outgrowth, morphological differences in the hindlimbs and forelimbs are specified and determined in the mesenchyme of the ectoderm. Skeletal elements and connective tissues of the limb are derived from mesenchymal cells of the LPM lineage, whereas somite derived cells migrate into the limb bud, giving rise to myogenic cells in muscle. From the somites, limb vasculature is formed, and ectodermal epithelial cells give rise to the skin epidermis (29).

The apical ectodermal ridge (AER) is a thickening at the tip of the ectoderm, beneath this is a region of undifferentiated mesenchymal cells, and these cells begin to differentiate after leaving this zone (Figure 1.2). The underlying mesoderm induces the AER, defining the proximodistal (PD) axis. The AER is one of the major signalling centres in the limb bud (30). The cartilaginous elements appear in the mesenchyme as the limb bud grows out, with differentiation beginning in the proximal part of the limb bud, proceeding distally. The mesenchyme underlying the AER referred to as the 'progress zone' proliferates and mediates the elongation of the limb bud. The 'zone of polarizing activity' (ZPA) is a block of tissue along the posterior side of the limb bud which defines the anterioposterior (AP) axis, and epithelial-mesenchymal interactions mediate the dorsoventral (DV) axis developmental axis (30). The development of the limb requires an integration of these axes for limb morphogenesis.

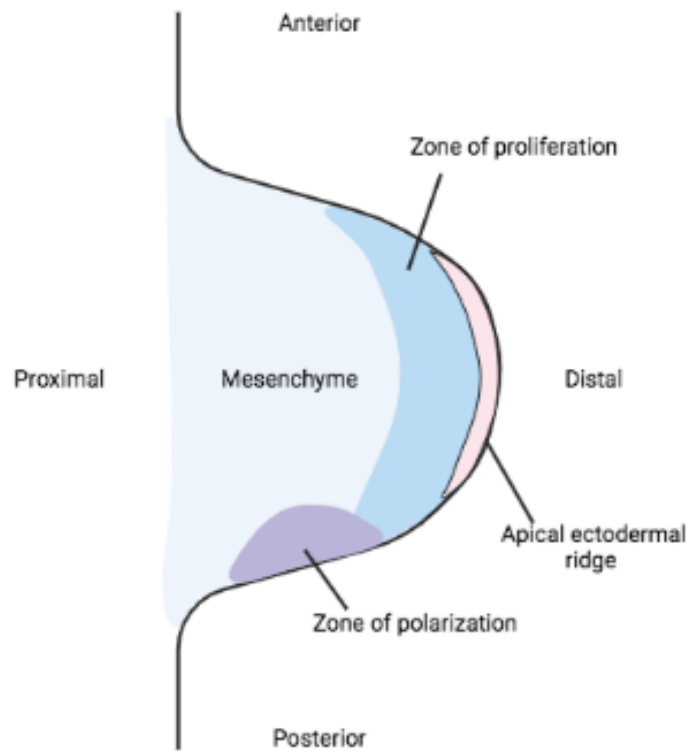


Figure 1.2: *The developing limb bud. Anterior-posterior and proximal-distal axis are shown. The apical ectodermal ridge (AER) is on the distal edge, with underlying the zone of proliferation and undifferentiated mesenchyme. The zone of proliferation (ZPA) is at the posterior base of the limb bud.*

Skeletal tissues, tendons, ligaments, and connective tissues arise from mesenchyme within in the limb bud. Cartilage differentiation begins by condensation of cells, a process of increased mesenchymal cell packaging, and these cartilage elements proceed in a proximal-distal direction (31). Over the developmental stages, the limb bud shape changes and elongates to form the 'elbow' and the distal region flattens and broadens in order to form the digital-plate. From the most proximal domain, skeletal elements are divided into the 'stylopod', the 'zeugopod', and most distally 'autopod' (29). Within the developing limb, the patterning of cartilage is the most studied structure as the development of both muscles and tendons are more intricate. In contrast to the skeletal structures, the muscle originates in the epaxial dermomyotome, a somite compartment outside of the limb bud, and migrates into the limb bud (30). As soon as the basic limb elements are formed, the apical ridge disappears, and the remaining development consists of the growth phase, where cartilaginous elements are mostly replaced by bone (29). Gene regulatory networks involved in embryonic patterning, differentiation, and proliferation are largely understood as a result of vertebrate limb bud development molecular analysis (28). During early limb development, the fundamental mechanisms directing elongation of the limb bud is thought to be similar in other regions of the embryo undergoing growth (29). It is important to understand how the pattern of skeletal tissues is established, and how cells communicate in order to form at the correct place and time.

1.2.2. Gene regulatory networks

Within the embryo, complex regulatory networks direct development, defining a central role in these integrated systems (32). The limb bud signalling system involves many pathways known to regulate morphogenesis, where these patterning signals interlink to coordinate the cell line specification and proliferation (33). To form a distinct pattern of chondrogenic elements, cells are differentially organised along the proximodistal, anteroposterior, and dorsoventral axes, regulated by fine-tuned gene networks (30).

The LPM expresses genes involved in specification of the limb type (forelimb/ hindlimb) and position of the limb, ensuring the correct limbs arise at precise positions along the AP axis (29). The mesodermal marker Brachyury related genes, *Tbx4* and *Tbx5*, are essential

regulators of limb outgrowth and patterning, with roles linked to signalling proteins FGF, BMP, and Wnt (34). During vertebrate limb development, the regulation loop of FGF and Wnt families play a pivotal role in limb initiation. Directly involved in this are the Tbx4 and Tbx5 genes, controlling the local production of FGFs in their respective limbs, and activating the Wnt/FGF signalling cascade (35).

Tbx4 and Tbx5 are expressed in the limb-forming regions and are important in limb identity with the Tbx4 gene specifically expressed in the forelimb and Tbx5 in the prospective hindlimb (34). The homeodomain transcription factor Pitx1 gene is expressed in the hindlimb but absent from the forelimb, with a key role in determining the difference between limb and generating hindlimb features (36). Mutations in Tbx5 and Pitx1 have been associated with human patient limb malformations, where a Tbx5 gain-of-function mutation results in skeletal deformations (37), and deletions in Pitx1 can cause lower-limb abnormalities including polydactyly (38). The Tbx5 mutations are responsible for Holt-Oram syndrome, characterised by defects in the upper limbs (39).

FGF-10 is expressed in the limb forming regions of the LPM and initiates normal limb bud development, demonstrated by Fgf-10 deficient mice which exhibit abolished limb bud initiation (40). During limb initiation, an FGF-8 and FGF-10 regulatory loop plays a key role in AER induction, where WNT factors regulate this, including Wnt-2b, Wnt-8c, and Wnt-3a signalling (41). In the ectoderm and AER, proximodistal patterning and outgrowth of the limb is regulated by Wnt signalling, by controlling the formation and maintenance of the AER (42). Wnt7a is also required for the regulation of SHH and is specifically expressed in the dorsal limb ectoderm, determining dorsal limb identity (43).

In the posterior region of the AER, FGF-4 is present during proliferation (44) and it has been demonstrated that during limb outgrowth and patterning, all three axes (dorsoventral, proximodistal, and anteroposterior) are linked through signalling of WNT7a, FGF-4, and SHH signalling (45). The AER is essential for correct patterning along the proximo-distal axis and limb bud outgrowth, and the polarizing region which is crucial for patterning along the antero-posterior axis is also established and maintained by FGFs (29). The expression of FGF-8 in the AER in response to FGF-10 signalling in the

mesenchyme establishes a positive feedback loop, whereby AER FGF-8 expression maintains mesenchyme FGF-10 (46).

The ZPA is a group of mesenchymal cells and is the second signalling centre of the limb. Within this polarizing region, Sonic Hedgehog (Shh) is expressed, mediating the activity of the ZPA (Figure 1.3) (42). Loss of skeletal elements along the proximodistal and anteroposterior axes result from the loss of FGF and SHH signalling, as both regulate the progenitor cell pool. Limb patterning and outgrowth are interconnected along these axes by epithelial-mesenchyme interactions mediated by FGFs in the AER and SHH in the mesenchyme. SHH maintains FGF expression and AER integrity, and FGF signalling from the AER is required for maintenance of SHH expression (42). Development along the proximo-distal and antero-posterior axes is linked by a positive feedback loop between the AER and polarising region. The apical ridge will regress if BMP-4 signalling levels are too high, therefore to maintain limb bud outgrowth, BMP-4 is controlled by the antagonist Gremlin in a negative feedback loop (47).

During the early stages of limb bud development, FGF expression is maintained in the AER, maintaining SHH expression in the polarizing region. Gremlin expression is regulated by SHH signalling, ensuring BMP activity is low in the mesoderm, and enforcing the FGF and SHH signalling positive feedback loop (Figure 1.4) (29). This feedback control mechanism is an example within development of a robust and reliable self-regulating system. In the distal mesenchyme underneath the AER, Wnt5a is expressed (48), and loss of Wnt5a results in reduced proliferation of the progressive zone and shortening of the skeleton with distal parts missing (49). When the AER and ZPA signalling regions are established, and a limb bud has formed, the limb can develop autonomously (29). For the outgrowth of the limb bud and progressive formation of skeletal elements along the proximodistal axis, the AER is essential with the key signal provided by FGFs. In order to generate the correct limb autonomy, the integration of patterning along all three limb axes is crucial, involving dorsal ectoderm Wnt-7a signals, AER FGFs, and SHH from the polarizing region (29).

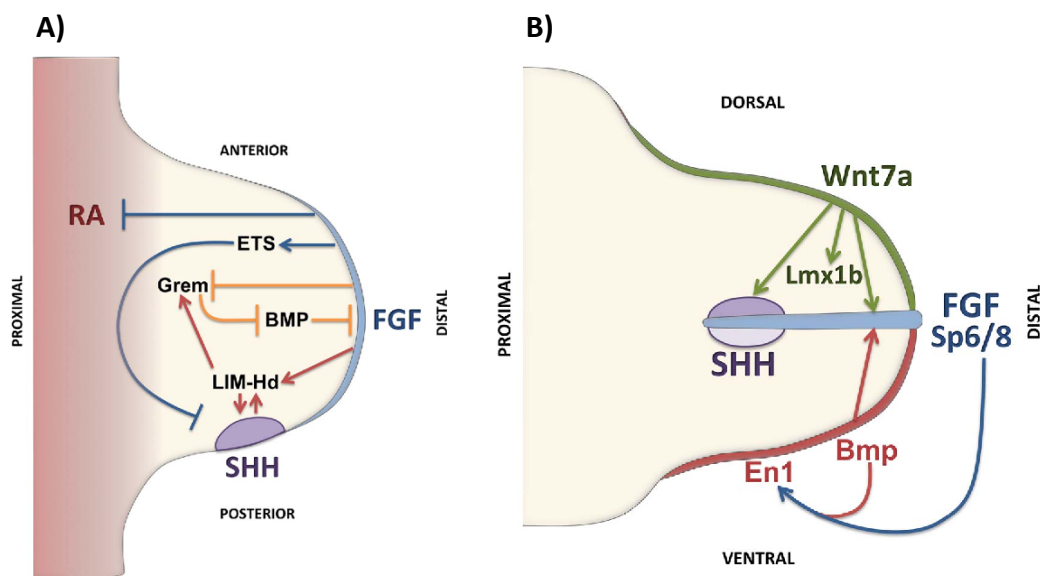


Figure 1.3: Coordination of limb development by crosstalk of pathways. A) AER and ZPA activity is maintained by the FGF-SHH positive feedback loop. The yellow lines indicate SHH/GREM1/FGF feedback loop and blue lines demonstrate Shh negative regulation by FGF targets. RA is restricted to the proximal limb and maintained by AER-FGF signals. B) AER positioning is regulated by dorso-ventral patterning, promoting Shh activation. Figure from Delgado et al (2017) *Developmental biology*.

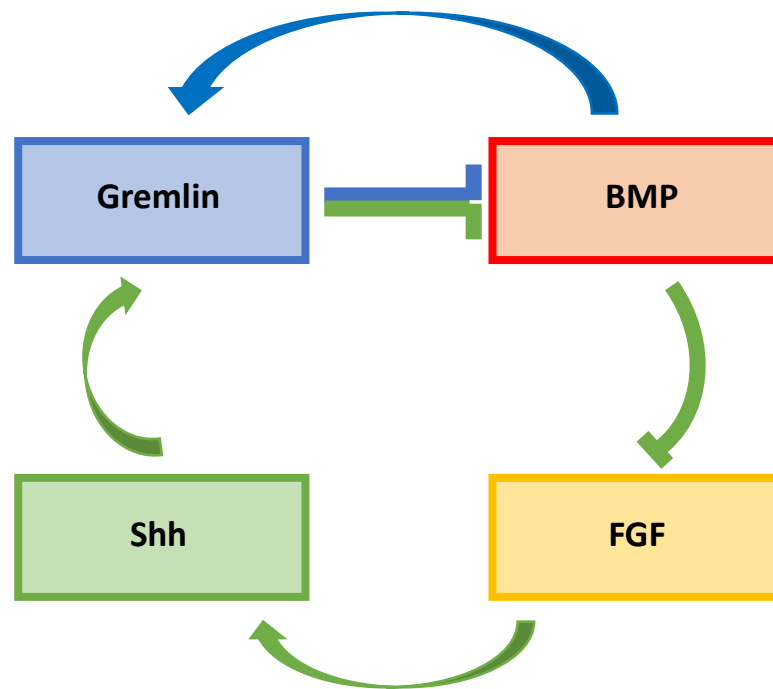


Figure 1.4: Limb bud development signal integration and feedback control. Within the developing limb bud mesoderm, Gremlin is a BMP antagonist. A positive feedback loop is established whereby BMP activity is kept low. From the apical ectodermal ridge, FGF signaling maintains the expression of Shh in the polarizing region. The polarizing region signaling of Shh maintains apical ectodermal ridge Fgf expression. Positive control is indicated by arrows where signaling molecules promote gene expression. Barred lines represent either prevention of gene expression or negative control of signaling by an antagonist. Blue lines show initiation loop with negative feedback, green lines show propagation loop with positive feedback.

1.2.3. Model organisms for studying vertebrate limb development

Models of limb bud development are extremely useful for complex molecular and genetic analysis and the success of these has allowed the development of techniques to experimentally manipulate limb buds that are genetically viable (28). For investigating skeletal development, the animal systems most commonly used are chick and mouse, each with their own advantages. Complementary experiments in the developing chick and genetic approaches in the mouse are responsible for enhancing knowledge of the underlying molecular events during limb development (30).

Through artificial gene knockouts and spontaneous mutations, mice have been used to study certain aspects of limb development, whereas the basic principles have been investigated in chick embryo, such as pattern formation and limb morphogenesis. Although the mouse embryo is a good model for the study of mammalian development, the chick embryo has been long studied due to the availability of fertile eggs, and the ability of the embryo to withstand microsurgical manipulations (29). A window can be made in the eggshell revealing the embryo and limb buds, resealed to continue development and then observe the effects of manipulations on limb development (50). These limb buds, composed of mesoderm and an outer layer of ectoderm, can be visualised on the flanks of the embryo following 3 days of incubation, after the main body axis structures are established. After 10 days the limbs main features are well developed (29). As an experimental model, the chick embryo has enhanced the study of development. This is due to the accessibility of the embryo and manipulative procedures, for example allowing molecular manipulations *in ovo*, where successive developmental stages can be examined (50).

1.2.4. Impact on disease

The processes of development initiate from a single cell to tissues and organs, forming complex functioning organisms. In regard to disease, it is important to understand development in order to gain an insight into developmental defects, cancer and ageing. Research focuses on model organisms such as chick, *Xenopus*, and zebrafish to study the fascinating genetic, molecular, and cellular mechanisms underlying embryogenesis,

complemented with mouse genetics. Progress in areas such as human disease genes, gene function using model organisms, stem cells, and bioartificial organs indicate the potential impact of developmental research on future medical applications (51). The formation of highly specialised organs are driven by morphogenetic processes, and the maintenance and repair of adult tissues such as bone and muscle use developmental signalling pathways and stem cells (52). During development, various tissues are formed by the proliferation and differentiation of embryonic cells, and identifying this process can lead to the restoration of non-functioning diseased organs (51). In some circumstances, signalling pathways that control normal development can be activated resulting in hyperproliferative conditions such as cancers (52).

1.3. The synovial joint

1.3.1. Development and structure

During embryonic development, joints form at the same time as bone formation and growth. Mesenchyme is the embryonic tissue that gives rise to bone, cartilage, and connective tissues of the body (53). The process of endochondral ossification gives rise to the bones and joints of the limbs, which initially develop as small limb buds on the sides of the embryo. As the limb bud grows, areas of the mesenchyme begin to differentiate into hyaline cartilage. This will form a model for future bone. Between the adjacent cartilage models, in an area called the joint interzone, the synovial joint will form (29). At the centre of the interzone region, cells will undergo cell death to form the joint cavity. The mesenchymal cells surrounding this will form the supporting ligaments and articular capsule, migrating out to the epiphyseal cartilage (54). Endochondral ossification will begin, converting the cartilage models to bone, and hyaline cartilage becomes the articular cartilage that covers the surface of bone within the synovial joint (53). Evidence has indicated that the growth plate cartilage and articular cartilage derive from different cell sources. These cells and types of cartilage are regulated by different signalling pathways (54).

The synovial joint (Figure 1.5) is the most common joint in mammals with the main purpose to allow movement (55). As the largest synovial joint in the body, the knee is an

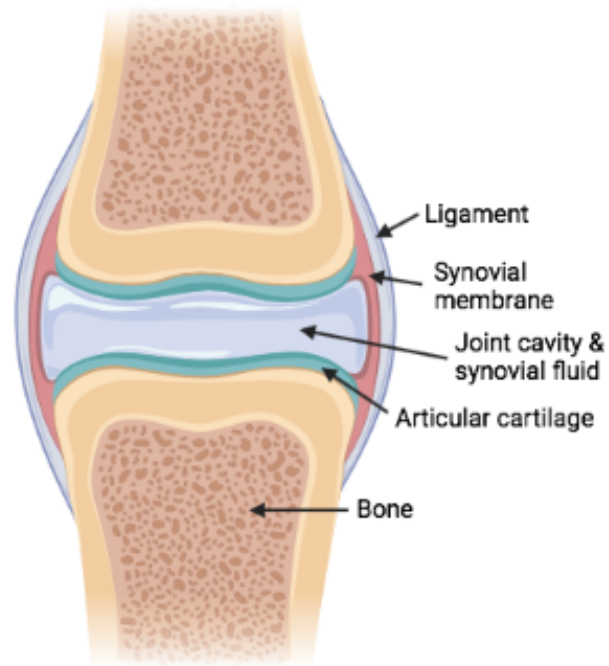


Figure 1.5: The synovial joint structure. The bones within a synovial joint are surrounded by a synovial capsule which secretes synovial fluid. The ends of the bones are covered in articular cartilage to reduce friction during movement.

extremely complex biomechanical system, composed of different tissues such as articular cartilage, perichondrium, ligaments, synovium, bursae, meniscus, articular fat pads, subchondral bone and all cells types in the bone marrow (56). The knee joint promotes complete stability and control under many different conditions, supporting both flexion and rotation (57). Synovial joint structure differs from cartilaginous and fibrous joints due to the presence of capsules which surround the articulating surfaces of the joint, containing a lubricating synovial fluid (55). Within a synovial joint, the articular capsule consists of a thick outer layer, the fibrous capsule, and an inner layer, the synovial membrane (Figure 1.5) (58). For the function of synovial joints, the joint capsule is vital as it protects the joint space (59). Bones are connected together by ligaments which are strong bands of fibrous connective tissue, allowing for joint movement but preventing excessive or abnormal movement. The synovial joint has additional support provided by muscles and tendons, which attach muscle to bone (53). If components of this complex biomechanical synovial joint system become altered or injured, it can result in disease, most commonly arthritis.

1.3.2. Endochondral ossification

The biological process known as endochondral ossification enables skeletal elements to develop from transient cartilage in vertebrate animals (Figure 1.6) (60). At the presumptive site of bone, cartilage is initially formed through mesenchyme condensation. A cartilage template is formed followed by chondrocyte proliferation and differentiation (61). This template has a similar shape to the bone it will eventually form, where chondrocytes at the centre of the cartilage undergo hypertrophic differentiation and apoptosis, vascular invasion and ossification by osteoblasts, before longitudinally spreading to metaphysis (54). Another ossification site forms at the epiphysis as the secondary ossification centre. In between these 2 ossification centres, cartilage forms the growth plate during skeletal growth (54). The cartilage between the joint cavity and secondary ossification centre permanently remains as articular cartilage. The proliferation and differentiation of chondrocytes is tightly regulated by different signalling molecules, and this complicated process is regulated by many molecules and signalling pathways, including Wnt, IHH, BMP, TGF- β , FGF, GDF5, and PTHrP (54).

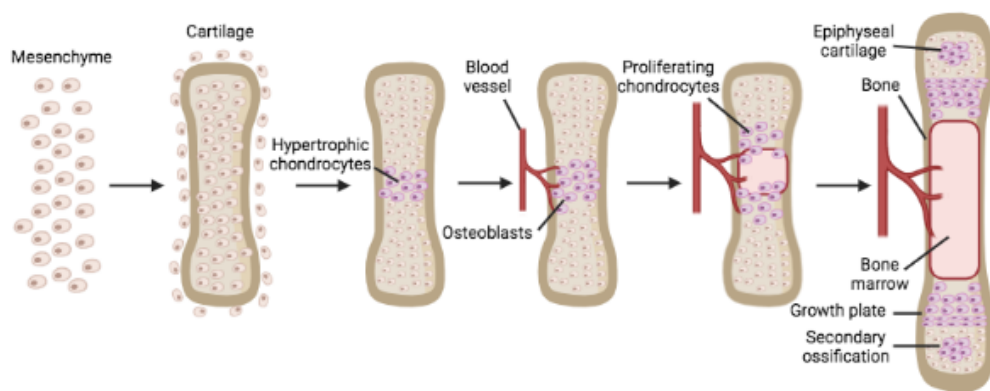


Figure 1.6: Endochondral ossification. The mechanism responsible for the formation of long bones of the skeleton. The embryonic cartilaginous model is replaced by bone, contributing to longitudinal growth.

1.3.3. Growth plate cartilage

Before differentiating into chondrocytes, mesenchymal progenitor cells proliferate and aggregate at mesenchymal condensations (62). In order to generate cartilage matrix, chondrocytes secrete extracellular matrix (ECM) proteins, such as type II collagen and aggrecan. Providing mechanical support, hyaline cartilage is the most common form of cartilage, found in joints, ribs, and growth plates. This type of cartilage has a major role in both long bone development and function (62). Long bone growth is driven by growth plate cartilage, whereas shock absorption and joint mobility is provided by articular cartilage.

The growth plate is separated into distinct zones of chondrocytes (Figure 1.7). In the resting zone, at the bones most epiphyseal side, chondrocytes proliferate slowly and differentiate into proliferating chondrocytes, expressing Col2a1 which encodes type II collagen (63). The proliferative zone contains proliferating chondrocytes expressing Col2a1 and ACAN (proteoglycan aggrecan) which produce important cartilage function matrix proteins. These chondrocytes then differentiate further into hypertrophic chondrocytes expressing Col10a1, for type X collagen and Ihh, for Indian Hedgehog (63). Hypertrophic chondrocytes in the hypertrophic zone are responsible for longitudinal bone growth, as they undergo mineralisation and are replaced by mineralized bone (62). The terminal hypertrophic chondrocytes express Spp1 (secreted phosphoprotein1), Ibsp (integrin-binding sialoprotein), and MMP13 (matrix metalloproteinase 13) (22). The chondrocyte transcription factors, including Sox9, RUNX2, and Osterix, ensure a precise coordination of events resulting in healthy osteogenesis (63).

1.3.4. Articular cartilage

Articular cartilage is found at the end of long bones in articulating joints. It is a flexible connective tissue which functions to provide a smooth surface for articulation with low friction and facilitating the transmission of load (64). The articular cartilage in joints can tolerate intensive and repetitive physical stress. However, it has an inability to heal following injury. This means that joints are sensitive to degradation and therefore

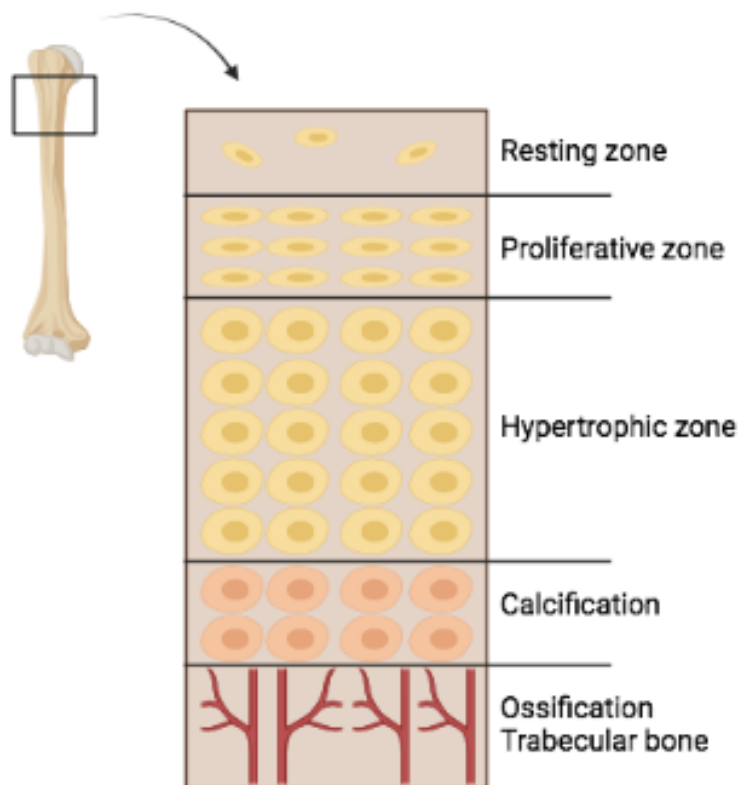


Figure 1.7: Growth plate structure. The cartilaginous part of long bones, where longitudinal growth takes place. The structure comprises of different zones of chondrocyte maturation.

development of diseases such as Osteoarthritis (OA) (65). Articular cartilage lacks blood vessels, lymphatics, and nerves, and has limited capacity for repair (64).

The mature articular cartilage, or hyaline cartilage, is translucent in appearance and contains unique constituents such as type II collagen, glycosaminoglycans (GAGs), and low cellularity (64). Human adult cartilage composition and cellular organisation is complex, where there are many matrix differences between different layers. The only cellular component of articular cartilage are chondrocytes, and these can have many different morphologies from larger and flatter in the deeper zones, to flattened at the surface (10). Depending on joint type, the surface chondrocytes can show distinct spatial patterns and differently orientated matrices (66). For example, the smooth surface of lubricin and horizontally orientated collagens helps attenuate friction of the articular cartilage during skeletal motion (67). Normal adult articular cartilage consists of chondrocytes and extracellular matrix (68). Chondrocytes synthesize the matrix components and the proteolytic enzymes to break them down, mediating normal turnover of matrix components (69). The cartilage ECM comprises mostly water, collagen, and proteoglycans, where proteoglycan turnover is rapid and collagen relatively slow. There are many factors that influence chondrocytes, such as the matrix components, structural and physical stimuli, and polypeptide growth factors and cytokines. Chondrocyte failure to maintain ECM component synthesis and degradation homeostasis results in a diseased state such as OA (70).

In human adult cartilage, chondrocytes are usually quiescent and maintain the matrix in a state of very low turnover. The abnormal repair and promotion of matrix destruction observed in OA is an important phenotype to understand. To reduce cartilage damage and promote repair, identifying major players within these pathways may provide targets for therapy (10). Studies within developmental biology have identified various signalling pathways and molecules involved in skeletal formation. Regenerative medicine and cell biology approaches have successfully enabled the induction of chondrocytes from somatic and pluripotent stem cells in vitro (71,72).

1.4. Pathophysiology of Osteoarthritis

1.4.1. Osteoarthritis phenotype

Osteoarthritis (OA) is a complex degenerative joint disease affecting millions of people worldwide, one of the most common forms of arthritis and chronic musculoskeletal disorders (69). Increasing evidence suggests that OA is a multifactorial, inflammatory disease of the entire synovial joint, with many phenotypes (73). The cause of OA is not understood, however, biomechanical forces placing stress on joints such as traumatic injuries of excessive and abnormal load bearing, may interact with other environmental, systemic and genetic factors. Combined, those could influence and contribute to the pathogenesis of OA (73).

The pathogenesis of OA includes changes in articular cartilage and subchondral bone tissue homeostasis, where multiple factors influence the disease initiation, progression and severity (74). Although OA is characterised by the progressive deterioration and loss of articular cartilage, there are structural and functional changes in the entire joint (73). Therefore, it is important to understand the complete pathogenesis of OA, including changes in the subchondral bone, synovium, menisci, ligaments, periarticular muscles and nerves, as well as the articular cartilage (75), where cellular changes and biomechanical stress combine to cause changes within the joint (Figure 1.8). For example, the formation of osteophytes, subchondral bone remodelling and the development of bone marrow lesions (76). Studies have demonstrated that age, obesity, and metabolic disease are major risk factors effecting disease development in OA (77).

In understanding the early development of OA, it is possible to target these changes to prevent or slow disease progression as forms of treatment (69). The pathophysiology mechanisms involved in OA include pro-inflammatory interleukins (IL-1b, IL-6, IL-8) and tumour necrosis factor- α (TNF- α). Through their signalling pathways, pro-catabolic mediators are also involved, including effects of nuclear factor κ B (NF κ B) and mitogen-activated protein (MAP) kinase signalling responses (78). As OA develops, many signalling pathways play important roles. For example, BMP, SRY-related protein 9 (SOX9), transforming growth factor β (TGF- β), and insulin-like growth factor (IGF) pathways.

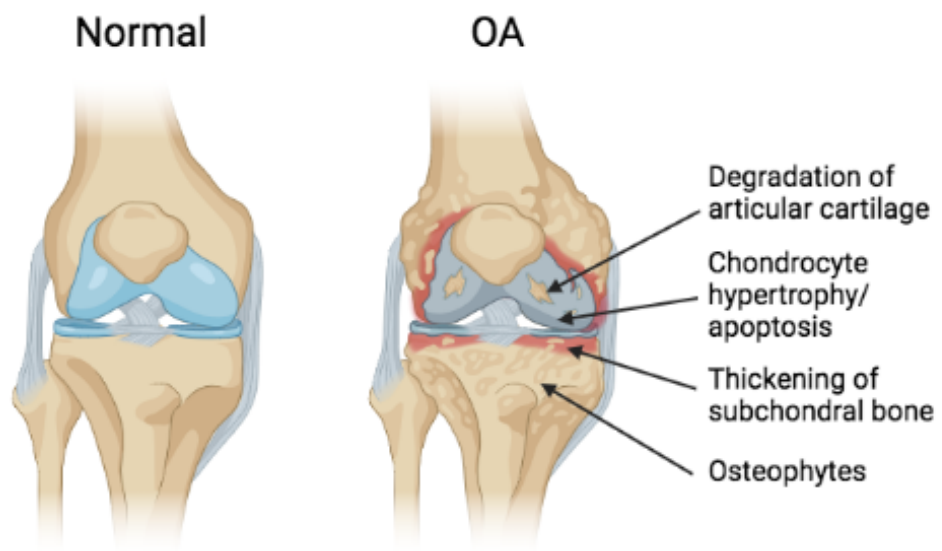


Figure 1.8: Osteoarthritis joint phenotype. Osteoarthritis is a degenerative joint disease characterized by degradation of articular cartilage, chondrocyte hypertrophy/apoptosis, thickening of subchondral bone and formation of osteophytes.

These pathways are involved in many processes such as chondrocyte metabolism, synthesis and degradation of ECM, cell proliferation, differentiation, apoptosis and inflammation (79).

Although in the disease initiation and progression of OA all joint tissues are affected, articular cartilage demonstrates the most destruction through aging, injury and disease (65). The function and viability of chondrocytes is compromised by inflammatory mediators, and mechanical and oxidative stress, as they undergo hypertrophic differentiation and early senescence, therefore becoming more sensitive to the effects of pro-catabolic and pro-inflammatory mediators (73).

1.4.2. Cartilage changes and Osteoarthritis

Chondrocytes are the cellular component of cartilage. Cytokines and growth factors secreted by chondrocytes regulate cartilage matrix synthesis and breakdown. In OA, this balance is disturbed (74). Within OA affected joints, cartilage, synovium and subchondral bone interact, impacting on cartilage function. Articular cartilage is altered and it is difficult to define the initiation of these pathological changes (10).

OA chondrocytes show a senescence secretory phenotype, including an overproduction of cytokines (interleukins 1 and 6), growth factors (e.g. epidermal growth factor) and matrix metalloproteinases (MMPs) (e.g. MMP-3 and MMP-13) (80). In OA chondrocytes, an increased expression of catabolic genes and decrease in anabolic gene expression are usually observed, disrupting the articular cartilage metabolic balance (81). The initiating factor that causes an imbalance between the repair and degradation of cartilage is unknown but may be influenced by inflammation causing an increase in enzyme activity, mechanical stress, or trauma causing a microfracture (69). During this imbalance, mediators of inflammation are produced, and chondrocytes are stimulated to release degradative enzymes. The release of proinflammatory cytokines, such as TNF α , IL-1 and IL-6, is caused by collagen and proteoglycan breakdown molecules. An increase in the cartilage degradation occurs when these cytokines bind to chondrocyte receptors which leads to further release of MMPs and inhibits the production of type II collagen (82). Due to the increased breakdown of collagen and decreased synthesis of type II collagen, the collagen

network is weakened. As a result of this disruption of homeostasis, the ECM decreases in proteoglycan content and increases in water content (83). There is also an increase in chondrocyte apoptosis (69).

An increase in anabolic and catabolic activity is observed in osteoarthritic cartilage. To begin with, the articular cartilage is maintained by an increase in matrix synthesis such as collagen, proteoglycans and hyaluronate and chondrocyte proliferation in the cartilage deep layers (84). However, with time, the changes in ECM and loss of chondrocytes cause the development of osteoarthritic changes (69). The articular cartilage degenerative changes become more severe over time. From cartilage softening, fibrillation of the superficial layers, fissuring and reduced cartilage thickness, to total destruction by cartilage thinning and exposure of the underlying subchondral bone plate (69).

1.4.3. Gene expression in Osteoarthritis

The gradual progression of cartilage degeneration observed in OA occurs alongside the decrease in gene expression of SOX9, ACAN, and COL2A1 (85). During OA progression, the expression of WNT antagonists DKK1 and FRZB are lost and hypertrophic markers RUNX2, COL10A1 and IHH increase (85). In addition to this, DKK1 and FRZB negatively correlate with OA grading, and RUNX2 and IHH have a significantly positive correlation (85).

Using RNA-seq, the gene expression changes in damaged OA cartilage compared with intact cartilage from the same joint were investigated (86). Within this study, differentially expressed genes and dysregulated pathways were identified. For example, a decreased expression of chondrogenic genes SOX9, SOX6, COL11A2, COL9A1/2/3, ACAN and HAPLN1 were demonstrated in damaged OA cartilage. There was also an increase in non-chondrogenic gene expression of COL1A1, COMP and FN1, and an altered pattern of secreted proteinase expression. The study did not identify an alteration in expression of major inflammatory cytokines (86). PhenomeExpress system analyses identified significant networks of differentially expressed genes to include mitotic cell cycle, Wnt signalling, apoptosis, and matrix organisation. These pathways were influenced by transcription factors FOSL1, AHR, E2F1 and FOXM1 (86). This concludes that damaged

cartilage possesses gene expression changes with a non-chondrogenic response from altered secreted proteinase and matrix protein expression (86).

Differentially expressed genes between OA and healthy control samples were also identified using meta-analysis, revealing 449 upregulated and 241 downregulated genes (87). Within these results, the transcription factors FOS, TWIST1, POU2F1, SMARCA4 and CREBBP decreased in mice with OA, and may play an important role in OA pathology (87). Another study confirmed expression patterns of 1619 dysregulated genes from a surgically induced model of early OA. These dysregulated genes included COL2A1, MMP13, ADAMTS5, CTSC, PTGES and CXCR4 (88).

In joint repair, MSCs have a crucial role, however their changes in characteristics affected by OA severity are unknown. Gene expression changes were evaluated in subchondral bone MSCs in knee OA, in relation to the progression of osteochondral damage. This identified STMN2, PTHLH and GREM1 as the most consistent upregulated genes in damaged tissue (89). Interestingly, these gene expression changes were not observed in chondrocytes, indicating that they are MSC specific. The gene expression patterns described in this study indicate a potential involvement of MSCs in cartilage calcification, bone formation and mineralisation, identifying several gene candidates for therapeutic targeting (89).

In articular cartilage, gene expression was analysed between healthy and OA cartilage identifying 1717 genes significantly differentially expressed (90). Within these genes, there was significant enrichment for genes involved in skeletal development, for example TNFRSF11B and FRZB. Inflammatory genes such as CD55, PTGES and TNFAIP6 were confirmed to be upregulated in OA cartilage (90). Focussing on these differentially expressed genes between OA and healthy tissues may provide useful for developing novel treatments.

1.5. microRNAs

1.5.1. Biogenesis and mechanism

Epigenetic mechanisms alter the expression of genes independent of changes in the DNA sequence and this regulation of genome activity induced by environmental factors can influence disease development (91). microRNAs (miRNAs) are a family of small, single stranded, non-coding RNAs with a sequence length of 19 to 23 nucleotides, first identified in *C.elegans* in the 1990s (92). The functional group of small RNAs that they belong to also include Piwi-interacting RNAs (piRNA) and short interfering RNAs (siRNAs) responsible for RNA interference (RNAi) (93). miRNAs are post-transcriptional regulators of gene expression, and function through base-pairing with “seed sequences” (94). This complementary binding of miRNA to a target mRNA represses gene expression by mediating translational cleavage, inhibition, or degradation (95). Many microRNAs are highly conserved which indicates that they play an important role in biological processes (96), and are involved in epigenetic regulation alongside DNA methylation and histone modification (97).

The dominant pathway in which miRNAs are processed is the canonical biogenesis pathway (Figure 1.9) (98). In this miRNA biogenesis pathway, miRNAs are transcribed as long primary transcripts (pri-miRNAs) before being processed into small hairpin precursor miRNAs (pre-miRNAs). These are then transported to the cytoplasm and cleaved by Dicer into functional, mature miRNAs (99). RNA polymerase II primarily mediates the transcription of miRNA genes. The 3' end of the pri-miRNA contain a hairpin structure which is cleaved and processed in the nucleus by the enzyme Drosha, releasing pre-miRNAs (100). A complex known as the microprocessor complex is formed of Drosha and its co-factor DGCR8 (DiGeorge syndrome critical region gene 8) (101). The pre-miRNA is processed and exported to the cytoplasm by an exportin 5 (XPO5)/RanGTP complex (102).

In the cytoplasm, Dicer, an RNase III type endonuclease responsible for cleavage of pre-miRNAs, recognizes the pre-miRNA. This results in the generation of a mature miRNA duplex, approximately 22 nucleotides long, following removal of the terminal loop. The mature miRNA is loaded onto an Argonaute (AGO) protein family member, in an ATP-

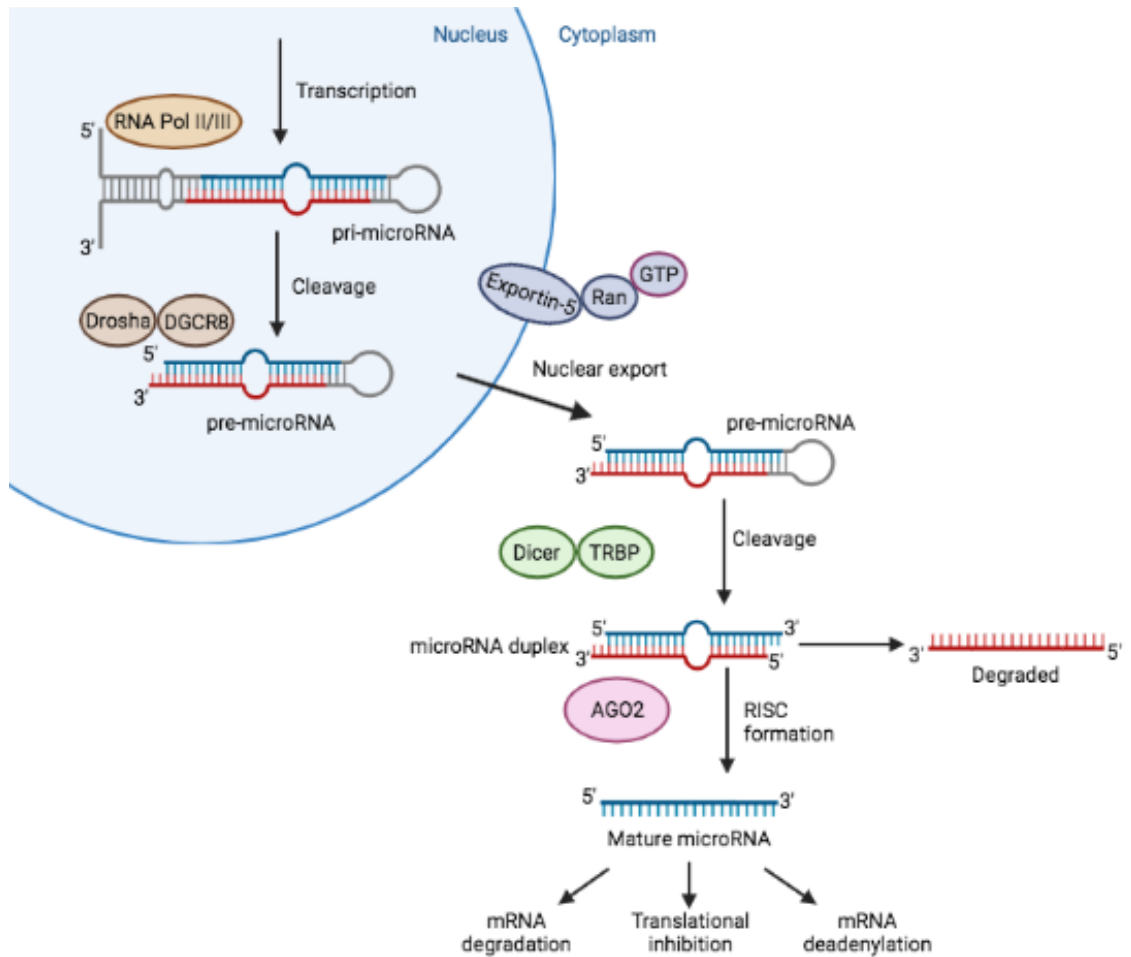


Figure 1.9: microRNA biogenesis. microRNAs are transcribed as primary transcripts (*pri-microRNA*) and processed into hairpin loop structures, precursor microRNA (*pre-microRNA*) but *Drosha* and cofactor. *Pre-microRNA* is transported to the cytoplasm but *Exportin-5*, before cleavage by *Dicer* and cofactor to form 2 complementary strands. The mature strand is loaded onto the RISC complex, complementary base pairing to target mRNA, usually in the 3'UTR, most commonly to repress translation.

dependant manner, forming a complex called the miRNA-induced silencing complex (miRISC) (103). The name of the mature strand of miRNA is determined by its directionality: the 3' strand originates from the 3' end of the pre-miRNA hairpin, and the 5' strand from the 5' end (98). Either of these strands derived from the mature miRNA duplex can be loaded into the AGO protein (104). The cellular environment or cell type influences the proportion of either AGO-loaded 3p or 5p strand of miRNA, where they may be present in almost equal proportions or predominantly only one (105). The RISC complex selects and recruits the guide strand of RNA, and the complementary strand is usually degraded (99). Following binding to the RISC, the miRNA guides the complex to a specific mRNA sequence, inducing inhibition of target gene translation and mRNA deadenylation and decapping (99).

miRNAs most typically suppress expression by binding to a specific sequence at the 3' untranslated region (UTR) of their target messenger RNAs (mRNAs), inhibiting translation or destabilising the mRNA (97). However, it has also been reported that miRNAs interact with other regions such as the coding sequence, gene promoters, and 5' UTR which contain miRNA binding sites (106). Under certain conditions, miRNAs have been shown to activate gene expression, opposing their function as repressors (107). For example, an interaction of miRNA with a promoter region can induce transcription (108), whereas binding to coding regions and 5'UTR silence gene expression (109,110). To control the rate of translation, and even transcription, studies have demonstrated that miRNAs may be moved from different subcellular compartments, although this interplay is under investigation (111). In addition to the canonical pathway, there are also multiple non-canonical miRNA biogenesis pathways which use different combinations of canonical pathway proteins such as AGO2, exportin 5, Dicer and Drosha (98).

During many cellular functions, such as apoptosis and differentiation, miRNAs are implicated to play a role, and are critical for normal development (112). Several biological disease processes, such as cardiovascular disease and cancer, have been associated with changes in miRNA expression (94). Previous studies suggest an important role for epigenetics in the progression of OA, observing gene expression changes in diseased cartilage (113). However, the complete role of miRNAs in OA remains unknown. Due to

their stability and ease of detection, interest has been focussed on the area of miRNAs, in particular as biomarkers for disease activity. There are many studies that demonstrate the release of miRNAs into extracellular fluids, and consequently these extracellular miRNAs may be used as biomarkers for different diseases (98). These extracellular miRNAs may also play a role in intercellular communication (114), and even portray hormone-like activities (115).

1.5.2. microRNAs in skeletal development

During embryonic development, the importance of microRNAs is almost omnipresent, contributing to the development of most cells and organs (116). In skeletal development, miRNAs important roles are demonstrated by the mutation or deletion of Dicer which prevents the biogenesis of miRNAs (117). At the early stages of embryonic development, conditional knockout of Dicer in the limb mesenchyme leads to the formations of smaller limbs (118). In the developing joint, enhanced hypertrophy is shown in Dicer null growth plates, in addition to a lack of chondrocyte proliferation (118). Skeletal growth defects and premature death result from the conditional knockout of Dicer in chondrocytes (119), and the phenotype in conditional Drosha knockouts is also very similar (120).

During skeletal formation, it is well known that miRNAs play a role in chondrogenic and osteogenic differentiation (121,122). Mesenchymal stem cells (MSCs) generate both connective and skeletal tissue. Surface expression markers define the identity of MSCs, of which many have been identified as miRNA targets (24). In the musculoskeletal system, miRNAs can act as both positive and negative factors influencing related signalling pathways, with studies showing a role in many aspects of bone biology including endochondral ossification (16). For example, osteogenic control of MSCs by miRNAs -17, -433, and -31 inhibit osteogenic differentiation whereas miRNAs -34a, -21, and -96 promote differentiation into osteoblasts (123).

The interplay between miRNAs and signalling is complex, and two important pathways for skeletal development are BMP and Wnt (124). Different miRNAs are reported to regulate osteogenesis transcription factors such as Runx2, and importantly molecules in the Wnt

and BMP signalling pathways which control osteoblast differentiation (125). In skeletogenesis, BMPs are profoundly involved, and several miRNAs regulate BMP signalling both positively and negatively (126). For example, miR-133 and miR-135 are described as negative regulators of osteogenesis by targeting Runx2 and Smad5, inhibiting osteogenic differentiation (126). The inhibition of Wnt/b-catenin pathway receptors is the main mechanism whereby miRNAs affect Wnt signalling (124). For example, during osteoblast differentiation miR-218 is upregulated resulting in an increase in osteoblast markers (Alpl, Runx2, Bglap) which correlate with decreased expression of Sfrp2, Sost, and Dkk2 (124). Other pathways, such as Notch, IGFs, and hedgehogs involved in skeletal tissue differentiation are post-transcriptionally regulated by miRNAs (124). A subset of miRNAs associated with osteoblast commitment, differentiation and identity have been termed 'osteomiRs' (127), and there are also miRNAs that silence osteogenic associated genes within non-bone tissues (24). During development of the skeletal system, osteomiRs target non-collagenous glycoproteins and proteoglycans for example BSP, OCN, and osteonectin. This regulates matrix mineralisation through targets implicated (128). For example, miR-29a and -29c play a role in maturing osteoblasts, where their expression increases during late osteogenesis (128). When embedded in the matrix, osteoblast differentiation into osteocytes can be directly or indirectly regulated by miRNAs (24). Even before this matrix calcification, the proliferating osteoprogenitors secrete proteins which are regulated by miRNAs such as OPN (24).

At different stages of skeletal development and osteogenesis, miRNAs and their targets play an essential role. A disruption to these processes may result in severe skeletal malformations and deformities, providing an interesting study topic. Many of the miRNA regulated targets during bone marrow MSC differentiation are only predicted, and further experiments are needed to validate these.

1.5.3. microRNAs during chondrogenesis

In chondrocytes, many miRNAs are expressed, creating a complex gene regulatory network as each miRNA can regulate many target genes (62). During chondrogenesis, transcription factors and signalling molecules have been identified as miRNA targets which therefore regulate this process and may be useful for the repair and engineering of

cartilage (129,130). Although SOX9 has shown to induce many different miRNA expression levels, a particularly responsive example is miR-140 (131). The skeletal phenotype of miR-140 null mouse shows the growth plate proliferating chondrocytes to decrease (132,133), which may be due to the ability of miR-140 to alter the cell cycle by targeting Sp1 (134).

During *in vitro* hMSC chondrogenesis, many miR-140-5p targets have been identified including FZD6 and RALA (135). In both hMSC and ATDC5 models of chondrogenesis, miR-455 is SOX9 inducible and also co-regulated with miR-140 (135,136). During early chondrogenic differentiation, miR-455-3p has also been shown to have a role targeting RUNX2 (137), and potentially HDAC8 and HDAC2 (138). DNA methylation may also be impacted during chondrogenesis by miR-455-3p targeting DNMT3A (139). It has previously been shown that premature hypertrophic chondrocyte differentiation and a delayed differentiation of resting to proliferating chondrocyte occurs as a result of miR-140 deficiency (133). Targets of miR-140 have been identified, however, the significance of the miR-140 regulatory role for each target remains to be determined. These targets include DNPEP, PDGFRA, HDAC4, SMAD3 and RALA (140–143).

The role of miRNAs in regulating cartilage development and homeostasis has been reported in many studies, using both *in vitro* and *in vivo* approaches (144). During MSC chondrogenesis, miR-29a expression decreases, and the expression of miR-29a is repressed by SOX9, suggesting a role in chondrogenesis induction (145,146). However, in regulating cartilage homeostasis, the functional role of miR-29a is currently unknown. Upon chondrocyte differentiation, several miRNAs are downregulated and negatively regulate the process. For example, during chondrocyte differentiation of mouse C3H10T1/2 cells miR-145 was downregulated (147). Chondrocyte differentiation is inhibited by miR-145 as SOX9 is a direct target of miR-145 and expression is suppressed. This leads to reduced mRNA levels of chondrocyte markers, for example COL2A1, COL9A1, COL11A1 and ACAN (62).

There are many more miRNAs that promote chondrogenesis *in vitro*, for example miR-574-3p is upregulated during MSC chondrogenic differentiation, and may be part of a

positive feedback loop promoting chondrogenesis (148). Upon chondrocyte differentiation of mouse MSCs, miR-335 expression increases with its host gene MEST, creating another feedback loop enhancing chondrogenesis (149). In human MSCs during chondrocyte differentiation, miR-199a was also upregulated (150).

During hypertrophic differentiation of chondrocytes, miR-1 was found to be downregulated, and miR-1 overexpression in chicken primary chondrocytes and HCS-2/8 cells reduced ACAN expression (151). miR-375 was also downregulated upon chondrocyte differentiation in chicken limb mesenchymal cells, and miR-375 inhibition increased chondrogenic differentiation (152). In mouse chondrocytes, miR-1247 was reported to be expressed, where it creates a negative feedback loop with SOX9 expression and may play a role in the regulation of SOX9 function (153). Inhibition of chondrocyte differentiation also increases miR-221 expression (154). Chondrocyte differentiation is also negatively regulated by miR-448 in human bone marrow MSCs and human chondrosarcoma cells. Expression of a component of the canonical Wnt-signalling pathway, LEF1, is suppressed by miR-449, and this reduces proteoglycan production and downregulates COL2A1 and SOX9 expression (155).

The complex integration of miRNAs show that many have the potential to regulate MSC differentiation and lineage determination. Other examples in mouse MSCs include miR-24, miR-199b, miR-101, miR-124a and miR-199a, which are all upregulated during differentiation into chondrocytes, and downregulated miR-18 and miR-19 (156).

1.5.4. Cartilage specific microRNA expression

The importance of miRNA function in skeletal development and homeostasis is displayed during *in vivo* modulation of proteins involved in miRNA processing, for example Dicer and Drosha. A severe growth retardation phenotype was observed in mouse cartilage tissue, when type II collagen-producing cells were devoid of Dicer (119). The number of hypertrophic chondrocytes was increased, and proliferation of growth plate chondrocytes reduced, suggesting that proliferation and differentiation of growth plates is regulated by miRNAs (119).

The most abundant miRNAs in somatic tissues, including chondrocytes, are let-7 miRNAs. The let-7 miRNA family have been shown to be required for normal growth plate chondrocyte proliferation (157). In Dicer-deficient chondrocytes, a let-7 miRNA target, HMGA2, was upregulated (119). In chondrocytes, an overexpression of Lin28a, a let-7 inhibitor, suppressed let-7 miRNA expression and reduced chondrocyte proliferation, resulting in a mild growth impairment. Predicted let-7 target genes were also upregulated (157). A mild skeletal phenotype was observed in Lin28a transgenic mice, however, miR-140 deficient/ Lin28a transgenic mice have a dramatic growth defect. As miR-140 has been shown to modulate chondrocyte differentiation, it has been suggested that, by regulating chondrocyte proliferation and differentiation, let-7 miRNAs and miR-140 coordinately regulate skeletal development (157).

miR-140 is encoded in an intron of the WWP2 gene sequence and is expressed in chondrocytes, and the expression of WWP2 and miR-140 is directly regulated by SOX9 (134), where an upstream region of the pri-miRNA-140 gene possesses chondrocyte-specific promoter activity (158). In chondrocytes, miR-365 was identified as a mechanosensitive miRNA, targeting HDAC4 to stimulate hypertrophic differentiation. Following this, in response to IL-1 β stimulation or cyclic loading, miR-365 was shown to be upregulated in chondrocytes of articular cartilage (159). As experimental evidence suggests significant roles for miRNAs in cartilage development, homeostasis and pathology, the potential for miRNAs to become therapeutic targets for cartilage disease has demonstrated the importance of understanding the role of each miRNA in chondrocytes and cartilage tissue.

1.6. microRNAs and Osteoarthritis

1.6.1. Differential expression of microRNAs in cartilage

Generally, the differentially expressed miRNAs in cartilage from normal and osteoarthritis patients are not consistent across studies. Figure 1.10 summarises research identifying miRNAs dysregulated in OA and their impact on cartilage. These microarray and RNA-Seq screens of expression may differ due to differences in the samples (117). The expression of published microRNAs in OA has been analysed, identifying 46 differentially expressed.

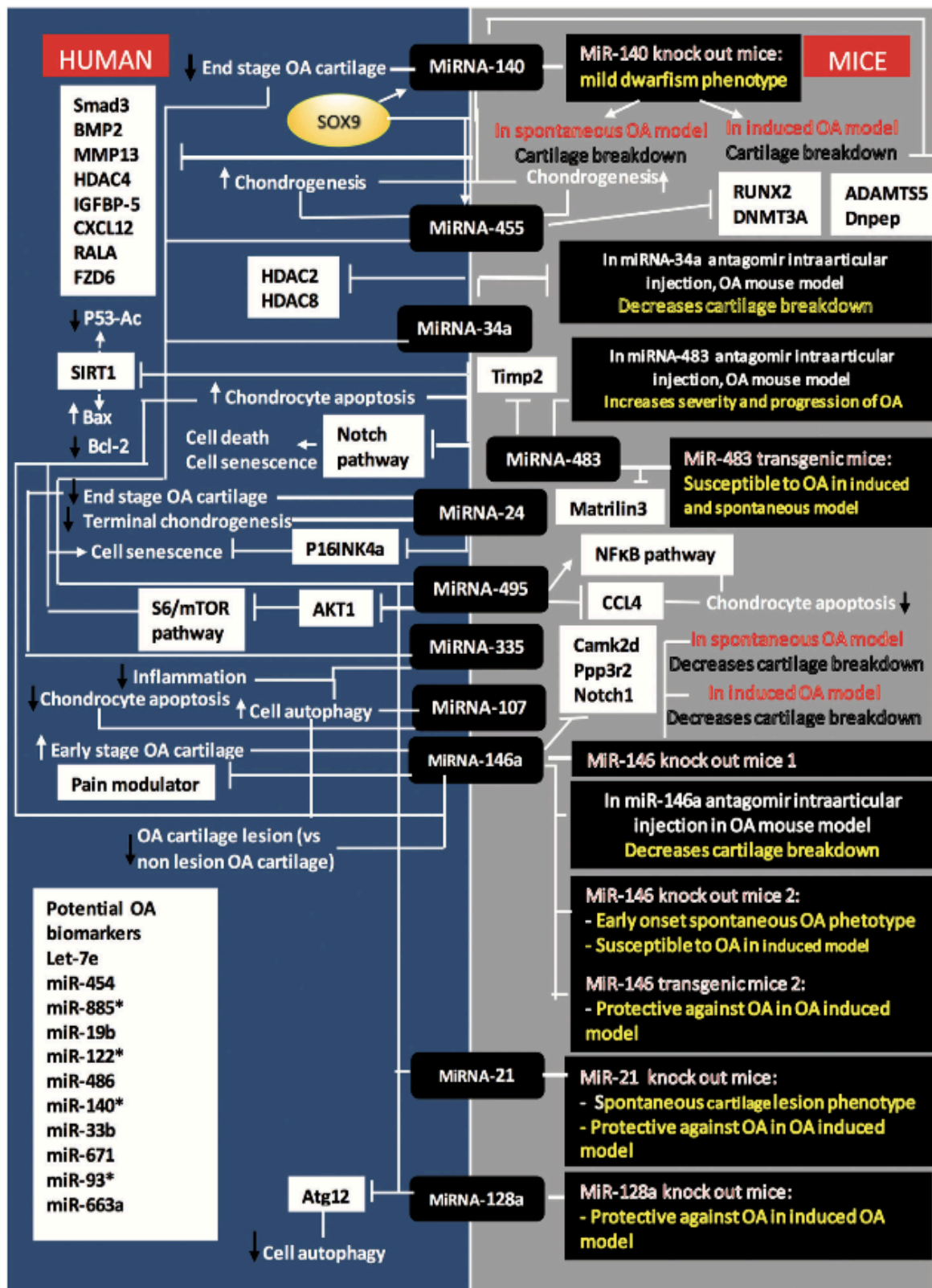


Figure 1.10: Roles of microRNAs in Osteoarthritis. Human cartilage, cells and plasma data is shown on the left, with complementary data from mouse models on the right. Schematic demonstrates research identifying microRNAs which are dysregulated in osteoarthritic cartilage and their impact on chondrogenesis (Swingler et al, 2020).

In chondrocytes, these miRNAs are involved in many different processes including differentiation, metabolism, ECM degradations, apoptosis, autophagy and inflammation (160). AGO2 immunoprecipitation has also been used to assess functional miRNAs in the RISC complex within chondrocytes, where cells taken from OA and normal cartilage identified miR-27b-3p as the most abundant (161). Another technique performing mRNA-Seq and miRNA-Seq from OA lesion and normal cartilage enabled an interactome of differentially expressed mRNAs and miRNAs to be identified (162). Within this data, in OA lesions miR-99a-3p was downregulated, targeting 36 mRNAs including FZD1, ITGB5 and GSF6. In contrast to this, miR-143-5p is upregulated in OA lesions, targeting 16 mRNAs including DCAKD, AMIGO1 and SMAD3 genes (162).

There are many reasons which could explain these different results. For example, the heterogeneous nature of human OA cartilage could explain why samples analysed by different research groups are varied. Within cartilage specimens of a similar OA grade, there may be different ratios of either chondrocytes contributing to ECM breakdown and chondrocytes actively attempting to repair ECM (144). Variations could also depend on analysis of hip or knee articular cartilage. On top of this, cartilage analysed at different stages of OA could affect the results. For example, a particular miRNA could be expressed at higher levels either in early or late-stage OA. Levels of miRNA may change throughout disease progression and it is important to determine target genes and the pathways they regulate in order to understand disease mechanisms.

It was shown that an early onset of OA and aging in mice was caused by miR-140 deficiency, and an accelerated development of OA was observed in OA induced mice (132). Elevated expression levels of miR-146a have been identified in OA cartilage and plasma from OA patients. In chondrocytes, this miRNA is responsive to pro-inflammatory cytokines (163,164). However, it is unknown whether miR-146a has beneficial or adverse effects on chondrocytes, as results have been published for both arguments (144). The levels of miR-483 and miR-146a also show an increase in OA cartilage. In human and mouse OA cartilage, miR-483 has been identified to be upregulated (165,166). Studies have shown that this miRNA, located in the insulin-like growth factor 2 (IGF2) gene, is differentially expressed during human chondrocyte differentiation (144).

In both OA and in response to inflammatory cytokines, the levels of miR-29a are altered (167), and in cartilage from a rat OA model and also in human OA samples, miR-365 levels were higher than controls (168). Another miRNA, miR-181a, was found to be increased in OA facet joint cartilage but decreased in knee OA cartilage (169). This is another example that could demonstrate how miRNAs can have varied functions in chondrocytes at different anatomical locations (144). miR-23b was also found to be upregulated in human OA chondrocytes in a separate study (170).

Members of the miR-181 family are expressed in both hypertrophic chondrocytes and chondrocytes from developing human cartilage (171), and higher levels of miR-181a were found in OA facet joint cartilage compared to control specimens (169). It has also been reported that mouse OA cartilage has higher levels of miR-181b, and by inhibiting with miR-181b antagomir intra-articular injection, the effects of OA were reduced (172). However, in contrast, decreased levels of the miR-181 have also been reported in human OA articular tissue (173). It has been discovered that miR-181a is highly expressed in chicken chondrocytes and directly targets to suppress the pro-chondrogenic gene CCN1 (CCN family member 1) and aggrecan (174).

The number of miRNAs and small samples sizes analysed in previous studies could be a limiting factor in identifying miRNAs with potential to become biomarkers in disease such as OA. Although it has been shown that many miRNAs are altered in disease, it is unclear whether this dysregulation is a cause of disease or a downstream effect (144). A few targets of miR-140 have been identified, for example in the human chondrocytic C28/I2 cells, miR-140 directly targets MMP13 mRNA, suppressing IL-1 β induced MMP13 expression (175). In OA chondrocytes, a downstream mediator of the TGF- β , Smad3, was shown to reduce miR-140 expression (176). An overexpression of miR-140 also downregulated IL-1 β -induced Adamts5 expression (177).

In response to IL-1 β stimulation, it has also been shown that miR-145 is increased in OA chondrocytes. The downregulation of type II collagen and aggrecan expression caused by IL-1 β treatment was also reversed by miR-145 inhibition, and SMAD3 has been identified

as a miR-145 target (147). MiR-145 was shown also to target SOX9 in human articular chondrocytes (178). There are many miRNAs linked with regulation during cartilage development, articular cartilage homeostasis, maintenance of articular chondrocytes in cartilage and OA, through diverse mechanisms (62).

For normal development and cellular function, epigenetic control of gene expression is essential, and it is evident that epigenetic regulation is altered in OA (179). In another study, the expression of 4 miRNAs (has-miR-138-5p, has-miR-146a-5p, has-miR-335-5p, and has-miR-9-5p) were found to be upregulated in OA patient cartilage compared to control (97). However, these results were not significantly related to clinical data demonstrating the need for further studies to assess cartilage miRNAs.

One of the most studied miRNAs in cartilage biology is miR-140, as it is known to be highly expressed in chondrocytes. As previously discussed, transgenic miR-140 knockout mice have been generated, where homozygous knockout mice displayed mild dwarfism phenotypes and craniofacial defects, such as short endochondral bones and reduced longitudinal growth of the skull (132,133). The post-natal articular cartilage in these mice was examined and showed accelerated ECM degradation compared with control (132). Results for miR-140 expression patterns in OA are contradictory, as reports have shown both increased (180) and decreased levels (177). As miR-140 has been shown to function in chondrocyte differentiation and cartilage homeostasis regulation, the altered expression of miR-140 in OA could be expected.

1.6.2. Implicated roles for microRNAs in Osteoarthritis

Many signalling pathways have been shown to regulate and be regulated by miRNAs, including those implicated in OA (117). For example, a number of miRNAs regulate and are regulated by TGF β and TGF β /Smad signalling, where the expression of miR-140 is reduced by TGF β (181) and SMAD3 identified as a target of miR-140-5p (142). Another example is the chondrocyte miR-29 reduced expression by TGF β (146) which is Smad3 dependant (182). In addition to this, miR-29 can suppress TGF β signalling (146). These feedback loops can again be demonstrated in chondrocytes, where miR-455 expression is induced by TGF β and also supresses TGF β signalling through targeting of SMAD2 (180). In

chondrocyte hypertrophy, miR-483 expression is significantly decreased, and overexpression resulted in a downregulation of SMAD4 which reduced ECM production and suppressed chondrogenesis (183). The role of microRNAs in the pathogenesis of OA is still unclear, although it is evident that they impact on signalling pathways associated with the disease.

Research of miRNAs has implicated a role in the regulation of apoptosis, autophagy and senescence, mechanisms involved in OA pathogenesis (117). In chondrocytes, miR-34a was identified to be involved in apoptosis, whereby a miR-34a inhibitor suppressed IL-1 chondrocyte apoptosis (184). In human OA cartilage, miR-34a expression is increased and its target SIRT1 decreased (185). This resulted in an increase in chondrocyte apoptosis through less acetylation of p53, decrease in Bcl-2 and increased Bax expression. In chondrocytes overexpressing miR-34a, markers of autophagy were also decreased (186). It has also been reported that miR-34a targets the Notch pathway, increasing chondrocyte cell death and senescence (187). In these studies, miR-34a inhibitor intraarticular injection into an OA model diminishes the destruction of cartilage (185,187).

Markers of senescence, including the cell cycle inhibitor P16INK4a, increase in terminal chondrogenesis and OA and are regulated by miR-24, which subsequently decreases in OA (188). In human OA cartilage, miR-495 levels are elevated (189). Markers of senescence (SA- β -gal and p16) are increased via AKT1 and the S6- mTOR system targeting when miR-495 is overexpressed, increasing chondrocyte apoptosis. Following intraarticular injection of a miR-495 inhibitor in a rat OA model, both chondrocyte apoptosis and OA decreased. Another study identified CCL4 as a potential target of miR-495, whereby inhibition of the miRNA suppressed apoptosis by activating the NF κ B pathway (190). In order to prevent apoptosis during cell stress, autophagy can be activated, and particular miRNAs have been shown to regulate this. For example, in OA chondrocytes, miR-335-5p expression was lower and overexpression caused a reduction in inflammation and increased autophagy (191). Overexpression of miR-107 in OA chondrocytes also increased autophagy and inhibited apoptosis (192).

In osteoarthritic patients, articular cartilage-derived MSCs (OA-MSCs) were transfected with miR-365 inhibitor which suppressed the expression of chondrogenic, hypertrophic, and osteogenic gene expression (193). An overexpression of miR-365 in mouse articular cartilage also resulted in an upregulation of OA markers and hypertrophy (193). From this it was concluded that miR-365 regulates chondrogenesis by activating mineralization, hypertrophic and osteogenic genes during OA pathogenesis, providing important implications for cartilage repair therapies (193).

1.6.3. microRNAs as biomarkers of Osteoarthritis

Multiple studies have suggested that miRNAs may be useful as biomarkers for various bone pathologies (194). miRNAs can be recovered from the blood or other fluids to represent markers of skeletal disorders. There is potential for plasma levels of microRNAs to be used as biomarkers of OA disease as they exhibit good stability in circulation (117). Many studies have investigated this, including the identification of let-7e, miR-454 and miR-885-5p as potentially OA progression predictive. In this research, let-7e decreased in OA patient plasma compared with control (195).

In OA plasma, 12 microRNAs were identified in a different study to have levels statistically different compared with controls in two cohorts (164). Another study identified 70 differentially expressed microRNAs from 2578 in normal plasma compared to OA, with miR-19b-3p and miR-486-5p positive correlating with disease severity (196). Independent factors for the risk of knee OA were also identified as miR-19b-3p, miR-122-5p and miR-486-5p (196). In control plasma against OA, 2549 microRNAs were measured in a study and 279 identified as differentially expressed. After validation, potential biomarkers were identified as miR-140-3p, miR-33b-3p and miR-671-3p (197). In these studies, no microRNAs were validated across all data. This may be due to differences in methodologies and also patient groups or sample number (117). Specific circulating microRNAs have also been measured as potential biomarkers of OA (198–201).

1.6.4. Therapeutic use of microRNAs in Osteoarthritis

For miRNA mimics or inhibitors to be used therapeutically, they need to be taken up into the tissues of the joint successfully, for example the articular cartilage (117). The largest hurdle surrounding miRNAs as therapeutics is the delivery without systemic toxicity. To investigate this, most studies use miRNA-mimic/ inhibitor -expressing lentivirus by intraarticular injection in mouse models of OA. Although examining cartilage shows efficacy, it does not show if the microRNA has direct uptake in the cartilage. Instead, measuring confirmed miRNA targets within the cartilage tissue can be used. Lentivirus was used to deliver miR-128a into the joint, and uptake into chondrocytes was demonstrated by in situ hybridisation (ISH), in addition to miR-128a mimic increasing OA score (202).

In a similar experiment to this, another study delivered miR-483 lentivirus intraarticularly, using ISH and co-expressed GFP expression to indicate cartilage uptake in mid and deep zone chondrocytes (203). GFP-tag was also used to demonstrate virus penetration in a study of miR-101 adenoviral delivery in a rat OA model (204). It is unlikely that this procedure will be translated to man, since viral delivery to the mouse knee is associated with various risks, and there are non-viral systems of delivery being developed (117). An inhibitor of miR-483 has non-virally been delivered directly to the joint and still portrays functional outcome (203). This has also been achieved in the DMM model of OA, by intraarticular short antisense LNA oligonucleotide injection. This study showed a decrease in OA markers and histological OA improvement (205).

Particles produced by the majority of cells called exosomes can also be used to package microRNAs. This way, microRNAs can circulate in the bloodstream, with cells taking up the exosomes (206). Exosomes produced by hMSCs and transfected with miR-92a-3p have been used to inject intraarticularly into a OA mouse model, demonstrating miRNA expression in cartilage chondrocytes by ISH and a functional effect (207). Another example of this is the use of miR-140-5p transfected synovial MSC exosomes to intraarticularly inject into a rat model, showing decreased OA (208). These studies in

rodent models suggest that exosomes may be used for microRNA therapeutic delivery, although trials to the human joint are yet to be started (117).

Exosomal miRNAs have also been measured as biomarkers of OA, using the synovial fluid of OA patients compared to control. This showed that several miRNAs have differential levels in OA, and could help to understand OA disease pathogenesis and miRNAs as therapeutic targets (209). The function of miRNAs as therapeutic targets is particularly relevant with complex diseases due to the ability for targeting interactomes (210). It is important to optimise the stability and delivery efficiency of miRNAs to specific tissue, target, or cell population, considering the effects of an individual miRNA with several different targets (194).

1.7. microRNA-455

1.7.1. microRNA-455 expression in cartilage

microRNA-455 (miR-455) is a member of a broadly conserved family of non-coding RNA expressed in most of the phylum (211). The precursor sequence of miR-455 is present on the human chromosome 9 at locus 9q32 consisting of 96 base pairs (212). In humans the miR-455-3p strand (shown to be the guide strand on www.mirbase.org) is present in 2 isoforms, miR-455-3p.1 and miR-455-3p.2, which have a one nucleotide difference (211). Canonical miRNA targeting uses base pairing of the seed region, nucleotides 2-7 of the miRNA, to mRNA target sites in the 3'UTR (213). The miR-455 seed region is demonstrated as 5' CCUGGAC 3'.

The expression of miR-140 and miR-455 has been shown to increase in OA cartilage (180), these miRNAs are both located within introns of protein-coding genes (Wwp2 and Col27a1 respectively). The product of Col27a1 is a cartilage collagen, type XXVII collagen alpha 1 chain (214). The cartilage basis of the developing skeleton shows Col27a1 expression, particularly in the growth plate proliferative zone, and expression is also seen in the articular cartilage of adult mice (214–216). Smad2, activin receptor 2B and chordin-like 1 have been validated as miR-455-3p direct targets and demonstrate that miR-455 abrogates Smad-dependant signalling (180). It is suggested that a change in miR-455

expression would lead to altered TGF-activin A signalling through the Smad2/3 pathway, hypothesising a potential mechanistic link between OA pathology and miRNAs that regulate the Smad pathway (180). An important aspect in maintenance of articular cartilage is TGF signalling, as a decrease in TGF signalling through the Smad2/3 pathways results in OA changes within the joint (217). miR-455 could also possibly indirectly regulate Col27a1 expression, for example through effects on TGF signalling.

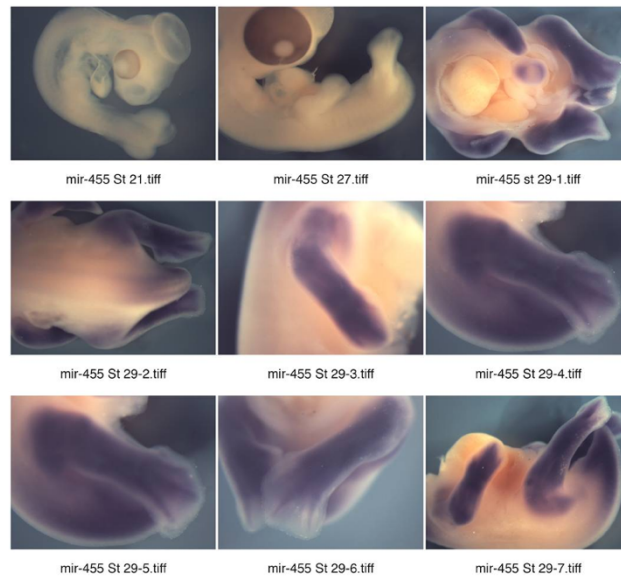
A whole-mount in situ hybridisation was performed and this showed expression of miR-455 in the developing long bones of chick, becoming more restricted to developing joints with time (Figure 1.11). This miR-455 expression was observed in the cartilage and perichondrium (180). There was also expression of miR-455 in muscle, supporting a study that showed miR-455 expression in myotubes following TWEAK (a proinflammatory cytokine) treatment (218). The expression in long bones and joints was also confirmed in a mouse embryo in situ hybridisation, observing miR-455 expression in developing skull sutures and in the interdigital region of the developing mouse paw. Where miR-455 is expressed, the developmental processes involve apoptosis within these tissues, and miR-455 may regulate this (180). During chondrogenesis in adult articular cartilage, miR-455 is expressed, and also has differential expression in OA. It has the potential to modulate cartilage homeostasis by altering TGF β signalling.

1.7.2. microRNA-455 null mouse model

The microRNA-455 null mouse model was created by Dr. Tracey Swingler in the Clark Lab at UEA. Previous targeted deletion of miR-455 in a mouse model resulted in a disruption to Col27a1 expression and a perinatal lethal phenotype. To avoid this disruption to Col27a1 and therefore perinatal lethal phenotype, the CRISPR Cas (Clustered Regularly Interspaced Short Palindromic Repeats and CRISPR associated (Cas)) genome editing technique was utilised to create miR-455 null mice. Oligonucleotides were designed against the miR-455 genomic sequence and mixed with Cas protein before pronuclear injection into one day single cell mouse embryos from the C57BL/6J mouse line (The Jackson Laboratory). Two cell embryos were then implanted into the mouse oviducts and off-spring genotyped for the absence of miR-455.

The phenotype of these miR-455 null mice is currently being investigated by Dr. Tracey Swingler within the Clark Lab at UEA (Figure 1.12).

A)



B)

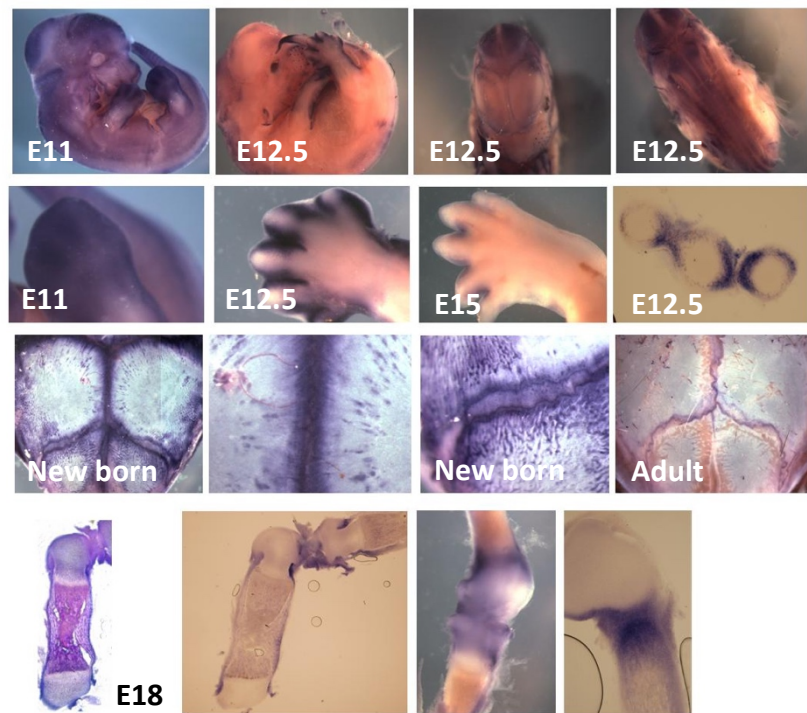


Figure 1.11: microRNA-455 expression in the developing embryo. A) Whole-mount ISH. Expression of miR-455 during chick embryo development demonstrates expression in developing limbs and perichondrium. Expression is detected from HH30 onwards. B) Mouse ISH. miR-455 expression visible in interdigital regions, developing joints, growth plates and perichondrium. Sections show staining in and around cartilage (180).

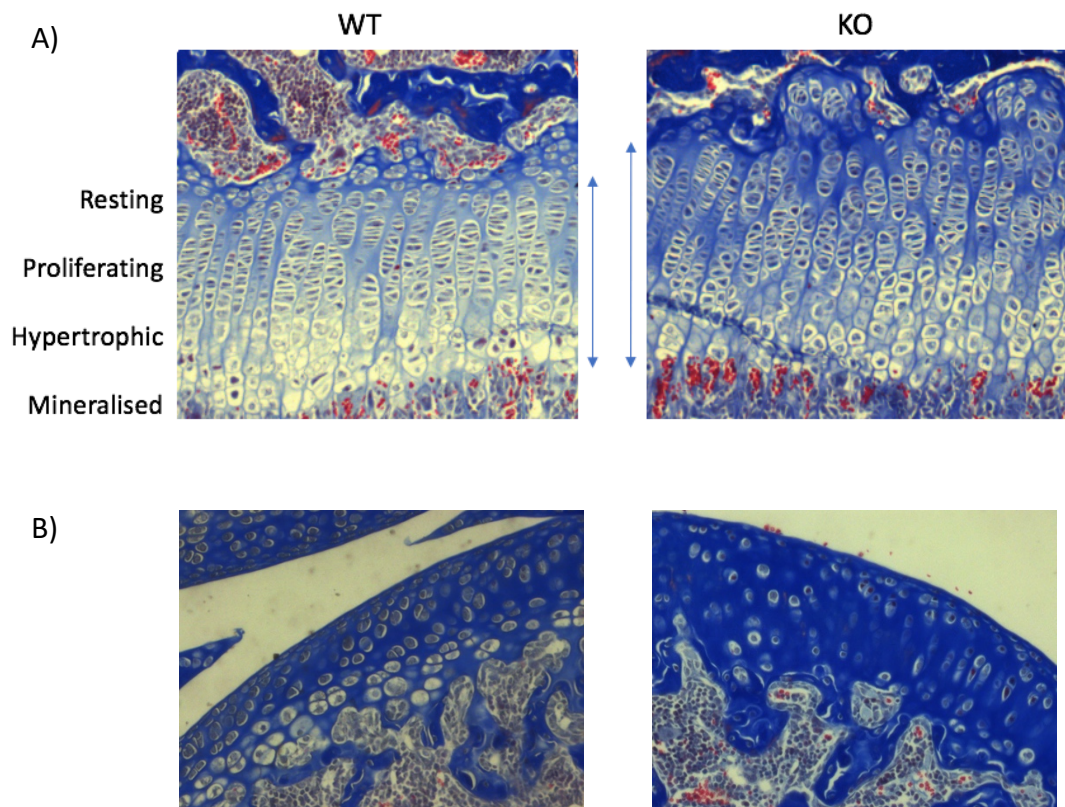


Figure 1.12: *microRNA-455 null mouse model. A) Growth plate Massons Trichome stain. The growth plate may be larger in miR-455 null growth plate, possibly more calcification (red) and increased matrix production. The proliferative zone could also be increase in miR-455 null. B) Articular cartilage Massons Trichome stain. Increased collagen (blue), increased calcification (red) and possibly hypo-cellular cartilage in deep zone.*

(Dr Tracey Swingler – unpublished data)

1.7.3. microRNA-455 during mesenchymal stem cell differentiation

In ATDC5 cells, miR-455-3p has been shown to function as an activator for early chondrogenic differentiation, directly targeting Runt-related transcription factor 2 (Runx2) to inhibit expression (137). A study demonstrated that miR-455-3p regulates DNMT3A expression, and *in vitro* DNMT3A modulates miR-455-3p expression (139). High DNMT3A expression levels were observed in miR-455-3p deletion mice, compared to low levels in wild-type mice. In miR-455-3p deletion mice, there was also a thinner cartilage thickness (139). In the same study, the degenerate process during chondrogenic differentiation was inhibited when overexpressing miR-455-3p, by regulating DNA methylation of cartilage development genes and pathways (139). It was previously found that during chondrogenic differentiation in human adipose-derived stem cells (hADSCs), there were high expression levels of miR-455-3p (219). It has also been demonstrated that miR-455-3p plays a role in the chondrogenic differentiation of hMSCs and in regulating OA (137,138,220). A recent paper has suggested that miR-455 knockout mice have an elevated expression of genes related to cartilage degeneration, and cartilage degeneration similar to OA was observed. This study also identified hypoxia inducible factor-2a (HIF-2a) as a direct target for miR-455, a catabolic factor for cartilage homeostasis. In addition to this, overexpression of miR-455 protected cartilage degeneration in a mouse OA model (221).

Chondrogenic differentiation in hMSCs may be regulated by miR-455-3p by targeting Runx2, HDAC2, and HDAC8, and miR-455-3p directly targets DNMT3A to downregulate expression (139). Between normal and OA cartilage, DNA has been shown to be differentially methylated (222), and the effect of DNA methylation in the pathophysiology of OA is becoming increasingly evident. The progression of OA is present with methylation changes to both catabolic and developmental associated genes in cartilage, for example MMP13, SOX9 and ADAMTS4 (223–225). DNA methylation is a crucial regulator of chondrocyte differentiation, where miR-455-3p and DNMT3 could modulate DNA methylation, coregulating chondrogenic differentiation of hMSCs (139). miR-455 may also regulate brown adipocyte differentiation and mitochondrial biogenesis (226).

1.7.4. microRNA-455 in disease

In addition to chondrogenic differentiation, recent studies have shown that many pathologies are regulated by miR-455. miR-455 has been implicated in various human cancers including colon cancer (227), prostate cancer (228,229), hepatocellular carcinoma (230), gastric cancer (231), pancreatic cancer (232), and non-small cell lung cancer (233). Within these studies, miR-455-3p acts as a tumour suppressor, influencing processes such as cell proliferation and apoptosis. Additional literature supports a role of miR-455 in cell proliferation, suggesting an importance during inflammation and extracellular matrix accumulation in diabetic nephropathy (234). A role of miR-455 in neurodegenerative diseases has also been investigated, revealing miR-455-3p as a potential biomarker and possible therapeutic target for Alzheimer's Disease (212).

Considering this, it is apparent that miR-455 may have a role in ageing and age-related pathologies. To support this, miR-455-3p has been demonstrated to be significantly deregulated in aged mice, and may play a functional role in muscle atrophy (235). miR-455 has also been implicated as an important component in the development and progression of multiple sclerosis disease (236). Data has revealed that miR-455-regulated signalling network may be a potential therapeutic target for human metabolic disorders (226).

1.8. Identification of microRNA target genes

1.8.1. microRNAs and their targets

As a multifactorial disease affecting the whole joint, OA has a complex pathogenesis involving different mechanisms and interactions between multiple tissues in the joint. To develop methods for diagnosis and treatment of OA, understanding this complex process is essential (69). An essential step in understanding the role of miRNAs as regulatory molecules is the identification of downstream miRNA targets (237). It is known that miRNAs target key signalling mediators in OA, such as Smad, NF κ B, WNT, and the TGF β signalling pathways. However, in chondrocytes, several miRNAs that are highly upregulated or downregulated in OA do not have identified and confirmed targets (94).

Many cellular processes can be controlled by miRNAs as they suppress specific target gene expression. In any cell type, one miRNA can affect many target genes, therefore altering multiple pathways (144).

miRNAs are significant in regulating skeletal development and homeostasis, demonstrated in thousands of published reports on miRNAs in the biology and disease of both cartilage and bone. During tissue development, disease, or cellular stress, an altered expression of miRNAs can impact on different cellular processes. For example, cell differentiation, metabolism, proliferation or apoptosis (144). At the post-transcriptional level, up to 60% of protein coding genes are regulated by miRNAs, despite miRNAs making up only 1-5% of the human genome (238). Since miRNAs have been shown to have significant regulating roles in biological pathways during normal development and metabolism, the role of aberrant miRNA expression in disease pathogenesis has become an increasingly interesting topic (239).

Studies have focussed on identifying changes in expression levels of miRNAs, either tissue-based or circulating, with the aim to identify potential diseases associated biomarkers or new disease mechanisms (144). There have been many miRNAs differentially expressed in human OA cartilage tissue or serum samples compared with control, it is important to now focus on the mechanisms and pathways in which these miRNAs are targeting. Regardless of whether the aim is to enhance tissue repair and regeneration or to attenuate disease, approaches should focus on determining miRNA function both *in vitro* and *in vivo* (144).

In recent epigenetic studies, many miRNAs have been identified to be involved in the pathogenesis of OA. These miRNAs may regulate expression by direct binding to anabolic or catabolic miRNAs at a post-transcriptional level to repress translation. It has also been indicated that miRNAs may regulate gene expression in OA at upstream levels, such as targeting signalling pathways or transcription factors, before their transcription (81). The future of miRNAs has great potential for OA diagnosis and therapeutic intervention biomarkers. A better understanding of how miRNA interactions impact on the pathology of OA will be important, as miRNAs can regulate the expression of several target genes.

For example, the overexpression or downregulation of a specific miRNA could provide a useful therapeutic approach (240). It is therefore extremely important to focus on identifying the specific miRNA target mRNA interactome, and the biological pathways these regulate.

1.8.2. Methods for identifying microRNA targets

To completely understand the function of miRNAs, it is important to identify real miRNA targets. This section describes techniques currently developed to study miRNAs and their targets. There are many *in silico* approaches available as miRNA target prediction programmes based on assumptive miRNA target recognition (241). These bioinformatic approaches are based on the assumption that target recognition requires conserved pairing to the miRNA seed region (237). Another approach for identifying miRNA targets is miR-CLIP (miRNA UV crosslinking and immunoprecipitation), where, to identify miRNA targets, a bioinformatic approach can be combined with high throughput CLIP data (245).

In the post-transcriptional regulation of gene expression, RNA-binding proteins (RBPs) play an important role. The position of binding sites of RBPs enables a greater understanding of molecular level transcript regulation (246). These interactions between protein and RNA can be studied using CLIP on a genome-wide scale when combined with high-throughput sequencing such as HITS-CLIP (highthroughput sequencing of RNA isolated by CLIP) or CLIP-seq (247). The development of individual-nucleotide resolution UV crosslinking and immunoprecipitation (iCLIP) has enabled the identification of protein-RNA crosslink sites on a genome wide scale (248).

As described, miRNAs guide Argonaute (AGO) proteins to specific target sites within their target mRNAs to regulate biological processes (249). The miRNA-mRNA base pairing occurs mainly in the 'seed region' spanning nucleotides 2-8 of the 21-22 nucleotide miRNA (250). There have been many miRNA targets identified through bioinformatic analysis, however false-positive and -negative rates are high. An empirical method to identify miRNA target sites is Ago HITS-CLIP, which, *in vivo*, maps the global transcriptome of Ago:miRNA:mRNA 'ternary' complexes. The complex between Argonaute proteins,

miRNAs and their target transcripts has been studied using HITS-CLIP (251). From this data, the direct pairing of a miRNA and target mRNA cannot be deduced. However, both miRNA and mRNA Argonaute direct binding sites were detected, and this enables endogenous mRNA target sites to be discovered (252).

The standard HITS-CLIP protocol has minor modifications to accommodate the association of Ago with the two RNA species (miRNAs and target mRNAs) (250). The high-throughput sequencing of RNAs crosslinked to Argonaute proteins can reveal miRNA binding sites and miRNA targets (242). miRNA targets were also studied using Argonaute CLIP-Seq, where the miRNA targetome was shown to be diverse across different cell types (253). In order to identify endogenous miRNA-target sites, iCLIP has also been used in *C. elegans* by isolating AGO-bound RNAs, which produced miRNA-target chimeras that identify miRNA targets (106). To increase the resolution of RNA-protein binding to a near nucleotide level, various methods of CLIP have been developed, allowing specific binding sites to be identified (254). New CLIP methods, such as irCLIP (255) and eCLIP (256), have also been developed, improving efficiency through combination of iCLIP with optimization at many steps. Protocols that amplify cDNAs include iCLIP, eCLIP, and irCLIP, and ensure protein-RNA crosslink sites are identified across the transcriptome (257).

In addition to this, the CLASH technique was derived from a modified version of CLIP called CRAC (UV crosslinking and analysis of cDNAs (258). The identification of RNA-RNA interactions without bioinformatic predictions by CLASH can be applied to the miRNA interactome (259). To identify novel miRNA targets, AGOCLASH is the method used, revealing miRNA-mRNA interactions bound by AGO proteins (260). However, CLASH and similar protocols using RNA ligation to capture miRNA-mRNA interactions have a low ligation efficiency, suggesting that many interactions are uncaptured (249). Another method for detecting microRNA-target interactions is Chimera PCR (ChimP). This protocol enables the analysis of miRNA targeting in different conditions, thereby validating or testing specific miRNA-target interactions (261). Understanding miRNA function and mRNA interactions is also commonly studied using the luciferase reporter gene assay (262). The firefly luciferase assay has been adapted to explore the target gene effect of miRNA-mediated post-transcriptional regulation (262). In order to identify miRNA targets

in the future, it is important to modify the efficiency of these protocols and therefore enable the study of miRNA interactions in different physiological conditions and compare the targets of miRNA family members.

1.8.3. CRISPR/Cas genome editing and microRNAs

1.8.3.1. CRISPR/Cas9 gene editing system

In a variety of fields, genome editing has enabled the generation of more accurate cellular and animal models of pathological processes (263). Clustered regularly interspaced short palindromic repeats (CRISPR)- Cas associated nucleases are efficient for genome engineering in eukaryotic cell lines and to generate genetically modified (GM) animals, progressing gene editing from concept to clinic (264).

CRISPR/Cas9 is a gene editing platform derived from a bacterial adaptive immune defence system (265). The development of CRISPR/Cas9 technology enables an easy and effective gene editing system (Figure 1.13). Within CRISPR/Cas9, an engineered single guide RNA (sgRNA) and a Cas9 endonuclease form a complex which recognises a target DNA sequence. A double-stranded break in genomic DNA is introduced which is subject to DNA repair (266). Within the sgRNA, there is often a unique 20bp sequence, complementary to the target DNA site and followed by a PAM (protospacer adjacent motif) of “NGG” or “NAG” upstream (267). The PAM is a short DNA sequence which is essential for Cas9 protein compatibility (263). A sgRNA will bind to its target sequence, where the Cas9 will precisely cleave the DNA to generate a double-stranded break (DSB) (268). Following this, genome repair is initiated by DNA-DSB repair mechanisms. There are two DNA repair mechanisms used with the CRISPR/Cas9 system: error-prone non-homologous end joining (NHEJ) and error-proof homology-directed repair (HDR) (269).

CRISPR/Cas9 technology was first applied in mammalian cells as a tool to edit the genome in 2013 (266,270), and since then its uses have been expanded from genomic sequence alteration or correction, to epigenetic and transcriptional modifications (263). There are three developed strategies for CRISPR/Cas9 genome editing: plasmid-bases, whereby a

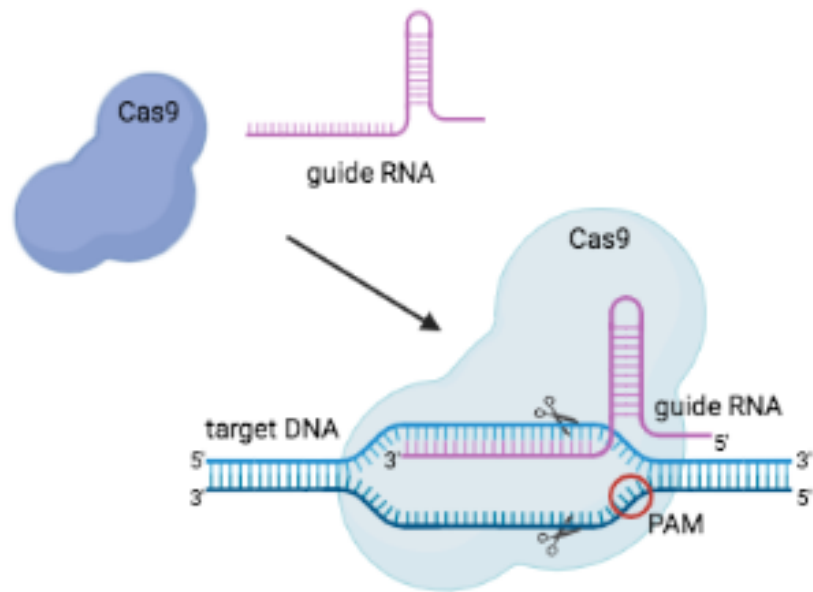


Figure 1.13: CRISPR/Cas9 system schematic. Site-specific DNA cleavage by the nuclease Cas9 directed by complementary between guide RNA and target sequences. On the opposite strand is a protospacer-adjacent motif (PAM). The double-stranded breaks (DSBs) are repaired by either nonhomologous end-joining (NHEJ) or by homology-directed repair (HDR).

plasmid is used to encode sgRNA and Cas9 protein (266); direct Cas9 mRNA and sgRNA intracellular delivery (271); and the direct sgRNA and Cas9 protein delivery (272).

Although double-stranded DNAs have been most commonly used in the past as donor templates for CRISPR/Cas9 genome engineering (273), ssDNA or single-stranded donor oligonucleotides (ssODNs) show a greater performance in mammalian systems (264). ssODNs allow shorter homology arms and provide higher insertion efficiencies in comparison to dsDNA templates, becoming the preferred template for HDR applications (274). An example of this method is the use of ssODN-mediated in-frame deletion with CRISPR/Cas9 methodology in patient-derived iPSCs for research (275). Using optimized ssODNs also improves the efficiency of CRISPR 'knock-in' methods (276). Each individual genome editing experiment using the CRISPR/Cas system requires well-researched design parameters (277).

As previously discussed, microRNAs play a key role in gene expression regulation, impacting development and disease. The CRISPR/Cas9 system has been shown to robustly reduce specific mature miRNA expression, maintaining this in both *in vitro* and *in vivo* models (278), providing an excellent strategy to modify miRNA expression. The over or under expression of miRNAs during development can result in organ system defects, and with CRISPR/Cas9 technology each individual miRNA function can be studied (279). For example, specific CRISPR knockouts of individual miRNAs were performed in embryonic mouse stem cells to study cardiac differentiation (279). A CRISPR/Cas9-mediated *in vivo* system was also developed to knockout miRNAs in a genetically engineered mouse model to study lung tumorigenesis (280). The knock-out of specific miRNAs, both conditional and complete knockout, can reveal downstream effects on cellular functions and phenotype (281).

In regard to skeletal development and pathologies, CRISPR systems are used extensively in musculoskeletal research, with potential for clinical therapies and treatments in orthopaedic practice (282). These applications in orthopaedic disease include both 'knock-out' and 'knock-in' cell and vertebrate animal models, where novel adaptations are enhancing the use of CRISPR (282). An example of CRISPR/Cas9-based gene editing for

investigating OA therapies was the study performing intra-articular injection in an induced OA mouse model (282). From this, CRISPR-mediated ablation of NGF was found to alleviate OA pain, and deleting IL-1 β or MMP-13 reduces structural damage (282). This suggests that gene editing by CRISPR-based methods may be useful to identify drug targets, treatments and therapeutic strategies for OA (282).

1.8.4. *microRNAs and the future*

To completely understand the cellular networks regulated by miRNAs, it is essential to identify their endogenous targets *in vitro* and *in vivo* (283). This knowledge will be important to anticipate the many consequences of miRNA function and manipulation for therapeutic intervention. To fully exploit miRNA therapeutic potential, both gain- and loss- of function strategies are needed. Recently, approaches to deliver oligonucleotides that either mimic or inhibit miRNA expression are being explored, providing a basis for tissue specific delivery systems (284). This may include miRNA-targeting oligonucleotide delivery by liposome-encapsulating or nanoparticle- associated delivery, administered through intravenous or subcutaneous routes (285).

Preclinical and clinical applications of small RNAs are expanding alongside studies of miRNAs. There are increasing reports suggesting a use for miRNAs as modulators of drug resistance, biomarkers for pathogenic conditions, and as medical intervention drugs for most human health conditions (286). The diverse effects that arise from miRNA regulation make them attractive drug targets, particularly for diseases with multifactorial aetiology and no current effective treatment (286). Currently, miRNA therapies are progressing through clinical trial phases, with the potential for both diagnostic and interventional medicine in the future (286). To support miRNAs as future therapeutics, small molecule drugs have already been successfully designed pharmacologically in order to pleiotropically target pathways or multiple targets (287,288). This will enable the study of miRNA to expand, with therapeutics focussing on epigenetic targets (286). It is important to understand how biological processes are modulated by miRNAs outside of their canonical function, and which mRNA targets they regulate, in order to advance the clinical development of miRNA treatments in the future.

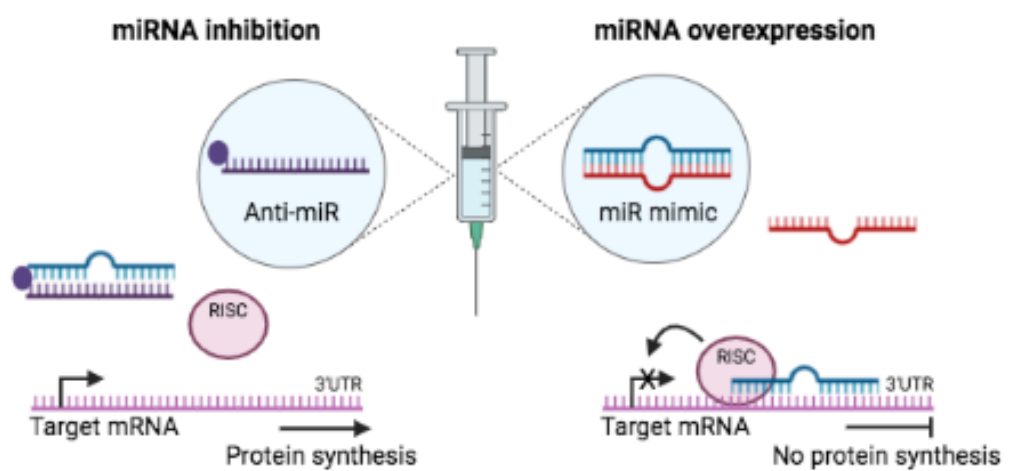


Figure 1.14: The future of microRNAs. miRNAs have a huge potential for therapeutic applications in the future. Approaches to deliver ‘anti-miRs’ and ‘miR mimics’ are being explored, aiming to either inhibit (left) or overexpress (right) specific miRNAs in disease phenotypes.

1.9. Hypothesis and Aims

This thesis aims to explore the role of microRNA-455 during skeletal development and cartilage tissue. The hypothesis is that altering miR-455 expression disrupts skeletal development and impacts the cartilage gene expression profile. By identifying the genes regulated by miR-455, this will increase understanding on the mechanisms involved in skeletal development, and findings can be implemented in the treatment of disease.

The following aims will be addressed throughout this thesis:

- To explore the role of miR-455 during hMSC differentiation using Osteogenesis and Chondrogenesis assays and overexpressing or inhibiting miR-455 before measuring gene expression by qPCR.
- To analyse the gene expression profile of miR-455 null mouse adult cartilage from knee joints using mRNA-seq.
- To evaluate the gene expression profile of the SW1353 Chondrosarcoma cell line following overexpression and inhibition of miR-455 by mRNA-seq analysis.
- To explore the role of miR-455 during chick limb bud development by mRNA-seq following microinjection of either miR-455 mimic or antagomir.
- Identify potential novel miR-455 targets using CRISPR/ Cas-mediated HDR.

Chapter 2

Materials & methods

2. MATERIALS & METHODS

2.1. microRNA-455 during MSC differentiation

2.1.1. Cell lines and cell culture

2.1.1.1. Mesenchymal stem cells

The Mesenchymal Stem Cells (MSCs) are isolated from human bone marrow. MSCs are maintained in MSCGMTM Mesenchymal Stem Cell Growth Medium (Lonza) at 37°C in 5% (v/v) CO₂, changing the Lonza MSCGMTM every 5 days. MSC lines from 3 donors 2454e, 2802f, and 071508a were used.

2.1.2. Transfection using Lipofectamine 3000

The MSCs were plated in 96-well plates. For adipogenesis and osteogenesis 100µL cells/well were plated at a density of 5×10^4 cells/mL in a flat-bottom 96-well plate and for chondrogenesis 100 µL cells/well were plated at a density of 6.7×10^6 cells/mL in a U-bottom 96-well plate and grown for 24 hours (80-90% confluence). A 96-well plate was used for each time-point. For the mock transfection, miR-455 mimic and cel-mir-39, 6µL (adipogenesis and osteogenesis) or 9µL (chondrogenesis) were prepared in 200µL Opti-MEMTM Medium (Gibco, USA). For each condition, 8µL Lipofectamine™ 3000 (Invitrogen, USA) was diluted in 200µL Opti-MEMTM Medium. These were mixed together and incubated for 10-15 minutes at room temperature. Following this, 10µl were added to each well. The transfected cells were incubated for 3 days at 37°C in 5% CO₂.

Table 2.1: miRCURY LNA miRNA (Qiagen) products.

| Product name | Sequence 5' to 3' |
|-----------------------------|------------------------|
| hsa-miR-455-3p | AGAUCAGAAGGUGACUGUGGCU |
| Negative Control Cel-miR-39 | UCACCGGGUGUAAAUCAGCUUG |
| hsa-miR-455-3p | TGTATATGCCCATGGACTGC |
| Negative Control A | TAACACGTCTATACGCCCA |

2.1.3. MSC differentiation

2.1.3.1. Adipogenesis

Following transfection, MSC adipogenesis was induced. The media was replaced with 100 μ L adipogenic culture medium (Table 2.2) and incubated for 3 days. The adipogenic culture medium was then replaced with adipogenic maintenance medium and incubated for 4 days. This cycle was repeated twice within 14 days. Adipogenesis time points were Days 0, 3, 7, 10, and 14.

Table 2.2: Adipogenic culture medium and adipogenic maintenance medium final concentration and volume.

| | Final concentration | Volume |
|---|----------------------------|---------------|
| Adipogenic culture medium | | |
| DMEM (high glucose) +1%P/S + Sodium Pyruvate | | 21.9mL |
| 10% FBS | | 2.5mL |
| Dexamethasone | 1 μ M | 250.0 μ L |
| Insulin | 10 μ g/mL | 25.0 μ L |
| IBMX methyl-isobutylxanthine | 500 μ M | 250.0 μ L |
| Indomethacin | 60 μ M | 15.0 μ L |
| Rosiglitazone | 2 μ M | 5.0 μ L |
| IGF-1 | 20nM | 25.0 μ L |
| Adipogenic maintenance medium | | |
| DMEM (high glucose) +1%P/S + Sodium Pyruvate | | 22.5mL |
| 10% FBS | | 2.5mL |
| Insulin | 10 μ g/mL | 25.0 μ L |

2.1.3.2. Chondrogenesis

To induce MSC chondrogenesis, the media was replaced with 100µL chondrogenic culture medium (Table 2.3) and replaced every 3 days for 14 days. Chondrogenesis time points were Days 0, 3, 7, 10, and 14.

Table 2.3: Chondrogenic culture medium final concentration and volume.

| | Final concentration | Volume |
|---|---------------------|---------|
| Chondrogenic culture medium | | |
| DMEM (high glucose) +1%P/S + Sodium Pyruvate | | 48.4mL |
| TGF-β3 | 10ng/mL | 50.0µL |
| Dexamethasone | 100nM | 50.0µL |
| ITS+L premix | 1x | 500.0µL |
| L-ascorbic acid-2-phosphate | 50µg/mL | 500.0µL |
| Proline | 40µg/mL | 500.0µL |

2.1.3.3. Osteogenesis

MSC osteogenesis was induced by replacing the Lonza media with OsteoMAX-XF (Sigma-Aldrich) containing 90mL OsteoMAX-XF Basal Medium and 10mL 10x OsteoMAX-XF supplement, and replaced every 3 days. Osteogenesis time points were Days 0, 1, 2, 3, and 4 for miRNA and mRNA analysis, with the addition of Day 5 for Alizarin red staining.

2.1.4. Quantitative Real Time Polymerase Chain Reaction (RT-qPCR)

2.1.4.1. Cells to cDNA

The medium was removed from the 96-well plate and cells washed twice with DPBS (Gibco, USA). Following this, 30µL Cells-to-cDNA cell lysis buffer (Ambion, USA) was added to each well and the lysates were transferred to a 96-well PCR plate. The PCR plate was then incubated for 15 minutes at 75°C to inactivate RNases. After cooling to room temperature, 1µL DNase I and 3µL DNase I Buffer (10X) were added to each well in order to remove genomic DNA contaminants. The 96-well plate was then incubated for 15

minutes at 37°C followed by 5 minutes at 75°C. From the DNase-treated samples, 8µL were transferred into a new 96-well PCR plate and 1µL random primers (Invitrogen, USA) and 3µL of 10mM dNTP mix (Bioline, UK) were added. To initiate priming, the PCR plate was incubated for 5 minutes at 70°C and then chilled on ice. To each well, a mixture was added containing 4µL First strand buffer (5x) (Invitrogen, USA), 2µL 0.1M dithiothreitol (DTT) (Invitrogen, USA), 1µL ddH₂O (Sigma, W4502), 0.5µL Moloney Murine Leukemia Virus (M-MLV) reverse transcriptase, and 1µL Rnasin ribonuclease inhibitor (40 units/µL) (Promega, USA). The samples were incubated for 50 minutes at 37°C, followed by 15 minutes at 75°C. After adding 30µL nuclease-free water, samples were stored at -20°C.

2.1.4.2. miRCURY LNA miRNA PCR

For highly sensitive Real Time PCR detection of miRNA levels, the miRCURY LNA miRNA PCR Kit (Qiagen) was used. From all timepoints, 2 µl of differentiation RNA samples were added to 96 well PCR plate with wells containing 2µl 5x miRCURY RT Reaction Buffer (Qiagen), 1µl 10x miRCURY RT Enzyme Mix (Qiagen), and 5µl RNase-free H₂O. The total volume of 10µl was incubated at 42°C for 60 minutes and 95°C for 5 minutes. The cDNA was diluted 1/80 and stored at -20°C.

2.1.4.3. Taqman Real Time PCR mRNA

For the RT-qPCR reactions, MicroAmp optical 96-well plates (Applied Biosystem, USA) were used. For analysis of mRNA, primers were designed using the Universal ProbeLibrary System Assay Design and ordered from Qiagen. Following the cells-to-cDNA protocol, each well contained 5µl cDNA templates, with reagent quantities shown in Table 2.4 total volume 25µl. The plates were sealed with adhesive cover film and qPCR was performed on an ABI 7500 real-time PCR system (Applied Biosystems), with cycle conditions set at 50°C for 2 minutes and 95°C for 10 minutes, followed by 95°C for 15 seconds and 60°C for 1 minute for 40 cycles.

Table 2.4: Taqman qPCR reagents and volumes.

| Reagent | 18S | Gene of interest |
|--|---------|------------------|
| 2x qPCRBIO Probe Mix Lo-ROX (PCR Biosystems) | 8.33µl | 8.33µl |
| Forward Primer (10µM) | 0.5µl | 0.5µl |
| Reverse Primer (10µM) | 0.5µl | 0.5µl |
| Probe (Roche) | 0.5µl | 0.25µl |
| ddH ₂ O | 10.17µl | 10.42µl |

2.1.4.4. SYBR Green Real Time PCR miRNA

The U6 snRNA miRCURY LNA miRNA PCR Assay (Qiagen) primer set was used as a reference gene, and miR-455-3p miRCURY LNA miRNA PCR Assay (Qiagen) to target mature miRNA, both containing forward and reverse primers. MicroAmp optical 96-well plates (Applied Biosystems, USA) were used and each well contained 4µl cDNA from the miRCURY LNA miRNA PCR reaction, with reagent quantities shown in Table 2.5, total volume 10µl. The plates were sealed with adhesive cover film and qPCR was performed on an ABI 7500 real-time PCR system (Applied Biosystems), with cycle conditions set at 95°C for 30 seconds followed by and 95°C for 10 seconds, 58°C for 15 seconds and 72°C for 10 seconds for 40 cycles.

Table 2.5: SYBR green qPCR reagents and volumes for detecting microRNA.

| Reagent | U6 | miR-455-3p |
|--|--------|------------|
| SYBR Green I (Sigma-Aldrich) | 0.18µl | 0.18µl |
| 2x qPCRBIO Probe Mix Lo-ROX (PCR Biosystems) | 5µl | 5µl |
| PCR Primer Mix (Qiagen) | 1µl | 1µl |

2.1.4.5. Statistical analysis

Statistical analysis was performed using Microsoft Excel 2019. Expression levels of mRNA were normalised to the housekeeping reference gene. The $2^{-\Delta\Delta CT}$ method was applied for comparative RT-qPCR analysis. Prism 8 was used to present data as mean \pm standard error for independent experimental repeats. Statistical p-values from unpaired t-tests were created in Prism 8.

2.1.5. Cell staining

2.1.5.1. Alizarin Red staining

Alizarin Red staining was used to stain osteocytes containing calcium in differentiated human mesenchymal stem cells. To prepare the reagents, 40nM Alizarin Red Solution at pH 4.2 was dissolved overnight before passing through a 0.2 μ M filter and 10% cetylpyridinium in 10nM sodium pyruvate buffer was prepared at pH7. The MSCs were incubated with 40nM Alizarin Red solution for 30 minutes at room temperature. Following this, the cells were washed thoroughly with 100 μ l ddH₂O and imaged using AxioVision Digital Imaging Software.

The dye was eluted with 50 μ l cetylpyridinium (10%), and once solubilized the stain was transferred to a 96-well plate. The absorbance was measured at 620nM using the Wallac Envision programme. Data was analysed using Microsoft Excel 2019.

2.2. Mouse cartilage microRNA-455 knockout

2.2.1. Mouse WT and KO lines

The miR-455 null mouse model was used, as described in 1.7.2. The C57BL/6J mouse line was used as wild-type control (The Jackson Laboratory).

2.2.2. Cartilage microdissection

To analyse gene expression in articular cartilage knee joint tissue between wild-type and miR-455 knockout mice, knee cartilage microdissection was performed. The cartilage

microdissection protocol was adapted from Gardiner et al (2014) supplementary file; microdissection of knee joint tissues (289), as previously described (290). Joints were dissected from the hind limbs. The skin and musculature were removed before separating the joint by dividing the collateral and cruciate ligaments and removing the menisci. Under a microscope, the cartilage was dissected using a disposable sterile scalpel no.15 (Swann-Morton, UK). Cartilage was collected from both the tibia and femur of the joint in RNAlater (Invitrogen), snap frozen in liquid nitrogen and stored at -80°C.

2.2.3. Cell lines and cell culture

2.2.3.1. SW1353 cell line

The SW1353 cell line is derived from human chondrosarcoma of the humerus. SW1353 cells are maintained in DMEM, high glucose, GlutaMAX™ supplement (Gibco, USA), containing 10% (v/v) heat-inactivated fetal bovine serum (FCS) (Gibco, USA), 100U/ml penicillin, and 100µg/ml streptomycin (Sigma-Aldrich, USA) at 37°C in 5% (v/v) CO₂.

2.2.4. Lipofectamine 3000 transfection

SW1353 cells were plated in 6-well plates at a density of 1.5×10^5 cells/mL and grown for 24 hours (80-90% confluence). A 6-well plate was used for each condition. For miR-455 mimic, mimic control, miR-455 inhibitor, and inhibitor control, 1.5µl were prepared in 100µl Opti-MEM™ Medium (Gibco, USA) for an optimum concentration of 50nM. For each well, 3.75µl Lipofectamine™ 3000 (Invitrogen, USA) was diluted in 100µl Opti-MEM™ Medium (Gibco, USA). The two were then mixed together and incubated for 10-15 minutes at room temperature. Following this, 200µl were added to each well. The transfected cells were incubated for 48 hours at 37°C in 5% CO₂.

2.2.5. Total RNA isolation from cultured cells

2.2.5.1. Trizol RNA extraction

RNA was extracted from the SW1353 cell line after transfection with miR-455 mimic, mimic control, miR-455 inhibitor, and inhibitor control in a 6-well plate. To each well, 500µl of Trizol/TriReagent (1ml Trizol per 50-100mg) was added and mixed before

transferring to a 2ml Eppendorf tube on ice (2 wells of the same condition per tube). Tubes were centrifuged at 4°C at 13000rpm for 5 minutes. The supernatant was transferred to a new 2ml Eppendorf tube and left at RT for 5 minutes. To each tube, 300µl of chloroform (300µl in 1.5ml or 200µl in 1ml) was added and vortexed. The tubes were then left at RT for 2 minutes and centrifuged at 4°C for 15 minutes at 13000rpm. On ice, 750µl RNase-free isopropanol was added to new 1.5ml Eppendorf tubes. The aqueous phase (approximately 750µl) was also added to the isopropanol tubes and vortexed. The tubes were placed at -20°C overnight. Following this, the tubes were centrifuged at 4°C for 10 minutes at 13000rpm, producing an RNA pellet. On ice, the isopropanol was removed, 1ml 80% EtOH added, and centrifuged at 4°C for 1 minute at 13000rpm. The 80% EtOH wash was then repeated and EtOH removed. The pellet was left on ice to air dry for 10 minutes. The RNA was resuspended in 30µl RNase-free H₂O and the RNA Nanodrop was used to quantify RNA concentrations.

2.2.5.2. TURBO DNase treatment

To DNase treat the RNA, the TURBO DNA-free Kit (Ambion) was used. To the RNA, 0.1 volume of 10x TURBO DNase Buffer (Ambion) and 1µl TURBO DNase Enzyme (Ambion) was added and incubated at 37°C for 20-30 minutes. A 0.1 volume of DNase Inactivation Reagent was then added and incubated at room temperature for 5 minutes. The RNA was transferred to a clean Eppendorf after centrifuging the samples at 10000xg for 1.5 minutes. RNA stored at -80°C.

2.2.5.3. Qiagen RNeasy Mini kit

RNA was extracted from the SW1353 cell line after transfection with miR-455 mimic, mimic control, miR- 455 inhibitor, and inhibitor control in a 6-well plate, according to the Qiagen RNeasy Mini Kit. To each well, 350µl buffer RLT was added to lyse the cells and transferred to an Eppendorf before vortexing. To the lysate, 1 volume 70% ethanol was added and mixed well before transferring to a RNeasy Mini spin column in a 2ml collection tube and centrifuged for 15 seconds at 8000xg. The column was then washed with 350µl buffer RW1. For DNase digestion, a volume of 80µl DNase I incubation mix (10µl DNase I + 70µl buffer RDD) was added to the column membrane and incubated for 15 mins at 20-30°C. The column was then washed with 350µl buffer RW1, followed by 2

500µl buffer RPE washes. In a 1.5ml collection tube, the RNA was eluted in 30µl RNase-free water. The RNA Nanodrop was used to quantify RNA concentrations and determine 260/280 and 260/230 ratios.

2.2.6. Total RNA extraction from cartilage tissue

2.2.6.1. Mouse articular cartilage

The cartilage from 2 mouse knee joints were microdissected and pooled. The cartilage was ground to a fine powder under liquid nitrogen. Trizol was added immediately to the ground cartilage (1mL/100mg cartilage), mixed and incubated on ice for 5 minutes. The ground cartilage was centrifuged at 4°C for 10 minutes at 9500g and supernatant recovered. To ensure the dissociation of nucleoproteins, the supernatant was incubated at room temperature for 5 minutes. Following this, 200µl chloroform per mL Trizol was added, vortexed and incubated at room temperature for 2 minutes. The Trizol/chloroform mixture was centrifuged at 4°C for 15 minutes at 12000g. The aqueous layer was recovered into an ice-cold RNase free 1.5mL Eppendorf tube.

2.2.6.2. mirVana™ miRNA Isolation kit

Total RNA was isolated from the cartilage according to the mirVana™ miRNA Isolation Kit, Total RNA Isolation Procedure. To the aqueous phase, 1.25 volumes of 100% ethanol was added, and this lysate/ ethanol mixture was passed through a filter cartridge by centrifuging for 15 seconds at 10000xg. The filter was then washed with 700µl miRNA wash solution 1 followed by 2 washes with 500µl miRNA wash solution 2/3. The RNA was eluted in 50µL RNase-free water and stored at -80°C. The RNA Nanodrop was used to quantify RNA concentrations and determine 260/280 and 260/230 ratios.

2.2.7. Electrophoresis for RNA integrity

2.2.7.1. Gel electrophoresis

To check RNA integrity before gene expression analysis, agarose gel electrophoresis was used on RNA samples with high concentration. A 1.5% agarose gel was prepared (2.25g agarose in 150ml 0.5xTBE, add 15µl EtBr). For each sample, 1µl of RNA and 5µl Ambion

gel loading buffer II (8546G) were loaded. The gel was run at 100V for 30 minutes and then imaged. The 28S and 18S bands should be visible in a 2:1 ratio (28S:18S) for good quality RNA.

2.2.7.2. Bio-Rad Experion Automated Electrophoresis system

To assess RNA integrity from samples with lower concentrations, the Experion RNA StdSens Analysis Kit (Bio-Rad) was used. Before use, electrodes were cleaned, and gel stain prepared. The RNA StdSens chip was primed on the Experion Priming Station (Bio-Rad) after addition of 9µl gel-stain to the gel priming well (GS) and priming station set to pressure setting B and time setting 1. The RNA StdSens chip was then loaded with 5µl RNA loading buffer into each sample well 1-12 followed by 1µl sample per well. To the second GS well, 9µl gel-stain was added, 9µl filtered gel into well G, and 5µl RNA loading buffer with 1µl RNA ladder into well L. The chip was then vortexed using the Experion Vortex Station II (Bio-Rad) before being placed in the Experion Automated Electrophoresis Station (Bio-Rad). The Experion Software (Bio-Rad) was used to create a new RNA StdSens eukaryotic total RNA run.

2.2.8. Quantitative Real Time Polymerase Chain Reaction (RT-qPCR)

2.2.8.1. SuperScript II Reverse Transcription

Following RNA extraction, cDNA was synthesised using SuperScript II reverse transcriptase (Invitrogen, USA). In a 96 well PCR plate, 1µg RNA from SW1353 cells was diluted in 9µg H₂O, and 100ng RNA from mouse articular cartilage was diluted in 9µl H₂O. To each well, 2µl random primers (Invitrogen, USA) were added and incubated at 70°C for 10 minutes. On ice, 9µl master mix was added, containing 1µl SuperScript II reverse transcriptase (Invitrogen, USA), 4µl First Strand Buffer (5X) (Invitrogen, USA), 2µl 0.1M DTT (Invitrogen, USA), 1µl 10mM dNTP mix (Biolone, UK), and 1µl RNasin Ribonuclease Inhibitor (Promega, USA). The plate was then incubated at 42°C for 60 minutes, followed by 70°C for 10 minutes. The cDNA from SW1353 cells was diluted 1/100, and cDNA from mouse articular cartilage was diluted 10/100, and stored at -20°C.

2.2.8.2. miRCURY LNA miRNA PCR

For highly sensitive Real Time PCR detection of miRNA levels, the miRCURY LNA miRNA PCR Kit (Qiagen) was used. RNA extracted from SW1353 cells and mouse articular cartilage was diluted 5ng/ μ l and 2 μ l was added to 96 well PCR plate with wells containing 2 μ l 5x miRCURY RT Reaction Buffer (Qiagen), 1 μ l 10x miRCURY RT Enzyme Mix (Qiagen), and 5 μ l RNase-free H₂O. The total volume of 10 μ l was incubated at 42°C for 60 minutes and 95°C for 5 minutes. The cDNA was diluted 1/40 and stored at -20°C.

2.2.8.3. Taqman Real Time PCR mRNA

For the Taqman Real Time PCR (qPCR) reactions, MicroAmp optical 96-well plates (Applied Biosystems, USA) were used. For analysis of mRNA, primers were designed using the Universal ProbeLibrary System Assay Design tool, and Oligos ordered from Sigma-Aldrich. The reference gene used was 18S. Each well contained 10 μ l cDNA (1ng) from the SSII RT reaction, with reagent quantities shown in Table 2.4 loaded per well, total volume 25 μ l. The plates were sealed with adhesive cover film and qPCR was performed on an ABI 7500 real-time PCR system (Applied Biosystems), with cycle conditions set at 50°C for 2 minutes and 95°C for 10 minutes, followed by 95°C for 15 seconds and 60°C for 1 minute for 40 cycles.

2.2.8.4. SYBR Green Real Time PCR miRNA

The U6 snRNA miRCURY LNA miRNA PCR Assay (Qiagen) primer set was used as a reference gene, and miR-455-3p miRCURY LNA miRNA PCR Assay (Qiagen) to target mature miRNA, as described above in 1.1.4.4.

2.2.8.5. Statistical analysis

Statistical analysis was performed using as described above in 2.1.4.5.

2.2.9. mRNA-seq Novogene & Bioinformatic analysis

Eukaryotic transcriptome libraries were created by Novogene using the Illumina NovaSeq platform (PE150), HiSeq system (Paired-end 150).

Bioinformatic analysis was performed with the assistance of Prof. Simon Moxon at UEA. To check the quality of reads, FASTQC was run followed by TrimGalore to trim adapter sequences and low quality reads. Transcripts were obtained from Ensembl and Kallisto was used to map reads (pseudalignment) to all transcripts. To identify differential expression between different conditions, Sleuth was run (R tool). This analysis produced a table of normalised counts, fold changes and p-values for differentially expressed genes, and a PCA plot to show how the samples cluster. Following this analysis, the data sets were used to explore differentially expressed (DE) gene expression across samples. Gene Ontology (GO) enrichment analysis (<http://geneontology.org>) was used to identify biological processes, cellular locations and molecular functions that are impacted by the overexpression or inhibition of miR-455.

2.3. Limb bud development and microRNA-455

2.3.1. Model organism

Chick embryos were used as the model organism due to the accessibility of the embryo to manipulative procedures. Development was observed *in ovo* at multiple stages. The Hamburger-Hamilton (HH) series of chronological stages in chick development were used to stage the embryos (291).

2.3.2. Microinjection into chick limb bud

Embryos were accessed through a window cut in the eggshell at HH20-21. The chorion membrane was removed with forceps, 2 drops of PBS +P/S were dropped onto the membrane before removing the amnion membrane with a 25-gauge needle. Using a 1ml syringe and 25-gauge needle, Indian ink (1 drop per 1.5ml PBS + P/S) was injected underneath the embryo. The allantois was then removed using no.5 forceps. Oligos were dissolved at 65°C in a heat block for 2-3 minutes. Needles containing 4µl Oligo at 1mM were set up for microinjection using a microscope. The right-side anterior limb buds were injected with either Scrambled sequences (AM-Scr) for control, antagomir-455 (AM-455), or miR-455 mimic (miR455m). Starting at the top of the limb bud, 3-5 injections were made down the limb bud. Following this, 2-3ml of albumin was removed using a 10ml syringe and 21-gauge needle. The window was resealed with tape and eggs incubated for 24 hours at 37°C.

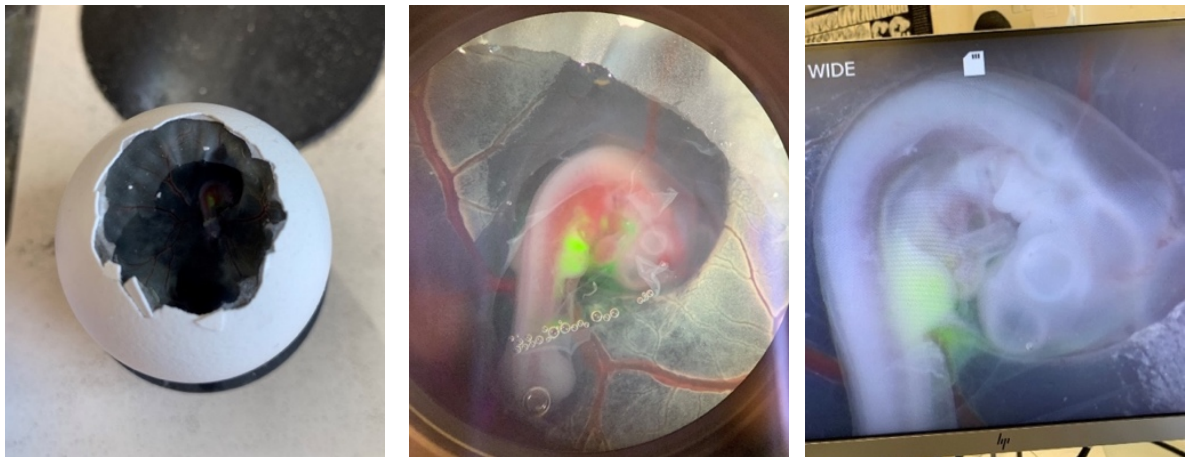


Figure 2.1: Chick limb bud microinjection. Egg windowing and microinjection into HH20-21 chick embryos. Antagomir and mimic can be visualised by fluorescence in the developing limb bud.

2.3.3. Embryo harvest and limb bud dissection

Embryos were harvested 24 hours after injection at HH24-25. The injected limb buds were observed under fluorescent microscope for GFP and dissected into PBS. After removing PBS, each limb bud was snap frozen in liquid nitrogen and stored at -80°C.

2.3.4. RNA extraction from chick limb bud

2.3.4.1. Qiagen RNeasy Micro kit

RNA was extracted from 8x AM-Scr, 8x AM-455, and 8x miR455m injected limb buds separately according to the Qiagen RNeasy Micro Kit. The limb bud tissue was disrupted and homogenized by the addition of 350µl and vortexed for 30 seconds. To the lysate, 1 volume 70% ethanol was added and mixed well before transferring to a RNeasy MinElute spin column in a 2ml collection tube and centrifuged for 15 seconds at 8000xg. The column was then washed with 350µl buffer RW1. A volume of 80µl DNase I incubation mix (10µl DNase I + 70µl buffer RDD) was added to the column membrane and incubated for 15 mins at 20-30°C. The column was then washed with 350µl buffer RW1, followed by 500µl buffer RPE, and finally 500µl 80% ethanol. In a 1.5ml collection tube, the RNA was eluted in 14µl RNase-free water. The RNA Nanodrop was used to quantify RNA concentrations and determine 260/280 and 260/230 ratios.

2.3.5. Quantitative Real Time Polymerase Chain Reaction (RT-qPCR)

2.3.5.1. SuperScript II Reverse Transcription

Following RNA extraction, cDNA was synthesised using SuperScript II reverse transcriptase (Invitrogen, USA) as described above. The cDNA was diluted 10/100 and stored at -20°C.

2.3.5.2. miRCURY LNA miRNA PCR

For highly sensitive Real Time PCR detection of miRNA levels, the miRCURY LNA miRNA PCR Kit (Qiagen) was used as described above where RNA extracted from the limb buds was diluted 5ng/µl. The cDNA was diluted 1/40 and stored at -20°C.

2.3.5.3. SYBR Green Real Time PCR mRNA

For the Real Time PCR (qPCR) reactions, MicroAmp optical 96-well plates (Applied Biosystems, USA) were used. For analysis of mRNA, primers were designed for *Gallus_gallus* in the Integrated DNA Technologies Custom Primer Design Tool, and Oligos ordered from Sigma-Aldrich. The reference gene used was GAPDH. Each well contained 5µl cDNA (1ng) from the SSII RT reaction, with reagent quantities shown in Table 2.6, total volume 15µl. The plates were sealed with adhesive cover film and qPCR was performed on an ABI 7500 real-time PCR system (Applied Biosystems), with cycle conditions set at 95°C for 30 seconds followed by and 95°C for 5 seconds, 58°C for 15 seconds and 72°C for 10 seconds for 40 cycles.

Table 2.6: SYBR green qPCR reagents and volumes for detecting mRNA.

| Reagent | GAPDH | Gene of interest |
|--|-------|------------------|
| SYBR Green PCR Master Mix (Applied Biosystems) | 7.5µl | 7.5µl |
| Forward Primer (10µM) | 0.5µl | 0.5µl |
| Reverse Primer (10µM) | 0.5µl | 0.5µl |
| ddH ₂ O | 1.5µl | 1.5µl |

2.3.5.4. SYBR Green Real Time PCR miRNA

The U6 snRNA miRCURY LNA miRNA PCR Assay (Qiagen) primer set was used as a reference gene, and miR-455-3p miRCURY LNA miRNA PCR Assay (Qiagen) to target mature miRNA, as described above in 1.1.4.4.

2.3.5.5. Statistical analysis

Statistical analysis was performed as described above in 2.1.4.5.

2.3.6. mRNA-seq Novogene

Eukaryotic transcriptome libraries were created by Novogene and data analysed as described above in 2.2.9.

2.4. Identifying microRNA-455 targets

2.4.1. Cell lines and cell culture

2.4.1.1. SW1353 cell line

The SW1353 cell line is derived from human chondrosarcoma of the humerus. SW1353 cells are maintained in DMEM, high glucose, GlutaMAX™ supplement (Gibco, USA), containing 10% (v/v) heat-inactivated fetal bovine serum (FCS) (Gibco, USA), 100U/ml penicillin, and 100µg/ml streptomycin (Sigma-Aldrich, USA) at 37°C in 5% (v/v) CO₂.

2.4.1.2. DF1 cell line

The DF1 cell line is a cell line of chicken embryo fibroblasts. DF1 cell are maintained in DMEM, high glucose, GlutaMAX™ supplement (Gibco, USA), containing 10% (v/v) heat-inactivated fetal bovine serum (FCS) (Gibco, USA), 100U/ml penicillin, and 100µg/ml streptomycin (Sigma-Aldrich, USA) at 37°C in 5% (v/v) CO₂.

2.4.2. 3'UTR Luciferase Reporter Assay

2.4.2.1. Transformation of 3'UTR into SW1353 cells

SW1353 cells were plated in 96-well plates at a density of 6×10^4 cells/mL and incubated for 24 hours at 37°C. The plasmids were diluted in nuclease free H₂O to a 100ng/µl. For each transfection, 1 µl WT/MT 3'UTR plasmid DNA, 0.075µl miR-455 mimic and mimic control (Qiagen) at 66.7µM, and 0.2µl p3000 Reagent (Invitrogen, USA) were prepared in 4µl Opti-MEM™ Medium (Gibco, USA). For each well, 0.2µl Lipofectamine™ 3000 (Invitrogen, USA) was diluted in 5µl Opti-MEM™ Medium (Gibco, USA). The two were then mixed together and incubated for 10-15 minutes at room temperature before being added to each well. A mock control was performed alongside 5 independent transfections for each WT/MT 3'UTR of interest. The transfected cells were incubated for 48 hours at 37°C in 5% CO₂.

2.4.2.2. Luciferase Reporter Assay

The media in the 96-well plate was replaced with 50µl fresh media. The luciferase assay was performed as per the Dual-Glo Luciferase assay system (Promega) protocol. To each well, 50µl Dual-Glo Luciferase assay reagent (Promega) was added and incubated for 15 minutes. The firefly luminescence was measured using a luminometer. Then, 50µl of Dual-Glo Stop & Glo reagent (Promega) was added to each well and incubated for 10 minutes. The Renilla luminescence was measured using a luminometer. The ratio of luminescence from the experimental reporter, firefly, to the luminescence from the control reporter, Renilla was calculated. This ratio is then normalised to a ratio of control wells.

2.4.3. microRNA-target interactions by CRISPR/Cas9 genome engineering

2.4.3.1. miR-CRISPR sgRNA design

For each selected gene, sgRNA was designed using the miR-CRISPR web tool. This platform selects CRISPR/Cas9 target sequences close to the predicted MRE of interest. The organism of interest, Human, was selected and search mode selected as user-defined 'custom sequence'. The gene of interest 3'UTR was copied from Ensembl and predicted MRE seed position and length entered from the miRanda algorithm at microrna.org. As the PX330 backbone vector was used in mammalian cells, the input sgRNA design parameters were "Mammalian U6" and "4bp (BsmBI, Bbcl, BsaI)" in the Promoter/RE field. More efficient cleavage is yielded by NGG PAMs so this was selected before 'Get CRISPR Targets'. The output page returns an algorithm with information of the selected target gene and miRNA of interest, ranked on distance from MRE and identity of PAM sequence. The designed Forward and Reverse oligos for adding the spacer sequence to a chimeric sgRNA backbone into the PX330 vector included the overhangs included for cloning and were ordered from Sigma-Aldrich.

2.4.3.2. HDR-mediated MRE replacement ssODN design

To perform HDR-mediated MRE replacement, 2 barcoded single stranded oligodeoxynucleotide (ssODN) donor templates were designed with the 5'-N₆₀-tag-N₆₀-3' format. The N₆₀ corresponds to homology arms 60nt upstream and downstream of the MRE seed sequence of interest and the barcodes used were T7 (5'-

TAATACGACTCACTATAGGG-3') and T3 (5'-AATTAACCCTCACTAAAGGGA-3'). For each gene of interest, 2 ssODNs were designed: ssODN^{mut-MRE} and ssODN^{WT-MRE}. The tag^{mut} was generated by replacing the MRE with a T7 barcode, and the tag^{WT} was generated by inserting a T3 barcode downstream of the MRE sequence. This created 2 ssODNs with the following structure:

ssODN^{mut-MRE}: 5'-N₆₀-[MRE seed deletion]T7-N₆₀-3'

ssODN^{WT-MRE}: 5'-N₆₀-MRE-T3-N₆₀-3'

In order to prevent any further cleavage following HDR replacement, in the ssODN, the PAM is mutated, and ordered from IDT as 4nmol Ultramers.

2.4.3.3. pX330 backbone vector

The pX330 vector was ordered from Addgene as a stab culture. The bacteria was streaked on a LB-AMP plate and incubated overnight at 37°C before inoculating an overnight culture of multiple colonies, and isolating the plasmid DNA using the QIAprep spin mini prep kit (Qiagen). Glycerol stocks were created by adding 500µl bacteria culture to 500µl glycerol and stored at -80°C.

Table 2.7: pX330 primer and sequence.

| Primer name | Sequence 5' to 3' |
|-------------|------------------------|
| pX330_Seq | ACTATCATATGCTTACCGTAAC |

2.4.3.4. sgRNA cloning into pX330 vector

The sgRNA oligos were annealed and cloned into the pX330 backbone vector.

2.4.3.4.1. pX330 digest

To digest the pX330 backbone vector, 1µg pX330 was mixed with 1µl FastDigestBbsI (Thermofisher), 1µl FastAP (Thermofisher), 2µl 10x FastDigest Buffer (Thermofisher), and Xµl ddH₂O for 30 minutes at 37°C.

2.4.3.4.2. Gel purification of digested pX330

Digested pX330 samples were diluted to 1µg in 17µl H₂O, and 3µl 6x Gel Loading Dye Purple (New England BioLabs), was added to each. Each 20µl sample was loaded onto a 1% agarose gel (1g Agarose + 100ml TAE buffer), alongside 5µl 1kb ladder (New England BioLabs), and run for 1 hour at 120V. The dye was developed by placing the gel in 200ml TAE buffer containing 10µl Ethidium Bromide for 15 minutes. The digested plasmid bands were cut out us under UV light and gel imaged using a Biorad Gel Doc.

The digested pX330 was gel purified using the QIAquick Gel Extraction Kit (Qiagen). To 1 volume of gel. To dissolve the gel, 3 volumes of buffer QG was added and incubated at 50°C for 10 minutes, vortexing every 2 minutes. The solution colour was checked for yellow before adding 1 volume isopropanol and mixed. To bind the DNA, the sample was added to a QIAquick column (Qiagen) and centrifuged for 1 minutes at 17900xg. The column was then washed with 750µl buffer PE. In a 1.5ml Eppendorf, the DNA was eluted in 30µl Elution Buffer (Qiagen), and the concentration of recovered plasmid determined by Nanodrop.

2.4.3.4.3. Oligo annealing and phosphorylation

The forward and reverse sgRNA spacer oligos were resuspended in nuclease free H₂O to a concentration of 100µM. To phosphorylate and anneal each pair of oligos, 1µl oligo1 (100µM), 1µl oligo2 (100µM), 1µl 10x T4 ligation buffer (Thermofisher), 6.5µl ddH₂O, and 0.5µl T4 PNK (Thermofisher) were added to a 96-well PCR plate. The total 10µl volume was incubated in a thermocycler at 37°C for 30 minutes, followed by 95°C for 5 minutes and then ramped down to 25°C and 5°C per minute.

2.4.3.4.4. Ligation into pX330 vector

The ligation reaction was set up with 1µl phosphorylated and annealed oligo duplex (1/250 dilution), 50ng digested pX330 vector, 1µl 10x T4 ligase buffer (New England BioLabs), Xµl ddH₂O, and 1µl QuickLigase (New England BioLabs), for a total volume of 100µl. This was incubated at room temperature for 10 minutes. A control ligation

reaction was performed where the annealed sgRNA oligo duplex was replaced with H₂O in order to assess sgRNA spacer sequence cloning success into destination vector.

2.4.3.4.5. Transformation

To transform competent bacteria, 50µl of Stellar Competent E.coli HST08 cells (Clontech) were thawed on ice. On ice, 2µl ligation reaction and 50µl E.coli were gently mixed and incubated for 30 minutes. The transformation tubes were then heat shocked at 42°C for 45 seconds before placing back on ice for 2 minutes. This was then added to 950µl pre-warmed LB media and put in the shaker at 225rpm for 1 hour at 37°C. The bacteria was pelleted by centrifuging at 2500xg for 3 minutes and 800µl of the LB media was removed. The pellet was resuspended in the remaining 200µl media and plated on LB-Agar-Amp plates (100µl Ampicillin + 100ml LB-Agar for 6 plates) with 10µl, 50µl, and 100µl E.coli. The plates were incubated overnight at 37°C.

Overnight cultures were set up from colonies on the LB-Agar-Amp plates containing 100µl E.coli. From each plate, 10 colonies were picked and grown overnight in 5ml LB-Amp (100ml LB + 100µl Amp for 20 colonies), in a shaker at 225 rpm and 37°C.

2.4.3.4.6. Isolation of plasmid DNA

The bacterial overnight culture was pelleted by centrifuging at 4000rpm for 10 minutes. The QIAprep Spin MiniPrep Kit was used as the bacteria cells were resuspended in 250µl Buffer P1 (Qiagen) and transferred to an eppendorf before adding 250µl Buffer P2 (Qiagen) and mixed until clear. To the lysis reaction, 350µl Buffer N3 was added, mixed, and centrifuged for 10 minutes at 17900xg. The supernatant was applied to a QIAprep spin column (Qiagen), before centrifuging for 1 minutes. The QIAprep spin column was then washed with 750µl Buffer PE. In a clean Eppendorf, the DNA was eluted with 50µl Elution Buffer (Qiagen). To confirm the presence of the correct sgRNA spacer, Sanger Sequencing (Source Bioscience) was used with the pX330_Seq primer (Sigma-Aldrich).

2.4.3.5. HDR-mediated MRE engineering into SW1353 cell line

SW1353 cells were plated in 12-well plates at a density of 1.5×10^5 cells/mL and incubated for 24 hours at 37°C. The ssODNs were resuspended in nuclease free H₂O to a concentration of 100µM. For each transfection, 1µg pX330-sgRNA plasmid DNA, 0.5µg ssODN^{WT-MRE} oligo (100µM), 0.5µg ssODN^{mut-MRE} oligo (100µM), and p3000 Reagent (Invitrogen, USA) were prepared in 75µl Opti-MEMTM Medium (Gibco, USA). For each well, 3µl LipofectamineTM 3000 (Invitrogen, USA) was diluted in 75µl Opti-MEMTM Medium (Gibco, USA). The two were then mixed together and incubated for 10-15 minutes at room temperature before being added to each well. An untransfected control was performed alongside 3 independent transfections for each sgRNA/target MRE locus. The transfected cells were incubated for 48 hours at 37°C in 5% CO₂.

2.4.3.6. DNA/RNA extraction from MRE engineered cells

SW1353 cells were harvested 48 hours post-transfection by incubating with trypsin (0.01%) for 5 minutes at 37°C. To neutralise the trypsin, 1mL media was added and the cells were centrifuged for 3 minutes at 500xg. Cells were washed with PBS, before snap freezing and stored at -80°C.

2.4.3.6.1. Qiagen Allprep DNA/RNA mini kit

From each cell sample, DNA and RNA were simultaneously extracted using the Qiagen Allprep DNA/RNA mini kit. To each frozen pellet, 350µl buffer RLT (Qiagen) was added to lyse the cells. The homogenized lysate was transferred to an Allprep DNA spin column (Qiagen) and centrifuged for 30 seconds at 8000xg. For total RNA purification, 1 volume 70% ethanol was added to the flow-through and transferred to a RNeasy spin column (Qiagen), before centrifuging for 15 seconds at 8000xg. The column was then washed with 700µl buffer RW1 (Qiagen) followed by 500µl buffer RPE. In a new 1.5mL collection tube, the RNA was eluted in 30µl RNase-free H₂O and stored at -80°C. The RNA Nanodrop was used to quantify RNA concentrations and determine 260/280 and 260/230 ratios.

The Allprep DNA spin column was placed in a new 2mL collection tube and washed with 500µl Buffer AW1 (Qiagen), followed by 500µl Buffer AW2. In a new 1.5mL collection tube, the DNA was eluted in 100µl Elution Buffer (Qiagen) and stored at -20°C.

2.4.3.6.2. ExoSAP-IT Cleanup

As residual ssODNs can interfere with qPCR analysis, the gDNA sample was treated with ExoSAP-IT (Thermofisher). For a reaction volume of 14µl, 10µl gDNA sample was mixed with 4µl ExoSAP-IT and incubated at 37°C for 15 minutes to degrade remaining ssODNs, followed by 80°C for 15 minutes to inactivate the ExoSAP-IT Reagent. The DNA sample was stored at -20°C.

2.4.3.7. Quantitative Real Time Polymerase Chain Reaction (RT-qPCR)

2.4.3.7.1. Qiagen QuantiTect RT kit

To generate cDNA from 1µg total RNA, the Qiagen QuantiTect RT kit was used. For the genomic DNA elimination, 1µg RNA was diluted in 12 µl RNase-free H₂O and 2µl 7x gDNA Wipeout buffer (Qiagen) was added for a total volume of 14 µl. This was incubated for 2 minutes at 42°C and placed on ice. For the Reverse Transcription master mix, 1µl Quantiscript Reverse Transcriptase (Qiagen), 4µl 5x Quantiscript RT buffer (Qiagen), 1µl RT Primer mix (Qiagen), and the 14 µl template RNA were mixed for a total volume 20µl. This was incubated for 15 minutes at 42°C, followed by 3 minutes at 95°C to inactivate the reverse transcriptase. The cDNA was stored at -20°C.

2.4.3.7.2. SYBR Green Real-Time PCR

For the Real Time PCR (qPCR) reactions, MicroAmp optical 96-well plates (Applied Biosystems, USA) were used. For the qPCR reaction, specific primers approximately 100-150nt upstream of each MRE seed sequence of interest were designed with a T_m of 60-65°C. The reverse primers were synthesised complementary to the designed MRE^{mut} and MRE^{WT} (T7 and T3) barcodes. Primers were ordered from Sigma-Aldrich.

For each MRE, the combinations of template and primers in Table 2.8 were run. Each sample well contained 1µl template DNA, with reagent quantities shown in Table 2.9

loaded per well, total volume 20 μ l. The plates were sealed with adhesive cover film and qPCR was performed on an ABI 7500 real-time PCR system (Applied Biosystems), with cycle conditions set at 98°C for 30 seconds, followed by 98°C for 10 seconds and 60°C for 1 minute for 40 cycles.

Table 2.8: Combinations of template and primers for microRNA-target interactions by CRISPR/Cas9 genome engineering qPCR.

| Sample | F Primer | R Primer | Template | Annotation |
|--------|--------------|----------|----------|-------------|
| A | MRE specific | T3 Rev | gDNA | WT MRE gDNA |
| B | MRE specific | T7 Rev | gDNA | MT MRE gDNA |
| C | MRE specific | T3 Rev | cDNA | WT MRE cDNA |
| D | MRE specific | T7 Rev | cDNA | MT MRE cDNA |

Table 2.9: qPCR reagents for microRNA-target interactions by CRISPR/Cas9 genome engineering.

| Reagent | Volume |
|--|------------|
| Template DNA (gDNA or cDNA) | 1 μ l |
| Forward Primer (10 μ M) | 1 μ l |
| Reverse Primer (10 μ M) | 1 μ l |
| SsoAdvanced Universal SYBR Green Supermix (BioRad) | 10 μ l |
| Nuclease-free H ₂ O | 7 μ l |

2.4.3.7.3. Statistical analysis

The cycle of threshold (Ct) values were obtained for reactions A, B, C, and D and for each transfected well, technical triplicate average Ct was calculated. The MRE^{mut}/MRE^{WT} gDNA (gDNA T7/T3) ratio $[2^{(-B)}/2^{(-A)}]$ and the MRE^{mut}/MRE^{WT} cDNA (cDNA T7/T3) ratio $[2^{(-D)}/2^{(-C)}]$ were determined and the average ratios for biological replicates of triplicate transfections were calculated. Data was displayed in a bar chart as average gDNA MRE^{mut}/MRE^{WT} ratio and average cDNA MRE^{mut}/MRE^{WT} ratio.

2.4.3.7.4. MRE-score calculation

The MRE-score was calculated to determine whether the MRE^{mut} is enriched in the cDNA samples. This can be calculated by dividing cDNA MRE^{mut}/MRE^{WT} ratio by the gDNA MRE^{mut}/MRE^{WT} ratio $[(2^{(-D)}/2^{(-C)})/[(2^{(-B)}/2^{(-A)})]]$.

If the MRE-score is >1 , this suggests that there is functional miRNA-target regulation. To determine if enrichment is significant, a t-test was used by comparing gDNA MRE^{mut}/MRE^{WT} ratios between biological replicates to the cDNA MRE^{mut}/MRE^{WT} ratio.

$$\frac{\text{cDNA } MRE^{mut}/MRE^{WT}}{\text{gDNA } MRE^{mut}/MRE^{WT}} = \frac{2^{(-D)}/2^{(-C)}}{2^{(-B)}/2^{(-A)}}$$

MRE Score = 1
MRE: inactive

MRE Score > 1
MRE: active

MRE Score < 1
MRE: stabilizing

Figure 2.2: MRE score calculation. This determines whether the MRE^{mut} is enriched in cDNA samples.

Chapter 3

***The role of microRNA-455-3p
during mesenchymal stem cell
differentiation***

3. The role of microRNA-455-3p during mesenchymal stem cell differentiation

3.1. Introduction

Within the bone marrow compartment, mesenchymal stem cells contribute to mesenchymal tissue regeneration, and can be isolated for *in vitro* studies. These cells can be manipulated and differentiated into mesodermal lineages such as chondrogenic, osteogenic and adipogenic cells. During mesenchymal stem cell differentiation, many microRNAs have been shown to have a regulatory role, including miR-455. For example, it was previously reported that miR-455 is a regulator of brown adipogenesis, possibly through targeting adipogenic suppressors (292). It has also been demonstrated that miR-455 regulates the process of chondrogenic differentiation in hMSCs, altering methylation levels of genes involved in the development of cartilage (139). The involvement of miR-455 is supported by an upregulation of miR-455-3p in chondrogenesis of MSCs, where it may function as an early chondrogenic differentiation activator possibly by inhibiting RUNX2 expression (137). At the post-transcriptional level, osteogenic-related gene expression is also regulated by multiple miRNAs (293). Previous research strongly suggests that microRNAs have regulatory roles in the differentiation of MSCs, although a specific role for miR-455 has not been identified. To investigate this further, this experiment determines the expression of miR-455-3p during chondrogenesis, osteogenesis and adipogenesis and from these results explores the role of miR-455-3p in both chondrogenesis and osteogenesis.

3.2. Results

3.2.1. microRNA-455-3p expression during hMSC differentiation

During *in vitro* differentiation assays of human mesenchymal stem cells as described in chapter 2.1, direct miR-455-3p expression levels were measured by qPCR (Figure 3.1). The results demonstrated that miR-455 increases during adipogenesis until day 3 and expression then decreases. From day 10 onwards there is no significant difference in miR-455 expression between differentiating and non-differentiating control. Similarly, miR-

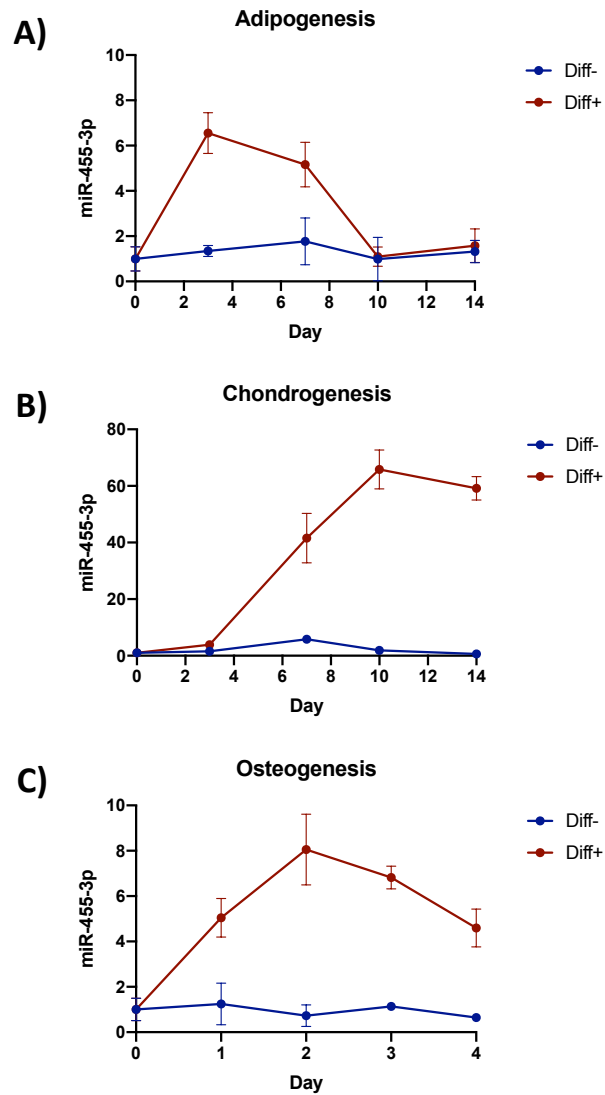


Figure 3.1: Expression of miR-455-3p during hMSC differentiation assays described in chapter 2.1. Comparison of differentiating cells to undifferentiated control. A) Adipogenesis assay day 0 to day 14 shows an initial increase of miR-455-3p at day 2, before decreasing to day 10. B) Chondrogenesis assay day 0 to day 14 shows an increase in miR-455-3p from day 3 to 10. C) Osteogenesis assay day 0 to day 4 shows an increase in miR-455-3p until day 2. (n=9, error bars +/- SD).

455 increases during osteogenesis until day 2 of differentiation, decreasing from day 2 onwards but remaining significantly higher than undifferentiated control. The chondrogenesis assay also demonstrated an initial increase in miR-455 expression to day 3, which rapidly increases from day 3 to day 10 where miR-455 is highest. The expression of miR-455 remains level from day 10 to day 14.

These results demonstrate that at the beginning of all 3 hMSC differentiation assays miR-455 increases, before decreasing in both adipogenesis and osteogenesis. The expression level of miR-455 during adipogenesis and osteogenesis remains low during differentiation. In comparison to this, miR-455 continues to increase during chondrogenesis, reaching peak expression level at day 10. From day 3, the expression of miR-455 during chondrogenic differentiation is significantly higher compared with adipogenic and osteogenic differentiation. This could suggest that miR-455 is required at initial stages of hMSC differentiation, but not to proceed in both adipogenesis and osteogenesis. The higher levels of miR-455 during chondrogenesis suggest that miR-455 is important during chondrogenic differentiation.

3.2.2. A complex role for microRNA-455-3p during osteogenesis

Human mesenchymal stem cells were differentiated into osteoblasts using a 5-day osteogenesis assay. During this assay, Osteogenic marker genes were measured. The increase in Osteogenic markers genes confirmed that the assay successfully differentiated hMSCs towards an osteogenic lineage (Figure 3.2). Samples from 3 individual MSC donors were used independently. Biological replicates of each MSC donor were performed and this data was combined. Within the assay, MSCs were transfected with either Cel-39 control, miR-455 mimic, Neg Ctrl A control, or miR-455 inhibitor. At time points day 0, 1, 2, 3, and 4, gene expression levels for chondrogenic marker genes were measured using qPCR, including COL1A1, COL1A2, BMP2, ALP and RUNX2.

Cells transfected with miR-455 inhibitor were compared to control, where data revealed that expression levels of all osteogenic marker genes were not significantly different. Despite this, it is apparent that expression levels of RUNX2 are higher in cells transfected with miR-455 inhibitor, particularly at day 2 (Figure 3.2). This is supported by a decreased

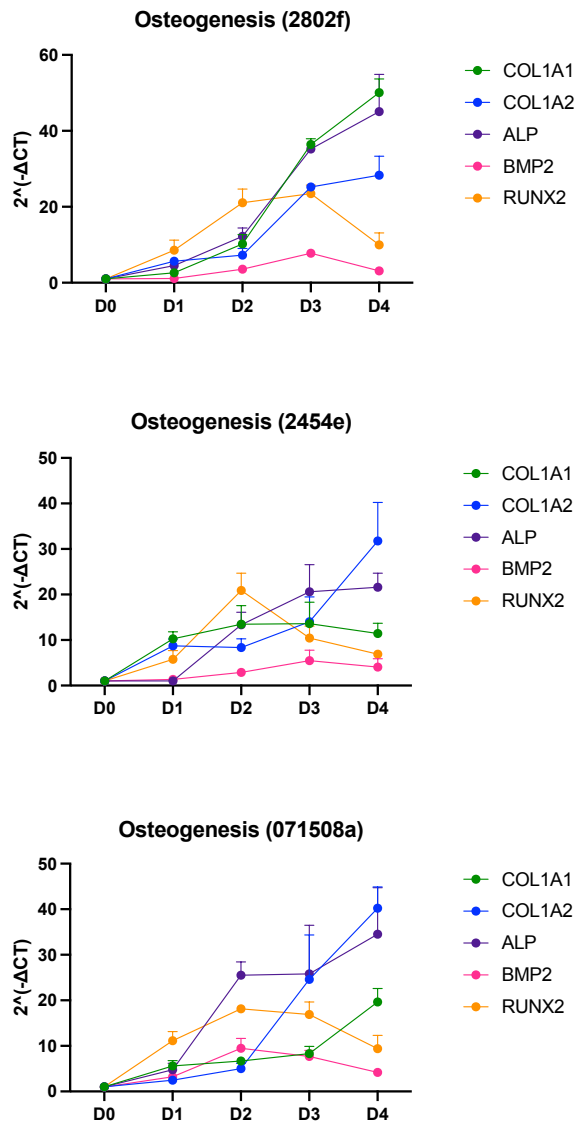


Figure 3.2: Osteogenesis differentiation assay. Independent cell lines from 3 donors were used for osteogenic differentiation: 2802f, 2454e and 071508a ($n=3$ for each cell line). Osteogenic marker genes COL1A1, COL1A2, ALP, BMP2 and RUNX2 were measured at D0, D1, D2, D3 and D4 of differentiating hMSCs using qPCR. The increase in Osteogenic marker genes during the osteogenesis assay confirmed that the hMSCs were differentiating into an osteogenic lineage. ($n=9$, error bars +/- SD).

expression of RUNX2 at day 2 when miR-455 is overexpressed using a mimic (Figure 3.3), and this expression pattern can also be observed for BMP2. With the addition of a miR-455 mimic, expression levels of COL1A1, COL1A2 and ALP show a general increase, although not consistently significant (Figure 3.3). For example, the biggest increase in gene expression when miR-455 is overexpressed is day 4 for both COL1A2 and ALP, whereas this is observed from day 2 onwards for COL1A1. Alizarin red staining also demonstrated minimal differences between control groups and inhibiting or overexpressing miR-455 (Figure 3.5), therefore differences in gene expression during osteogenesis are not significant.

This data suggests that miR-455-3p may have a role in osteogenesis, although whether this promotes or inhibits osteogenic differentiation is unclear. Within this assay, an overexpression of miR-455 has a greater impact on osteogenesis compared with miR-455 inhibition. As the osteogenic marker genes COL1A1, COL1A2, and ALP increase when miR-455 is overexpressed, but BMP2 and RUNX2 decrease (Figure 3.3), it is difficult to conclude a specific regulatory role.

3.2.3. Overexpression of microRNA-455-3p suppresses chondrogenesis

To explore the role of miR-455 during chondrogenesis, human mesenchymal stem cells were differentiated into chondrocytes using a 14-day chondrogenesis assay. An increase in chondrogenic marker genes throughout this assay confirmed differentiation into a chondrogenic lineage (Figure 3.6). Samples from 3 individual MSC donors were used independently. Biological replicates of each MSC donor were performed and this data was combined. Within the assay, MSCs were transfected with either Cel-39 control, miR-455 mimic, Neg Ctrl A control, or miR-455 inhibitor. At time points day 0, 3, 7, 10, and 14, gene expression levels for chondrogenic marker genes were measured using qPCR, including COL2A1, COL10A1, SOX9, ACAN, RUNX2, and PRELP.

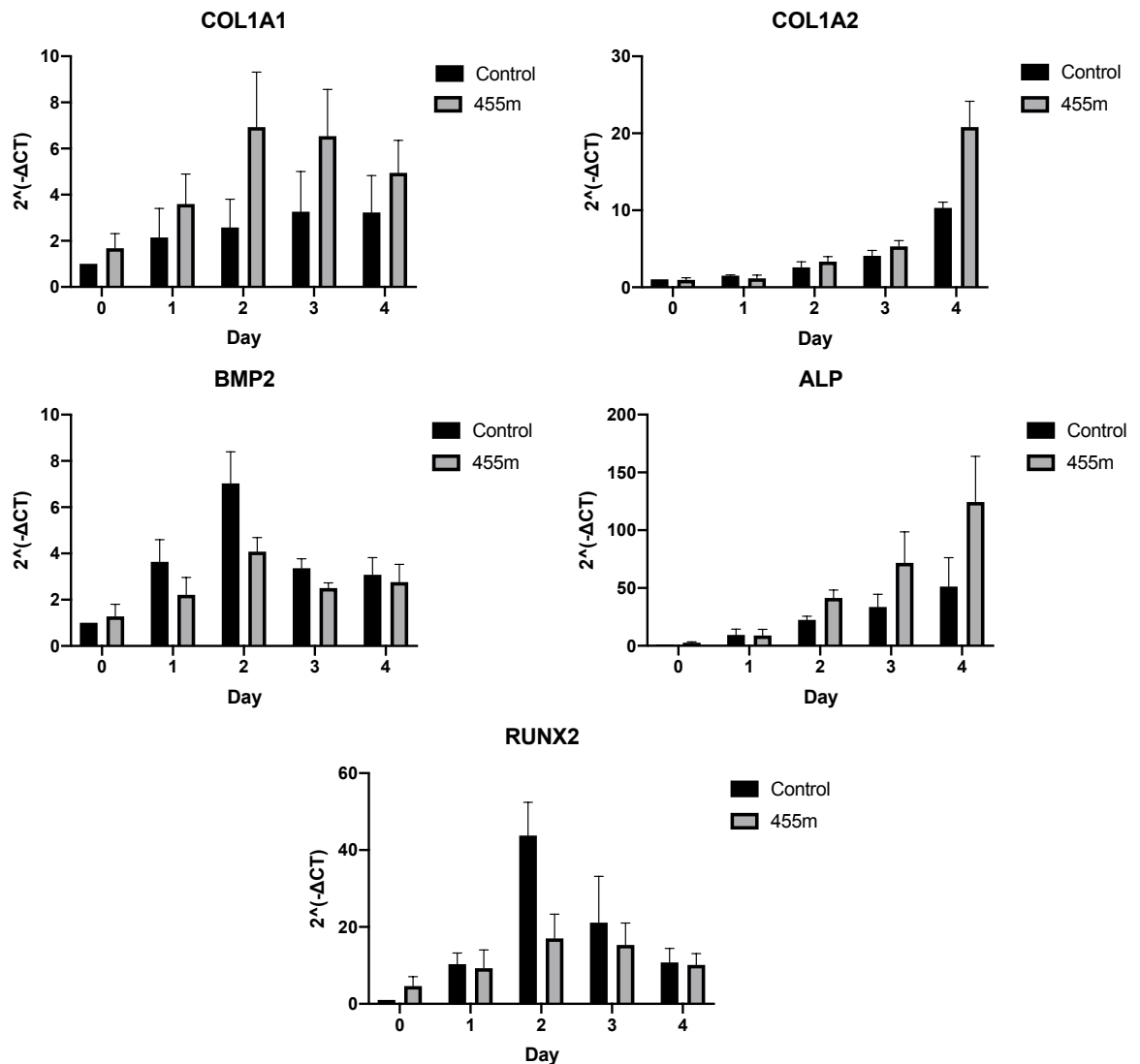


Figure 3.3: Osteogenic marker gene expression during hMSC osteogenesis assay (mimic). hMSC were transfected with either mimic Control (Cel-39) or miR-455 mimic prior to osteogenic differentiation for 4 days. Gene expression was measured for osteogenic marker genes COL1A1, COL1A2, BMP2, ALP, and RUNX2 by qPCR. For each gene, the results combine data from 3 biological replicates from each of the 3 hMSC donor cell lines: 2454e, 2802f, 071508a. (n=9, error bars +/- SD).

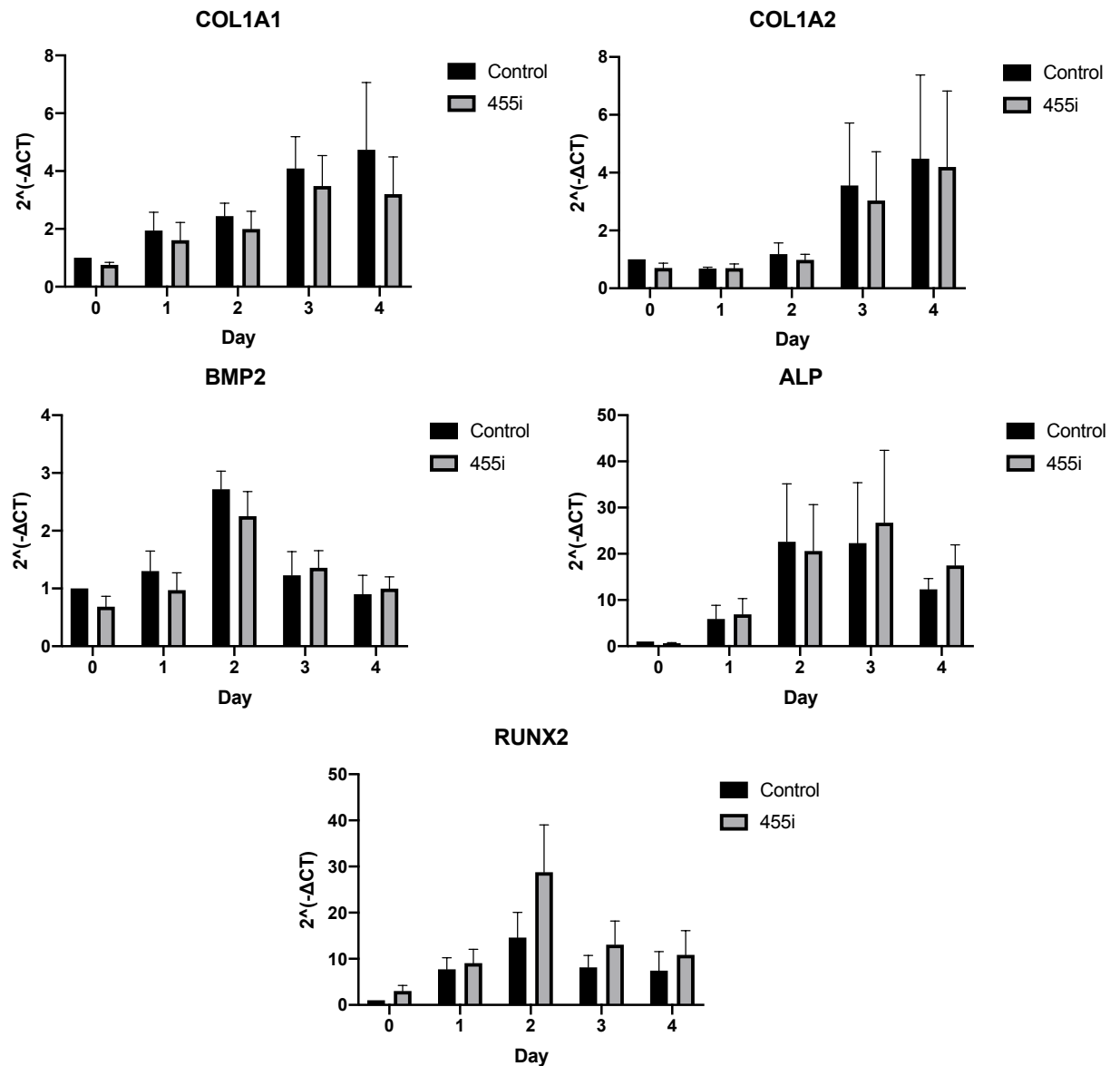


Figure 3.4: Osteogenic marker gene expression during hMSC osteogenesis assay (inhibitor). hMSC were transfected with either inhibitor Control (Neg Ctrl A) or miR-455 inhibitor prior to osteogenic differentiation for 4 days. Gene expression was measured for osteogenic marker genes COL1A1, COL1A2, BMP2, ALP, and RUNX2 by qPCR at each time point. For each gene, the results combine data from 3 biological replicates from each of the 3 hMSC donor cell lines: 2454e, 2802f, 071508a (n=9, error bars +/- SD).

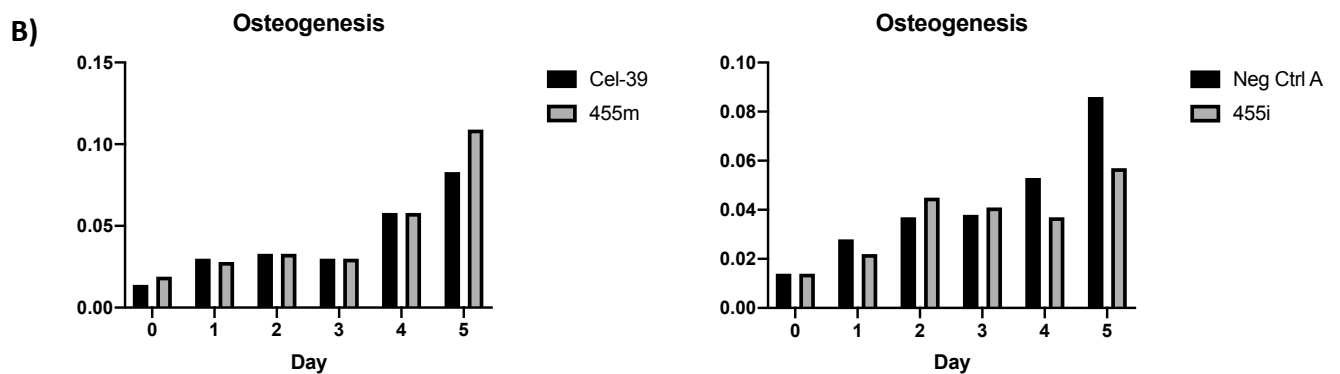
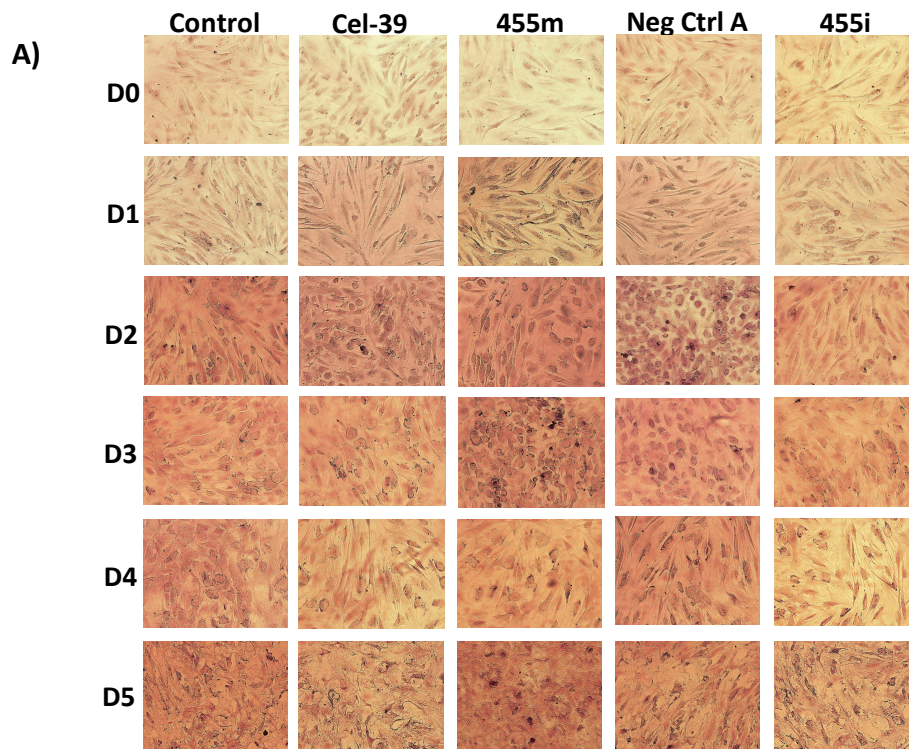


Figure 3.5: Alizarin red staining of hMSCs during osteogenic differentiation. Cells were fixed and stained with Alizarin red at D0, D1, D2, D3, D4 and D5 of the osteogenic differentiation assay. A) Images indicate that there is little difference in staining between control samples and samples transfected with miR-455 mimic or miR-455 inhibitor, possibly an increase in staining when miR-455 is overexpressed. B) Absorbance measured from eluted dye suggests a small increase in staining at day 5 in miR-455 mimic samples, and a small decrease and days 4 and 5 in miR-455 inhibitor samples, although this is not statistically significant ($n=3$, $p>0.05$).

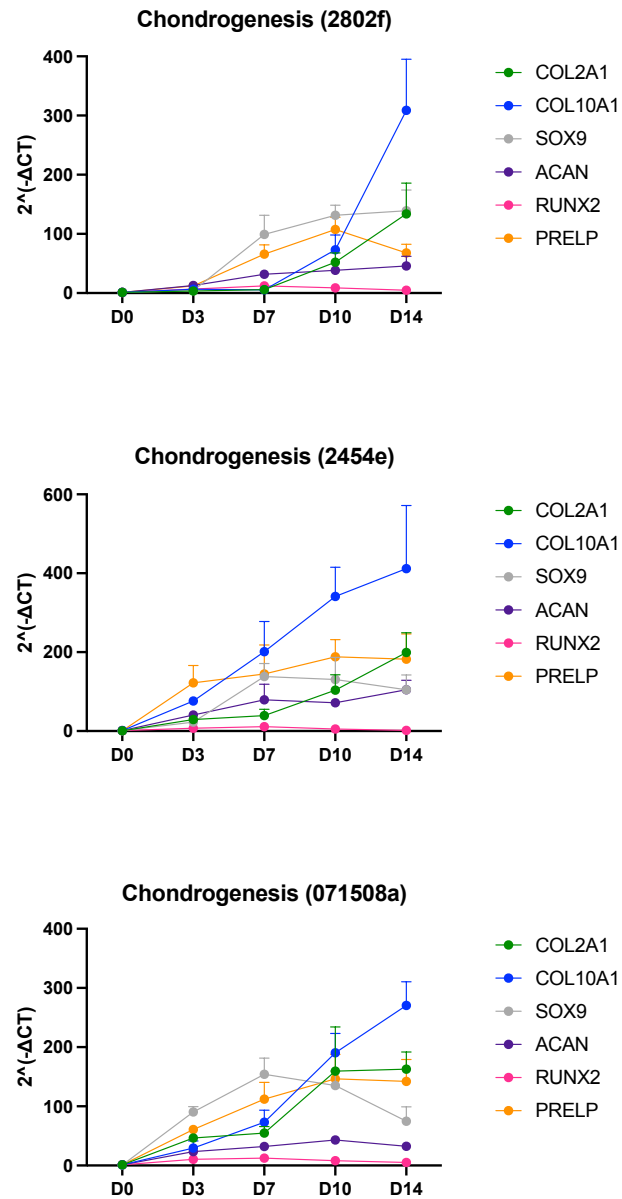


Figure 3.6: Chondrogenesis differentiation assay. Independent cell lines from 3 donors were used for chondrogenic differentiation: 2802f, 2454e and 071508a ($n=3$ for each cell line). Chondrogenic marker genes COL2A1, COL10A1, SOX9, ACAN, RUNX2 and PRELP were measured at D0, D3, D7, D10 and D14 of differentiating hMSCs using qPCR. The increase in Chondrogenic marker genes during the chondrogenesis assay confirmed that the hMSCs were differentiating into a chondrogenic lineage. ($n=9$, error bars \pm SD).

Cells transfected with miR-455 mimic were compared to control. The data revealed that expression levels of all chondrogenic marker genes were significantly decreased in cells transfected with miR-455 mimic (Figure 3.7). This was most apparent for both SOX9 and PRELP gene expression, which increased significantly less during differentiation in cells transfected with miR-455 mimic compared with control cells. These results were supported by data demonstrating a general increase in chondrogenic marker genes in cells transfected with miR-455 inhibitor compared with control, although not always statistically significant (Figure 3.8). Interestingly, the effect of the miR-455 inhibitor was not as severe compared with miR-455 mimic. For example, there was no significant difference in COL2A1, SOX9, and ACAN expression between miR-455 inhibitor and control. Although most timepoints had no significant difference in COL10A1 expression, day 14 showed a statistically significant increase in gene expression in samples where miR-455 had been inhibited. From day 7 onwards, RUNX2 and PRELP expression was also higher when miR-455 was inhibited (Figure 3.8).

These results suggest that an overexpression of miR-455-3p may suppress chondrogenesis. Although it may be hypothesised that inhibiting miR-455-3p has the opposite effect by promoting chondrogenesis, the result of miR-455 inhibition is similar to control chondrogenesis hMSC assays. This data may suggest that an increase in miR-455 impacts negatively during the chondrogenic differentiation process.

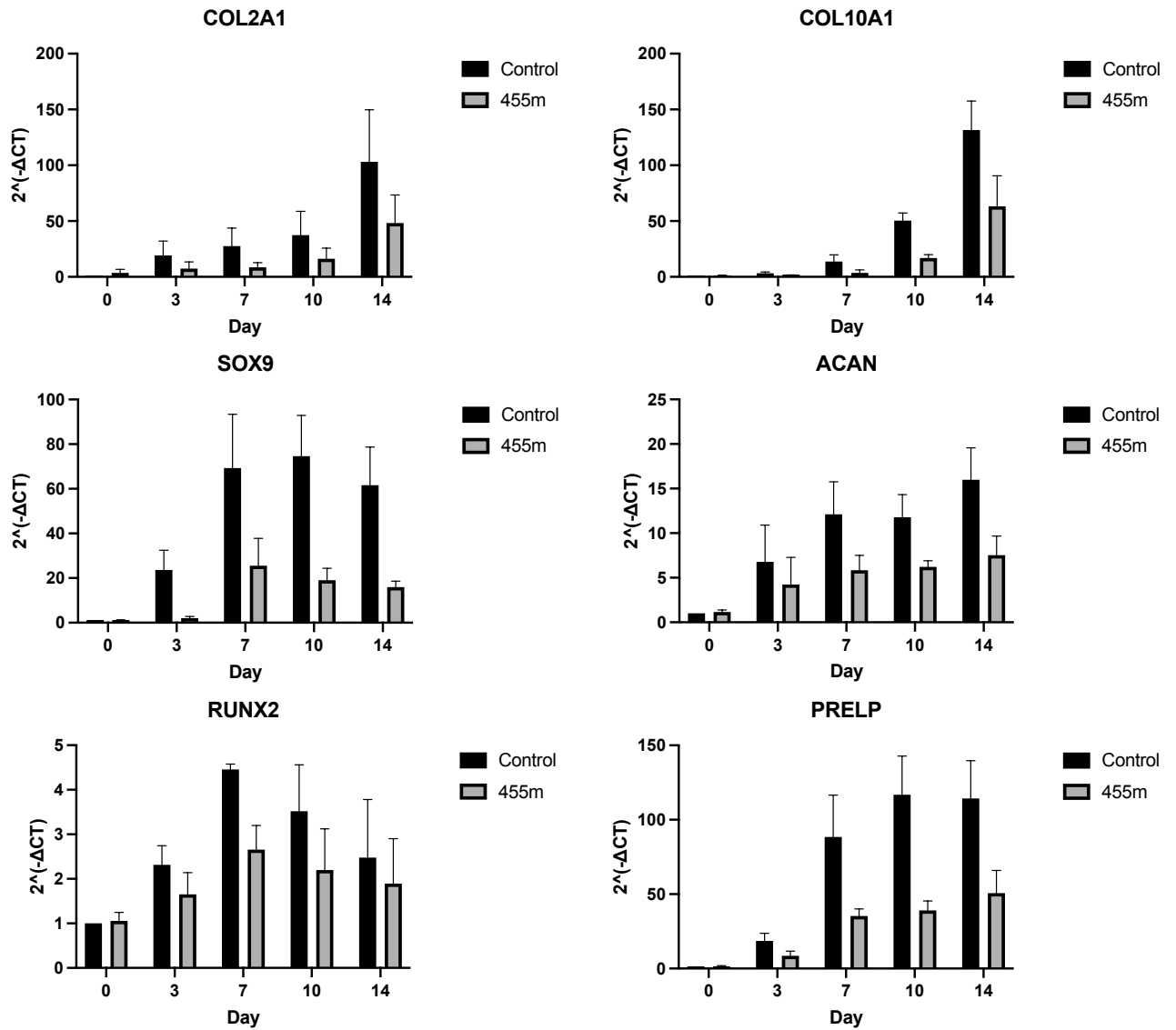


Figure 3.7: Chondrogenic marker gene expression during hMSC chondrogenesis assay (inhibitor). hMSC were transfected with either mimic control (Cel-39) or miR-455 mimic prior to chondrogenic differentiation for 14 days. Gene expression was measured for chondrogenic marker genes COL1A1, COL10A1, SOX9, ACAN, RUNX2 and PRELP by qPCR. Results combine data from 3 biological replicates from each of the 3 hMSC donor cell lines: 2454e, 2802f, 071508a. (n=9, error bars +/- SD).

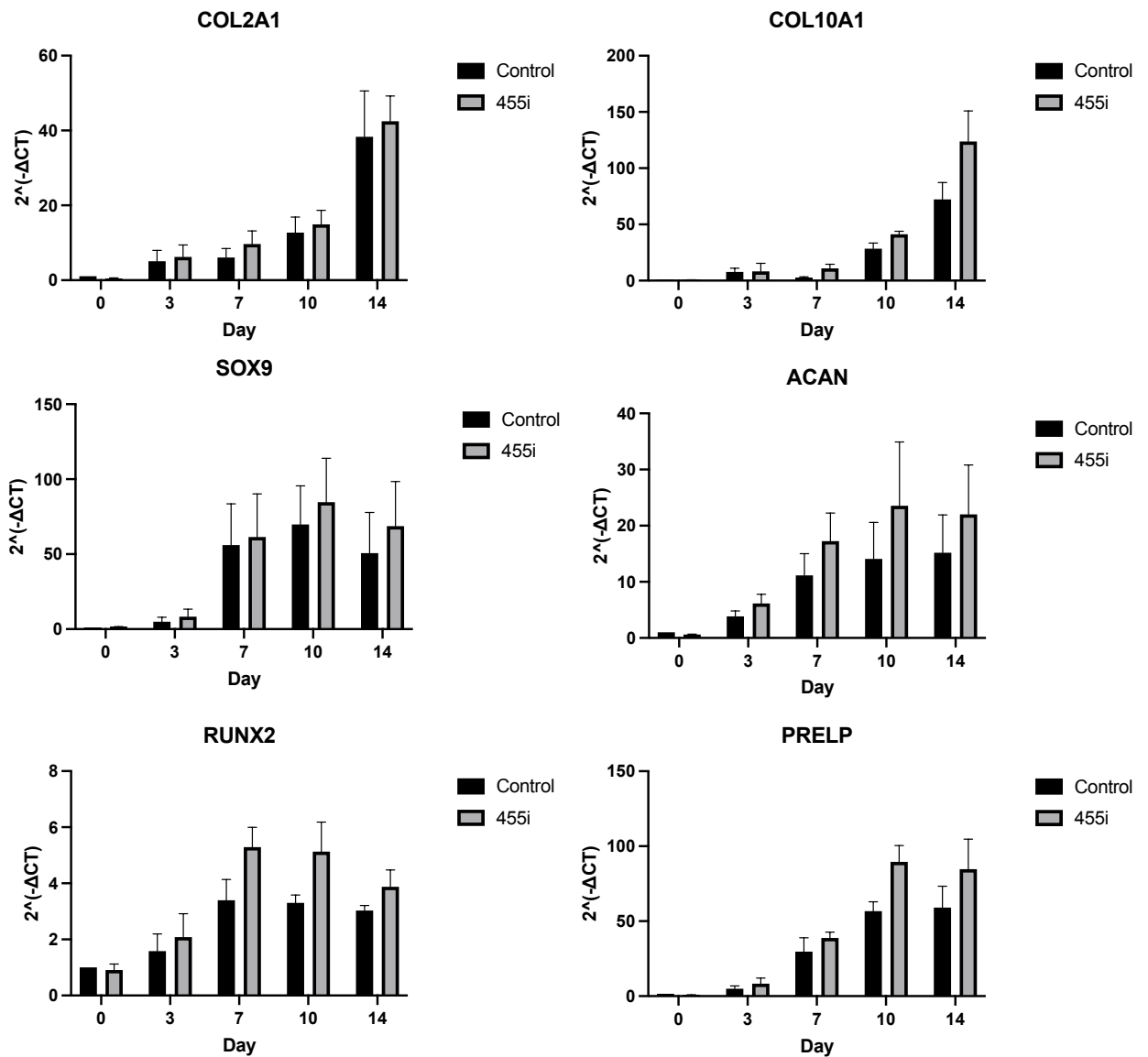


Figure 3.8: Chondrogenic marker gene expression during hMSC chondrogenesis assay (inhibitor). hMSC were transfected with either inhibitor control (Neg Ctrl A) or miR-455 inhibitor prior to chondrogenic differentiation for 14 days. Gene expression was measured for chondrogenic marker genes COL1A1, COL10A1, SOX9, ACAN, RUNX2 and PRELP by qPCR. Results combine data from 3 biological replicates from each of the 3 hMSC donor cell lines: 2454e, 2802f, 071508a. (n=9, error bars +/- SD).

3.1. Discussion

As miR-455-3p initially increases during differentiation of hMSCs in adipogenesis, osteogenesis and chondrogenesis, it is evident that miR-455 has a role in the differentiation of hMSCs. This could suggest that miR-455 is required to initiate differentiation. The change in miR-455 levels between each differentiation process indicates that miR-455 is most important during chondrogenesis, since upregulation continues during chondrogenic differentiation in comparison to a decrease during adipogenic and osteogenic differentiation.

Although miR-455 increases during chondrogenesis, an overexpression of miR-455 results in a decrease in chondrogenic marker gene expression. This could suggest that miR-455 is required at a particular expression level, and if this is not maintained chondrogenesis is dysregulated. Inhibition of miR-455, however, did not demonstrate a significant difference in chondrogenic gene expression in most cases. An overexpression of miR-455 may have a greater impact on chondrogenesis compared with miR-455 knockdown/inhibition. Additionally, transfection of miR-455 mimic during osteogenesis had a greater effect compared with miR-455 inhibitor, increasing osteogenic marker gene expression.

These results suggest that miR-455-3p has a role in hMSC differentiation, in particular chondrogenesis, although the mechanism is unclear. Interestingly, overexpression of miR-455 decreases chondrogenic differentiation and this is something to explore further. Analysis of adult cartilage and chondrocytes in addition to differentiation and developing chondrocytes will give greater insight into a role of miR-455-3p in cartilaginous tissue.

Chapter 4

***Functions of microRNA-455-3p
in cartilage***

4. Functions of microRNA-455-3p in cartilage

4.1. Introduction

Since data has demonstrated that miR-455-3p may have a role in chondrogenesis, this was explored further in adult mouse articular cartilage and the cell line SW1353. As a chondrosarcoma cell line, SW1353 cells were used as an *in vitro* model, and the miR-455 conditional knockout mouse was used as an *in vivo* model to study the role of miR-455 in cartilage and chondrocytes. Previous work has identified cartilage-specific microRNAs, including observation of miR-455-3p in the growth plate and perichondrium during development. To develop on this, it is important to study adult cartilage and compare the role of miR-455 during chondrogenesis and in chondrocytes of mature cartilage. Articular cartilage from null miR-455 mouse knee joints can be dissected to study gene expression in the absence of miR-455, and potentially identify novel cartilage-specific targets. *In vivo* studies can be combined with *in vitro*, where manipulation of miR-455 expression is easily achieved. These experiments explore the role of miR-455 at a molecular level, using mRNA-seq to measure gene expression following an alteration in miR-455 expression levels. The aim is to reveal the consequences of miR-455 overexpression and inhibition/complete knockout both *in vivo* and *in vitro* and identify novel miR-455 target genes.

4.2. Results

4.2.1. Mouse cartilage microdissection

The articular cartilage from WT and miR-455 null mice was microdissected from the tibia and femur of both hind-legs and pooled (Figure 4.1B). RNA was extracted from these samples, pooling 3 mice together (articular cartilage from 6 knee joints in total) with an average final concentration of 70ng/ul. The expression of miR-455 was measured by qPCR in the samples (n=3), confirming that miR-455 KO cartilage did not express miR-455 (Figure 4.1A). To check the purity of articular cartilage, bone marker genes (COL1A1 and TRAP) and cartilage marker genes (COL2A1 and ACAN) were measured against bone samples (Figure 4.1C, D). The results demonstrated that the articular cartilage samples expressed minimal bone marker genes but significant cartilage marker genes. From this, it

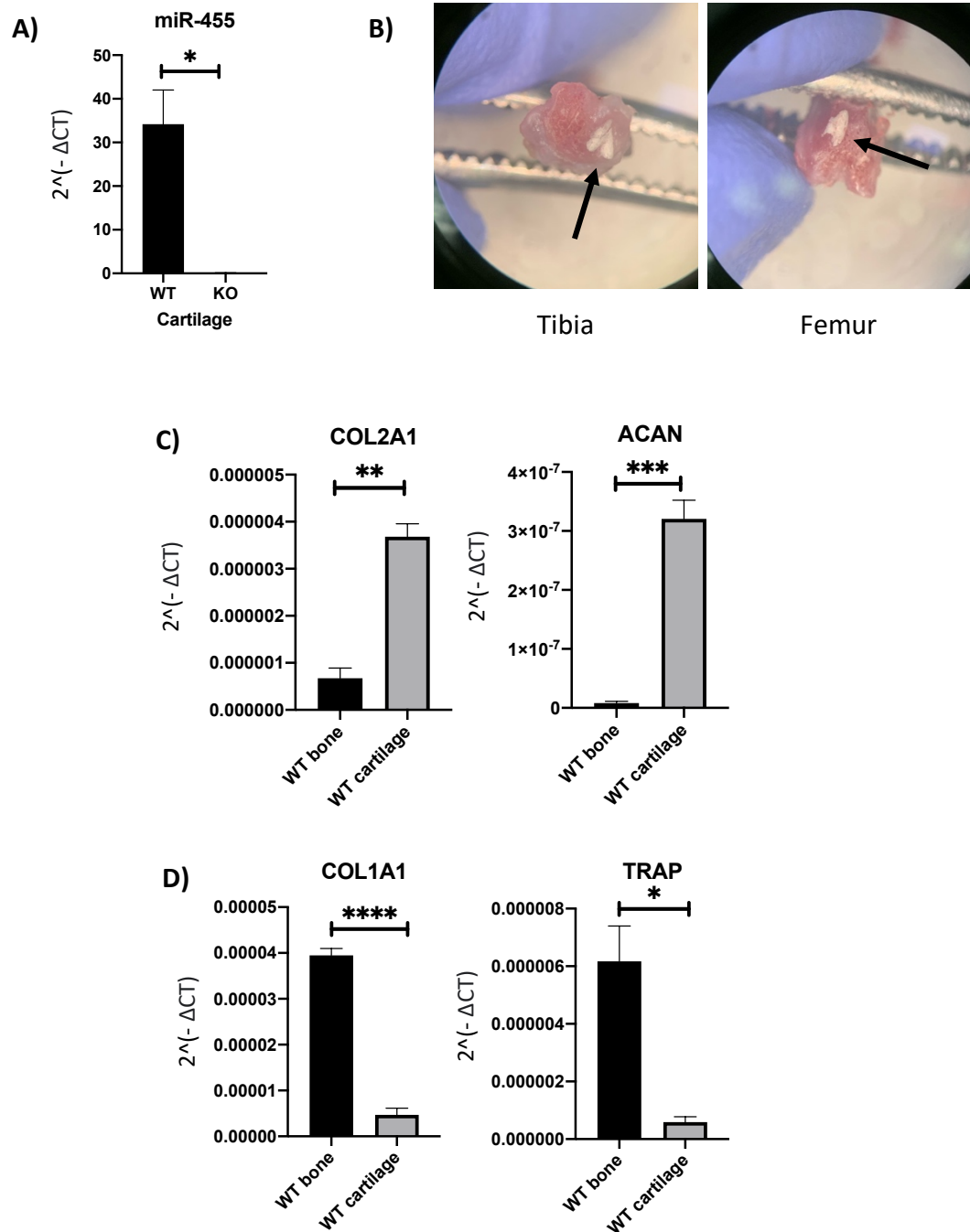


Figure 4.1: Mouse articular cartilage microdissection. (A) miR-455 expression levels in WT and miR-455 KO articular cartilage samples measured by qPCR. (B) Articular cartilage microdissection technique from mouse tibia (left) and femur (right). Arrows indicate articular cartilage that has been removed. (C) Cartilage marker gene expression genes COL2A1 and ACAN in mouse bone and micro dissected articular cartilage samples. (D) Bone marker gene expression genes COL1A1 And TRAP in mouse bone and micro dissected articular cartilage samples ($n=3$, $p<0.05$, error bars +/- SEM).

can be concluded that the samples contain almost pure articular cartilage without bone contamination.

4.2.2. miR-455 null cartilage mRNA-seq

Following mRNA-seq of WT and miR-455 articular cartilage samples (n=3), analysis showed that in some cases, the changes in differentially expressed (DE) genes are quite subtle and most are lowly expressed. For DE genes ($q \leq 0.05$), there were a total of 28 DE genes, of which 22 were upregulated (Figure 4.2B). The PCA plot indicated that there is not a lot of separation between gene expression within the WT and KO samples (Figure 4.2A). Despite this, for DE genes ($q \leq 0.05$), GO analysis revealed enrichment across all GO categories indicating an enrichment for genes involved in different biological processes, cellular components and molecular functions (Figure 4.2C). Within this set of genes, biological processes involved in chondrocyte differentiation, cartilage morphogenesis, endochondral bone growth, and extracellular matrix organization are enriched (Table 4.1, Table 4.2). These genes include COL6A1, COL6A2, COL14A1, LOXL2, AEBP1, and VCAN (Figure 4.3).

This data set was also analyzed to identify DE expressed genes ($p \leq 0.05$) between miR-455 KO articular cartilage and WT articular cartilage. The analysis identified 872 DE genes, of which 323 were downregulated in miR-455 KO samples (Figure 4.4A). GO analysis also showed greater enrichment for genes (Figure 4.4B). Within this data, biological processes with genes significantly upregulated in miR-455 KO articular cartilage include ECM organisation, chondrocyte/ cartilage development (including growth plate cartilage), chondrocyte differentiation, endochondral bone growth, and metabolism of collagen. Similar gene enrichment was observed in molecular functions and cellular components such as ECM structure and binding. Examples of genes involved in these processes include ACAN, COL2A1, COL10A1, SOX9 (cartilage markers), and COL1A1, ALPL, TRAP1, RUNX2 (bone markers) (Figure 4.5). RNA-seq data was validated by qPCR (Appendix 9 and 10).

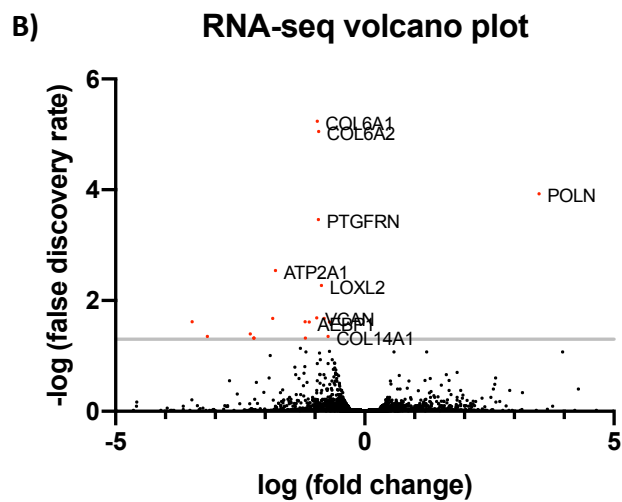
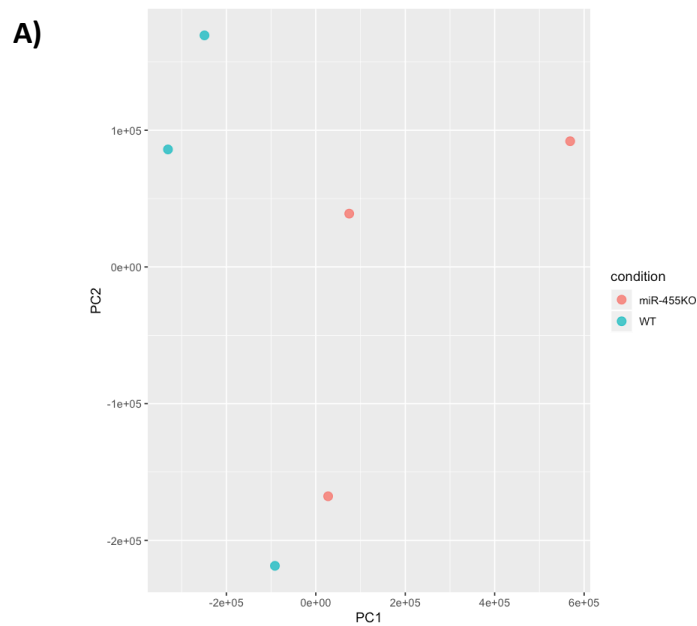


Figure 4.2: miR-455 null cartilage RNA-seq data analysis. A) PCA plot demonstrating that there is little separation between WT (blue) and miR-455 KO (red) cartilage samples. B) RNA-seq volcano plot showing differentially expressed ($q \leq 0.05$) genes, of the 28 DE genes, 22 genes were significantly upregulated and 3 downregulated.

Table 4.1: Table of significantly ($q \leq 0.05$) upregulated genes in miR-455 KO cartilage samples with enrichment for biological processes. Overlapping genes are highlighted in bold.

| Biological Processes | Gene |
|---|--|
| Chondrocyte morphogenesis GO:0090171 | COL6A1, COL6A2, COL14A1 |
| Extracellular matrix organization GO:0030198 | COL6A1, COL6A2, LOXL2, VCAN, AEBP1, COL14A1 |
| Growth plate cartilage chondrocyte differentiation GO:0003418 | COL6A1, COL6A2, COL14A1 |
| Cartilage morphogenesis GO:0060536 | COL6A1, COL6A2, COL14A1 |
| Chondrocyte differentiation involved in endochondral bone morphogenesis GO:0003413 | COL6A1, COL6A2, COL14A1 |
| Chondrocyte differentiation GO:0002062 | COL6A1, COL6A2, LOXL2, COL14A1 |
| Endochondral bone growth GO:0003416 | COL6A1, COL6A2, COL14A1 |
| Collagen fibril organization GO:0030199 | LOXL2, AEBP1, COL14A1 |

Table 4.2: Table of significantly ($p \leq 0.05$) upregulated genes in miR-455 KO cartilage samples with enrichment for endochondral-related human phenotype ontologies.

| Human Phenotype Ontology | Gene |
|-------------------------------|--|
| Abnormality of lower limb | COL6A1, COL6A2, AEBP1, FN1, LIFR, DDR2, FBN1, BGN, EVC, PRDM5, SERPINF1, MYO9A, TNNI2, CAV1, ACTA1, COL2A1, SH3PXD2B, PLOD1, ANTXR1, DST, COL6A3, TNNT3, DYNC2LI1, ABCC9, TRPS1, COMP, TWIST1, ERLIN2, FLNB, COL1A1, HOXA11, RPS6KA3, GMPPB, CCN2, COL3A1 |
| Abnormal diaphysis morphology | FN1, LIFR, DDR2, FBN1, BGN, EVC, ACTA1, COL2A1, SH3PXD2B, SERPINH1, SGMS2, ALPL, P4HB, AIP, DYNC2LI1, TRPS1, COMP, FLNB, COL1A1, HOXA11, RPS6KA3, FAM20C |
| Platyspondyly | DDR2, BGN, KCNJ8, COL2A1, SERPINH1, SGMS2, ALPL, SPARC, ABCC9, PLOD3, COMP, FLNB, COL1A1 |

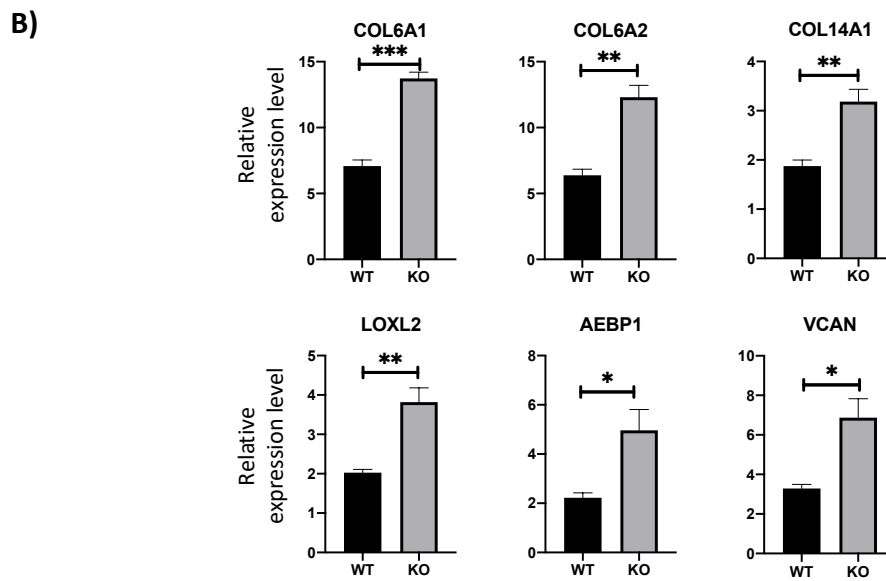
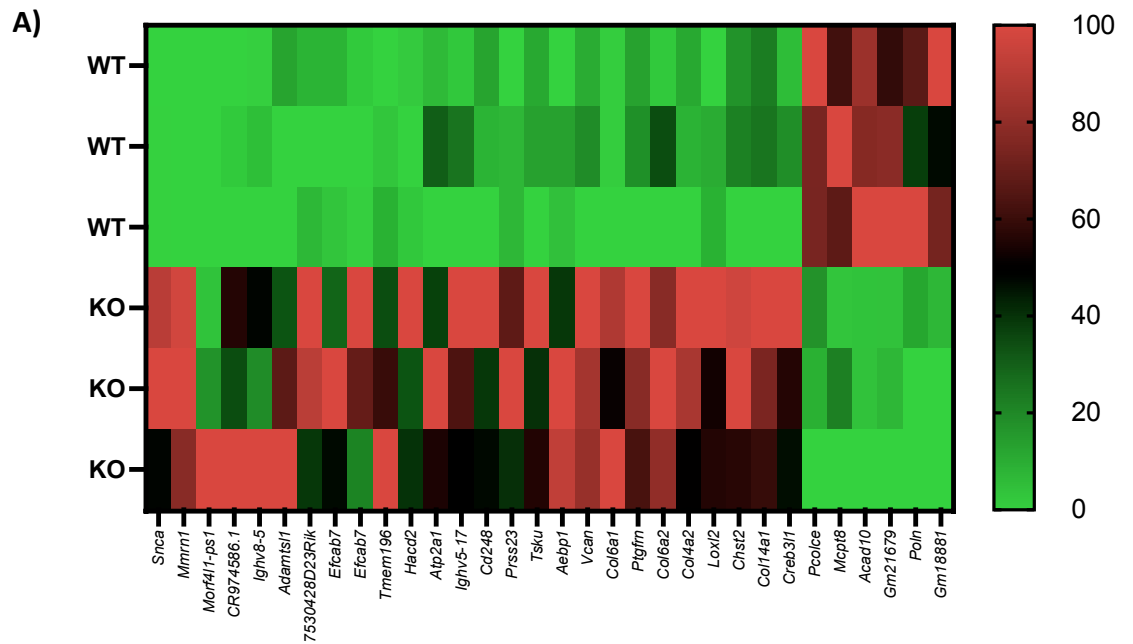


Figure 4.3: miR-455 null cartilage RNA-seq data ($q \leq 0.05$). A) Heat map showing differentially expressed ($q \leq 0.05$) genes between miR-455 KO and WT cartilage. B) RNA-seq analysis of genes significantly ($q \leq 0.05$) upregulated in miR-455 KO cartilage involved in endochondral biological processes.

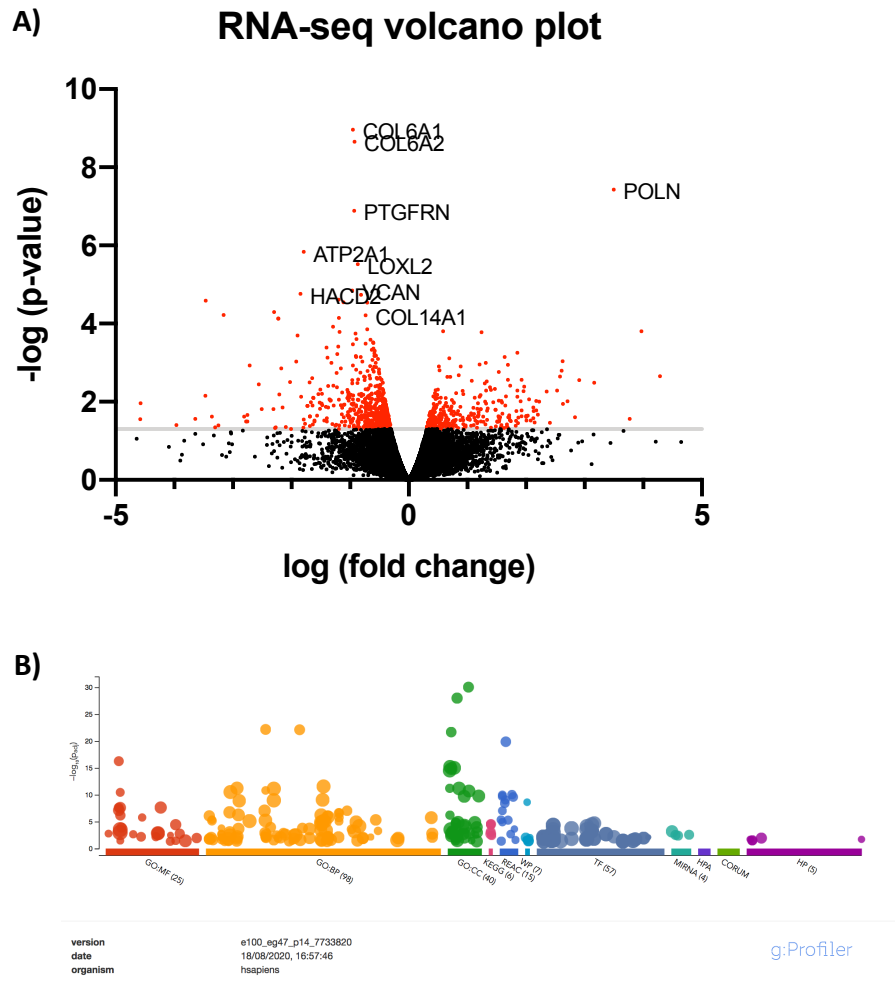


Figure 4.4: miR-455 null cartilage RNA-seq data ($p \leq 0.05$). A) RNA-seq volcano plot showing differentially expressed ($p \leq 0.05$) genes, of the 872 DE genes, 549 genes were significantly upregulated and 323 downregulated. B) GO analysis of significantly ($p \leq 0.05$) upregulated genes in miR-455 KO cartilage samples indicates enrichment in all categories indicating an enrichment for genes involved in different biological processes (orange), cellular components (green) and molecular functions (red).

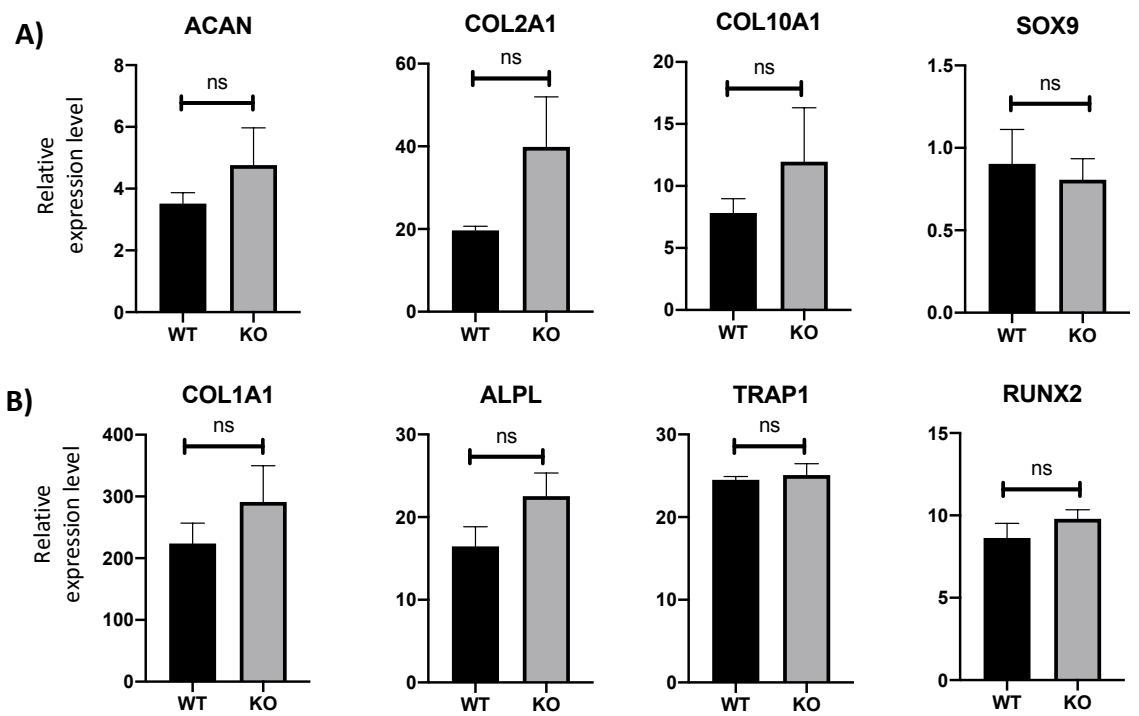


Figure 4.5: RNA-seq data showing upregulated genes ($p \leq 0.05$) in miR-455 null articular cartilage. (A) Cartilage marker genes ACAN, COL2A1, COL10A1 and SOX9 are upregulated in the miR-455 KO articular cartilage compared with WT control. (B) Bone marker genes COL1A1, ALPL, TRAP1 and RUNX2 are also upregulated in the miR-455 KO articular cartilage compared with WT control.

4.2.3. mRNA-seq overexpressing and inhibiting miR-455 in SW1353 cells

To enhance this data further, *in vitro* studies were performed using the SW1353 cell line. Cells were transfected with either a miR-455 mimic or inhibitor and compared with controls. For each sample group, expression of miR-455-3p was measured using qPCR to validate mimic or inhibitor efficacy (Figure 4.6A). These samples (n=3) were used for mRNA-seq and the PCA plot demonstrated separation between groups (Figure 4.6B). Volcano plot analysis revealed that overexpression of miR-455 in cells resulted in 522 DE genes ($q \leq 0.1$), of which 404 were upregulated and 118 downregulated (Figure 4.6C). For samples where miR-455 was inhibited, 657 DE genes were identified, where 328 were upregulated and 329 downregulated (Figure 4.6D). Interestingly, miR-455 overexpression resulted in more upregulated genes than downregulated, whereas inhibiting miR-455 resulted in a similar number of DE genes both upregulated and downregulated. From this data, GO analysis revealed enrichment in all categories. Surprisingly, the groups of DE genes with GO enrichment were genes upregulated ($q \leq 0.1$) in miR-455 mimic cell samples and genes downregulated ($q \leq 0.1$) in miR-455 inhibitor cell samples (Figure 4.7).

4.2.4. Downregulating miR-455 results in skeletal system development phenotype

In order to combine this data, comparison of DE genes with expression 'upregulated in miR-455 KO articular cartilage', 'upregulated in SW1353 cells transfected with miR-455 inhibitor', and 'downregulated in SW1353 cells transfected with miR-455 mimic' was analysed. This was to identify potential targets of miR-455, since such target gene expression level could increase in response to a miR-455 inhibitor/knockout and decrease in response to a miR-455 mimic. Although no overlap between all 3 data groups was observed, 16 DE genes overlapped between both 'up in KO' and 'up in inhibitor' samples (Figure 4.7). Using GO analysis, this set of DE genes showed enrichment for 'skeletal system development' and 'collagen-containing extracellular matrix' (Table 4.3). These genes included FGF8, COL3A1, TIMP1, PHOSPHO1, SNAI1, PRELP and ANXA4, where heat map analysis demonstrates increased expression levels in miR-455 KO cartilage compared to WT, and SW1353 cells transfected with miR-455 inhibitor compared to control.

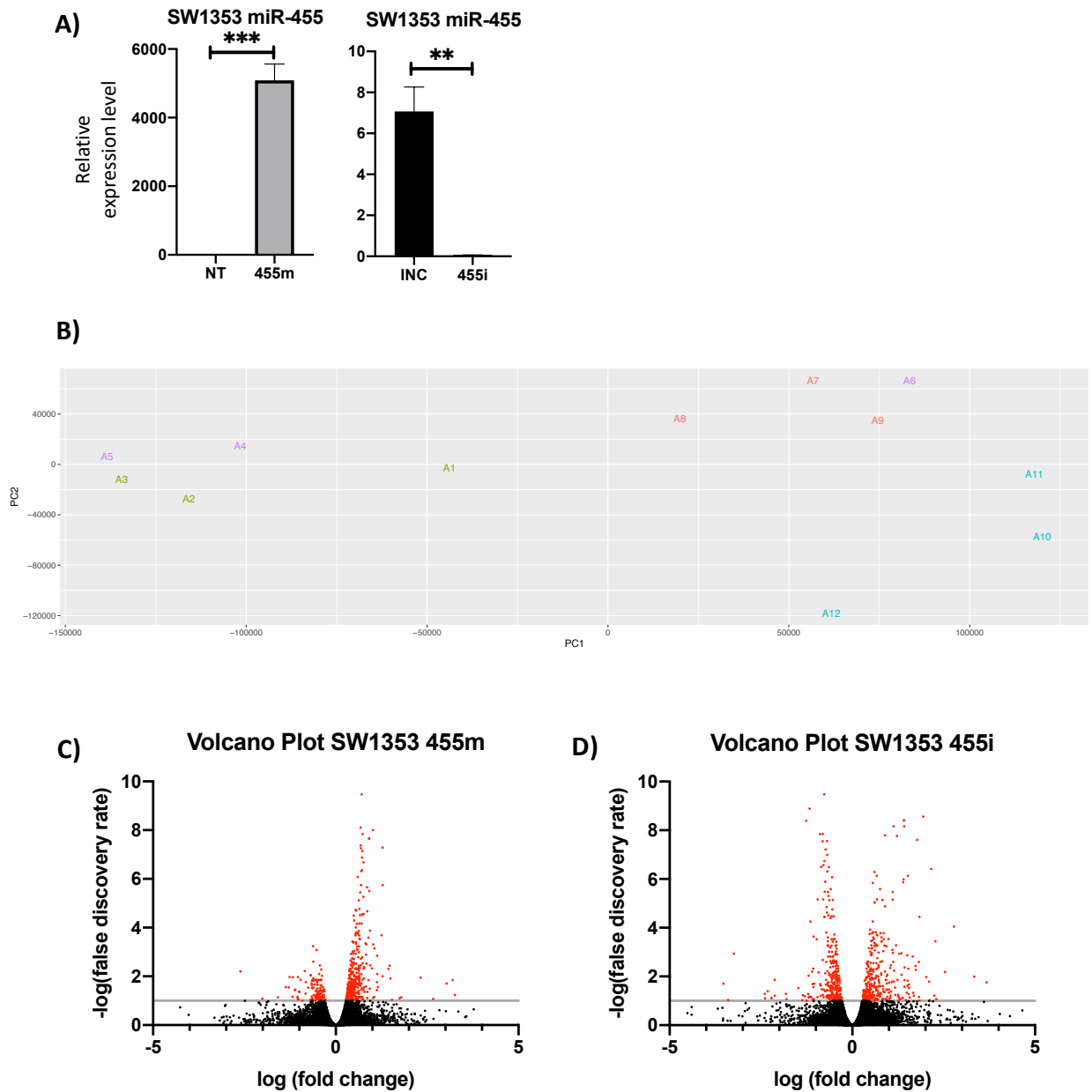


Figure 4.6: RNA-seq data showing genes ($q \leq 0.1$) in SW1353 cells transfected with miR-455 mimic and inhibitor. (A) miR-455 expression in RNA-seq samples. (B) PCA plot demonstrating separation between SW1353 control and +/- miR-455 samples (red = inhibitor control, green = mimic control, blue = miR455 inhibitor, purple = miR455 mimic). (C) RNA-seq volcano plot showing miR-455 mimic differentially expressed ($q \leq 0.1$) genes, with 404 genes significantly upregulated and 118 downregulated. (D) RNA-seq volcano plot showing miR-455 inhibitor differentially expressed ($q \leq 0.1$) genes, with 328 genes significantly upregulated and 329 downregulated.

Table 4.3: Table of gene ontology for common genes combining RNA-seq data from SW1353 cells +/- miR-455 ($q \leq 0.1$) and miR-455 KO cartilage ($p \leq 0.05$), revealing enrichment for skeletal phenotypes.

| Gene ontology | Gene |
|--|---|
| Skeletal system development GO:0001501 | <i>FGF18, COL3A1, TIMP1, PHOSPHO1, SNAI1, PRELP</i> |
| Collagen-containing extracellular matrix GO:0062023 | <i>COL3A1, TIMP1, PHOSPHO1, ANXA4, S100A10</i> |

4.3. Discussion

This data demonstrates that miR-455-3p could play a role in cartilage and osteochondral development. RNA-seq from miR-455 KO mouse articular cartilage indicates that DE genes resulting from a knockout of miR-455 are implemented in biological processes involved in chondrocyte differentiation, cartilage morphogenesis, endochondral bone growth, and extracellular matrix organization. Analysis also identified enrichment for genes associated with abnormality of the limb. Interestingly, these genes are upregulated in the miR-455 KO cartilage, suggesting that a knockout of miR-455 could upregulate osteochondral-related processes.

When combining this data with RNA-seq from SW1353 cells either overexpressing or inhibiting miR-455, DE genes upregulated in miR-455 KO cartilage and miR-455 inhibited cells were associated with skeletal system development and collagen-containing extracellular matrix. This supports hMSC data, where an overexpression of miR-455 resulted in a downregulation of chondrogenic gene markers. Although specific genes have been identified as upregulated or downregulated by miR-455 overexpression or downregulation, the regulatory mechanisms implemented by miR-455 are unclear. It is important to identify possible miR-455 targets and their downstream effects.

From this data, it can be concluded that miR-455 has a role in cartilage, particularly during chondrogenic development. To explore this further, studying miR-455 within a developmental model will provide more details on the mechanisms regulated by miR-455 during skeletal development.

Chapter 5

***Limb bud development and
microRNA-455-3p***

5. Limb bud development and microRNA-455-3p

5.1. Introduction

Previous experiments have indicated a role for miR-455-3p in the developing skeletal system. Combining RNA-seq data from both miR-455-3p knockout mice and SW1353 cells transfected with a miR-455-3p inhibitor revealed upregulation of genes for the GO terms “skeletal system development” and “collagen-containing ECM”. This dysregulation of genes as a result of altered miR-455-3p levels suggest a role for miR-455-3p in skeletal development. In addition to this, whole-mount in situ hybridisation demonstrates miR-455-3p expression in the developing limb of both chick and mouse embryo, particularly in the growth plate and perichondrium. Differentiation assays of mesenchymal stem cells also suggested potential implications on chondrogenesis and osteogenesis following miR-455-3p overexpression. To explore this further in a developmental system, the chick embryo was used due to its accessibility of the embryo and ability to withstand manipulative procedures, with the aim of identifying a role of miR-455-3p during limb bud development

5.2. Results

5.2.1. Overexpression of miR-455 inhibits chick limb bud formation

Chick embryos were microinjected in the right-side anterior limb buds with either Scrambled sequences (AM-Scr) for control, antagomir-455 (AM-455), or miR-455 mimic (miR455m). Starting at the top of the limb bud, 3-5 injections were made down the limb bud at HH18-19 and imaged 24 hours after injection. Images demonstrated no apparent difference in the limb bud development between AM-455 and AM-Scr injected embryos, however, a reduction in the limb bud size of 455m injected embryos was observed and a delay in limb bud development compared with control embryos (Figure 5.1). After 24 hours, at HH24-25, embryos demonstrated approximately a 30% decrease in limb bud size of 455m samples compared with both AM-455 and AM-Scr, and similarly after 48 hours at HH27-28 (Figure 5.2).

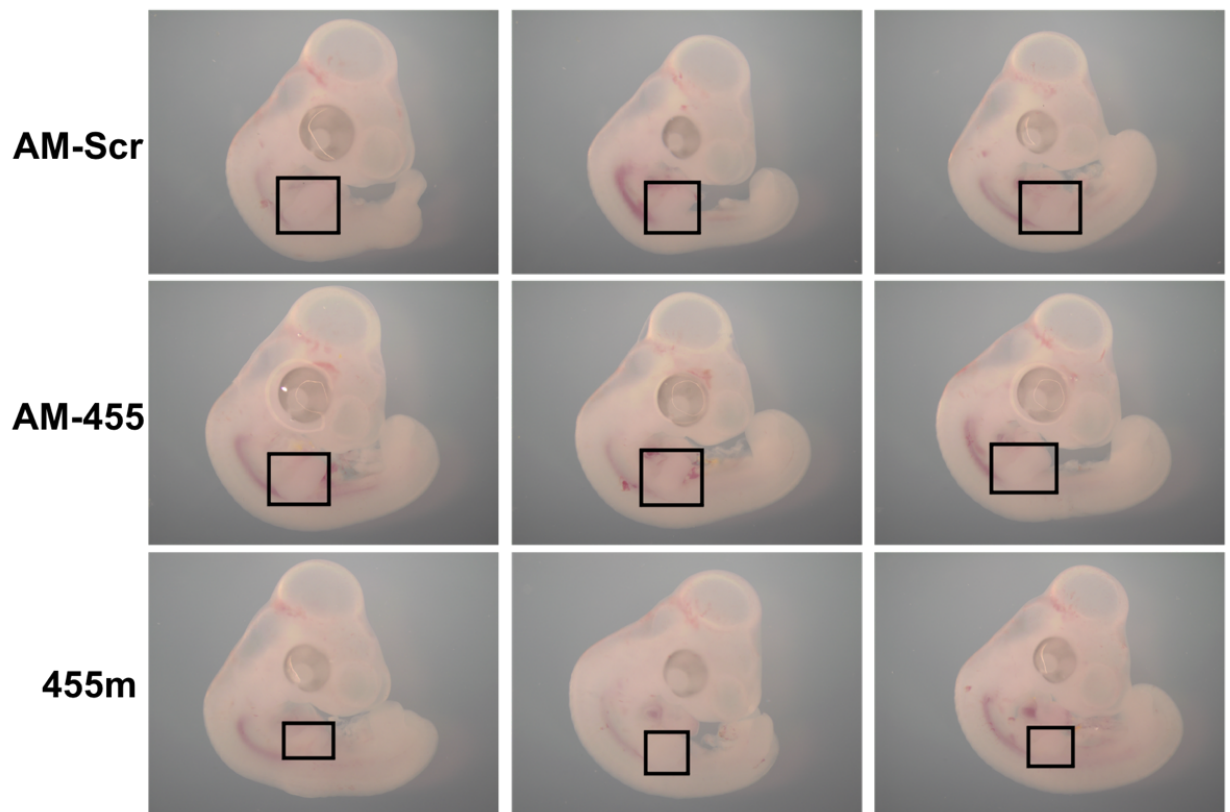


Figure 5.1: Microinjection of miR-455-3p mimic and antagomir into the developing chick limb bud. A) Images taken of chick embryo 24hr after microinjection of AM-Scr, AM-455 or 455 mimic at HH24-25 (total n=27, n=9 per condition). Black boxes indicate relative limb bud size, the area of these boxes were measured and an average for each condition calculated. These results indicated approximately a 30% decrease in limb bud size when miR-455 is overexpressed compared with control.

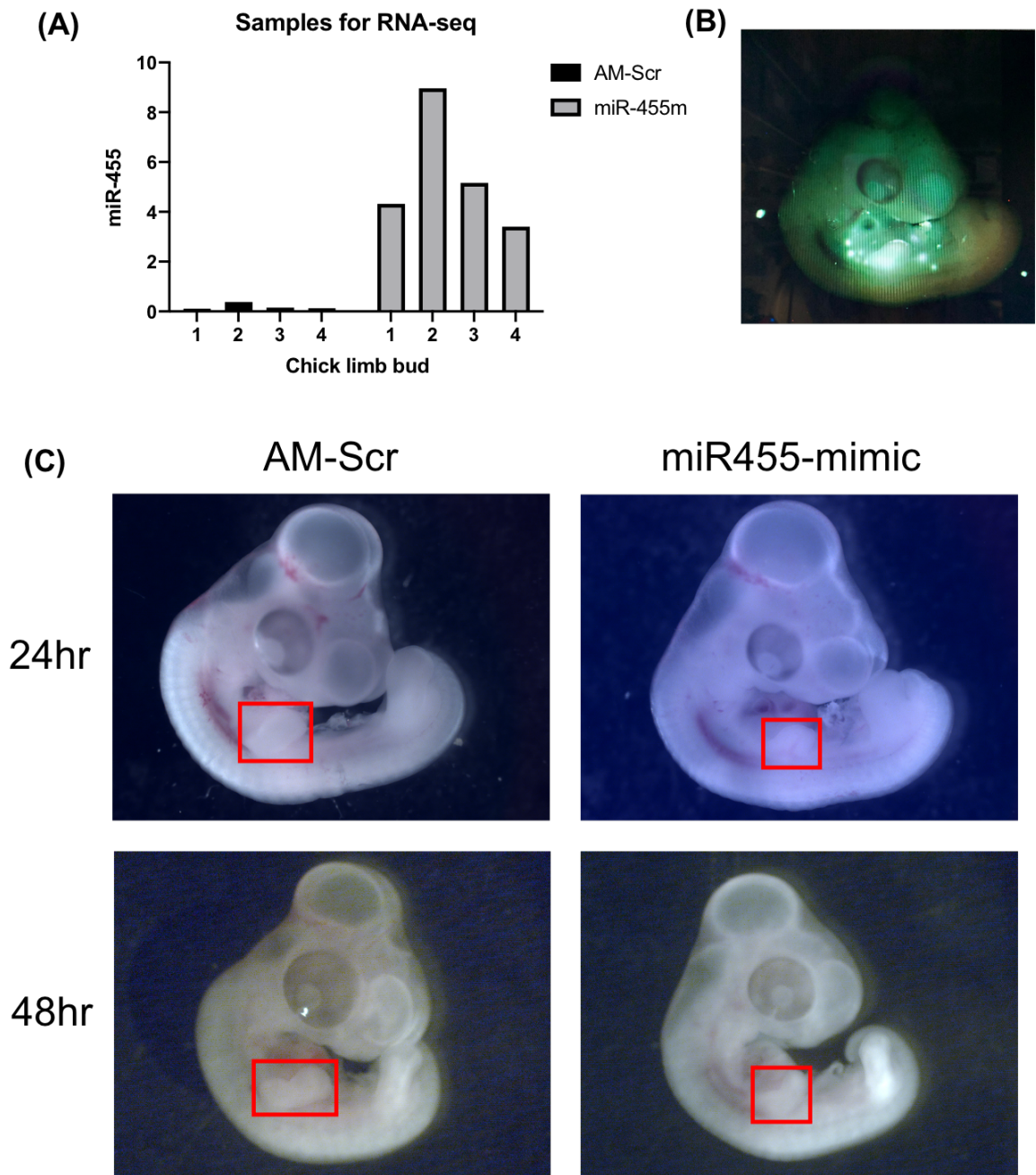


Figure 5.2: Overexpression of miR-455-3p inhibits chick limb bud formation. A) Expression of miR-455-3p in AM-Scr control samples and miR-455 overexpression limb bud samples used for RNA-seq. B) GFP-tagged miR-455 probe visualisation showing localization in limb bud. C) Chick embryo images indicating smaller limb bud size in limb buds overexpressing miR-455 compared to control at 24hr (HH24-25) and 48hr (HH27-28) post-microinjection. These results indicated approximately a 30% decrease in limb bud size when miR-455 is overexpressed compared with control at both 24hr and 48hr.

RT-qPCR confirmed an increased in miR-455-3p in limb buds injected with 455m compared to AM-Scr, and 4 samples of each condition were used for mRNA-seq (n=4). The PCA plot showed separation between the two groups. Initial bioinformatic analysis identified 2842 differentially expressed (DE) genes ($p \leq 0.05$), of which 1630 genes were upregulated in the 455m samples and 1212 genes downregulated in the 455m samples compared to AM-Scr control (Figure 5.3). Gene Ontology (GO) analysis showed enrichment in all categories including Molecular Function, Cellular Components, and Biological Pathways. Interestingly, Human Phenotype Ontology analysis of downregulated genes in 455m samples showed enrichment for genes involved in Brachydactyly (HP:0001156), a shortening of the fingers and toes due to unusually short bones, and Polydactyly (HP:0010442), additional fingers or toes, indicating a skeletal development phenotype (Table 5.1). Within significantly upregulated genes from 455m limb buds, enrichment for genes involved in Global developmental delay (HP:0001283) were reported.

5.2.2. Dysregulation of development-related signalling pathway genes

Signalling pathways are essential during development, and it is important that these remain regulated correctly in order for normal development to proceed. Within the developing limb bud, these include Wnt/ β -Catenin, Hedgehog (Hh), TGF β (transforming growth factor-beta) and BMP (bone morphogenic protein), and FGF (fibroblast growth factor) signalling pathways. Within the RNA-seq data, many genes involved in these pathways are dysregulated when miR-455 is overexpressed (Figure 5.4). For example, WNT2, 3A, 4, 6, and 10A are all significantly upregulated ($p \leq 0.05$) in 455m samples compared with AM-Scr. Another WNT related gene, DKK3 (Dickkopf WNT Signalling Pathway Inhibitor 3), is significantly downregulated in the presence of miR-455 mimic.

When miR-455 is overexpressed, there are also many differentially expressed genes involved in the Hh pathway, in particular Sonic Hedgehog (Shh) which is significantly upregulated. In addition to this, GLI1 (GLI Family Zinc Finger 1) is upregulated in response to miR-455 overexpression, whereas GLI3 (GLI Family Zinc Finger 3) is downregulated, both GLI1 and GLI3 have been linked to polydactyly phenotypes (294–297). Other dysregulated Hh pathway related genes include upregulated PTCH2 (Patched 2) and SMO

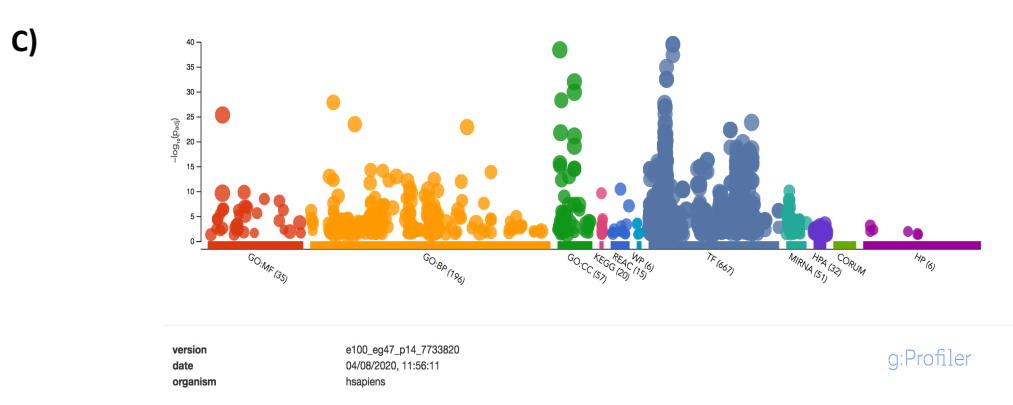
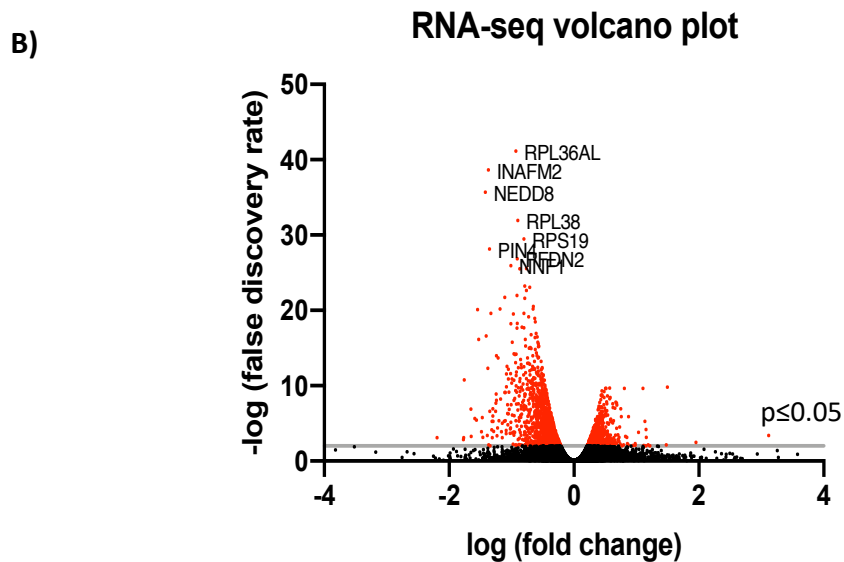
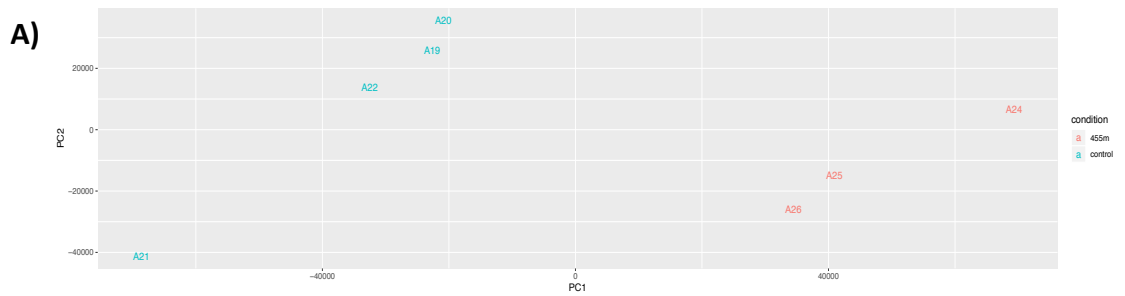


Figure 5.3: RNA-seq data from chick limb bud overexpressing miR-455-3p. A) PCA plot showing clustering of samples from miR-455 mimic and AM-Scr control, indicating separation in gene expression profiles. B) RNA-seq volcano plot. Data points in red indicate DE genes ($p \leq 0.05$). C) GO analysis of differentially expressed ($p \leq 0.05$) genes shows enrichment in all categories suggesting an enrichment for genes involved in different biological processes (orange), cellular components (green) and molecular functions (red).

Table 5.1: RNA-seq data from chick limb bud overexpressing miR-455-3p. DE genes ($p \leq 0.05$) demonstrate enrichment for genes involved in brachydactyly and polydactyly, both phenotypes related to limb development.

| Human Phenotype Ontology | Gene |
|-----------------------------|--|
| Brachydactyly HP:0001156 | <i>TRIP11, ATRX, KIAA0753, RIN2, ADNP, KAT6B, SOS1, RB1, AKT1, PIK3CA, EIF2AK3, BBS5, TRPS1, DYNC2H1, WDR60, GHR, GNAS, MAP3K7, OFD1, CDH11, SOS2, EVC, LZTFLI1, SMC3, TRIO, PCNT, LBR, CUL4B, ARID2, SHOC2, RAD21, MBTPS1, LIG4, ATP7A, KIF15, WASHC5, IFT140, FAM149B1, NEK1, RERE, EVC2, SIK3</i> |
| Polydactyly HP:0010442 | <i>KIAA0753, AKT3, ADNP, PIK3CA, BBS5, FAM92A, DYNC2H1, AHI1, WDR60, ARL13B, CC2D2A, OFD1, FLI1, EVC, LZTFLI1, JMJD1C, CENPF, PIBF1, LBR, ZNF423, WASHC5, IFT140, FAM149B1, CCND2, NEK1, FBLN1, RERE, CEP55, EVC2, TGFBR1</i> |

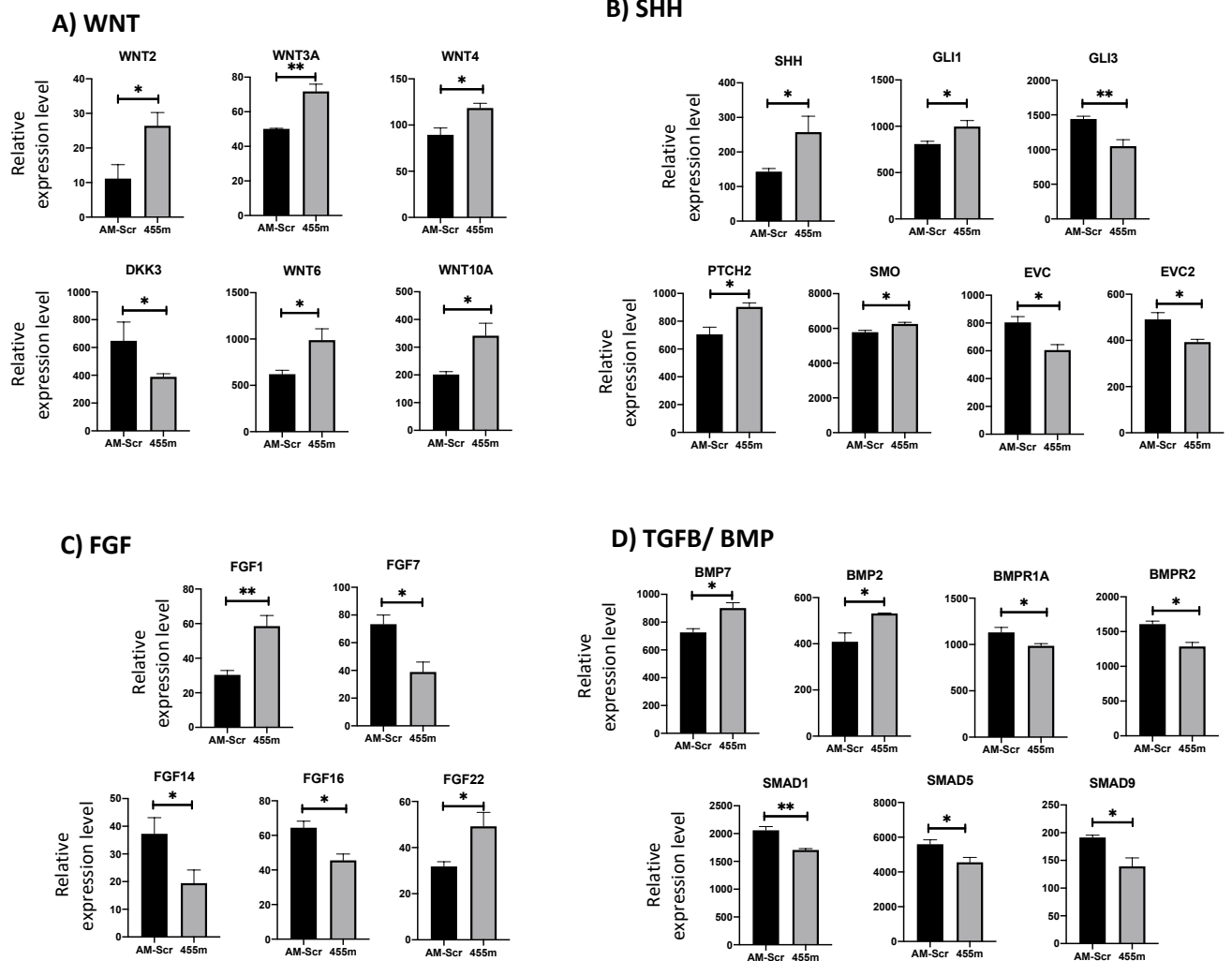


Figure 5.4: Dysregulation of development-related signalling pathway genes ($p \leq 0.05$) in limb buds overexpressing miR-455-3p. A) Wnt/ β -Catenin pathway-related genes. B) Sonic hedgehog (Shh) pathway-related genes. C) Fibroblast growth factor (FGF) pathway-related genes. D) Transforming growth factor-beta (TGF β) and Bone morphogenic protein (BMP) pathway-related genes.

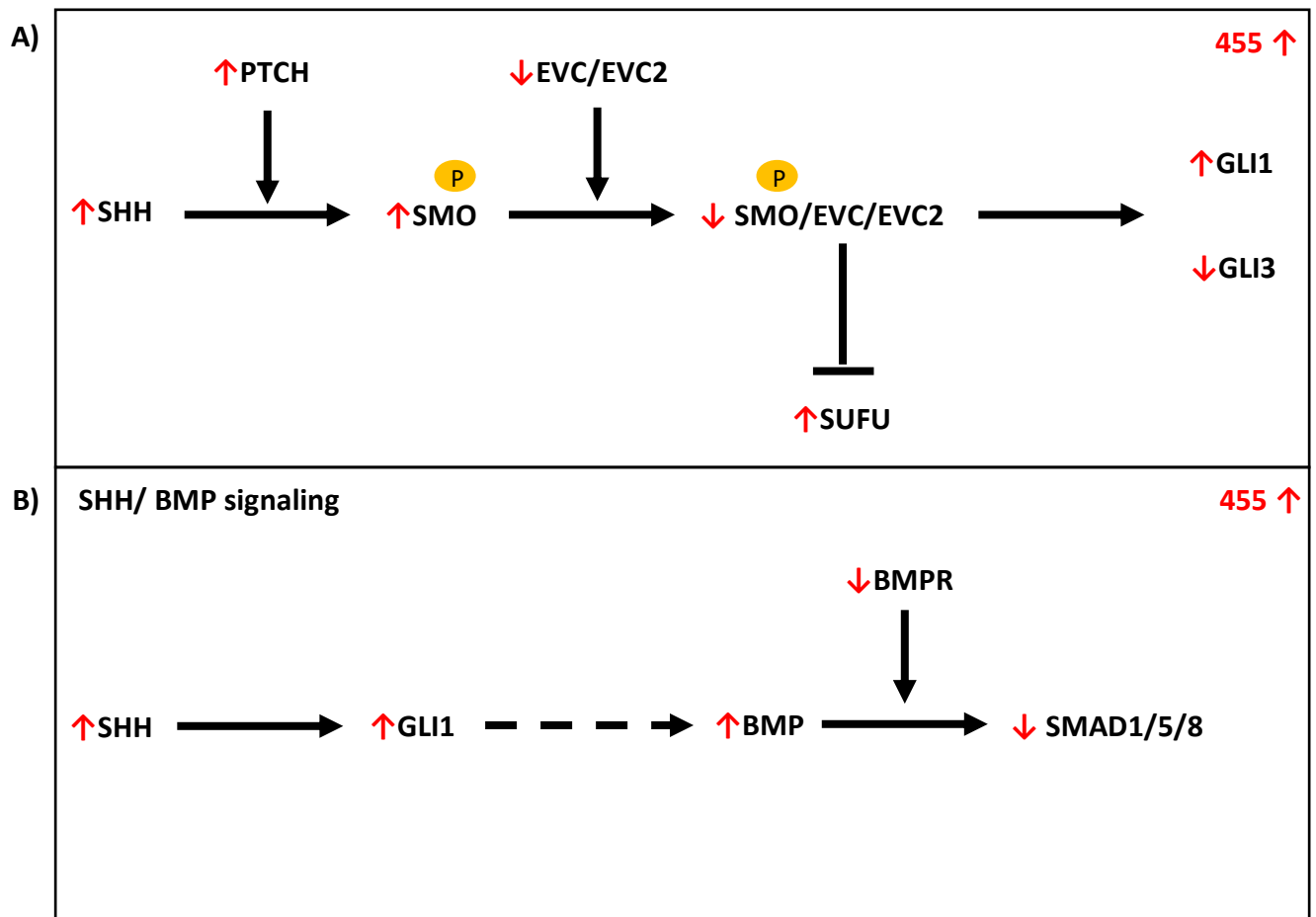


Figure 5.5: Combining development-related signalling pathways. A) Shh signalling molecule and the downstream pathway. The red arrows indicate the direction of gene expression level in response to miR-455 overexpression. Shh is upregulated in response to overexpressing miR-455. B) The Shh and BMP signalling pathway's form a signalling loop, and the mechanism for this is currently unknown (dotted line). From the gene expression results following miR-455 overexpression, it could be hypothesised that when miR-455 is overexpressed, the increase in GLI1 expression as a result of Shh upregulation may impact BMP and its downstream pathway during development.

(Smoothed, Frizzled Class Receptor), and downregulated EVC (EvC Ciliary Complex Subunit 1) and EVC2 (EvC Ciliary Complex Subunit 2), which function in bone formation, endochondral growth and skeletal development (298,299).

The TGF β / BMP signalling pathways have fundamental roles in both postnatal bone homeostasis and embryonic skeletal development (300). In chick limb buds overexpressing miR-455, BMP2 and BMP7 gene expression is upregulated, whereas BMPR1A and BMPR2 expression is downregulated. BMP2 is essential for skeletal development and regeneration, where dysregulation leads to skeletal anomalies (301) such as brachydactyly (302), and BMP7 has been associated with degradation of the ECM (303). Downstream of BMP receptors and ligands, SMAD1, 5 and 9 are all downregulated following overexpression of miR-455.

During vertebrate skeletal development, FGF pathways are essential in regulating limb bud development, including mesenchymal condensation, chondrogenesis, and osteogenesis (304). Overexpression of miR-455 in limb buds results in DE genes involved in FGF signalling pathways. For example, FGF7, 16, and 14 are downregulated and FGF1 and 22 are upregulated. The FGF family possess broad functions in embryonic development, and dysregulation of these genes may influence cell differentiation and proliferation (305).

These findings suggest that an overexpression of miR-455-3p may be detrimental to the developing limb. The altered expression of genes related to all developmental signalling pathways indicates that miR-455 plays a role in the regulation of skeletal development. A possible crosstalk between these signalling pathways creates a complex role for miR-455 regulation. The Shh and BMP signalling pathways form a signalling loop, and the mechanism for this is currently unknown. A proposed mechanism could be hypothesised that an overexpression of miR-455 increases GLI1 expression. Within this mechanism, GLI1 upregulation is a result of an increase in Shh, which forms a positive feedback loop with BMP (Figure 5.5). There are many aspects of the signalling involved in skeletal development that could be explored further, to identify the specific role of miR-455-3p.

Table 5.2: RNA-seq data showing disruption to cell cycle. GO analysis from chick limb bud overexpressing miR-455 compared to Scrambled control identified enrichment for biological processes including cell cycle (GO:0007049) and negative regulation of cell cycle (GO:0045786). The table illustrates differentially expressed genes within the samples.

| Biological Processes | Gene |
|---|---|
| Cell cycle GO:0007049 | WAC PPP1R12A USP8 ZMYND11 ATRX RHOA CCPG1 MDM1 DLG1 EML4 CCP110 SENP6 E2F8 EVI5 RIPK1 SASS6 PDS5B TET2 PER2 HBP1 LRRCC1 CNTRL CHMP2B CETN2 TSG101 RB1 CEP135 ROCK1 GTF2H1 BRCA2 ANLN PIAS1 CCNI DBF4 PARD6B SRPK2 PBRM1 TCF7L2 CNOT4 RAB11A NEDD9 KMT2E E2F6 USP3 OFD1 ERCC4 ATAD5 BACH1 CDK17 ARNTL NDE1 ORC5 SMC3 MDM2 CDC27 CENPF PIBF1 PCNT PDS5A CUL5 CUL4B LIMK2 POLE3 E2F5 FBXO7 TRAPPC12 CBX3 BCL2 PSMA1 KIF15 WASHC5 USP33 UBR2 SMARCA1 MSH4 UBE2E1 CCND2 TASOR NEK1 SMC4 NDC80 CDC14A TFDP1 SEPTIN10 EDN1 KIF1B ERN1 ITGB1 XPO1 MZT1 TAF2 CHFR SIAH1 WASL PKP4 AZI2 ANAPC10 |
| Negative regulation of cell cycle GO:0045786 | HEXIM1 RPL23 CDK2AP2 LAMTOR2 GAS2L1 PPP1R9B PSMC5 NOP53 CDK5 PSMD13 TAF6 RASSF1 APBB1 PSMB6 CDK2 SHFM1 CBX5 PSMD4 WDR76 MLST8 TIMELESS SIPA1 FANCD2 PEA15 RPL24 PSMD3 IK HTRA2 ESPL1 KAT2A BCL2L1 LAMTOR1 CDK5RAP3 PPM1G PSMA5 SLC9A3R1 PCNA E2F1 PSMB3 CDT1 PSMB4 PSMD11 CDC6 PSMC1 RAD51 TFAP4 TNKS1BP1 NAA10 PSMD9 MAD2L1 CHMP1A PSMD2 PSMB7 WDR6 PSMA3 PSMA7 CHMP2A AK1 SLC25A33 PSMD10 CDK9 BMP7 CALR PSMA4 AKT2 NABP2 RPA2 TBRG4 MIF TRIAP1 EME1 CAMK2N1 PSMD14 BLM HSP90AB1 EED CDK5RAP1 NUBP1 ANAPC15 ZNF385A BMP2 RBBP7 MYBBP1A CDK5R1 |

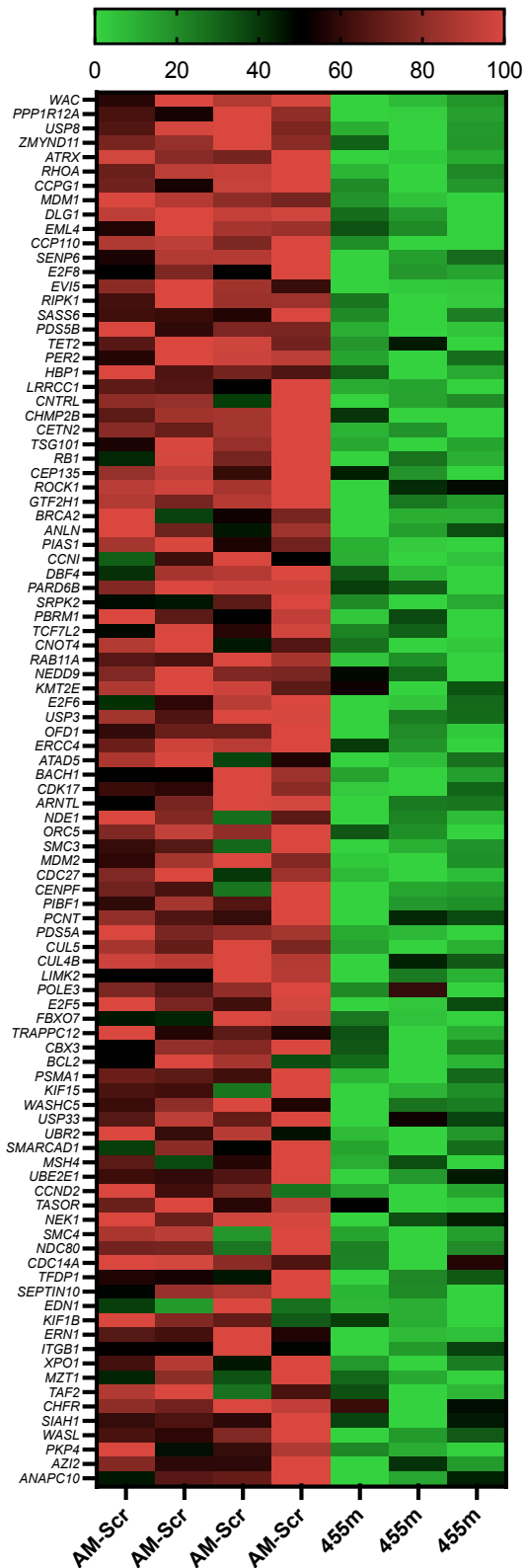


Figure 5.6: Heat map of differentially expressed genes ($p \leq 0.05$) identified by GO analysis associated with the cell cycle in limb buds overexpressing miR-455-3p compared with scrambled control. Genes are downregulated following overexpression of miR-455.

Table 5.3: RNA-seq data showing abnormal mitochondria and metabolism. GO analysis from chick limb bud overexpressing miR-455 compared to Scrambled control identified enrichment for human phenotype ontology including abnormality of the mitochondrion (HP:0012103) and abnormality of mitochondrial metabolism HP:0003287). The table illustrates differentially expressed genes within the samples.

| Human Phenotype Ontology | Gene |
|---|--|
| Abnormality of the mitochondrion HP:0012103 | <i>FUS, NDUFB3, NDUFA6, NDUFS6, NDUFA13, HSD17B10, MRPS14, OPA3, NDUFS2, HTRA2, ECHS1, GTPBP3, SLC25A4, ND6, NDUFV1, TXN2, FOXRED1, MICOS13, ATAD3A, NDUFS7, HADHA, ETFA, TIMM50, COX15, SDHD, HMGCL, NDUFB9, NDUFS8, NDUFA2, SDHA</i> |
| Decreased activity of mitochondrial respiratory chain HP:0008972 | <i>NDUFB3, NDUFA6, NDUFS6, NDUFA13, MRPS14, NDUFS2, ECHS1, GTPBP3, NDUFV1, TXN2, FOXRED1, NDUFS7, TIMM50, COX15, SDHD, NDUFB9, NDUFS8, NDUFA2, SDHA</i> |
| Abnormality of mitochondrial metabolism HP:0003287 | <i>NDUFB3, NDUFA6, NDUFS6, NDUFA13, MRPS14, OPA3, NDUFS2, HTRA2, ECHS1, GTPBP3, ND6, NDUFV1, TXN2, FOXRED1, MICOS13, ATAD3A, NDUFS7, HADHA, ETFA, TIMM50, COX15, SDHD, HMGCL, NDUFB9, NDUFS8, NDUFA2, SDHA</i> |

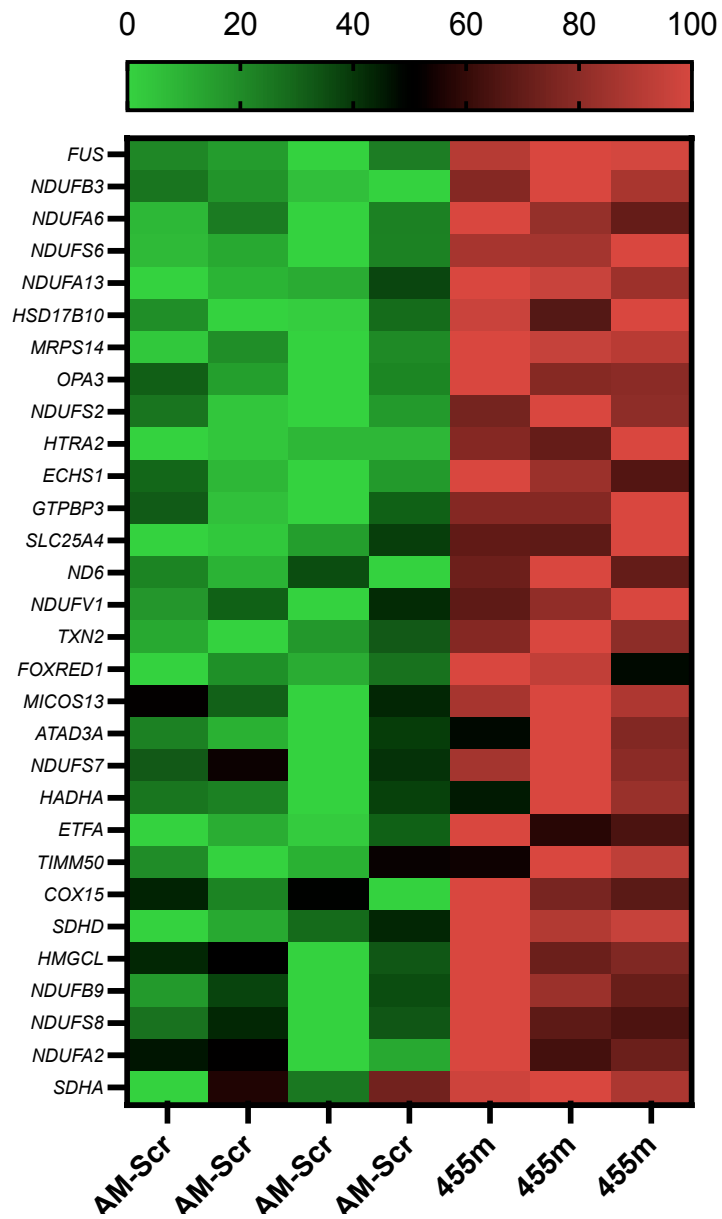


Figure 5.7: Heat map of differentially expressed genes ($p \leq 0.05$) identified by GO analysis associated with abnormal mitochondria in limb buds overexpressing miR-455-3p compared with scrambled control. Genes are upregulated following overexpression of miR-455.

5.2.3. Disruption to cell cycle and abnormal mitochondria

Further GO analysis revealed an enrichment for dysregulated genes associated with a disruption to the cell cycle in limb bud samples overexpressing miR-455-3p (Table 5.2). Differentially expressed genes were enriched for the GO biological processes terms cell cycle (GO:0007049) and negative regulation of cell cycle (GO:0045786), and also GO human phenotype ontology terms including abnormality of the mitochondrion (HP:0012103) and abnormality of mitochondrion metabolism (HP:0003287) (Table 5.3).

Heat map analysis revealed that differentially expressed genes ($p \leq 0.05$) associated with the cell cycle in limb buds overexpressing miR-455-3p were downregulated (Figure 5.6), whereas genes associated with abnormal mitochondria were upregulated (Figure 5.7). The phenotype observed in limb buds overexpressing miR-455-3p could be explained by an alteration to the cell cycle or abnormal mitochondria, phenotypes which are closely linked. When there is a disruption to the cell cycle or mitochondrial abnormality, this can result in reduced or delayed development and growth. An explanation for this could be that miR-455-3p targets a transcription factor that regulates these genes, as either a promoter of cell cycle-related genes or repressor of abnormal mitochondria-related genes.

5.2.4. miR-455-3p targets the transcription factor CREB1

Since there were many genes identified with enrichment associated with different biological processes, the next step was to explore common transcription factors within the data. The 2842 differentially expressed genes in developing limb buds overexpressing miR-455-3p were screened for transcription factors. Using *Transfac* transcription factor binding site predictions, CREB1 was identified as a common transcription factor. On further analysis, the downregulated genes involved in disruption to cell cycle all have a common promoter sequence for the transcription factor CREB1, motif: RTGACGYGT CAN (TF:M11221) (Table 5.4). As CREB1 expression is downregulated in limb buds as a result of miR-455-3p overexpression, *Target scan* was used to screen for binding sites. This screen revealed that CREB1 is a predicted target of miR-455-3p. To validate this, a luciferase assay was performed in the DF-1 chicken fibroblast cell line to confirm that CREB1 is a

target of miR-455-3p (Figure 5.8). For CREB1, following transfection, the expression of luciferase was decreased by overexpression of miR-455-3p which was then rescued by a mutation in the miR-455-3p target site within the UTR. This confirmed that CREB1 is a potential target of miR-455-3p. Therefore, the differentially expressed genes in response to an overexpression of miR-455-3p could be a result of downregulated expression of CREB1, where CREB1 acts as a transcriptional activator. If CREB1 regulates the expression of genes associated with the cell cycle, dysregulation of these genes due to a decrease in CREB1 could result in abnormalities.

Table 5.4: Downregulated genes ($p \leq 0.05$) identified by GO analysis associated with the cell cycle in limb buds overexpressing miR-455-3p were screened for common transcription factors and CREB1 was identified using Transfac transcription factor binding site predictions.

| Transcription factor | Gene |
|---|--|
| Factor: CREB1; motif: RTGACGYGTCAN TF:M11221 | WAC, PPP1R12A, USP8, ZMYND11, ATRX, RHOA, CCPG1, MDM1, DLG1, EML4, CCP110, SENP6, E2F8, EVI5, RIPK1, SASS6, PDS5B, TET2, PER2, HBP1, LRRCC1, CNTRL, CHMP2B, CETN2, TSG101, RB1, CEP135, ROCK1, GTF2H1, BRCA2, ANLN, PIAS1, CCNI, DBF4, PARD6B, SRPK2, PBRM1, TCF7L2, CNOT4, RAB11A, NEDD9, KMT2E, E2F6, USP3, OFD1, ERCC4, ATAD5, BACH1, CDK17, ARNTL, NDE1, ORC5, SMC3, MDM2, CDC27, CENPF, PIBF1, PCNT, PDS5A, CUL5, CUL4B, LIMK2, POLE3, E2F5, FBXO7, TRAPPC12, CBX3, BCL2, PSMA1, KIF15, WASHC5, USP33, UBR2, SMARCAD1, MSH4, UBE2E1, CCND2, TASOR, NEK1, SMC4, NDC80, CDC14A, TFDP1, SEPTIN10, EDN1, KIF1B, ERN1, ITGB1, XPO1, MZT1, TAF2, CHFR, SIAH1, WASL, PKP4, AZI2, ANAPC10 |

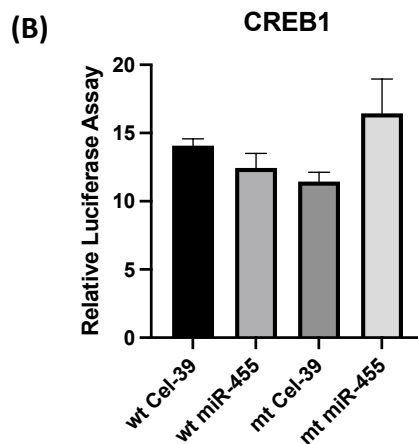
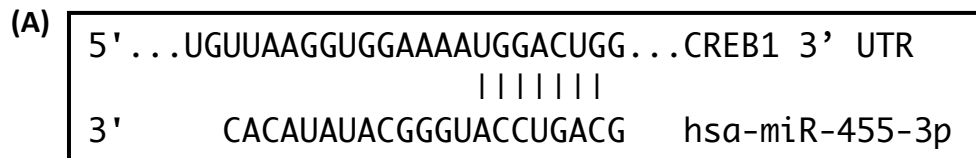


Figure 5.8: miR-455-3p targets CREB1. A) Target scan revealed that CREB1 is a predicted target of miR-455. B) Luciferase assay performed in the DF-1 cell line confirmed that miR-455 could directly target CREB1. The expression of luciferase was decreased by overexpression of miR-455-3p (wt miR-455) which was then rescued by a mutation in the miR-455-3p target site (mt miR-455) within the UTR. (n=3, error bars +/- SEM).

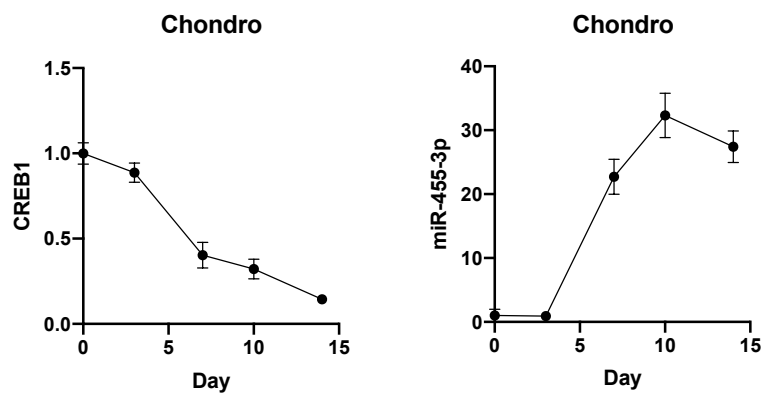


Figure 5.9: CREB1 during chondrogenesis. During chondrogenic differentiation of hMSCs, CREB1 expression and miR-455-3p expression were measured by qPCR at D0, D3, D7, D10 and D14. qPCR analysis showed that CREB1 expression decreases as chondrogenesis progresses, while miR-455-3p increases. (n=3, error bars +/- SD).

5.2.5. CREB1 siRNA phenocopies miR-455-3p in chondrogenesis

To explore the relationship between miR-455-3p and CREB1 during chondrogenesis, CREB1 expression was measured at Day 0, 3, 7, 10 and 14 using the chondrogenesis assay described in Chapter 2 (Figure 5.9). Initial analysis revealed that CREB1 expression was significantly higher at day 0 compared with day 14, demonstrating an opposite trend to miR-455-3p expression which increases from day 0 to day 14. During the chondrogenesis assay, CREB1 expression decreases whilst miR-455-3p expression increases from day 3. The most significant decrease in CREB1 expression is from day 3 to day 7, correlating with the most significant increase in miR-455-3p expression from day 3 to day 7. This supports CREB1 as a target of miR-455-3p, suggesting this interaction may have a role in chondrogenesis.

The role of miR-455-3p/CREB1 during chondrogenesis was investigated further using the hMSC chondrogenesis assay. hMSCs were transfected with either CREB1 siRNA to knockdown CREB1 expression, or miR-455-3p mimic to overexpress miR-455. As previously discussed (Figure 3.7), an overexpression of miR-455-3p resulted in a decrease in chondrogenic marker gene expression compared with control. This experiment was repeated in the same hMSC donor line using CREB1 siRNA and demonstrated that inhibiting CREB1 also resulted in a significant decrease in chondrogenic marker gene expression. As with miR-455 overexpression, this was most evident in SOX9 expression (Figure 5.10).

Although CREB1 decreases during chondrogenesis, these results indicate that CREB1 is required for the initiation of chondrogenic differentiation since siRNA knockdown resulted in a significant decrease in chondrogenic marker genes (Figure 5.10). As CREB1 siRNA phenocopies miR-455 mimic in transfected hMSCs, this could suggest that the miR-455 overexpression phenotype is a result of directly targeting the transcription factor CREB1 and the downstream effects on chondrogenesis. As miR-455-3p levels are low at the beginning of chondrogenesis, an overexpression of miRNA and therefore downregulation of CREB1 results in a decrease in chondrogenic marker gene expression and therefore may inhibit chondrogenesis. If the chondrogenesis assay were to be

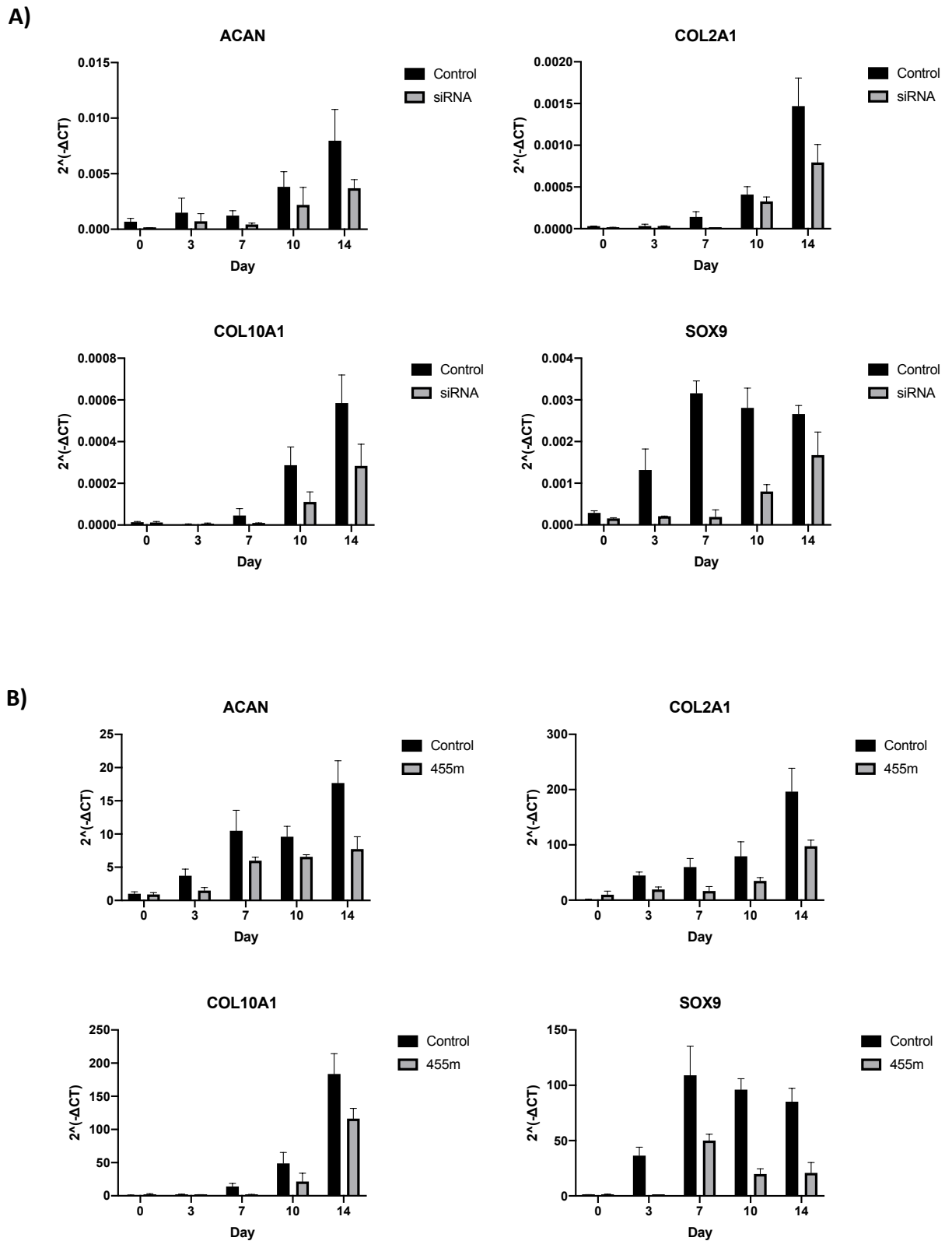


Figure 5.10: CREB1 siRNA phenocopies miR-455-3p in hMSC chondrogenesis. A) Chondrogenic marker gene expression during hMSC chondrogenesis assay, transfected with CREB1 siRNA compared to control. B) Chondrogenic marker gene expression during hMSC chondrogenesis assay, transfected with miR-455 mimic compared to control. Gene expression was measured for COL1A1, COL10A1, SOX9 and ACAN by qPCR. Results combine data from 3 biological replicates from 1 hMSC donor cell line (2802f). (n=3, P<0.05, error bars +/- SD).

extended after 14 days, this phenotype may be observed as a delay in chondrogenesis, as chondrogenic genes do increase but at a slower rate than control.

5.2.6. CREB1 siRNA phenocopies miR-455-3p in hMSC's

Following this, hMSC's were transfected with either CREB1 siRNA or miR-455-3p mimic and gene expression compared with control. The expression of dysregulated genes identified by RNA-seq were measured by qPCR (Figure 5.11). These included mitochondrial genes *NDUFA5*, *ND4*, *ND6*, *FOXRED1*, *COX15*, *TOMM40* and *TIMM50* which were upregulated in limb buds overexpressing miR-455-3p. In addition to this, hMSC's overexpressing miR-455 also resulted in an increase in *ND6*, *FOXRED1* and *COX15* gene expression. A similar increase in gene expression of *ND6*, *FOXRED1* and *COX15* was also observed in hMSC's with downregulated of CREB1 expression. *TOMM40* and *TIMM50* expression increased when miR-455 was overexpressed but decreased when CREB1 was inhibited. This could suggest that changed in *TOMM40* and *TIMM50* expression following overexpression of miR-455 is not related to a downregulation of its target CREB1. Although in hMSCs *NDUFA5* and *ND4* expression decreased in response to miR-455 mimic transfection, this expression pattern was also observed in hMSC's transfected with CREB1 siRNA, suggesting that overexpressing miR-455 and inhibiting CREB1 results in a similar phenotype.

The expression of cell cycle genes identified by RNA-seq were also measured in these samples (Figure 5.12). These genes, *E2F8*, *TFDP1*, *POLE3*, *BCL2*, *ORC5* and *CUL4B*, were downregulated in limb buds overexpressing miR-455-3p. In hMSC's, the overexpression of miR-455 by mimic transfection also resulted in a downregulation of the cell cycle-related genes with the exception of *CUL4B*. Additionally, a downregulation of these genes was observed in hMSC's transfected with CREB1 siRNA. This suggest that CREB1 siRNA phenocopies miR-455 mimic in hMSCs. The data indicates that changes in gene expression as a result of miR-455 overexpression may be due to miR-455 targeting and therefore downregulating CREB1 expression.

Within the Cyclic AMP (cAMP)/ PKA pathway, transcription is regulated by the direct phosphorylation of the transcription factors CREB, CREM, and ATF1 (306). Because of this,

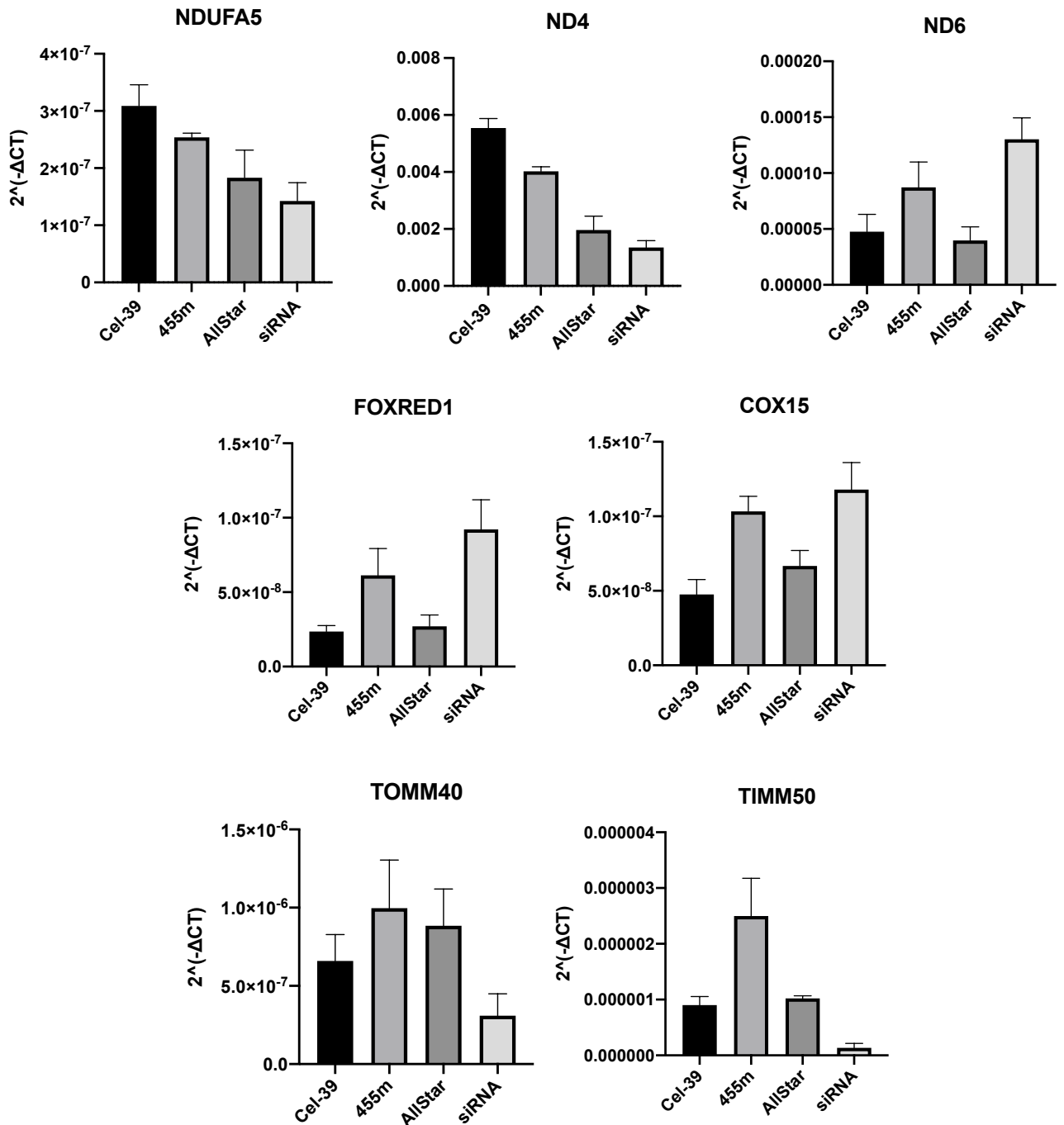


Figure 5.11: CREB1 siRNA phenocopies miR-455-3p in hMSCs. Mitochondrial gene expression was measured in hMSCs transfected with CREB1 siRNA compared to siRNA control (AllStar), and miR-455 mimic compared to mimic control (Cel-39). Gene expression was analysed for NDUFA5, ND4, ND6, FOXRED1, COX15, TOMM40 and TIMM50 by qPCR. All genes other than TOMM40 and TIMM50 followed similar expression patterns in hMSCs transfected with CREB1 siRNA and miR-455 mimic. Results combine data from 3 biological replicates from 1 hMSC donor cell line (2802f). (n=3, error bars +/- SEM).

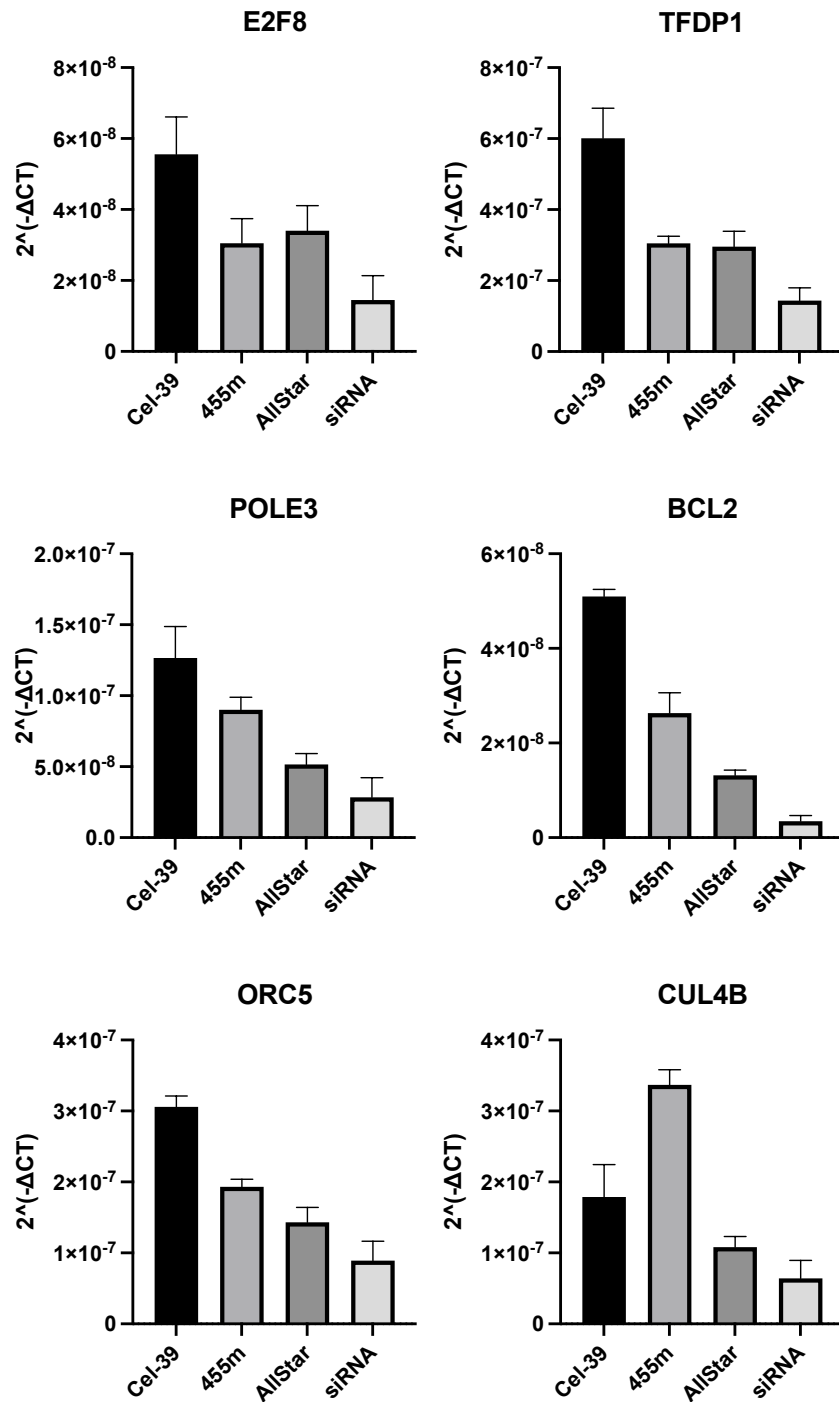


Figure 5.12: CREB1 siRNA phenocopies overexpression of miR-455-3p in hMSCs. Cell cycle gene expression was measured in hMSCs transfected with CREB1 siRNA compared to control, and miR-455 mimic compared to control. Gene expression was analysed for E2F8, TFDP1, POLE3, BCL2, ORC5 and CUL4B by qPCR. All genes other than CUL4B followed similar expression patterns in hMSCs transfected with CREB1 siRNA and miR-455 mimic. Results combine data from 3 biological replicates from 1 hMSC donor cell line (2802f). (n=3, error bars +/- SEM).

CREM and ATF1 (in addition to CREB1) expression levels were also measured in hMSCs transfected with either miR-455 mimic or CREB1 siRNA (Figure 5.13). The results confirmed that miR-455 overexpression and CREB1 siRNA downregulated CREB1 expression. This was also observed with CREM expression, where levels were lower in miR-455 mimic and CREB1 siRNA samples. ATF1 expression was not altered in response to miR-455 overexpression or CREB1 knockdown. These results suggest that overexpression of miR-455-3p may impact the cAMP pathway.

5.2.7. Skeletal tissues and CREB1

Within the 3 RNA-seq data-sets described in Chapter 4 and Chapter 5, CREB1 expression is consistent. Chick limb buds overexpressing miR-455-3p demonstrate a significant downregulation in CREB1 which is also observed in SW1353 cells transfected with miR-455 mimic (Figure 5.14). Although the expression of CREB1 is upregulated in miR-455 KO mouse articular cartilage, this is less significant. In these samples, overexpression of miR-455-3p has a greater effect than inhibiting miR-455, and this follows with previous experiments described in previous chapters, including hMSC chondrogenesis. The expression of CREB1 was also measured in both WT and miR-455 KO mouse bone samples. Interestingly, CREB1 expression was significantly upregulated in miR-455 KO samples, suggesting that downregulation of miR-455 has a greater effect on bone than articular cartilage. Since previous research has demonstrated an increase in miR-455-3p in human OA articular cartilage, human NOF control samples and OA articular cartilage were measured for CREB1 expression. These results demonstrated that CREB1 is significantly lower in OA samples compared with control, possibly as a result of the increase in miR-455-3p expression.

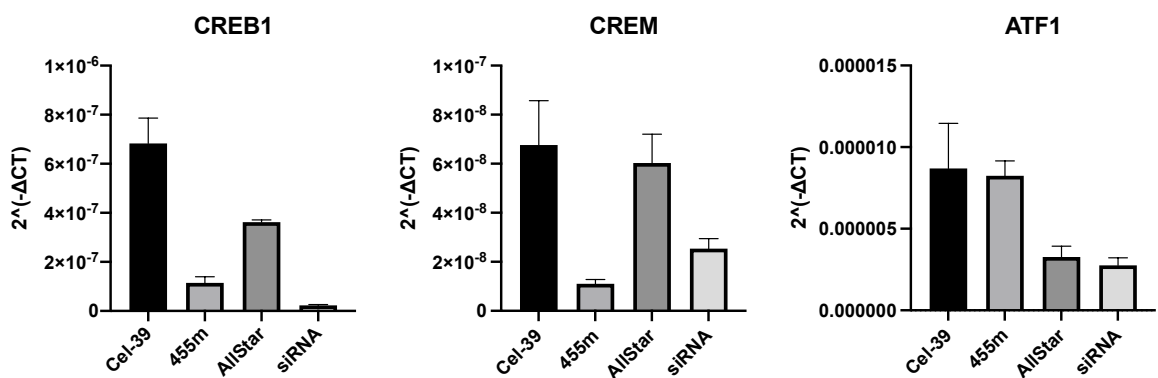


Figure 5.13: CREB1 siRNA phenocopies miR-455-3p in hMSCs. Gene expression of CREB1, CREM and ATF1 was measured in hMSCs transfected with CREB1 siRNA compared to control, and miR-455 mimic compared to control by qPCR. Both CREB1 and CREM followed similar expression patterns in hMSCs transfected with CREB1 siRNA and miR-455 mimic. Results combine data from 3 biological replicates from 1 hMSC donor cell line (2802f). (n=3, error bars +/- SEM).

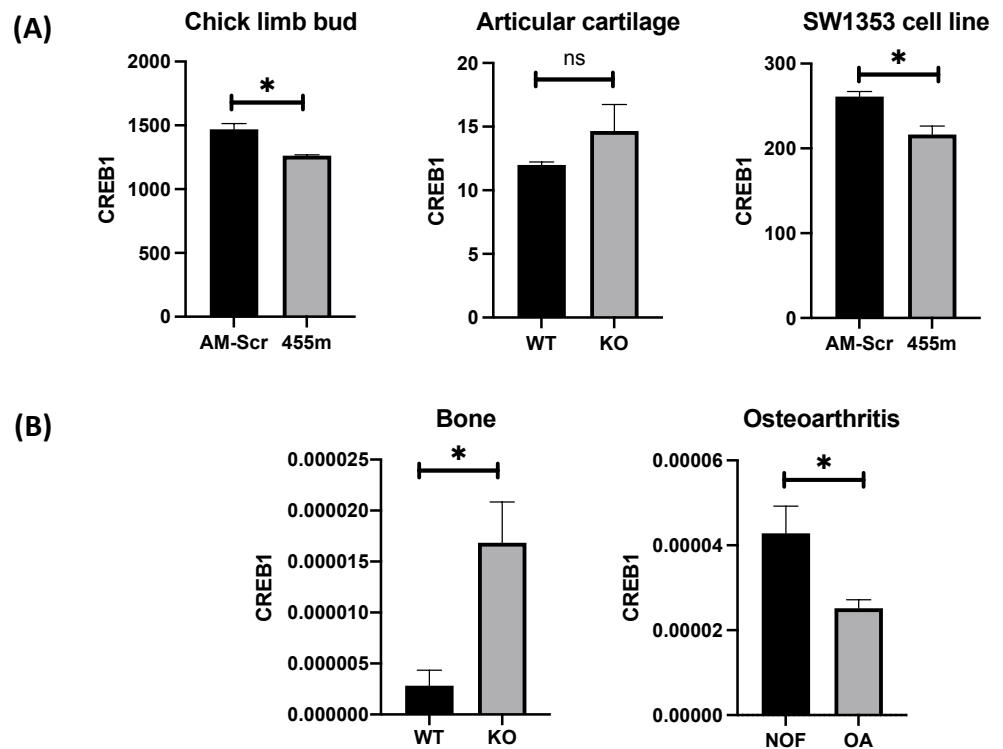


Figure 5.14: CREB1 expression across skeletal samples. (A) RNA-seq data results of CREB1 expression levels in chick limb buds overexpressing miR-455, miR-455 KO mouse articular cartilage, and SW1353 cell line transfected with miR-455 mimic and inhibitor. (B) qPCR analysis of CREB1 in miR-455 KO mouse tibia bone samples and human knee OA samples. ($n=3$, $P<0.05$, error bars \pm SEM).

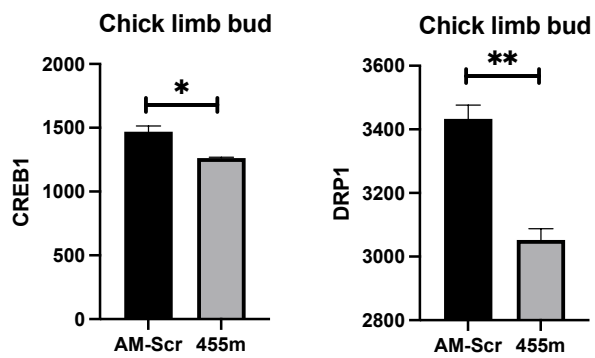


Figure 5.15: Comparison of CREB1 and DRP1 expression levels. Chick limb buds overexpressing miR-455 compared to AM-Scr control demonstrate a decrease in CREB1 and DRP1 expression. (n=3, P<0.05, error bars +/- SEM).

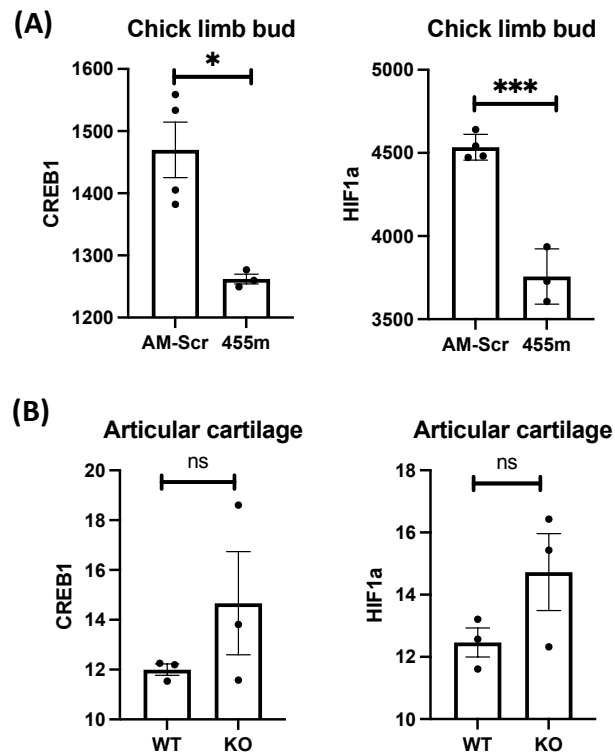


Figure 5.16: Comparison of CREB1 expression levels and HIF1a expression. A) Chick limb buds overexpressing miR-455 compared to AM-Scr control demonstrating the relationship between an increase in CREB1 expression and HIF1a. B) Articular cartilage from miR-455 KO mouse compared to WT showing correlation between an increase in CREB1 expression and HIF1a. (n=3, P<0.05, error bars +/- SEM).

5.3. Discussion

An overexpression of miR-455-3p in the developing chick limb bud results in a visual phenotype of smaller limb bud size compared to control (n=9). Interestingly, inhibition of miR-455-3p by antagomir did not result in a visual phenotype, where no difference was observed compared with control. This data supports previous gene expression analysis in mouse cartilage, where altered levels of miR-455 expression resulted in a dysregulation of genes associated with skeletal system development. Analysis of RNA-seq data from limb buds overexpressing miR-455-3p revealed that developmental pathways are dysregulated within these samples. Whilst exploring this further, data analysis demonstrated a disruption to the cell cycle and abnormal mitochondria when miR-455 is overexpressed.

In order to uncover a mechanism by which miR-455 regulates the development of the limb, the CREB1 transcription factor was identified as a miR-455-3p target, regulating many cell cycle related genes. This was confirmed by the phenotype similarity between miR-455 overexpression and CREB1 knockdown in hMSCs, and their effect on cell cycle and mitochondrial related genes. Analysis revealed a possible role of CREB1 in skeletal tissues, including the disease phenotype OA, since CREB1 is downregulated in OA tissue.

There are many possible mechanisms by which the miR-455-3p/CREB1 interaction may regulate chondrogenesis and the developing limb. One of these is the regulation of DRP1 by CREB1. Overexpression of miR-455-3p and therefore a downregulation of CREB1 results in a downregulation of DRP1 in the developing chick limb (Figure 5.15). During the cell cycle, different phases exhibit changes in mitochondrial morphology (307). The morphology of mitochondria, in particular mitochondrial fission, required DRP1 (308). There is an increase in fission and DRP1 expression during the S & G2M cell cycle phases (308). Since an overexpression of miR-455-3p results in a downregulation of CREB1 and consequently DRP1, this may lead to a G2M arrest, terminating the cell cycle and reducing proliferation.

Another mechanism could be the interaction between CREB1 and HIF-1a as it was observed that in chick limb buds overexpressing miR-455-3p and downregulated CREB1,

there was also a significant decrease in HIF1a expression (Figure 5.16). To support this, articular cartilage from miR-455-3p KO mouse revealed an increase in both CREB1 and HIF1a expression. HIF1a regulates cellular response to hypoxia, and it has previously been described that HIF-1a has a role in cartilaginous tissues, where a downregulation of HIF1a causes growth plate defects and cell death (309). This could explain the phenotypes observed in tissues with an overexpression of miR-455-3p, as this results in a downregulation of both CREB1 and HIF1a, impacting on hypoxic response and HIF-1a and cell survival in tissues. Further experiment should be performed to explore the interaction between miR-455-3p and CREB1, and the role of CREB1 during chondrogenesis and chondrogenic tissues.

Chapter 6

Identifying microRNA-455-3p targets

6. Identifying microRNA-455-3p targets

6.1. Introduction

The post transcriptional regulation of target genes by microRNAs is an essential element of eukaryotic gene regulation. miRNA response elements (MRE) complementary target transcripts form the miRNA induced silencing complex (miRISC). The understanding of miRNA mechanisms has enhanced due to advances in methodologies. Despite this, the study of direct miRNA-target interactions *in vivo* presents as a challenge. Fulga et al have described an experimental protocol, identifying specific miRNA-MRE interactions in situ by CRISPR/Cas9 genome engineering (310). This has enabled investigation of a putative miRNA-target interaction within a pool of cells, eliminating the need for generating transgenic animals or clonal cells lines (310). The protocol was performed in HEK-293T cells, and before now has not been used to study miRNA-target interactions in cartilage. The aim of this research was to optimize CRISPR/Cas9 genome engineering in SW1353 cells, identifying miR-455-3p novel target interactions *in vivo*.

6.1.1. Assessing microRNA-455 activity by CRISPR-mediated HDR

Previous advances in methodologies have improved the understanding of miRNA biogenesis and mechanisms in which miRNAs repress their targets, however, the physiological relevance of direct miRNA-target interactions remains a challenge (310). An experimental protocol has been described using CRISPR/Cas9-mediated genome engineering to directly interrogate miRNA-MRE interactions (310). It is extremely likely that miRNAs regulate a large number of genes, since their target recognition is mainly controlled by short 'seed' sequences (283). Cell culture systems can offer valuable information to directly investigate miRNA function and role in human cells.

Literature has described this technique using CRISPR-mediated homology-directed repair, designing short oligonucleotide donors in order to assess MRE activity in human cells, and subsequently analyse the consequences of blocking specific miRNA-MRE interactions (283). This approach co-transfects Cas9/sgRNA targeting a MRE into cultured cells, with

two 140nt single-stranded DNA (ssDNA) oligonucleotide templates for HDR (283). The first HDR template inserts a T3 'barcode' downstream of the target MRE maintaining the MRE, whilst the second replaces the MRE with a T7 'barcode'. These two cell populations can be identified from a pooled sample by using a primer specific to the MRE of interest, and primers binding the T3 and T7 'barcodes' (283). In a heterogenous mixture of transiently transfected cells, the MRE activity can be assessed. For example, with an active MRE, mRNA containing the T7 'barcode' and MRE deleted will be higher when compared to the intact MRE T3 'barcode' (283). qPCR is used to quantify this with T3 and T7 primers on complementary DNA (cDNA), and the T3 and T7 integration efficiencies are assessed by qPCR of genomic DNA (gDNA) from the same cells compared to cDNA results (283). The MRE is active within the cell type if the T7/T3 ratio is significantly higher in the cDNA compared with gDNA. An increase in this indicates the extent of this (283).

This has been tested in HEK293T cells, for three putative miR-92a targets (C9orf7, PCMTD1, MAPRE1) which were identified by CLASH (259). The CLASH assay, however, cannot discriminate between direct and indirect regulation by miRNA. The analysis of this experiment revealed that despite direct miRNA-MRE predicted binding, only one target (C9orf7) deletion of MRE affected transcript abundance. This was not shown in the PCMTD1 and MAPRE1 MREs, suggesting that miR-92a does not play a role in regulating these transcripts in this cell type (283). This protocol may be implemented in different cell lines and scaled up for multiplex studies (310).

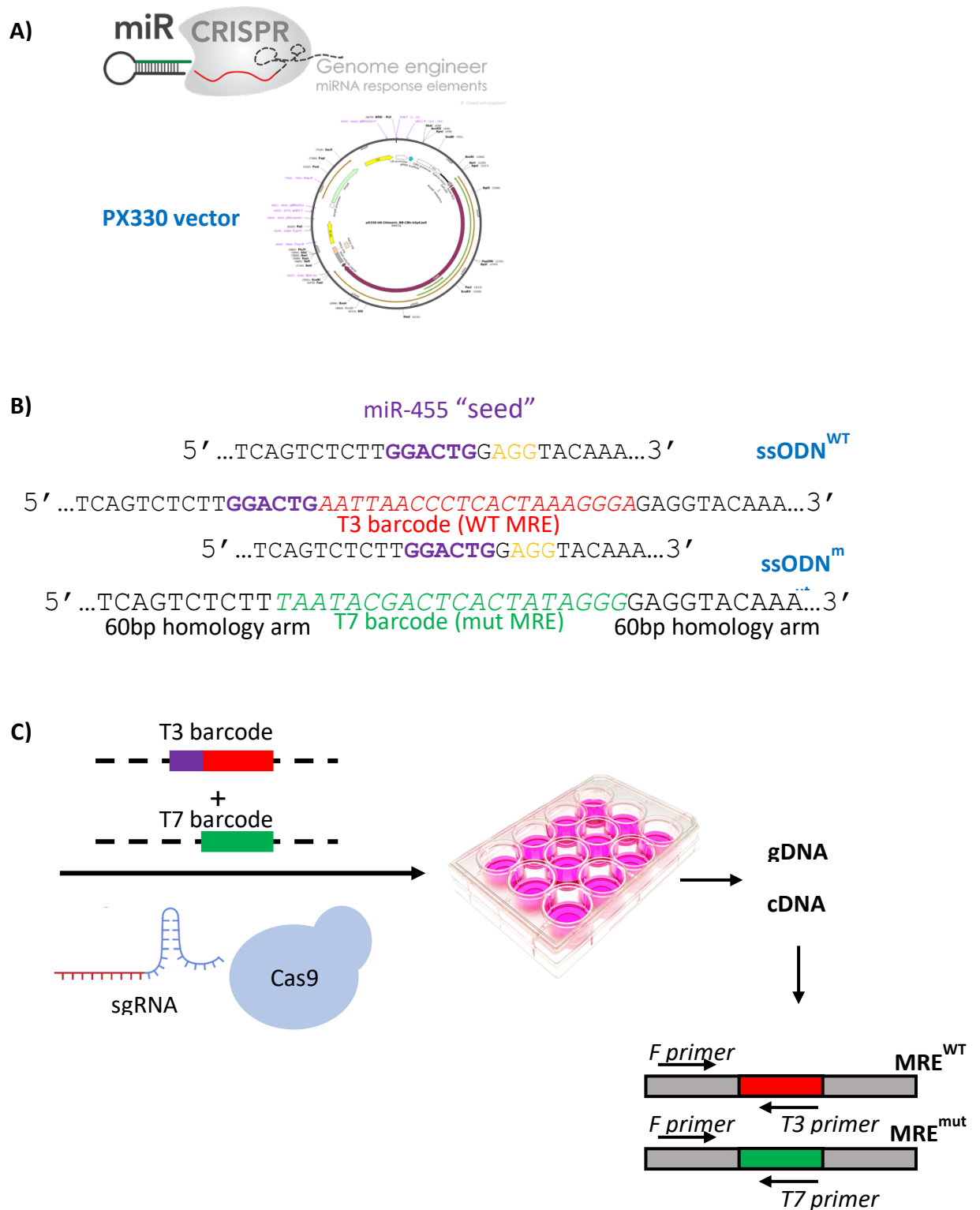


Figure 6.1: CRISPR-mediated HDR and MRE activity protocol. Schematic as described by Bassett et al. 2014. A) miR-CRISPR is used to design sgRNA. B) ssODN design for DKK3 and miR-455-3p. C) Transfection of ssODN, sgRNA and Cas9 into SW1533 cells. gDNA and cDNA extracted and qPCR performed.

6.2. Results

6.2.1. Optimization and protocol development in SW1353 cells

The microRNA-target interactions by CRISPR/Cas9 genome engineering protocol was developed in the SW1353 cell line, due to its extensive use in cartilage-related *in vitro* research and successful transfection efficiency. The genes DKK3 and CLOCK have previously been identified in the lab as miR-455-3p targets and were therefore used to optimize the CRISPR/Cas9 genome engineering protocol in SW1353 cells. Firstly, to confirm that DKK3 and CLOCK are direct targets of miR-455-3p, luciferase assays were performed. For both genes, following transfection, the expression of luciferase was decreased by overexpression of miR-455-3p which was then rescued by a mutation in the miR-455-3p target site within the UTR. This provides confirmation that DKK3 and CLOCK are targets of miR-455-3p (Figure 6.2).

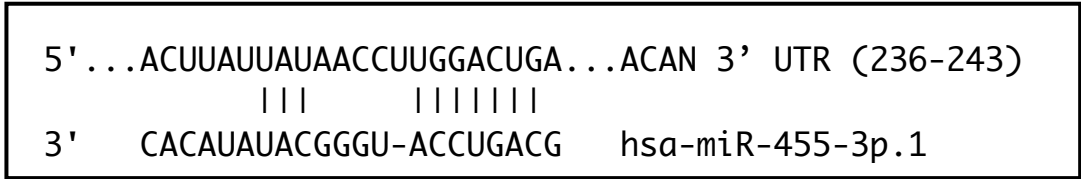
The miRanda algorithm (microrna.org) provided predicted MRE seed position for each target gene, and sgRNA were designed using the miR-CRISPR tool. Both WT-MRE and mut-MRE ssODNs were designed and transfected into SW1353 cells alongside pX330-sgRNA plasmid DNA using Lipofectamine 3000. After 48 hours, DNA and RNA were extracted from each cell sample and qPCR performed (Figure 6.1). For DKK3, MRE score calculation revealed a score of 1.56 (Figure 6.2). As this value is greater than 1, this suggests that there is functional miRNA-target regulation. Analysis of the qPCR data demonstrated that the T7/T3 ratio for DKK3 was significantly different higher in cDNA compared with gDNA. An increase in ratio in the cDNA suggests that the MRE is active, as its deletion results in increasing amounts of transcript being produced. In the gDNA, the T7/T3 ratio is used to estimate the relative integration efficiency of the T7 and T3 oligos. For CLOCK, MRE score calculation revealed a score of 0.82. As this value is less than 1, this suggests that the MRE is stabilizing. Although the T7/T3 ratio was higher in cDNA samples compared to control, this was not significantly different. This may suggest an absence of miR-455-CLOCK regulation within the cell line SW1353. This conflicts luciferase assay data and could demonstrate that CLOCK downregulation as a result of miR-455-3p overexpression could be due to downstream regulation rather than direct interaction between CLOCK and miR-455-3p.

This data provides an example of how this CRISPR/Cas9 genome engineering protocol can distinguish between primary and secondary miRNA targets and could overcome limitations in the luciferase assay providing a more accurate representation of miRNA mediated gene regulation.

6.2.2. Validating RNA-seq data and identifying novel miR-455-3p targets

Following CRISPR/Cas9 genome engineering protocol optimization in SW1353 cells, predicted miR-455-3p target genes selected from RNA-seq data-sets described above were analysed. In miR-455 null mouse articular cartilage, ACAN expression was upregulated. This gene is interesting in terms of skeletal tissue, as it is a member of the aggrecan/versican proteoglycan family. The protein encoded by ACAN is an integral part of the ECM in cartilaginous tissue, and upregulation in miR-455 null mouse cartilage could suggest a skeletal phenotype. TargetScan identified ACAN as a miR-455-3p targets and following miRanda analysis, predicted MRE seed position for ACAN was selected and experimental design was performed. Analysis of qPCR data demonstrated that the T7/T3 ratio was significantly different higher in cDNA compared with gDNA, suggesting that the MRE is active (Figure 6.3). This was supported score calculation which revealed a score of 1.91, where a value greater than 1 suggests an active MRE. Since a complete knockout of miR-455-3p in mouse articular cartilage resulted in an upregulation of ACAN, and CRISPR/Cas9 genome engineering validated ACAN MRE to be active in SW1353 cells, it can be concluded that ACAN is a direct target of miR-455-3p.

Further analysis of RNA-seq data from miR-455 null mouse articular cartilage, SW1353 cells inhibiting miR-455-3p and chick limb buds overexpressing miR-455-3p was performed. This revealed PRELP as a common gene in groups 'downregulated in limb buds overexpressing miR-455-3p', 'upregulated in SW1353 cells inhibiting miR-455-3p' and 'upregulated in miR-455 null mouse articular cartilage' (Figure 6.4A). In addition to this, during hMSC chondrogenesis assays, PRELP expression levels decrease in response to cell transfection with miR-455 mimic-3p, and increase following transfection with a miR-455-3p inhibitor (Figure 6.4C). PRELP (proline and arginine rich end leucine rich repeat protein) is another interesting gene in relation to ECM. The protein encoded by PRELP is



ACAN MRE Score = 1.91

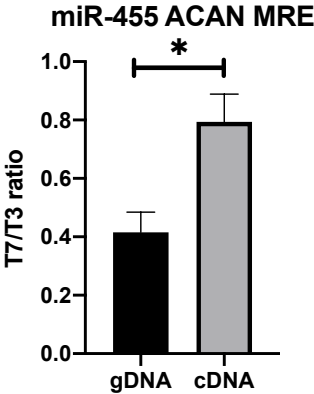


Figure 6.3: Validation of RNA-seq data. A) Predicted alignment of ACAN 3'UTR MRE and miR-455-3p seed sequence. B) CRISPR/Cas9 genome editing data to identify active MRE and MRE score calculation (n=3, P<0.05, error bars +/- SEM).

present in connective tissue ECM, binding type I collagen to basement membranes and type II collagen to cartilage. TargetScan identified PRELP as a miR-455-3p targets and following miRanda analysis, a predicted MRE seed position for PRELP was selected and experimental design was performed. Analysis of qPCR data demonstrated that the T7/T3 ratio was significantly different higher in cDNA compared with gDNA, suggesting that the MRE is active (Figure 6.5). This was supported by the score calculation which revealed a score of 1.25, where a value greater than 1 suggests an active MRE. This data suggests that PRELP is a direct target of miR-455-3p, and this interaction could be involved in the mechanism for the phenotype observed in cartilage tissues as a result of miR-455-3p overexpression or downregulation.

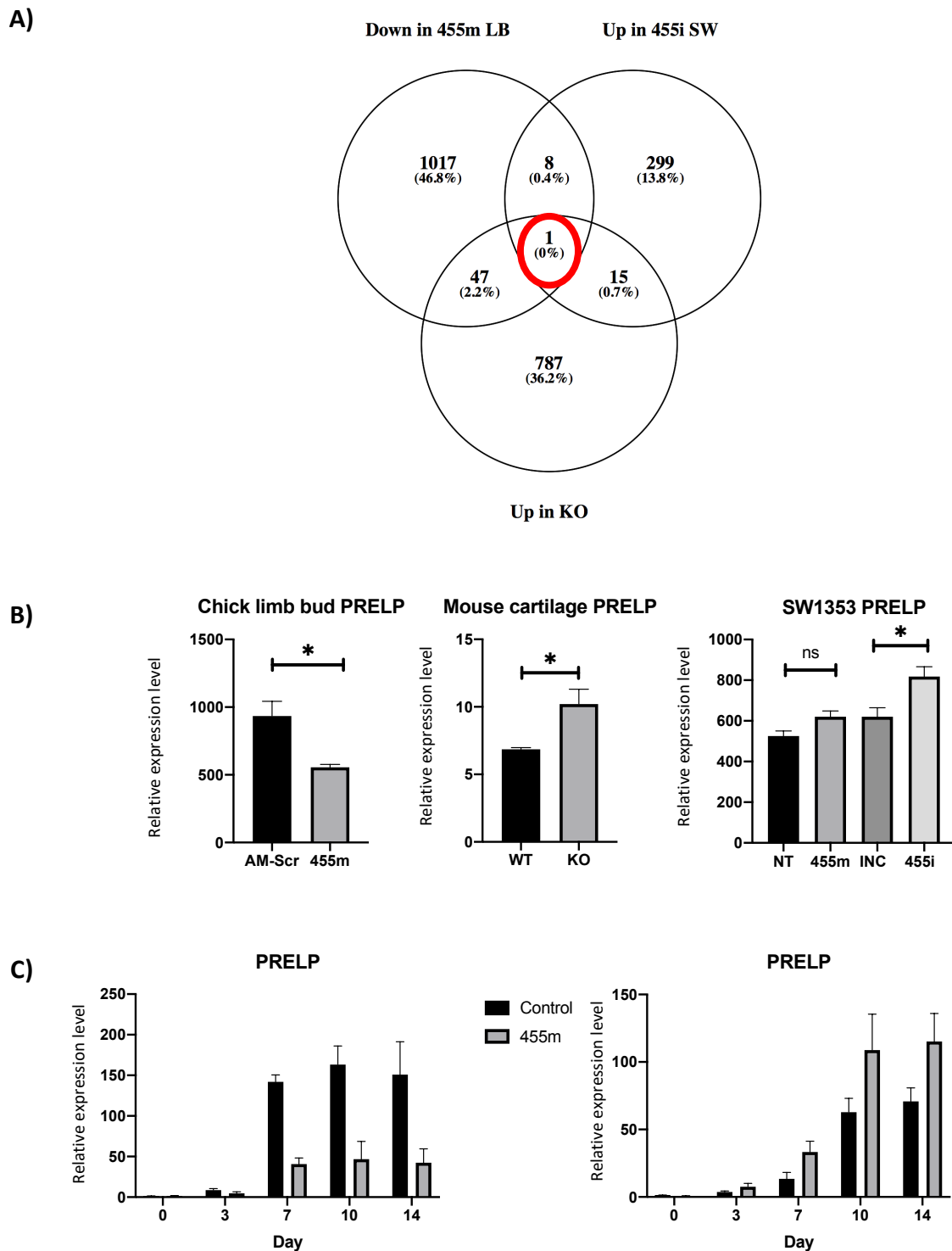


Figure 6.4: PRELP expression across cartilage samples. PRELP is a gene related to ECM and cartilage. A) Ven diagram demonstrating 1 common gene 'down in 455m limb bud', 'up in 455i SW1353 cells' and 'up in miR-455 KO cartilage'. B) Expression levels of PRELP decrease in chick limb buds overexpressing miR-455, increase in miR-455 KO articular cartilage samples, and also increase in SW1353 cells transfected with a miR-455 inhibitor. C) During hMSC chondrogenesis assays, PRELP expression levels decrease in response to cell transfection with miR-455 mimic, and increase following transfection with a miR-455 inhibitor.

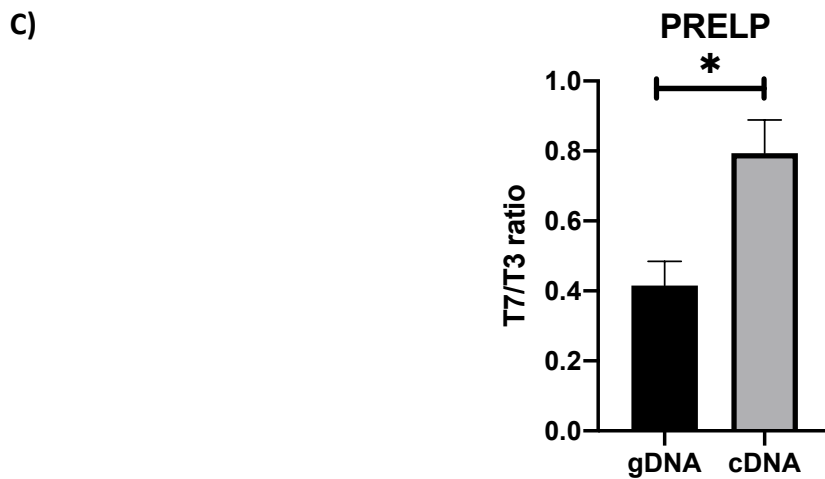
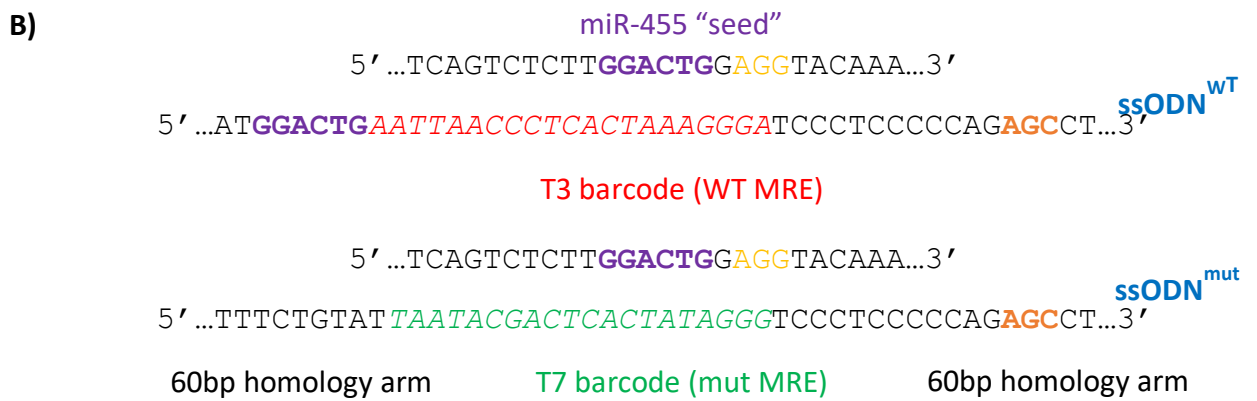
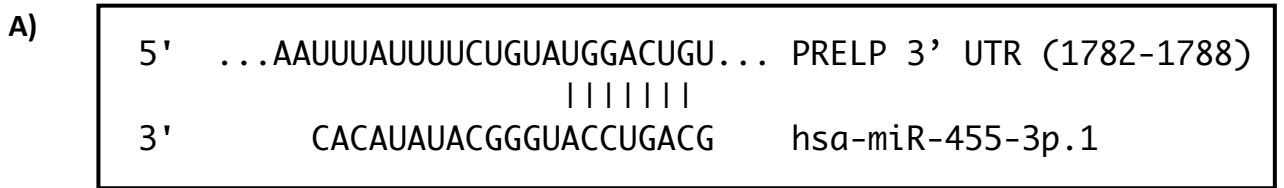


Figure 6.5: Identifying PRELP as a target of miR-455-3p. A) Using Target scan, PRELP was identified as a miR-455-3p.1 predicted target. Predicted consequential pairing of target region (top) and miRNA (bottom). B) ssODN experimental design for CRISPR/Cas9 engineering. C) T7/T3 ratio between PRELP gDNA and cDNA, demonstrating that PRELP is a direct target of miR-455-3p.

6.1. Discussion

These results show that the CRISPR/Cas9 genome editing protocol to identify miRNA target genes has been successfully performed in SW1353 cells. Using this method in SW1353 cells will allow further miRNA-MRE interactions to be studied in cartilage research. The next step would be to optimize the technique in different cell lines, such as human articular chondrocytes or MSCs, to identify cell specific interactions. If this method can be transferred into human primary cell lines, it could be used to compare healthy articular cartilage samples and OA samples, to understand the regulatory roles of miRNAs in diseased and healthy tissues. To enhance this method further, research could focus on scaling up the protocol in order to study multiple miRNAs at one time. This could also be used to study multiple predicted targets of a miRNA in a single assay.

The protocol overcomes several limitations of previous methods to identify miRNA targets such as the luciferase assay. For example, they do not capture the endogenous miRNA-target stoichiometry, and therefore cannot identify physiological miRNA-mediated repression *in vivo*. In addition to this, capture-based techniques such as CLIP detect spatial-temporal binding between targets and miRNAs. As miRNA-target binding does not always mirror repressive action of miRNAs, this does not definitively identify function interactions (310). This protocol described by Fulga et al. demonstrates a direct validation of miRNA-MRE interactions under physiological conditions, impacting minimally on cellular homeostasis (310).

The targets validated by CRISPR/Cas9 genome engineering suggest that miR-455-3p has a role in cartilage development or maintenance, since ACAN and PRELP are both expressed in cartilaginous tissue. Further analysis is required to explore the role of miR-455-3p interactions with ACAN and PRELP, and the downstream consequences of this.

Chapter 7

Discussion

1. Discussion

Previous research has shown that miR-455 is expressed in the developing long bone, joints and cartilage and has also been identified as an activator for early chondrogenic differentiation. This research has aimed to explore the role of miR-455 during skeletal development and cartilage. Gene expression analysis has enabled potential miR-455 targets to be identified, and provided insight into the mechanisms regulated by miR-455 during chondrogenesis. These results provide a platform for exploring both osteochondral development and the role of miR-455 targets within these processes, and translating this to disease research.

1.1. microRNA-455-3p in cartilage and skeletal development

This research has demonstrated that miR-455-3p expression increases during chondrogenesis, and overexpression of miR-455-3p prior to differentiation results in a downregulation of the chondrogenic marker genes SOX9, COL2A1, ACAN and COL10A1. During adipogenesis and osteogenesis, miR-455-3p expression also increases at the beginning of differentiation. These findings oppose those of the Liao group (137–139), where overexpression of miR-455-3p increases chondrogenic markers. This model of chondrogenesis is in the ATDC5 cell line, whereas our data is from the hMSC model. Since we observe the same results from 3 independent hMSC cells lines, we can be confident that CREB1 acts as an activator of gene expression. This disagreement may be explained by, using different cofactors, CREB1 acts as a transcriptional repressor in ATDC5 cells.

Analysis of RNA-seq data from miR-455 null mouse articular cartilage suggests that miR-455-3p has a role in osteochondral development. Differentially expressed genes upregulated in miR-455 null cartilage are involved in osteochondral-related processes. In combination with SW1353 cells inhibiting miR-455-3p, RNA-seq analysis identified differentially expressed genes involved in skeletal system development. Data from hMSC's overexpressing miR-455-3p during chondrogenesis shows a downregulation of chondrogenic markers, supporting the hypothesis that altered miR-455-3p expression impacts chondrogenic differentiation.

In the chick limb bud, overexpression of miR-455-3p by microinjection inhibited limb bud development. RNA-seq data revealed many differentially expressed genes involved in developmental signalling pathways, indicating a dysregulation of development due to miR-455-3p overexpression. In addition to this, many mitochondrial genes were upregulated, and cell cycle genes downregulated, resulting in mitochondrial dysfunction and a disruption to the cell cycle. The majority of these genes are not miR-455-3p predicted targets, however, the CRE is overrepresented in their promoters, suggesting regulation by the transcription factor CREB1. In the chick limb bud, CREB1 is downregulated by miR-455-3p, and is predicted to be a miR-455-3p target. To validate this, the 3'UTR of CREB1 was subcloned into pmiRGLO downstream of luciferase. Following transfection, luciferase expression was decreased by miR-455-3p overexpression which was rescued by mutation in the miR-455-3p UTR target site, confirming CREB1 as a direct miR-455-3p target. Due to time constraints, CREB1 was not explored further as a potential mi-455-3p target. The next experiment would aim to validate CREB1 as a miR-455-3p target using the CRISPR/Cas9 genome engineering protocol described in Chapter 6.

During hMSC chondrogenesis, CREB1 levels decrease as miR-455-3p levels increase. In both cultured hMSCs and the hMSC chondrogenesis assay, silencing of CREB1 by siRNA phenocopied miR-455-3p overexpression, where chondrogenic marker genes were decreased. The expression of mitochondrial and cell cycle related genes were also differentially expressed in response to CREB1 siRNA and miR-455-3p overexpression, suggesting that the action of miR-455-3p is mediated by a downregulation of CREB1.

From this research, it can be hypothesised that miR-455-3p has a role in chondrogenesis, regulating the expression of CREB1. Within skeletal development, the impact of miR-455-3p demonstrates a significant regulatory mechanism to explore further. It may be possible in the future to use miR-455-3p inhibition to upregulate CREB1 and enhance chondrogenesis, consequently providing a platform in stem cells, tissue engineering, and regenerative medicine.

1.2. CREB1

The cAMP-response element binding protein 1 (CREB1) is part of the CREB family of activators which stimulate cellular gene expression. This occurs following phosphorylation at a conserved serine in response to cAMP, most commonly Ser-133 in CREB1 (311). The transcription factor binds to the CRE (cAMP response element) or a half site within a gene promoter (312). The phosphorylation of CREB1 enables dimerization and recognition of the transcriptional coactivator CBP (CREB1-binding protein) (313). This family of basic region/leucine zipper (bZIP) transcription factors also includes CREM (cAMP response element regulatory protein) and ATF1 (transcriptional activator 1), where CREB1, CREM and ATF1 can form heterodimers and homodimers (313).

Studies on mice have demonstrated that CREB1 has many tissue specific functions. Although a genome wide study suggested that approximately 4000 genes were regulated by CREB1, the induction of gene expression by cAMP is dependent on the recruitment of regulatory partners such as CBP (314). The generation of CREB1^{-/-} mice resulted in respiratory failure and lung development problems, leading to death at birth (315).

During endochondral ossification, cell proliferation is essential to control long bone growth (316). In multiple cell types, CREB1 has an important role in cell proliferation. G1 progression is extremely important in the growth plate, regulating chondrocyte proliferation through cyclin A and D1 (317). CREB1 is required for the regulation of these genes, which both have CREs in their promoters (318). Interestingly, previous research demonstrated that CREB recruitment leads to increased levels of MMP13 in both human articular chondrocytes and OA (319). It is well known that CREB1 is a critical regulator of cell differentiation and proliferation, and knockdown of CREB1 inhibits cell cycle transition. The mechanism to which CREB1 and other family members regulate cell cycle progression is unclear, although cell cycle related genes have been identified to be regulated by CREB1.

1.3. CREB1 in chondrogenesis and endochondral ossification

The expression of SOX9 is regulated by cAMP which induces chondrogenesis in micro-mass culture of chick limb bud mesenchymal cells (320). Within this study, CREB1 was highly expressed and phosphorylated during early stages of chondrogenesis, decreasing over time. This cell model demonstrated that, at the early stages of chick development, CREB1 is required for limb bud chondrogenesis. In addition to this, CREB1 has been reported to bind to the SOX9 promotor, inducing SOX9 expression (321).

During endochondral bone development, the CREB family of transcription factors have been identified as important (322). The DNA binding of CREB family members, including CREB1, CREM and ATF1 is disrupted by a dominant negative CREB1 inhibitor A-CREB (323). In growth plate chondrocytes of mice, the expression of a dominant negative A-CREB inhibitor resulted in short-limbed dwarfism and perinatal lethality, due to respiratory failure as a results of small rib cage circumference (Figure7.1) (322). These mutant chondrocytes portrayed a delay in hypertrophy and decrease in proliferative index. This is in contrast to wild-type cartilage during development, where there is an activation of CREB in proliferative zone chondrocytes (322). In addition to this, signalling molecules involved in development showed altered expression. In support of this data, It has previously been demonstrated that CREB activation is critical in chondrocytes (318).

Many signalling molecules are involved in the regulation of endochondral bone formation, and these mechanisms induce cartilage and bone gene expression programmes. This study demonstrates that the CREB family of activators function as critical intermediates within this process. The results suggest that the decreased proliferative zone in A-CREB mutant mice may be due to both a reduced rate of proliferation and also the cell cycles in which the chondrocytes undergo before exiting the cell cycle (322). This research concludes that CREB increases proliferation and promotes chondrocyte differentiation. Additionally, other CRE-binding proteins such as ATF2 may have an important function in bone development (324). Although this study indicates a critical role for the CREB family during proliferation, the mechanisms involving regulation of cell cycle progression in unknown. This in an important beginning for developmental research identifying chondrocyte target genes which, in response to mitogenic signals, are induced by CREB.

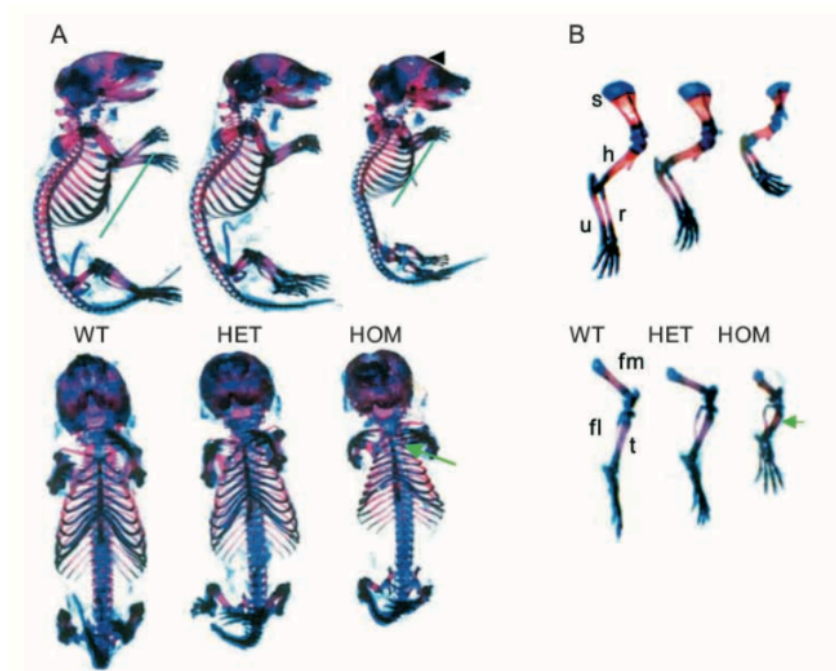


Figure 7.1: Inhibiting CREB1 in chondrocytes. The expression of A-CREB inhibitor in chondrocytes results in perinatal lethality due to reduced rib cage circumference and short-limbed dwarfism. Images demonstrate whole skeletal preparations of 18.5dpc littermates containing 0 (WT), 1 (HET), or 2 (HOM) alleles of the A-CREB transgene. Comparison of forelimbs and hindlimbs in the same embryos are also shown (Long et al, 2001).

During hMSC differentiation, it has been discovered that the cAMP/PKA/CREB pathway also has a role in osteogenic differentiation (325). Phosphorylated CREB was detected in hMSCs leading to PKA activation and stimulates osteogenic differentiation *in vitro* (326). From this study, a model for induction of osteogenesis in hMSCs by PKA signalling was derived, suggesting that cAMP induces direct expression of BMP target genes via CREB, and the expression of BMP2 results in the induction of bone formation (326). During osteochondrogenesis, SOX9 is a master transcription factor, whereby interaction between SOX9 and CREB was shown to be an active event as a result of BMP2 stimulation (327). Overexpressing CREB enhanced the action of SOX9, promoting BMP2 induced osteochondrogenic differentiation (327). It has been reported that the SOX9 proximal promoter is regulated by CREB, and mutations of the CREB binding site results in a reduction of SOX9 promoter activity (321). Multiple growth factor pathways, including IGF, TGF β , FGF, EGF and PDGF, also promote target gene expression via CREB1 (328,329).

It is also interesting that a study has identified CREB1 as a potential direct downstream target of miR-140 (330) – a microRNA extensively studied in regard to osteochondral elements, known to be coregulated with miR-455 (180). This research demonstrated that the function of miR-140 overexpression mimicked CREB1 knockdown on ECM degradation, where IL-1 β or TNF- α induced degradation was enhanced (330).

1.4. CREB1 and endochondral disease

Epiphyseal chondrodysplasia Muria type (ECDM) is a skeletal overgrowth disorder whereby a mouse model revealed a thickening of the hypertrophic growth plate and hypertrophic chondrocytes continue to proliferate (331). Following this, the study showed that in disease conditions, hypertrophic chondrocytes are signalled to induce CREB phosphorylation and increase expression of cyclin D1, which results in continued proliferation, leading to skeletal overgrowth (331). Neonatal-onset multisystem inflammatory disease (NOMID) is an auto-inflammatory disease which also affects chondrocytes and epiphyseal overgrowth in the joint (332). A study discovered that in chondroprogenitor cells, the CREB/ATF-binding site of the human SOX9 promoter was

critical for SOX9 overexpression, and NOMID chondrocyte hyperplastic capacity is dependent on the cAMP/PKA/CREB pathway (332).

In regard to Osteoarthritis and human articular chondrocytes, CREB was identified as the regulating factor able to bind to the MMP13 promoter following a specific CpG methylation, inducing MMP13 expression (319). This provides an epigenetic link between elevated MMP13 expression, osteoarthritic cartilage, and CREB. The active CREB/MMP13 axis in OA chondrocytes may cause the degeneration of cartilage and progression of OA (333). In a mouse OA model, a high expression of SGK1 was found which in turn inhibited the expression of CREB1 in chondrocytes (334). This suppressed chondrocyte proliferation and induced inflammation, providing further evidence of a regulatory role of CREB1 in chondrocytes and OA.

1.5. CREB1/ miR-455-3p interaction in chondrocytes

1.5.1. miR-455-3p/CREB1, DRP1 and the cell cycle

The overexpression of miR-455-3p in chick limb buds results in a decrease in CREB1 and also DRP1. DRP1 has a predicted transcription factor binding site for CREB1, suggesting that a decrease in CREB1 expression may result in a decrease in DRP1. During the cell cycle, different phases require changes in mitochondrial morphology, and cycles of mitochondrial fission and fusion are integrated within the cell cycle progression. It has also been demonstrated that tubular-intermediate and fragmented mitochondria requires mitochondrial fission (307). Tubular-intermediate and fragmented mitochondria morphology are observed at both S and G2M phases of the cell cycle, since there is an increase in fission at these phases. DRP1 levels were also shown to be highest during the G2M phase, increasing from G1/S to S and then G2M (307). Research has shown that mitochondrial fission required DRP1, and the reduction of DRP1 causes a robust hyperfusion phenotype (308). Inhibition of DRP1 causes a delay in G2/M cell cycle progression, triggering replication stress-mediated genome instability (308). The loss of DRP1 increases DNA damage and cell death.

From the process of endochondral ossification, it is clear that the cell cycle plays an essential role in proliferating chondrocytes (316). During osteogenic dysfunction, the DRP1-dependent mitochondrial pathways have a role during inflammation, where DRP1 upregulation is driven by oxidative stress (335). Since high levels of DRP1 could be a factor of TNF α -induced osteogenic dysfunction, this demonstrates that both overexpression and downregulation of DRP1 may result in mitochondrial dysfunction and altered cell cycle progression. The dysregulation of mitochondria is also related to ageing and age-related disease, including mitochondrial fusion and fission processes. It is interesting to mention that senescent cells have reduced levels of DRP1, decreasing capacity for mitochondrial biogenesis (336). Since OA is an age-related disease, correlating with a rise in senescent cells, this is an interesting aspect of future research to explore. In addition to this research, cartilage metabolism, mitochondria and osteoarthritis have all been linked, since chondrocyte are responsible for maintaining and repairing articular cartilage, and a failure of this process is observed in OA (337).

It is clear that a balance of mitochondrial fusion and fission is required to sustain the cell cycle and cellular functions, and many core mitochondrial fusion and fission regulators are emerging as stem cell regulators (338). Therefore, defects in genes involved in mitochondrial dynamics controlling fusion and fission can affect cellular differentiation, proliferation, reprogramming and aging (339). It has previously been demonstrated that a disruption to CREB activity in mitochondria leads to a dysregulation in mitochondrial genes. Since CREB regulates mitochondrial gene expression, a decrease in CREB activity may contribute to mitochondrial dysfunction (340). Research suggests that the DRP1 pathway may be a focus for the development of novel approaches for prevention and treatment of osteochondral disease, and this research demonstrates a possible regulatory mechanism through miR-455-3p/CREB1, providing a target for future therapy. This hypothesis provides a link between the mitochondrial dysfunction and dysregulation of the cell cycle observed when miR-455-3p is overexpressed, and the interaction between miR-455-3p/CREB1 which phenotypically appears to inhibit chondrogenesis.

miR-455-3p overexpression downregulates CREB1, which in turn leads to reduced expression of DRP1. Mitochondrial fission requires DRP1 and loss of DRP1 induces

mitochondrial hyperfusion, leading to abnormal mitochondria and metabolism. Since fission and DRP1 expression is usually increased in S & GM phases, the reduction in DRP1 may lead to termination of the cell cycle and therefore reduced proliferation. This could be a possible mechanistic explanation for the inhibition of limb bud development and chondrogenesis as a result of miR-455-3p overexpression.

1.5.2. miR-455-3p/CREB1, HIF1a and mitochondrial dysfunction

In several diseases, such as OA, there is a suggested protective role of hypoxia inducible factor-1a (HIF-1a) mediated mitophagy. The expression of HIF-1a has been shown to increase in human and mouse OA cartilage (341). This hypoxia-induced mitochondrial dysfunction was impaired further by HIF-1a knockdown, and under hypoxia conditions HIF-1a stabilisation alleviated apoptosis and senescence in chondrocytes (341). Surgery induced cartilage degeneration in an OA mouse model was also improved by HIF-1a stabilisation, suggesting HIF-1a mediated mitophagy could alleviate OA (341). As mitochondrial dysfunction leads to OA and disc degeneration (341), the upregulation of HIF-1a could provide a basis for future research.

The differentiation of MSCs into chondrocytes can be stimulated by hypoxia and HIFs, where their stability is essential to the effect of hypoxia on chondrogenic differentiation (342). Limb buds overexpressing miR-455-3p have a significant decrease in expression of HIF-1a, whereby miR-455 knockout mice show an increase in HIF-1a expression in the articular cartilage. Since CREB1 is a target of miR-455-3p, this can be explained as the transcription factor CREB1 constitutively binds to HIF-1a (343), and interactions between HIF-1a and CREB1 may be pivotal for chondrocyte survival. It was previously demonstrated that miR-455 expression increases in OA cartilage samples (180), and in NOF and OA samples, CREB1 expression was shown to decrease. A knockdown of miR-455-3p, and therefore increase in CREB1 expression, may stabilise HIF-1a and reverse mitochondrial dysfunction.

In cartilaginous tissues, hypoxia and HIF-1a have a pivotal role. Functionally inactivating HIF-1a in growth plates demonstrated defects caused by massive cell death (309). In

addition to this, HIF-1a has been shown to have an important function in matrix synthesis in articular chondrocytes, promoting matrix accumulation and decreasing degradation (344). Unpublished data phenotyping the miR-455 KO mouse suggests an increase in cartilaginous ECM matrix compared to WT. This could be explained by the increase in CREB1 and HIF-1a expression as a result of miR-455 absence. In addition to this, hMSC chondrogenesis differentiation assays overexpressing miR-455-3p show a decrease in chondrogenesis markers, suggesting differentiation into chondrocytes is inhibited by the addition of miR-455-3p. This is phenocopied in cells transfected with CREB1 siRNA, indicating that the downregulation of CREB1 in response to miR-455-3p may cause this phenotype and inhibit chondrogenesis, possibly through interactions with HIF-1a. Although HIF-1a may be involved in OA pathogenesis, for example an increased HIF-1a concentration in the synovial fluid of OA patients (345), HIF-1a expression has also been associated with degradative enzyme and hypertrophic marker downregulation, increasing redifferentiation in healthy and OA chondrocytes *in vitro* (344).

To conclude, overexpressing miR-455-3p decreases CREB1 expression in chondrocytes and the developing limb. This causes a developmental delay in the chick limb bud, and a differentiation block in hMSC chondrogenesis assay, suggesting high levels of miR-455-3p and low levels of CREB1 negatively impacts chondrogenesis. Increased levels of miR-455-3p and decreased expression of CREB1 in OA samples also mirrors this phenotype and could indicate that miR-455-3p/CREB1 have a role in regulating chondrocyte proliferation or cartilage degeneration. This demonstrates the therapeutic potential of miR-455 in treating OA, where a knockdown of miR-455 may alleviate OA symptoms in cartilage, possibly through interactions with HIF-1a.

1.6. miR-455-3p predicted targets

1.6.1. PRELP

PRELP (proline/arginine-rich end leucine-rich repeat protein) is a glycosaminoglycan and collagen binding protein. Expression of PRELP is high in basement membranes, cartilage and developing bone (346). Research has demonstrated that PRELP is highly expressed in developing bones, increasing during osteogenesis. The downregulation of PRELP also

reduced expression of osteogenic marker genes (347). PRELP deficiency is associated with Hutchinson-Gilford progeria, a disease of connective tissue, specifically collagen (348). Within the joint, MSCs found in the synovium display stable PRELP expression levels, whereas bone marrow MSCs display increased PRELP expression levels during *in vitro* chondrogenesis, suggesting that PRELP is a characteristic of intraarticular tissue MSCs (349). This could indicate that PRELP has a role in the maintenance of osteochondral tissues. An equilibrium between bone resorption by osteoclasts and bone formation by osteoblasts is essential for the integrity of the skeleton. PRELP has been shown to inhibit mouse osteoclastogenesis both *in vivo* and *in vitro*, reducing osteoclast specific gene expression (346). In multiple studies, PRELP was also shown to be upregulated in MSC cell pellets during chondrogenic differentiation (350,351).

Within this research, PRELP has been identified as a direct target of miR-455-3p. Initially identified by RNA-seq analysis, PRELP was a common gene in groups 'downregulated in limb buds overexpressing miR-455-3p', 'upregulated in SW1353 cells inhibiting miR-455-3p' and 'upregulated in miR-455 null mouse articular cartilage'. During hMSC chondrogenesis assays, PRELP expression levels also decreased when miR-455-3p was overexpressed and increased when miR-455-3p was downregulated. TargetScan identified PRELP as a miR-455-3p target, and CRISPR/Cas9 genome engineering confirmed that miR-455-3p directly targets PRELP. During control chondrogenesis assay samples, PRELP increases during chondrogenic differentiation, suggesting that miR-455-3p has a role in osteochondral differentiation, directly targeting genes highly expressed in skeletal tissues. This supports the hypothesis that overexpressing miR-455-3p inhibits or delays chondrogenesis by downregulating chondrogenic related genes both directly and indirectly.

1.6.2. Collagen VI

Collagen VI (ColVI) is a member of the collagen family, expressed in a wide range of tissues. There are 6 different genes which encode ColVI (COL6A1, COL6A2, COL6A3, COL6A4, COL6A5, COL6A6), as an extracellular matrix molecule (352). Originally, three ColVI chains were identified (a1, a2, a3) in humans, and later three additional genes encoding ColVI chains were also identified (a4, a5, a6) (353). ColVI is a component of the

ECM in articular cartilage and foetal bone. The pericellular matrix of adult cartilage has high ColVI expression, with a role in chondrocyte attachment and integrity (352). The use of soluble ColVI has also been used as a stimulus for the proliferation of both adult and OA chondrocytes (354).

Multiple musculoskeletal abnormalities have been linked to the mutation or loss of collagen VI including tissue ossification and osteoarthritis (355). Studies have shown that Col6a1^{-/-} mice have significant differences in trabecular bone structure such as lower bone volume, and also had lower cartilage degradation scores (355). As Col6a1^{-/-} mice age, the development of osteoarthritic joint degeneration is accelerated (356). The skeletal abnormalities exhibited by Col6a1^{-/-} mice include delayed development and ossification and increased osteoarthritic changes within the joint. A deficiency of collagen VI also induces osteopenia, and a reduced amount of collagen VI is reported in osteoporotic bone ECM (357).

Within miR-455 null articular cartilage samples, the expression of Col6a1, Col6a2 and Col6a3 are upregulated. Since the expression of miR-455-3p increases in OA cartilage compared with control (180), miR-455-3p could contribute to OA joint degeneration through targeting ECM related genes such as ColVI. In addition to this, miRbase revealed Col6a1 as a predicted target of miR-455-3p.

1.7. Future directions

Since this data suggests that miR-455-3p regulates chondrocyte differentiation by post-transcriptionally regulating the expression of the CREB1 transcription factor, there are multiple future research directions. There are many possibilities to explore regarding the regulation of chondrogenesis by miR-455-3p, many of which have been described above. Although this research identifies CREB1 as a potential miR-455-3p target, the downstream effects of this interaction needs further analysis. Both *in vivo* and *in vitro* analysis will enhance this data and identify a specific role for chondrogenic regulation by miR-455-3p/CREB1. Firstly, luciferase assay data identifying CREB1 as a direct target of miR-455-3p could be validated using MRE analysis by CRISPR/Cas9 genome engineering in hMSCs.

Future experiments should aim to identify how miR-455-3p/CREB1 is regulated, at what time point during chondrogenesis this is most active, and how miR-455-3p/CREB1 regulates these processes. For example, does miR-455-3p/CREB1 regulate chondrocyte proliferation and/ or mitochondrial dysfunction, or are there other targets that influence chondrogenesis. In addition to this, future experiments could explore further the miR-455 null mouse phenotype in the growth plate, for both chondrocyte proliferation, hypertrophy and mitochondrial function. In order to explore this, the following research could be performed.

1.7.1. Growth plate phenotype in miR-455 null

To explore the role of miR-455-3p in the mouse growth plate *in vivo*, the growth plate structure, chondrocyte proliferation and hypertrophy, and mitochondrial function can be studied. Within the miR-455 null mouse model, the growth plate and resting, proliferative and hypertrophic zones can be measured using Masson's Trichrome histological assessment and compared with WT. This can be supported by RNA-seq gene expression analysis to identify molecular phenotypic differences. The localisation of miR-455 in the developing growth plate can be visualised using whole-mount *in situ* hybridization (ISH), with both embryonic and post-embryonic stages. Within the growth plate, CREB1 can also be visualised by ISH and immunohistochemistry (IHC), comparing mRNA and protein expression in both miR-455 null and WT. This will reveal the spatial relationship between miR-455-3p and CREB1 expression, and the expression of CREB1 when miR-455 is absent.

Further analysis in the growth plate could measure cell proliferation using BrdU.

If there is a difference in cell proliferation, identified targets of miR-455-3p could be measured using IHC, in addition to cyclins, and this could identify mechanisms involved in this process. Another experiment could measure mitochondrial function in mouse tissue and compare between miR-455 null and WT. This can be achieved using the Agilent Seahorse assay, which identifies differences in mitochondrial metabolism. MitoTracker dyes can also be used in IHC for cartilage tissue.

Using a miR-455 complete knockout mouse as an experimental model also has limitations. Although miR-455 null tissues can be studied, there is the possibility that knockout of miR-455-3p during development could lead to compensation, since miRNA regulatory mechanisms are extremely complex. The development of a controllable, tamoxifen inducible miR-455 null mouse could improve future research, exploring the consequences of miR-455-3p knockout.

1.7.2. The role of miR-455-3p/CREB1 in chondrogenesis

Since an overexpression of miR-455-3p decreases CREB1 mRNA expression, it is important to also study CREB1 protein expression by western blot. CREB1 activity is regulated by phosphorylation and binding partners, and CREB1 phosphorylation can also be measured using western blot following transfection of miR-455-3p. Co-immunoprecipitation can measure other known binding partners.

In order to identify when miR-455-3p/CREB1 interaction is functioning during chondrogenesis, miR-455-3p mimic or CREB1 siRNA could be transfected at different time-points within the assay such as Day 0, 3, 7 or 10. Chondrogenic marker genes can then be measured across the time-points. Rather than inhibiting miR-455-3p by transfection of an inhibitor in cell lines, the complete knockout of miR-455-3p can be studied. Isolating bone marrow-derived stem cells from miR-455 null mice and culturing these cells will allow an *ex vivo* analysis of miR-455-null MSCs differentiating through chondrogenesis. The hypothesised outcome would be an increase in chondrogenesis which would demonstrate if miR-455-3p knockout leads to activation of chondrogenesis.

Gene regulation by microRNAs commonly involves feedback loops. To explore the potential feedback mechanisms between miR-455-3p and CREB1, CREB1 can be overexpressed using a lentiviral system. Following this, miR-455-3p expression can be measured and if miR-455 is transactivated by CREB1, the promoter can be defined using 5'RACE. A rescue experiment in chick embryo can also be performed. For example, chick limb buds microinjected with miR-455-3p mimic can be injected with CREB1 mimic to reveal if the inhibited limb bud development phenotype is rescued. In addition to this,

limb buds can be microinjected with a CREB1 inhibitor to reveal if this phenocopies miR-455-3p overexpression *in ovo*.

To demonstrate the impact of miR-455-3p and CREB1 on chondrogenic proliferation, hMSCs or human articular chondrocytes can be transduced with miR-455-3p or CREB1 shRNA lentivirus and cell proliferation can be measured using BrdU incorporation. This system can also be used to demonstrate the impact of miR-455-3p and CREB1 on mitochondrial dysfunction. The Agilent Seahorse assay can measure mitochondrial metabolism and Mitotracker dyes can reveal mitochondrial morphology.

1.7.3. Identification of miR-455-3p/CREB1 targets

Developing upon the chick limb bud RNA-seq data, it is important to identify specific targets of miR-455-3p/CREB1 during chondrogenesis. For this, the chondrogenesis assay can be used, with miR-455-3p mimic transfection and CREB1 siRNA transfection. From each timepoint, RNA-seq can be performed to identify differentially expressed genes. These can be assessed by pathway analysis for chondrogenesis involvement. Potential novel targets can be assessed by luciferase assay or CRISPR/Cas9 genome engineering. The MRE analysis by CRISPR/Cas9 genome engineering described in this research has the potential to be scaled up for multiplex studies (310). To develop this technique further, it would be useful to optimize the protocol for use in primary human articular chondrocytes and human MSCs. This will allow the study of cell-specific interactions between miR-455-3p and target genes. Many microRNA regulatory pathways differ between tissue type, and it would be interesting to compare this in SW1353 cells, human articular chondrocytes and MSCs. It would also be interesting to compare healthy articular cartilage samples and OA samples, to understand the regulatory roles of miRNAs in diseased and healthy tissues.

1.8. Final conclusions

To conclude, through many possible mechanisms, we have shown overexpression of miR-455-3p appears to inhibit chondrogenesis. This may be due to miR-455-3p targeting CREB1, resulting in a downregulation of CREB1 expression. Transcription factors and

miRNAs are commonly involved in feedback loops. Previous work has demonstrated that CREB1 can increase expression of SOX9, and SOX9 is a major activator of miR-455-3p. The repression of chondrogenesis observed when miR-455-3p is overexpressed could be a result of CREB1 and therefore SOX9 downregulation, decreasing osteochondrogenic gene transcription (Figure 7.2). It is also very likely that CREB1 has additional actions outside of the miR-455-3p feedback loop.

miR-455-3p could be present during differentiation to control the level of chondrocyte specific proliferation, and this could explain previous research where miR-455-3p is not detected at earlier stages of development. This also provides an explanation for why there were no differences observed in the developing chick limb bud following inhibition of miR-455-3p. Following with this hypothesis, an increase in miR-455-3p is required to control proliferation, however, overexpression results in insufficient proliferation. Since CREB1 is known to regulate cell proliferation and cell cycle transition, overexpression of miR-455-3p could inhibit the cell cycle by downregulating CREB1, resulting in dysregulation of the cell cycle. From a disease perspective, the knockdown of miR-455-3p may alleviate osteoarthritis, and an increase in CREB1 expression could promote regeneration. This provides a basis for future research, hypothesising that the role of miR-455-3p in chondrogenesis is to regulate the expression of CREB1 within this system.

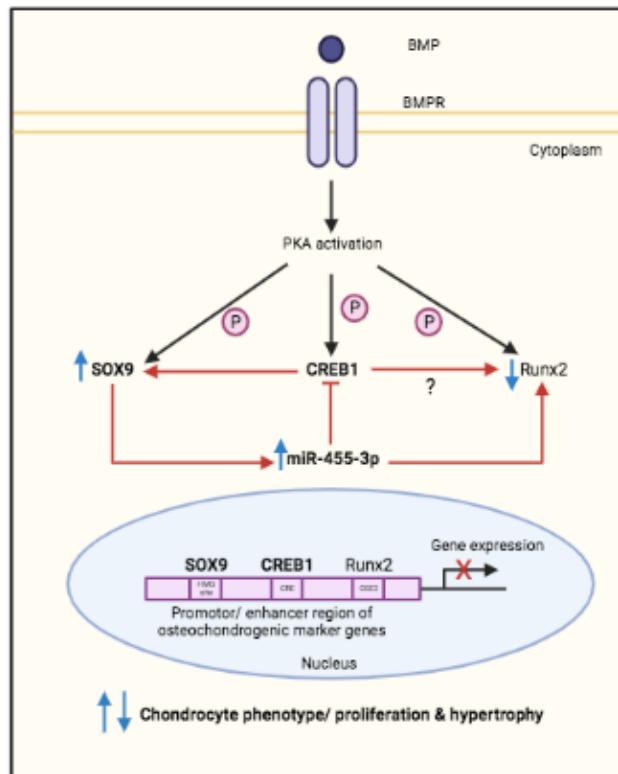


Figure 7.2: *miR-455-3p/ CREB1 schematic in chondrocytes. BMP2 induces PKA activation, phosphorylating downstream factors including SOX9, CREB1 and other osteochondrogenic factors. This then regulates transcription and function of these osteochondrogenic factors, where SOX9 and CREB1 directly interact. Red arrows indicate predicted miR-455-3p/ CREB1 feedback loop. Blue arrows indicate direction of expression, where miR-455-3p overexpression represses chondrogenic gene expression, due to direct regulation of CREB1 (Adapted from Zhao et al, 2008).*

Bibliography

1. Zulma, Gazit. Gadi, Pelled. Dima, Sheyn. Nadav, Kimelman. Dan G. Principles of Regenerative Medicine, Chapter 19 – Mesenchymal Stem Cells. First. 2008. 318–343 p.
2. Zulma, Gazit. Gadi, Pelled. Dima, Sheyn. Nadav, Kimelman. Dan G. Principles of Regenerative Medicine, Chapter 17 - Mesenchymal Stem Cells [Internet]. Second. 2011. 285–304 p. Available from: <https://doi.org/10.1016/B978-0-12-381422-7.10017-3>
3. Gafni Y, Pelled G, Zilberman Y, Turgeman G, Apparailly F, Yotvat H, et al. Gene therapy platform for bone regeneration using an exogenously regulated, AAV-2-based gene expression system. *Mol Ther* [Internet]. 2004;9(4):587–95. Available from: <http://dx.doi.org/10.1016/j.ymthe.2003.12.009>
4. Kim Y, Ryu J-S, Yeo J, Choi Y, Kim Y, Ko K, et al. Overexpression of TGF- β 1 enhances chondrogenic differentiation and proliferation of human synovium-derived stem cells. *Biochem Biophys Res Commun*. 2014;450(4):1593–9.
5. Gimble J, Kaplan DL. Comparative Chondrogenesis of Human Cell Sources in 3D Scaffolds. *J Tissue Eng Regen Med*. 2009;3(5):348–60.
6. Zuo Q, Cui W, Liu F, Wang Q, Chen Z, Fan W. Co-cultivated mesenchymal stem cells support chondrocytic differentiation of articular chondrocytes. *Int Orthop*. 2013;37(4):747–52.
7. Augustyniak E, Trzeciak T, Richter M, Kaczmarczyk J, Suchorska W. The role of growth factors in stem cell-directed chondrogenesis: a real hope for damaged cartilage regeneration. *Int Orthop*. 2015;39(5):995–1003.
8. Ullah I, Subbarao RB, Rho GJ. Human mesenchymal stem cells - Current trends and future prospective. *Biosci Rep*. 2015;35.
9. Horwitz, Edwin M. Andreef, Michael. Frassoni F. Mesenchymal Stromal Cells. *Curr Opin Hematol*. 2006;13(6):419–25.
10. Goldring MB. Chondrogenesis, chondrocyte differentiation, and articular cartilage metabolism in health and osteoarthritis. *Ther Adv Musculoskelet Dis*. 2012;4(4):269–85.
11. M.B. G, K. T, K. I. The control of chondrogenesis [Internet]. Vol. 97, *Journal of Cellular Biochemistry*. 2006. p. 33–44. Available from: <http://www.embase.com/search/results?subaction=viewrecord&from=export&id=L43050970%5Cnhttp://dx.doi.org/10.1002/jcb.20652%5Cnhttp://elvis.ubvu.vu.nl:9003/vulink?sid=EMBASE&issn=07302312&id=doi:10.1002%2Fjcb.20652&atitle=The+control+of+chondrogenesis&stilt>
12. Keller B, Yang T, Chen Y, Munivez E, Bertin T, Zabel B, et al. Interaction of TGF β and bmp signaling pathways during chondrogenesis. *PLoS One*. 2011;6(1).
13. Mueller MB, Fischer M, Zellner J, Berner A, Dienstknecht T, Prantl L, et al. Hypertrophy in mesenchymal stem cell chondrogenesis: Effect of TGF- β isoforms and chondrogenic conditioning. *Cells Tissues Organs*. 2010;192(3):158–66.
14. Bi W, Min Deng J, Zhang Z, Behringer R, Crombrugge D. Sox9 is required for cartilage formation. *Nat Genet*. 1999;25:85–9.
15. Chang SH, Oh C Do, Yang MS, Kang SS, Lee YS, Sonn JK, et al. Protein kinase C regulates chondrogenesis of mesenchymes via mitogen- activated protein kinase signaling. *J Biol Chem*. 1998;273(30):19213–9.

16. Dong S, Yang B, Guo H, Kang F. MicroRNAs regulate osteogenesis and chondrogenesis. *Biochem Biophys Res Commun*. 2012;418(4):587–91.
17. Miljkovic ND, Cooper GM, Marra KG. Chondrogenesis, bone morphogenetic protein-4 and mesenchymal stem cells. *Osteoarthr Cartil*. 2008;16(10):1121–30.
18. Prein C, Beier F. ECM Signalling in cartilage development and endochondral ossification. In: *Current topics in Developmental Biology*. 2019. p. (133) 25-47.
19. Mihelic R, Pecina M, Jelic M, Zoricic S, Kusec V, Simic P, et al. Bone Morphogenetic Protein–7 (Osteogenic Protein–1) Promotes Tendon Graft Integration in Anterior Cruciate Ligament Reconstruction in Sheep. *Am J Sport Med*. 2004;32(7):1619–25.
20. Zoricic S, Maric I, Bobinac D, Vukicevic S. Expression of bone morphogenetic proteins and cartilage-derived morphogenetic proteins during osteophyte formation in humans. *J Anat*. 2003;202(3):269–77.
21. Komori T. Regulation of osteoblast differentiation by transcription factors. *J Cell Biochem*. 2006;99(5):1233–9.
22. Komori T. Regulation of bone development and extracellular matrix protein genes by RUNX2. *Cell Tissue Res*. 2010;339(1):189–95.
23. Toyosawa S, Shintani S, Fujiwara T, Ooshima T, Sato A, Ijuhin N, et al. Dentin matrix protein 1 is predominantly expressed in chicken and rat osteocytes but not in osteoblasts. *J Bone Miner Res*. 2001;16(11):2017–26.
24. Sera SR, zur Nieden NI. microRNA Regulation of Skeletal Development. *Curr Osteoporos Rep*. 2017;15(4):353–66.
25. Grgurevic L, Macek B, Mercep M, Jelic M, Smoljanovic T, Erjavec I, et al. Bone morphogenetic protein (BMP)1-3 enhances bone repair. *Biochem Biophys Res Commun*. 2011;408(1):25–31.
26. Vukicevic S, Grgurevic L. BMP-6 and mesenchymal stem cell differentiation. *Cytokine Growth Factor Rev*. 2009;20(5–6):441–8.
27. Zhang Y, Wang F, Chen J, Ning Z, Yang L. Bone marrow-derived mesenchymal stem cells versus bone marrow nucleated cells in the treatment of chondral defects. *Int Orthop*. 2012;36:1079–86.
28. Zuniga A. Next generation limb development and evolution: Old questions, new perspectives. *Dev*. 2015;142(22):3810–20.
29. Wolpert L, Tickle C, Martinez Arias A, Lawrence P, Lumsden A, Robertson E, et al. *Principles of Development*. 5th ed. Oxford: Oxford University Press; 2015.
30. Hill RE, Lettice LA. Kaufman’s Atlas of Mouse Development Supplement, Chapter 15 - Limb Development. Academic Press; 2016. 193–205 p.
31. Pearse R, Scherz P, Campbell J, Tabin C. A cellular lineage analysis of the chick limb bud. *Dev Biol*. 2007;310(2):388–400.
32. Nowlan NC, Sharpe J, Roddy KA, Prendergast PJ, Murphy P. Mechanobiology of embryonic skeletal development: Insights from animal models. *Birth Defects Res Part C - Embryo Today Rev*. 2010;90(3):203–13.
33. Zeller R, Lopez-Rios J, Zuniga A. Vertebrate limb bud development: moving towards integrative analysis of organogenesis. *Nat Rev Genet*. 2009;10:845–58.
34. Rodriguez-Esteban C, Tsukui T, Yonei S, Magallon J, Tamura K, Izpisua Belmonte J. The T-box genes *Tbx4* and *Tbx5* regulate limb outgrowth and identity. *Nature*. 1999;398(6730):814–8.
35. Takeuchi JK, Koshiba-Takeuchi K, Suzuki T, Kamimura M, Ogura K, Ogura T. *Tbx5* and *Tbx4* trigger limb initiation through activation of the Wnt/Fgf signaling

- cascade. *Development*. 2003;130(12):2729–39.
36. Nemec S, Luxey M, Jain D, Huang Sung A, Pastinen T, Drouin J. Pitx1 directly modulates the core limb development program to implement hindlimb identity. *Development*. 2017;144:3325–2225.
 37. Postma A V., Van De Meerakker JBA, Mathijssen IB, Barnett P, Christoffels VM, Ilgun A, et al. A gain-of-function TBX5 mutation is associated with atypical Holt-Oram syndrome and paroxysmal atrial fibrillation. *Circ Res*. 2008;102(11):1433–42.
 38. Klopocki E, Kähler C, Foulds N, Shah H, Joseph B, Vogel H, et al. Deletions in PITX1 cause a spectrum of lower-limb malformations including mirror-image polydactyly. *Eur J Hum Genet*. 2012;20(6):705–8.
 39. Basson CT, Huang T, Lin RC, Bachinsky DR, Weremowicz S, Vaglio A, et al. Different TBX5 interactions in heart and limb defined by Holt-Oram syndrome mutations. *Proc Natl Acad Sci U S A*. 1999;96(6):2919–24.
 40. Min H, Danilenko DM, Scully SA, Bolon B, Ring BD, Tarpley JE, et al. Fgf-10 is required for both limb and lung development and exhibits striking functional similarity to *Drosophila* branchless. *Genes Dev*. 1998;12(20):3156–61.
 41. Kawakami Y, Capdevila J, Büscher D, Itoh T, Esteban CR, Belmonte JCI. WNT signals control FGF-dependent limb initiation and AER induction in the chick embryo. *Cell*. 2001;104(6):891–900.
 42. Yang Y, Kozin SH. Cell signaling regulation of vertebrate limb growth and patterning. *J Bone Jt Surg - Ser A*. 2009;91(SUPPL. 4):76–80.
 43. Parr BA, McMahon AP. Dorsalizing signal Wnt-7a required for normal polarity of D–V and A–P axes of mouse limb. *Nature*. 1995;374:350–3.
 44. Tanaka EM, Gann AAF. Limb Development: The budding role of FGF. *Curr Biol*. 1995;5(6):594–7.
 45. Yang Y, Niswander L. Interaction between the signaling molecules WNT7a and SHH during vertebrate limb development: Dorsal signals regulate anteroposterior patterning. *Cell*. 1995;80(6):939–47.
 46. Jin L, Wu J, Bellusci S, Zhang JS. Fibroblast growth factor 10 and vertebrate limb development. *Front Genet*. 2019;10(JAN):1–9.
 47. Bénazet JD, Zeller R. Vertebrate limb development: moving from classical morphogen gradients to an integrated 4-dimensional patterning system. *Cold Spring Harb Perspect Biol*. 2009;1(4):1–14.
 48. Geetha-Loganathan P, Nimmagadda S, Scaal M. Wnt signaling in limb organogenesis. *Organogenesis*. 2008;4(2):109–15.
 49. Yamaguchi TP, Bradley A, McMahon AP, Jones S. A Wnt5a pathway underlies outgrowth of multiple structures in the vertebrate embryo. *Development*. 1999;126(6):1211–23.
 50. Korn MJ, Cramer KS. Windowing chicken eggs for developmental studies. *J Vis Exp*. 2007;(8):2–3.
 51. Hsieh F. Impact of developmental biology on medicine. *J Formos Med Assoc*. 2000;99(2):86–91.
 52. Editorial. Developing disease. *Nat Cell Biol*. 2007;9(9):2007–2007.
 53. OpenStax. OpenStax CNX. In: *Anatomy & Physiology* [Internet]. 2016. Available from: <http://cnx.org/contents/14fb4ad7-39a1-4eee-ab6e-3ef2482e3e22@8.24>.
 54. Chijimatsu R, Saito T. Mechanisms of synovial joint and articular cartilage development. *Cell Mol Life Sci* [Internet]. 2019;76(20):3939–52. Available from:

<https://doi.org/10.1007/s00018-019-03191-5>

55. Oliveira I, Gon C, Lu R. Regenerative Strategies for the Treatment of Knee Joint Disabilities. 2017. 21–29 p.
56. Tarafder S, Lee C. Synovial Joint. In: In Situ Tissue Regeneration. 2016.
57. Abulhasan JF, Grey MJ. Anatomy and physiology of knee stability. *J Funct Morphol Kinesiol.* 2017;2(4).
58. Fenn S, Datir A, Saifuddin A. Synovial recesses of the knee: MR imaging review of anatomical and pathological features. *Skeletal Radiol.* 2009;38:317–28.
59. Ralphs J, Benjamin M. The joint capsule: structure, composition, ageing and disease. *J Anat.* 1994;503–9.
60. Long F, Ornitz DM. Development of the endochondral skeleton. *Cold Spring Harb Perspect Biol.* 2013;5(1):1–20.
61. Lefebvre V, Bhattaram P. Vertebrate skeletogenesis. *Curr Top Dev Biol.* 2010;90(C):291–317.
62. Mirzamohammadi F, Papaioannou G, Kobayashi T. microRNAs in cartilage development, homeostasis, and disease. *Curr Osteoporos Rep.* 2014;12(4):410–9.
63. Ağirdil Y. The growth plate: A physiologic overview. *EFORT Open Rev.* 2020;5(8):498–507.
64. Sophia Fox AJ, Bedi A, Rodeo SA. The basic science of articular cartilage: Structure, composition, and function. *Sports Health.* 2009;1(6):461–8.
65. Buckwalter J, Mankin H. Articular cartilage: degeneration and osteoarthritis, repair, regeneration, and transplantation. *Instr Course Lect.* 1998;47:487–504.
66. Wiley J, Link C. Proliferative re-modeling of the spatial organization of human superficial chondrocytes distant to focal early osteoarthritis (OA). 2012;62(2):489–98.
67. Camarero-Espinosa S, Rothen-Rutishauser B, Foster E, Weder C. Articular cartilage: from formation to tissue engineering. *Biomater Sci.* 2016;4(5):734–67.
68. Goldring MB, Marcu KB. Cartilage homeostasis in health and rheumatic diseases. *Arthritis Res Ther.* 2009;11(3).
69. Man GS, Mologhianu G. Osteoarthritis pathogenesis - a complex process that involves the entire joint. *J Med Life.* 2014;7(1):37–41.
70. Heijink A, Vanhees M, van den Ende K, van den Bekerom MP, van Riet RP, Van Dijk CN, et al. Biomechanical considerations in the pathogenesis of osteoarthritis of the elbow. *Knee Surgery, Sport Traumatol Arthrosc.* 2016;24(7):2313–8.
71. Oldershaw RA, Baxter MA, Lowe ET, Bates N, Grady LM, Soncin F, et al. Directed differentiation of human embryonic stem cells toward chondrocytes. *Nat Biotechnol.* 2010;28(11):1187–94.
72. Chijimatsu R, Ikeya M, Yasui Y, Ikeda Y, Ebina K, Moriguchi Y, et al. Characterization of Mesenchymal Stem Cell-Like Cells Derived from Human iPSCs via Neural Crest Development and Their Application for Osteochondral Repair. *Stem Cells Int.* 2017;2017.
73. Mobasheri A, Batt M. An update on the pathophysiology of osteoarthritis. *Ann Phys Rehabil Med [Internet].* 2016;59(5–6):333–9. Available from: <http://dx.doi.org/10.1016/j.rehab.2016.07.004>
74. Ashkavand Z, Malekinejad H, Vishwanath BS. The pathophysiology of osteoarthritis. *J Pharm Res [Internet].* 2013;7(1):132–8. Available from: <http://dx.doi.org/10.1016/j.jopr.2013.01.008>

75. Dieppe P. Developments in osteoarthritis. *Rheumatology*. 2011;50(2):245–7.
76. Goldring M, Goldring S. Articular cartilage and subchondral bone in the pathogenesis of osteoarthritis. *Ann N Y Acad Sci*. 2010;
77. Felson D, Anderson J, Naimark A, Walker A, Meenan R. Obesity and knee osteoarthritis. The Framingham Study. *Ann Intern Med*. 1998;109(1):18–24.
78. Liu-Bryan R, Terkeltaub R. Emerging regulators of the inflammatory process in osteoarthritis. *Nat Rev Rheumatol*. 2015;11(1):35–44.
79. Xu B, Li Y yao, Ma J, Pei F xing. Roles of microRNA and signaling pathway in osteoarthritis pathogenesis. *J Zhejiang Univ Sci B*. 2016;17(3):200–8.
80. Portal-Núñez S, Esbrit P, Alcaraz MJ, Largo R. Oxidative stress, autophagy, epigenetic changes and regulation by miRNAs as potential therapeutic targets in osteoarthritis. *Biochem Pharmacol*. 2016;108:1–10.
81. Zhang M, Lygrissea K, Wanga J. Role of MicroRNA in Osteoarthritis. *J Arthritis*. 2017;06(02).
82. Stannus O, Jones G, Cicuttini F, Parameswaran V, Quinn S, Burgess J, et al. Circulating levels of IL-6 and TNF- α are associated with knee radiographic osteoarthritis and knee cartilage loss in older adults. *Osteoarthr Cartil* [Internet]. 2010;18(11):1441–7. Available from: <http://dx.doi.org/10.1016/j.joca.2010.08.016>
83. Buckwalter J, Mankin H, Grodzinsky A. Articular cartilage and osteoarthritis. *Instr Course Lect*. 2005;54:465–80.
84. Goldring MB, Goldring SR. Osteoarthritis. *J Cell Physiol*. 2007;213(3):626–34.
85. Zhong L, Huang X, Karperien M, Post JN. Correlation between gene expression and osteoarthritis progression in human. *Int J Mol Sci*. 2016;17(7):1–14.
86. Dunn SL, Soul J, Anand S, Schwartz JM, Boot-Handford RP, Hardingham TE. Gene expression changes in damaged osteoarthritic cartilage identify a signature of non-chondrogenic and mechanical responses. *Osteoarthr Cartil* [Internet]. 2016;24(8):1431–40. Available from: <http://dx.doi.org/10.1016/j.joca.2016.03.007>
87. Tian H. Detection of differentially expressed genes involved in osteoarthritis pathology. *J Orthop Surg Res*. 2018;13(1):1–8.
88. Appleton CTG, Pitelka V, Henry J, Beier F. Global analyses of gene expression in early experimental osteoarthritis. *Arthritis Rheum*. 2007;56(6):1854–68.
89. Sanjurjo-Rodriguez C, Baboolal TG, Burska AN, Ponchel F, El-Jawhari JJ, Pandit H, et al. Gene expression and functional comparison between multipotential stromal cells from lateral and medial condyles of knee osteoarthritis patients. *Sci Rep*. 2019;9(1):1–12.
90. Ramos YFM, Den Hollander W, Bovée JVMG, Bomer N, Van Der Breggen R, Lakenberg N, et al. Genes involved in the osteoarthritis process identified through genome wide expression analysis in articular cartilage; the RAAK study. *PLoS One*. 2014;9(7).
91. Skinner MK. Environmental epigenetic transgenerational inheritance and somatic epigenetic mitotic stability. *Epigenetics*. 2011;2294.
92. Feinbaum R, Ambros V, Lee R. The *C. elegans* Heterochronic Gene *lin-4* Encodes Small RNAs with Antisense Complementarity to *lin-14*. *Cell*. 2004;116(116):843–54.
93. Kutter C, Svoboda P. miRNA, siRNA, piRNA: Knowns of the unknown. *RNA Biol*. 2008;5(4):181–8.
94. Sondag G, Haqqi T. The Role of MicroRNAs and Their Targets in Osteoarthritis. *Curr Rheumatol Rep*. 2016;18(8):56.

95. Moran Y, Agron M, Praher D, Technau U. The evolutionary origin of plant and animal microRNAs. *Nat Ecol Evol.* 2017;1(3):1–22.
96. Ibáñez-Ventoso C, Vora M, Driscoll M. Sequence relationships among *C. elegans*, *D. melanogaster* and human microRNAs highlight the extensive conservation of microRNAs in biology. *PLoS One.* 2008;3(7).
97. Kopańska M, Szala D, Czech J, Gabło N, Gargas K, Trzeciak M, et al. MiRNA expression in the cartilage of patients with osteoarthritis. *J Orthop Surg Res.* 2017;12(1):1–7.
98. O'Brien J, Hayder H, Zayed Y, Peng C. Overview of microRNA biogenesis, mechanisms of actions, and circulation. *Front Endocrinol (Lausanne).* 2018;9(AUG):1–12.
99. Tétreault N, De Guire V. MiRNAs: Their discovery, biogenesis and mechanism of action. *Clin Biochem [Internet].* 2013;46(10–11):842–5. Available from: <http://dx.doi.org/10.1016/j.clinbiochem.2013.02.009>
100. Lee Y, Ahn C, Han J, Choi H, Kim J, Yim J, et al. The nuclear RNase III Drosha initiates microRNA processing. *Nature.* 2003;425(September):1–5.
101. Han J, Lee Y, Yeom K-H, Kim Y-K, Jin H, Kim VN. The Drosha-DGCR8 complex in primary microRNA processing. *Genes Dev [Internet].* 2004;(18):3016–27. Available from: <http://www.pubmedcentral.nih.gov/articlerender.fcgi?artid=4078803&tool=pmcentrez&rendertype=abstract%0Ahttp://eutils.ncbi.nlm.nih.gov/entrez/eutils/elink.fcgi?dbfrom=pubmed&id=15549137&retmode=ref&cmd=prlinks%5Cnpapers3://publication/doi/10.1038/sj.emboj>.
102. Lund E, Güttinger S, Calado A, Dahlberg JE, Kutay U. Nuclear Export of MicroRNA Precursors. *Science (80-).* 2004;303(5654):95–8.
103. Ha M, Kim VN. Regulation of microRNA biogenesis. *Nat Rev Mol Cell Biol.* 2014;15(8):509–24.
104. Yoda M, Kawamata T, Paroo Z, Ye X, Iwasaki S, Liu Q, et al. ATP-dependent human RISC assembly pathways. *Nat Struct Mol Biol.* 2010;17(1):17–24.
105. Meijer H, Smith E, Bushell M. Regulation of miRNA strand selection: follow the leader? *Biochem Soc Trans.* 2014;42(4):1135–40.
106. Broughton JP, Lovci MT, Huang JL, Yeo GW, Pasquinelli AE. Pairing beyond the Seed Supports MicroRNA Targeting Specificity. *Mol Cell [Internet].* 2016;64(2):320–33. Available from: <http://dx.doi.org/10.1016/j.molcel.2016.09.004>
107. Vasudevan S. Posttranscriptional Upregulation by MicroRNAs. *Wiley Interdiscip Rev RNA.* 2012;3(3):311–30.
108. Dharap A, Pokrzywa C, Murali S, Pandi G, Vemuganti R. MicroRNA miR-324-3p induces promoter-mediated expression of RelA gene. *PLoS One.* 2013;8(11):4–8.
109. Forman JJ, Legesse-Miller A, Collier HA. A search for conserved sequences in coding regions reveals that the let-7 microRNA targets Dicer within its coding sequence. *Proc Natl Acad Sci U S A.* 2008;105(39):14879–84.
110. Zhang J, Zhou W, Liu Y, Liu T, Li C, Wang L. Oncogenic role of microRNA-532-5p in human colorectal cancer via targeting of the 5'UTR of RUNX3. *Oncol Lett.* 2018;15(5):7215–20.
111. Makarova JA, Shkurnikov MU, Wicklein D, Lange T, Samatov TR, Turchinovich AA, et al. Intracellular and extracellular microRNA: An update on localization and biological role. *Prog Histochem Cytochem [Internet].* 2016;51(3–4):33–49.

Available from: <http://dx.doi.org/10.1016/j.proghi.2016.06.001>

112. Li L, Jia J, Liu X, Yang S, Ye S, Yang W, et al. MicroRNA-16-5p Controls Development of Osteoarthritis by Targeting SMAD3 in Chondrocytes. *Curr Pharm Des*. 2015;21(35):5160–7.
113. Berenbaum F. Osteoarthritis as an inflammatory disease (osteoarthritis is not osteoarthrosis!). *Osteoarthr Cartil*. 2013;21(1):16–21.
114. Kosaka N, Iguchi H, Yoshioka Y, Takeshita F, Matsuki Y, Ochiya T. Secretory mechanisms and intercellular transfer of microRNAs in living cells. *J Biol Chem*. 2010;285(23):17442–52.
115. Iftikhar H, Carney GE. Evidence and potential in vivo functions for biofluid miRNAs: From expression profiling to functional testing: Potential roles of extracellular miRNAs as indicators of physiological change and as agents of intercellular information exchange. *BioEssays*. 2016;38(4):367–78.
116. Ivey KN, Srivastava D. microRNAs as developmental regulators. *Cold Spring Harb Perspect Biol*. 2015;7(7):1–9.
117. Swingler TE, Niu L, Smith P, Paddy P, Le L, Barter MJ, et al. The function of microRNAs in cartilage and osteoarthritis. *Clin Exp Rheumatol*. 2019;37(5):40–7.
118. Harfe B, McManus M, Mansfield J, Hornstein E, Tabin C. The RNaseIII enzyme Dicer is required for morphogenesis but not patterning of the vertebrate limb. *PNAS*. 2005;102(31):10898–903.
119. Kobayashi T, Lu J, Cobb BS, Rodda SJ, McMahon AP, Schipani E, et al. Dicer-dependent pathways regulate chondrocyte proliferation and differentiation. *Natl Acad Sci U S A*. 2008;105(6):1949–54.
120. Kobayashi T, Papaioannou G, Mirzamohammadi F, Kozhemyakina E, Zhang M, Blelloch R, et al. Early postnatal ablation of the microRNA-processing enzyme, Drosha, causes chondrocyte death and impairs the structural integrity of the articular cartilage. *Osteoarthr Cartil*. 2015;23(7):1214–20.
121. Hobert O. Gene regulation by transcription factors and microRNAs. *Science (80-)*. 2008;319(5871):1785–6.
122. Kapinas K, Delany AM. MicroRNA biogenesis and regulation of bone remodeling. *Arthritis Res Ther*. 2011;13(3):1–11.
123. Peng S, Gao D, Gao C, Wei P, Niu M, Shuai C. MicroRNAs regulate signaling pathways in osteogenic differentiation of mesenchymal stem cells (Review). *Mol Med Rep*. 2016;14(1):623–9.
124. Gámez B, Rodríguez-Carballo E, Ventura F. MicroRNAs and post-transcriptional regulation of skeletal development. *J Mol Endocrinol*. 2014;52(3).
125. Kang H, Hata A. The role of microRNAs in cell fate determination of mesenchymal stem cells: Balancing adipogenesis and osteogenesis. *BMB Rep*. 2015;48(6):319–23.
126. Inose H, Ochi H, Kimura A, Fujita K, Xu R, Sato S, et al. A microRNA regulatory mechanism of osteoblast differentiation. *Proc Natl Acad Sci U S A*. 2009;106(49):20794–9.
127. Eguchi T, Watanabe K, Hara ES, Ono M, Kuboki T, Calderwood SK. OstemiR: A Novel Panel of MicroRNA Biomarkers in Osteoblastic and Osteocytic Differentiation from Mesenchymal Stem Cells. *PLoS One*. 2013;8(3).
128. Kapinas K, Kessler CB, Delany AM. miR-29 suppression of osteonectin in osteoblasts: Regulation during differentiation and by canonical Wnt signaling. *J Cell Biochem*. 2009;108(1):216–24.

129. Hong E, Reddi A. MicroRNAs in chondrogenesis, articular cartilage, and osteoarthritis: implications for tissue engineering. *Tissue Eng Part B Rev.* 2012;18(6):445–53.
130. Lolli A, Colella F, De Bari C, van Osch GJVM. Targeting anti-chondrogenic factors for the stimulation of chondrogenesis: A new paradigm in cartilage repair. *J Orthop Res.* 2019;37(1):12–22.
131. Nakamura Y, He X, Kato H, Wakitani S, Kobayashi T, Watanabe S, et al. Sox9 is upstream of microRNA-140 in cartilage. *Appl Biochem Biotechnol.* 2012;166(1):64–71.
132. Miyaki S, Sato T, Inoue A, Otsuki S, Ito Y, Yokoyama S, et al. MicroRNA-140 plays dual roles in both cartilage development and homeostasis. *Genes Dev.* 2010;24(11):1173–85.
133. Nakamura Y, Inloes JB, Katagiri T, Kobayashi T. Chondrocyte-Specific MicroRNA-140 Regulates Endochondral Bone Development and Targets Dnpep To Modulate Bone Morphogenetic Protein Signaling. *Mol Cell Biol.* 2011;31(14):3019–28.
134. Yang J, Qin S, Yi C, Ma G, Zhu H, Zhou W, et al. MiR-140 is co-expressed with Wwp2-C transcript and activated by Sox9 to target Sp1 in maintaining the chondrocyte proliferation. *FEBS Lett [Internet].* 2011;585(19):2992–7. Available from: <http://dx.doi.org/10.1016/j.febslet.2011.08.013>
135. Barter MJ, Tselepi M, Gómez R, Woods S, Hui W, Smith GR, et al. Genome-wide microRNA and gene analysis of mesenchymal stem cell chondrogenesis identifies an essential role and multiple targets for miR-140-5p. *Stem Cells.* 2015;33(11):3266–80.
136. Karlsen T, Jakobsen R, Mikkelsen T, Brinchmann J. microRNA-140 targets RALA and regulates chondrogenic differentiation of human mesenchymal stem cells by translational enhancement of SOX9 and ACAN. *Stem Cells Dev.* 2013;23(3).
137. Zhang Z, Hou C, Meng F, Zhao X, Zhang Z, Huang G, et al. MiR-455-3p regulates early chondrogenic differentiation via inhibiting Runx2. *FEBS Lett [Internet].* 2015;589(23):3671–8. Available from: <http://dx.doi.org/10.1016/j.febslet.2015.09.032>
138. Chen W, Chen L, Zhang Z, Meng F, Huang G, Sheng P, et al. MicroRNA-455-3p modulates cartilage development and degeneration through modification of histone H3 acetylation. *Biochim Biophys Acta - Mol Cell Res [Internet].* 2016;1863(12):2881–91. Available from: <http://dx.doi.org/10.1016/j.bbamcr.2016.09.010>
139. Sun H, Zhao X, Zhang C, Zhang Z, Lun J, Liao W, et al. MiR-455-3p inhibits the degenerate process of chondrogenic differentiation through modification of DNA methylation article. *Cell Death Dis [Internet].* 2018;9(5). Available from: <http://dx.doi.org/10.1038/s41419-018-0565-2>
140. Tuddenham L, Wheeler G, Ntounia-Fousara S, Waters J, Hajihosseini MK, Clark I, et al. The cartilage specific microRNA-140 targets histone deacetylase 4 in mouse cells. *FEBS Lett.* 2006;580(17):4214–7.
141. Eberhart JK, He X, Swartz ME, Yan YL, Song H, Boling TC, et al. MicroRNA Mirn140 modulates Pdgf signaling during palatogenesis. *Nat Genet.* 2008;40(3):290–8.
142. Pais H, Nicolas FE, Soond SM, Swingler TE, Clark IM, Chantry A, et al. Analyzing mRNA expression identifies Smad3 as a microRNA-140 target regulated only at protein level. *Rna.* 2010;16(3):489–94.

143. Karlsen T, Jakobsen R, Mikkelsen T, Brinchmann J. microRNA-140 targets RALA and regulates chondrogenic differentiation of human mesenchymal stem cells by translational enhancement of SOX9 and ACAN. *Stem Cells Dev.* 2013;23(3).
144. McAlinden A, Im G. MicroRNAs in Orthopaedic Research: Disease Associations, Potential Therapeutic Applications, and Perspectives. *J Orthop Res.* 2018;36(1):33–51.
145. Guerit D, Brondello J-M, Chuchana P, Philipot D, Toupet K, Bony C, et al. FOXO3A regulation by miRNA-29a Controls chondrogenic differentiation of mesenchymal stem cells and cartilage formation. *Stem Cells Dev.* 2014;23(11):1195–205.
146. Le LTT, Swingler TE, Crowe N, Vincent TL, Barter MJ, Donell ST, et al. The microRNA-29 family in cartilage homeostasis and osteoarthritis. *J Mol Med [Internet].* 2016;94(5):583–96. Available from: <http://dx.doi.org/10.1007/s00109-015-1374-z>
147. Yang B, Kang X, Xing Y, Dou C, Kang F, Li J, et al. Effect of microRNA-145 on IL-1 β -induced cartilage degradation in human chondrocytes. *FEBS Lett [Internet].* 2014;588(14):2344–52. Available from: <http://dx.doi.org/10.1016/j.febslet.2014.05.033>
148. Guérit D, Philipot D, Chuchana P, Toupet K, Brondello JM, Mathieu M, et al. Sox9-Regulated miRNA-574-3p Inhibits Chondrogenic Differentiation of Mesenchymal Stem Cells. *PLoS One.* 2013;8(4).
149. Lin X, Wu L, Zhang Z, Yang R, Guan Q, Hou X, et al. MiR-335-5p promotes chondrogenesis in mouse mesenchymal stem cells and is regulated through two positive feedback loops. *J Bone Miner Res.* 2014;29(7):1575–85.
150. Laine S, Alm J, Virtanen S, Aro H, Laitala-Leinonen T. MicroRNAs miR-96, miR-124, and miR-199a regulate gene expression in human bone marrow-derived mesenchymal stem cells. *J Cell Biochem.* 2012;113(8):2687–95.
151. Sumiyoshi K, Kubota S, Ohgawara T, Kawata K, Nishida T, Shimo T, et al. Identification of miR-1 as a micro RNA that supports late-stage differentiation of growth cartilage cells. *Biochem Biophys Res Commun [Internet].* 2010;402(2):286–90. Available from: <http://dx.doi.org/10.1016/j.bbrc.2010.10.016>
152. Song J, Kim D, Chun CH, Jin EJ. MicroRNA-375, a new regulator of cadherin-7, suppresses the migration of chondrogenic progenitors. *Cell Signal [Internet].* 2013;25(3):698–706. Available from: <http://dx.doi.org/10.1016/j.cellsig.2012.11.014>
153. Martinez-Sanchez A, Murphy CL. miR-1247 functions by targeting cartilage transcription factor SOX9. *J Biol Chem.* 2013;288(43):30802–14.
154. Kim D, Song J, Jin EJ. MicroRNA-221 regulates chondrogenic differentiation through promoting proteosomal degradation of slug by targeting Mdm2. *J Biol Chem.* 2010;285(35):26900–7.
155. Paik S, Jung HS, Lee S, Yoon DS, Park MS, Lee JW. MiR-449a Regulates the chondrogenesis of human mesenchymal stem cells through direct targeting of lymphoid enhancer-binding factor-1. *Stem Cells Dev.* 2012;21(18):3298–308.
156. Suomi S, Taipaleenmäki H, Seppänen A, Ripatti T, Väänänen K, Hentunen T, et al. MicroRNAs regulate osteogenesis and chondrogenesis of mouse bone marrow stromal cells. *Gene Regul Syst Bio.* 2008;2008(2):177–91.
157. Papaioannou G, Inloes JB, Nakamura Y, Paltrinieri E, Kobayashi T. Let-7 and miR-140 microRNAs coordinately regulate skeletal development. *Proc Natl Acad Sci U S*

- A. 2013;110(35).
158. Yamashita S, Miyaki S, Kato Y, Yokoyama S, Sato T, Barrionuevo F, et al. L-Sox5 and Sox6 proteins enhance chondrogenic miR-140 MicroRNA expression by strengthening dimeric Sox9 activity. *J Biol Chem*. 2012;287(26):22206–15.
 159. Guan Y, Yang X, Wei L, Chen Q. MiR-365: a mechanosensitive microRNA stimulates chondrocyte differentiation through targeting histone deacetylase 4. *FASEB J*. 2011;25(12):4457–66.
 160. Cong L, Zhu Y, Tu G. A bioinformatic analysis of microRNAs role in osteoarthritis. *Osteoarthr Cartil*. 2017;25(8):1362–71.
 161. Haseeb A, Makki MS, Khan NM, Ahmad I, Haqqi TM. Deep sequencing and analyses of miRNAs, isomiRs and miRNA induced silencing complex (miRISC)-associated miRNome in primary human chondrocytes. *Sci Rep [Internet]*. 2017;7(1):1–10. Available from: <http://dx.doi.org/10.1038/s41598-017-15388-4>
 162. Coutinho De Almeida R, Ramos YFM, Mahfouz A, Den Hollander W, Lakenberg N, Houtman E, et al. RNA sequencing data integration reveals an miRNA interactome of osteoarthritis cartilage. *Ann Rheum Dis*. 2019;78(2):270–7.
 163. Yamasaki K, Nakasa T, Miyaki S, Ishikawa M, Deie M, Adachi N, et al. Expression of microRNA-146a in osteoarthritis cartilage. *Arthritis Rheum*. 2009;60(4):1035–41.
 164. Borgonio Cuadra VM, González-Huerta NC, Romero-Córdoba S, Hidalgo-Miranda A, Miranda-Duarte A. Altered expression of circulating microRNA in plasma of patients with primary osteoarthritis and in silico analysis of their pathways. *PLoS One*. 2014;9(6):20–5.
 165. Díaz-Prado S, Cicione C, Muiños-López E, Hermida-Gómez T, Oreiro N, Fernández-López C, et al. Characterization of microRNA expression profiles in normal and osteoarthritic human chondrocytes. *BMC Musculoskelet Disord*. 2012;13.
 166. Qi Y, Ma N, Yan F, Yu Z, Wu G, Qiao Y, et al. The expression of intronic miRNAs, miR-483 and miR-483*, and their host gene, *Igf2*, in murine osteoarthritis cartilage. *Int J Biol Macromol [Internet]*. 2013;61:43–9. Available from: <http://dx.doi.org/10.1016/j.ijbiomac.2013.06.006>
 167. Li X, Zhen Z, Tang G, Zheng C, Yang G. MiR-29a and MiR-140 protect chondrocytes against the anti-proliferation and cell matrix signaling changes by IL-1 β . *Mol Cells*. 2016;39(2):103–10.
 168. Yang X, Guan Y, Tian S, Wang Y, Sun K, Chen Q. Mechanical and IL-1 β responsive miR-365 contributes to osteoarthritis development by targeting histone deacetylase 4. *Int J Mol Sci*. 2016;17(4).
 169. Nakamura A, Rampersaud YR, Sharma A, Lewis SJ, Wu B, Datta P, et al. Identification of microRNA-181a-5p and microRNA-4454 as mediators of facet cartilage degeneration. *JCI Insight*. 2016;1(12):1–17.
 170. Song J, Kim D, Lee CH, Lee MS, Chun CH, Jin EJ. MicroRNA-488 regulates zinc transporter SLC39A8/ZIP8 during pathogenesis of osteoarthritis. *J Biomed Sci [Internet]*. 2013;20(1):1. Available from: *Journal of Biomedical Science*
 171. McAlinden A, Varghese N, Wirthlin L, Chang LW. Differentially Expressed MicroRNAs in Chondrocytes from Distinct Regions of Developing Human Cartilage. *PLoS One*. 2013;8(9).
 172. Song J, Lee M, Kim D, Han J, Chun CH, Jin EJ. MicroRNA-181b regulates articular chondrocytes differentiation and cartilage integrity. *Biochem Biophys Res Commun [Internet]*. 2013;431(2):210–4. Available from:

- <http://dx.doi.org/10.1016/j.bbrc.2012.12.133>
173. Tu M, Li Y, Zeng C, Deng Z, Gao S, Xiao W, et al. MicroRNA-127-5p regulates osteopontin expression and osteopontin-mediated proliferation of human chondrocytes. *Sci Rep*. 2016;6(December 2015):4–11.
 174. Sumiyoshi K, Kubota S, Ohgawara T, Kawata K, Abd El Kader T, Nishida T, et al. Novel role of miR-181a in cartilage metabolism. *J Cell Biochem*. 2013;114(9):2094–100.
 175. Liang Z, Zhuang H, Wang G, Li Z, Zhang H, Yu T, et al. MiRNA-140 is a negative feedback regulator of MMP-13 in IL-1 β -stimulated human articular chondrocyte C28/I2 cells. *Inflamm Res*. 2012;61:503–9.
 176. Tardif G, Pelletier JP, Fahmi H, Hum D, Zhang Y, Kapoor M, et al. NFAT3 and TGF- β /SMAD3 regulate the expression of miR-140 in osteoarthritis. *Arthritis Res Ther*. 2013;15(6).
 177. Miyaki S, Nakasa T, Otsuki S, Grogan S, Higashiyama R, Inoue A, et al. MicroRNA-140 is expressed in differentiated human articular chondrocytes and modulates interleukin-1 responses. *Arthritis Rheum* [Internet]. 2009;60(9):2723–30. Available from: <https://www.ncbi.nlm.nih.gov/pmc/articles/PMC3624763/pdf/nihms412728.pdf>
 178. Martinez-Sanchez A, Dudek KA, Murphy CL. Regulation of human chondrocyte function through direct inhibition of cartilage master regulator SOX9 by microRNA-145 (miRNA-145). *J Biol Chem*. 2012;287(2):916–24.
 179. Peffers MJ, Balaskas P, Smagul A. Osteoarthritis year in review 2017: genetics and epigenetics. *Osteoarthr Cartil* [Internet]. 2018;26(3):304–11. Available from: <https://doi.org/10.1016/j.joca.2017.09.009>
 180. Swingler TE, Wheeler G, Carmont V, Elliott HR, Barter MJ, Abu-Elmagd M, et al. The expression and function of microRNAs in chondrogenesis and osteoarthritis. *Arthritis Rheum*. 2012;64(6):1909–19.
 181. Tardif G, Hum D, Pelletier JP, Duval N, Martel-Pelletier J. Regulation of the IGFBP-5 and MMP-13 genes by the microRNAs miR-140 and miR-27a in human osteoarthritic chondrocytes. *BMC Musculoskelet Disord*. 2009;10(1):1–11.
 182. Qin W, Chung ACK, Huang XR, Meng XM, Hui DSC, Yu CM, et al. TGF- β /Smad3 signaling promotes renal fibrosis by inhibiting miR-29. *J Am Soc Nephrol*. 2011;22(8):1462–74.
 183. McAlinden A, Anderson B. miR-483 targets SMAD4 to suppress chondrogenic differentiation of human mesenchymal stem cells. *J Orthop Res*. 2017;35(11):2369–77.
 184. Abouheif MM, Nakasa T, Shibuya H, Niimoto T, Kongcharoensombat W, Ochi M. Silencing microRNA-34a inhibits chondrocyte apoptosis in a rat osteoarthritis model in vitro. *Rheumatology*. 2010;49(11):2054–60.
 185. Yan S, Wang M, Zhao J, Zhang H, Zhou C, Jin L, et al. MicroRNA-34a affects chondrocyte apoptosis and proliferation by targeting the SIRT1/p53 signaling pathway during the pathogenesis of osteoarthritis. *Int J Mol Med*. 2016;38(1):201–9.
 186. Endisha H, Datta P, Sharma A, Tavallaee G, Kapoor M. The role of microRNAs in osteoarthritis and ageing-related functional decline in joint tissues homeostasis. *Osteoarthr Cartil*. 2017;
 187. Zhang W, Hsu P, Zhong B, Guo S, Zhang C, Wang Y, et al. MiR-34a Enhances

- Chondrocyte Apoptosis, Senescence and Facilitates Development of Osteoarthritis by Targeting DLL1 and Regulating PI3K/AKT Pathway. *Cell Physiol Biochem*. 2018;48(3):1304–16.
188. Philipot D, Guérit D, Platano D, Chuchana P, Olivotto E, Espinoza F, et al. P16INK4a and its regulator miR-24 link senescence and chondrocyte terminal differentiation-associated matrix remodeling in osteoarthritis. *Arthritis Res Ther*. 2014;16(1):1–12.
 189. Zhao X, Wang T, Cai B, Wang X, Feng W, Han Y, et al. MicroRNA-495 enhances chondrocyte apoptosis, senescence and promotes the progression of osteoarthritis by targeting AKT1. *Am J Transl Res* [Internet]. 2019;11(4):2232–44. Available from: <http://www.ncbi.nlm.nih.gov/pubmed/31105831><http://www.pubmedcentral.nih.gov/articlerender.fcgi?artid=PMC6511756>
 190. Yang DW, Qian G Bin, Jiang MJ, Wang P, Wang KZ. Inhibition of microRNA-495 suppresses chondrocyte apoptosis through activation of the NF- κ B signaling pathway by regulating CCL4 in osteoarthritis. *Gene Ther* [Internet]. 2019;26(6):217–29. Available from: <http://dx.doi.org/10.1038/s41434-019-0068-5>
 191. Zhong G, Long H, Ma S, Shunhan Y, Li J, Yao J. miRNA-335-5p relieves chondrocyte inflammation by activating autophagy in osteoarthritis. *Life Sci* [Internet]. 2019;226(January):164–72. Available from: <https://doi.org/10.1016/j.lfs.2019.03.071>
 192. Zhao X, Li H, Wang L. MicroRNA-107 regulates autophagy and apoptosis of osteoarthritis chondrocytes by targeting TRAF3. *Int Immunopharmacol* [Internet]. 2019;71(April 2018):181–7. Available from: <https://doi.org/10.1016/j.intimp.2019.03.005>
 193. Hu N, Gao Y, Jayasuriya CT, Liu W, Du H, Ding J, et al. Chondrogenic induction of human osteoarthritic cartilage-derived mesenchymal stem cells activates mineralization and hypertrophic and osteogenic gene expression through a mechanomiR. *Arthritis Res Ther*. 2019;21(1):1–14.
 194. Valenti MT, Carbonare LD, Mottes M. Role of microRNAs in progenitor cell commitment and osteogenic differentiation in health and disease (Review). *Int J Mol Med*. 2018;41(5):2441–9.
 195. Beyer C, Zampetaki A, Lin N-Y, Kleyer A, Perricone C, Lagnocco A, et al. Signature of circulating microRNAs in osteoarthritis. *Ann Rheum Dis*. 2015;74(3).
 196. Kong R, Gao J, Si Y, Zhao D. Combination of circulating miR-19b-3p, miR-122-5p and miR-486-5p expressions correlates with risk and disease severity of knee osteoarthritis. *Am J Transl Res*. 2017;9(6):2852–64.
 197. Ntoumou E, Tzetis M, Braoudaki M, Lambrou G, Poulou M, Malizos K, et al. Serum microRNA array analysis identifies miR-140-3p, miR-33b-3p and miR-671-3p as potential osteoarthritis biomarkers involved in metabolic processes. *Clin Epigenetics*. 2017;9(1):1–15.
 198. Murata K, Yoshitomi H, Tanida S, Ishikawa M, Nishitani K, Ito H, et al. Plasma and synovial fluid microRNAs as potential biomarkers of rheumatoid arthritis and osteoarthritis. *Arthritis Res Ther*. 2010;12(3).
 199. Xia S, Tian H, Fan L, Zheng J. Peripheral Blood miR-181-5p Serves as a Marker for Screening Patients with Osteoarthritis by Targeting TNF α . *Clin Lab*. 2017;63(11):1819–25.
 200. Zhou Z, Tian F, An N, Zhang Y, Wang C, Guo L. MiR-300 Serves as Potential Biomarker to Screen Knee Osteoarthritis Patients by Targeting TNF α . *Clin Lab*.

- 2018;64(4):577–84.
201. Wan L, Zhao Q, Niu G, Xiang T, Ding C, Wang S. Plasma miR-136 can be used to screen patients with knee osteoarthritis from healthy controls by targeting IL-17. *Exp Ther Med*. 2018;16(4):3419–24.
 202. Lian WS, Ko JY, Wu RW, Sun YC, Chen YS, Wu SL, et al. MicroRNA-128a represses chondrocyte autophagy and exacerbates knee osteoarthritis by disrupting Atg12. *Cell Death Dis* [Internet]. 2018;9(9). Available from: <http://dx.doi.org/10.1038/s41419-018-0994-y>
 203. Wang H, Zhang H, Sun Q, Wang Y, Yang J, Yang J, et al. Intra-articular Delivery of Antago-miR-483-5p Inhibits Osteoarthritis by Modulating Matrilin 3 and Tissue Inhibitor of Metalloproteinase 2. *Mol Ther* [Internet]. 2017;25(3):715–27. Available from: <http://dx.doi.org/10.1016/j.ymthe.2016.12.020>
 204. Dai L, Zhang X, Hu X, Liu Q, Man Z, Huang H, et al. Silencing of miR-101 Prevents Cartilage Degradation by Regulating Extracellular Matrix-related Genes in a Rat Model of Osteoarthritis. *Mol Ther*. 2015;23(8):1331–40.
 205. Nakamura A, Rampersaud Y, Nakamura S, Sharma A, Zeng F, Rossomacha E, et al. microRNA-181a-5p antisense oligonucleotides attenuate osteoarthritis in facet and knee joints. *Ann Rheum Dis*. 2018;78(1).
 206. Latifkar A, Hur YH, Sanchez JC, Cerione RA, Antonyak MA. New insights into extracellular vesicle biogenesis and function. *J Cell Sci*. 2019;132(13):1–9.
 207. Mao G, Zhang Z, Hu S, Zhang Z, Chang Z, Huang Z, et al. Exosomes derived from miR-92a-3p overexpressing human mesenchymal stem cells enhance chondrogenesis and suppress cartilage degradation via targeting WNT5A. *Stem Cell Res Ther*. 2018;9(1):1–13.
 208. Tao SC, Yuan T, Zhang YL, Yin WJ, Guo SC, Zhang CQ. Exosomes derived from miR-140-5p overexpressing human synovial mesenchymal stem cells enhance cartilage tissue regeneration and prevent osteoarthritis of the knee in a rat model. *Theranostics*. 2017;7(1):180–95.
 209. Kolhe R, Hunter M, Liu S, Jadeja RN, Pundkar C, Mondal AK, et al. Gender-specific differential expression of exosomal miRNA in synovial fluid of patients with osteoarthritis. *Sci Rep* [Internet]. 2017;7(1):1–14. Available from: <http://dx.doi.org/10.1038/s41598-017-01905-y>
 210. Hensley AP, McAlinden A. The role of microRNAs in bone development. *Bone* [Internet]. 2021;143(August 2020):115760. Available from: <https://doi.org/10.1016/j.bone.2020.115760>
 211. Kumar S, Reddy AP, Yin X, Reddy PH. Novel MicroRNA-455-3p and its protective effects against abnormal APP processing and amyloid beta toxicity in Alzheimer's disease. *Biochim Biophys Acta - Mol Basis Dis* [Internet]. 2019;1865(9):2428–40. Available from: <https://doi.org/10.1016/j.bbadis.2019.06.006>
 212. Kumar S, Reddy PH. MicroRNA-455-3p as a potential biomarker for Alzheimer's disease: An update. *Front Aging Neurosci*. 2018;10(FEB):1–11.
 213. Chipman L, Pasquinelli A. miRNA Targeting: Growing beyond the Seed. *Cell*. 2019;35(3):215–22.
 214. Boot-Handford RP, Tuckwell DS, Plumb DA, Farrington Rock C, Poulosom R. A novel and highly conserved collagen (pro α 1(XXVII)) with a unique expression pattern and unusual molecular characteristics establishes a new clade within the vertebrate fibrillar collagen family. *J Biol Chem* [Internet]. 2003;278(33):31067–77. Available

from: <http://dx.doi.org/10.1074/jbc.M212889200>

215. Pace JM, Corrado M, Missero C, Byers PH. Identification, characterization and expression analysis of a new fibrillar collagen gene, COL27A1. *Matrix Biol.* 2003;22(1):3–14.
216. Plumb DA, Dhir V, Mironov A, Ferrara L, Poulosom R, Kadler KE, et al. Collagen XXVII is developmentally regulated and forms thin fibrillar structures distinct from those of classical vertebrate fibrillar collagens. *J Biol Chem.* 2007;282(17):12791–5.
217. Van Der Kraan PM, Goumans MJ, Blaney Davidson E, Ten Dijke P. Age-dependent alteration of TGF- β signalling in osteoarthritis. *Cell Tissue Res.* 2012;347(1):257–65.
218. Panguluri SK, Bhatnagar S, Kumar A, McCarthy JJ, Srivastava AK, Cooper NG, et al. Genomic profiling of messenger RNAs and microRNAs reveals potential mechanisms of TWEAK-induced skeletal muscle wasting in mice. *PLoS One.* 2010;5(1).
219. Zhang Z, Kang Y, Zhang Z, Zhang H, Duan X, Liu J, et al. Expression of microRNAs during chondrogenesis of human adipose-derived stem cells. *Osteoarthr Cartil.* 2012;20(12):1638–46.
220. Mao G, Zhang Z, Huang Z, Chen W, Huang G, Meng F, et al. MicroRNA-92a-3p regulates the expression of cartilage-specific genes by directly targeting histone deacetylase 2 in chondrogenesis and degradation. *Osteoarthr Cartil* [Internet]. 2017;25(4):521–32. Available from: <http://dx.doi.org/10.1016/j.joca.2016.11.006>
221. Ito Y, Matsuzaki T, Ayabe F, Mokuda S, Kurimoto R, Matsushima T, et al. Both microRNA-455-5p and -3p repress hypoxia-inducible factor-2 α expression and coordinately regulate cartilage homeostasis. *Nat Commun* [Internet]. 2021;12(1):1–13. Available from: <http://dx.doi.org/10.1038/s41467-021-24460-7>
222. Simon T, Jeffries M. The Epigenomic Landscape in Osteoarthritis. *Curr Rheumatol Rep.* 2017;
223. Yatabe T, Mochizuki S, Takizawa M, Chijiwa M, Okada A, Kimura T, et al. Hyaluronan inhibits expression of ADAMTS4 (aggrecanase-1) in human osteoarthritic chondrocytes. *Ann Rheum Dis.* 2009;68(6):1051–8.
224. Hashimoto K, Otero M, Imagawa K, De Andrés MC, Coico JM, Roach HI, et al. Regulated transcription of human matrix metalloproteinase 13 (MMP13) and interleukin-1 β (IL1B) genes in chondrocytes depends on methylation of specific proximal promoter CpG sites. *J Biol Chem.* 2013;288(14):10061–72.
225. Kim K II, Park YS, Im G II. Changes in the epigenetic status of the SOX-9 promoter in human osteoarthritic cartilage. *J Bone Miner Res.* 2013;28(5):1050–60.
226. Zhang H, Guan M, Townsend KL, Huang TL, An D, Yan X, et al. Micro RNA -455 regulates brown adipogenesis via a novel HIF 1 α - AMPK - PGC 1 α signaling network . *EMBO Rep.* 2015;16(10):1378–93.
227. Zheng J, Lin Z, Zhang L, Chen H. MicroRNA-455-3p inhibits tumor cell proliferation and induces apoptosis in HCT116 human colon cancer cells. *Med Sci Monit.* 2016;22:4431–7.
228. Zhao Y, Yan M, Yun Y, Zhang J, Zhang R, Li Y, et al. MicroRNA-455-3p functions as a tumor suppressor by targeting eIF4E in prostate cancer. *Oncol Rep.* 2017;37(4):2449–58.
229. Xing Q, Xie H, Zhu B, Sun Z, Huang Y. MiR-455-5p suppresses the progression of prostate cancer by targeting CCR5. *Biomed Res Int.* 2019;2019.
230. Qin L, Zhang Y, Lin J, Shentu Y, Xie X. MicroRNA-455 regulates migration and

- invasion of human hepatocellular carcinoma by targeting Runx2. *Oncol Rep.* 2016;36(6):3325–32.
231. Liu J, Zhang J, Li Y, Wang L, Sui B, Dai D. MiR-455-5p acts as a novel tumor suppressor in gastric cancer by down-regulating RAB18. *Gene* [Internet]. 2016;591(2):308–15. Available from: <http://dx.doi.org/10.1016/j.gene.2016.07.034>
 232. Xu B, Gong X, Zi L, Li G, Dong S, Chen X, et al. Silencing of DLEU2 suppresses pancreatic cancer cell proliferation and invasion by upregulating microRNA-455. *Cancer Sci.* 2019;110(5):1676–85.
 233. Li Y-J, Ping C, Tang J, Zhang W. MicroRNA-455 suppresses non-small cell lung cancer through targeting ZEB1. *Cell Biol Int.* 2016;40(6):621–8.
 234. Zhu X-J, Gong Z, Li S-J, Jia H-P, Li D-L. Long non-coding RNA Hottip modulates high-glucose-induced inflammation and ECM accumulation through miR-455-3p/WNT2B in mouse mesangial cells. *Int J Clin Exp Pathol.* 2019;12(7):2435–45.
 235. Jung HJ, Lee KP, Milholland B, Shin YJ, Kang JS, Kwon KS, et al. Comprehensive miRNA Profiling of Skeletal Muscle and Serum in Induced and Normal Mouse Muscle Atrophy during Aging. *Journals Gerontol - Ser A Biol Sci Med Sci.* 2017;72(11):1483–91.
 236. Torabi S, Tamaddon M, Asadolahi M, Shokri G, Tavakoli R, Tasharrofi N, et al. miR-455-5p downregulation promotes inflammation pathways in the relapse phase of relapsing-remitting multiple sclerosis disease. *Immunogenetics.* 2018;71:87–95.
 237. Nugent M. MicroRNAs: Exploring new horizons in osteoarthritis. *Osteoarthr Cartil* [Internet]. 2016;24(4):573–80. Available from: <http://dx.doi.org/10.1016/j.joca.2015.10.018>
 238. Friedman RC, Farh KKH, Burge CB, Bartel DP. Most mammalian mRNAs are conserved targets of microRNAs. *Genome Res.* 2009;19(1):92–105.
 239. He L, Hannon G. MicroRNAs: small RNAs with a big role in gene regulation. *Nat Rev Genet.* 2004;5:522–31.
 240. Trachana V, Ntoumou E, Anastasopoulou L, Tsezou A. Studying microRNAs in osteoarthritis: Critical overview of different analytical approaches. *Mech Ageing Dev.* 2018;171(September 2017):15–23.
 241. Peterson SM, Thompson JA, Ufkin ML, Sathyanarayana P, Liaw L, Congdon CB. Common features of microRNA target prediction tools. *Front Genet.* 2014;5(FEB):1–10.
 242. Imig J, Brunschweiler A, Brümmer A, Guennewig B, Mittal N, Kishore S, et al. MiR-CLIP capture of a miRNA targetome uncovers a lincRNA H19-miR-106a interaction. *Nat Chem Biol.* 2015;11(2):107–14.
 243. Darnell R. CLIP (Cross-linking and immunoprecipitation) identification of RNAs bound by a specific protein. *Cold Spring Harb Protoc.* 2012;7(11):1146–60.
 244. Fecko C, Munson K, Saunders A, Sun G, Begley T, Lis J, et al. Comparison of femtosecond laser and continuous wave UV sources for protein-nucleic acid crosslinking. *Photochem Photobiol.* 2007;
 245. Chou CH, Lin FM, Chou M Te, Hsu S heng Da, Chang TH, Weng SL, et al. A computational approach for identifying microRNA-target interactions using highthroughput CLIP and PAR-CLIP sequencing. *BMC Genomics* [Internet]. 2013;14(Suppl 1):S2. Available from: <http://www.biomedcentral.com/1471-2164/14/S1/S2>
 246. Sugimoto Y, König J, Hussain S, Zupan B, Curk T, Frye M, et al. Analysis of CLIP and

- iCLIP methods for nucleotide-resolution studies of protein-RNA interactions. *Genome Biol.* 2012;13(8):R67.
247. König J, Zarnack K, Rot G, Curk T, Kayikci M, Zupan B, et al. ICLIP - transcriptome-wide mapping of protein-RNA interactions with individual nucleotide resolution. *J Vis Exp.* 2011;(50):2–8.
 248. Huppertz I, Attig J, D’Ambrogio A, Easton LE, Sibley CR, Sugimoto Y, et al. iCLIP: Protein-RNA interactions at nucleotide resolution. *Methods.* 2014;65(3):274–87.
 249. Lu Y, Leslie CS. Learning to Predict miRNA-mRNA Interactions from AGO CLIP Sequencing and CLASH Data. *PLoS Comput Biol.* 2016;12(7):1–18.
 250. Moore MJ, Zhang C, Gantman EC, Mele A, Darnell JC, Darnell RB. Mapping Argonaute and conventional RNA-binding protein interactions with RNA at single-nucleotide resolution using HITS-CLIP and CIMS analysis. *Nat Protoc.* 2014;9(2):263–93.
 251. Chi SW, Zang JB, Mele A, Darnell RB. Ago HITS-CLIP decodes miRNA-mRNA interaction maps. 2010;460(7254):479–86.
 252. König J, Zarnack K, Luscombe NM, Ule J. Protein–RNA interactions: new genomic technologies and perspectives. 2012;13(February):77–83.
 253. Clark PM, Loher P, Quann K, Brody J, Londin ER, Rigoutsos I. Argonaute CLIP-Seq reveals miRNA targetome diversity across tissue types. *Sci Rep.* 2014;4:1–11.
 254. Stork C, Zheng S. Genome-Wide Profiling of RNA–Protein Interactions Using CLIP-Seq. *Methods Mol Biol.* 2016;1421(1):137–51.
 255. Zarnegar B, Flynn R, Shen Y, Do B, Chang H, Khavari P. irCLIP platform for efficient characterization of protein—RNA interactions. *Nat Methods.* 2016;13(6):489–92.
 256. Nostrand EL Van, Pratt G a, Shishkin A a, Gelboin- C, Fang MY, Sundararaman B, et al. Robust transcriptome-wide discovery of RNA binding protein binding sites with enhanced CLIP (eCLIP). *Nat Methods.* 2016;13(6):508–14.
 257. Haberman N, Huppertz I, Attig J, König J, Wang Z, Hauer C, et al. Insights into the design and interpretation of iCLIP experiments. *Genome Biol.* 2017;18(1):1–21.
 258. Granneman S, Kudla G, Petfalski E, Tollervey D. Identification of protein binding sites on U3 snoRNA and pre-rRNA by UV cross-linking and high-throughput analysis of cDNAs. *Proc Natl Acad Sci U S A.* 2009;106(24):9613–8.
 259. Helwak A, Kudla G, Dudnakova T, Tollervey D. Mapping the human miRNA interactome by CLASH reveals frequent noncanonical binding. *Cell [Internet].* 2013;153(3):654–65. Available from: <http://dx.doi.org/10.1016/j.cell.2013.03.043>
 260. Helwak A, Tollervey D. Mapping the miRNA interactome by cross-linking ligation and sequencing of hybrids (CLASH). *Nat Protoc.* 2014;9(3):711–28.
 261. Broughton J, Pasquinelli A. Detection of microRNA-Target Interactions by Chimera PCR (ChimP). In: *Methods in molecular biology.* 2018. p. 153–65.
 262. Jin Y, Chen Z, Liu X, Zhou X. Evaluating the MicroRNA targeting sites by luciferase reporter gene assay. *Methods Mol Biol.* 2013;936(4):117–27.
 263. Li H, Yang Y, Hong W, Huang M, Wu M, Zhao X. Applications of genome editing technology in the targeted therapy of human diseases: mechanisms, advances and prospects. *Signal Transduct Target Ther [Internet].* 2020;5(1). Available from: <http://dx.doi.org/10.1038/s41392-019-0089-y>
 264. Yoshimi K, Kunihiro Y, Kaneko T, Nagahora H, Voigt B, Mashimo T. SsODN-mediated knock-in with CRISPR-Cas for large genomic regions in zygotes. *Nat Commun.* 2016;7:2–11.

265. Al-Attar S, Westra ER, Van Der Oost J, Brouns SJJ. Clustered regularly interspaced short palindromic repeats (CRISPRs): The hallmark of an ingenious antiviral defense mechanism in prokaryotes. *Biol Chem*. 2011;392(4):277–89.
266. Cong L, Ran FA, Cox D, Lin S, Barretto R, Hsu PD, et al. Multiplex Genome Engineering Using CRISPR/Cas Systems. *Science*. 2013;339(6121):819–23.
267. Sternberg SH, Redding S, Jinek M, Greene EC, Jennifer A, Biophysics M, et al. DNA interrogation by the CRISPR RNA-guided endonuclease Cas9. *Nature*. 2014;507(7490):62–7.
268. Gasiunas G, Barrangou R, Horvath P, Siksnys V. Cas9-crRNA ribonucleoprotein complex mediates specific DNA cleavage for adaptive immunity in bacteria. *Proc Natl Acad Sci U S A*. 2012;109(39):2579–86.
269. Jackson SP, Bartek J. The DNA-damage response in human biology and disease. *Nature*. 2009;461(7267):1071–8.
270. Mali P, Yang L, Esvelt KM, Aach J, Guell M, DiCarlo JE, et al. RNA-guided human genome engineering via Cas9. *Science* (80-). 2013;339(6121):823–6.
271. Liu C, Zhang L, Liu H, Cheng K. Delivery Strategies for CRISPR-Cas9 Gene-Editing Systems. *HHS Public Access J Control Release*. 2017;266(816):17–26.
272. Biagioni A, Laurenzana A, Margheri F, Chillà A, Fibbi G, So M. Delivery systems of CRISPR/Cas9-based cancer gene therapy. *J Biol Eng [Internet]*. 2018;12(1):1–10. Available from: <http://dx.doi.org/10.1186/s13036-018-0127-2>
273. Shao Y, Guan Y, Wang L, Qiu Z, Liu M, Chen Y, et al. CRISPR/Cas-mediated genome editing in the rat via direct injection of one-cell embryos. *Nat Protoc*. 2014;9(10):2493–512.
274. Chen F, Pruett-Miller S, Davis S. Gene editing using ssODNs with engineered endonucleases. *Methods Mol Biol*. 2015;1239:251–65.
275. Hu Z, Zhou M, Wu Y, Li Z, Liu X, Wu L, et al. ssODN-Mediated In-Frame Deletion with CRISPR/Cas9 Restores FVIII Function in Hemophilia A-Patient-Derived iPSCs and ECs. *Mol Ther - Nucleic Acids [Internet]*. 2019;17(September):198–209. Available from: <https://doi.org/10.1016/j.omtn.2019.05.019>
276. Okamoto S, Amaishi Y, Maki I, Enoki T, Mineno J. Highly efficient genome editing for single-base substitutions using optimized ssODNs with Cas9-RNPs. *Sci Rep*. 2019;9(1):1–11.
277. Wang Y, Liu KI, Sutrisnoh NAB, Srinivasan H, Zhang J, Li J, et al. Systematic evaluation of CRISPR-Cas systems reveals design principles for genome editing in human cells. *Genome Biol*. 2018;19(1):1–16.
278. Chang H, Yi B, Ma R, Zhang X, Zhao H, Xi Y. CRISPR/cas9, a novel genomic tool to knock down microRNA in vitro and in vivo. *Sci Rep [Internet]*. 2016;6(October 2015):1–12. Available from: <http://dx.doi.org/10.1038/srep22312>
279. Zhang Z, Ursin R, Mahapatra S, Ian Gallicano G. CRISPR/CAS9 ablation of individual miRNAs from a miRNA family reveals their individual efficacies for regulating cardiac differentiation. *Mech Dev [Internet]*. 2018;150:10–20. Available from: <http://dx.doi.org/10.1016/j.mod.2018.02.002>
280. Hong H, Yao S, Zhang Y, Ye Y, Li C, Hu L, et al. In vivo miRNA knockout screening identifies miR-190b as a novel tumor suppressor. *PLoS Genet [Internet]*. 2020;16(11):1–17. Available from: <http://dx.doi.org/10.1371/journal.pgen.1009168>
281. Raab N, Mathias S, Alt K, Handrick R, Fischer S, Schmieder V, et al. CRISPR/Cas9-

- Mediated Knockout of MicroRNA-744 Improves Antibody Titer of CHO Production Cell Lines. *Biotechnol J*. 2019;14(5):1–9.
282. Zhao L, Huang J, Fan Y, Li J, You T, He S, et al. Exploration of CRISPR/Cas9-based gene editing as therapy for osteoarthritis. *Ann Rheum Dis*. 2019;78(5):676–82.
283. Bassett AR, Azzam G, Wheatley L, Tibbit C, Rajakumar T, McGowan S, et al. Understanding functional miRNA-target interactions in vivo by site-specific genome engineering. *Nat Commun*. 2014;5:1–11.
284. Krützfeldt J. Strategies to use microRNAs as therapeutic targets. *Best Pract Res Clin Endocrinol Metab* [Internet]. 2016;30(5):551–61. Available from: <http://dx.doi.org/10.1016/j.beem.2016.07.004>
285. Li Z, Rana TM. Therapeutic targeting of microRNAs: Current status and future challenges. *Nat Rev Drug Discov*. 2014;13(8):622–38.
286. Hanna J, Hossain GS, Kocerha J. The potential for microRNA therapeutics and clinical research. *Front Genet*. 2019;10(MAY).
287. Hopkins AL. Network pharmacology: The next paradigm in drug discovery. *Nat Chem Biol*. 2008;4(11):682–90.
288. McCall R, Miles M, Lascuna P, Burney B, Patel Z, Sidoran KJ, et al. Dual targeting of the cancer antioxidant network with 1,4-naphthoquinone fused Gold(i) N-heterocyclic carbene complexes. *Chem Sci*. 2017;8(9):5918–29.
289. Gardiner MD, Vincent TL, Driscoll C, Burleigh A, Bou-Gharios G, Saklatvala J, et al. Transcriptional analysis of micro-dissected articular cartilage in post-traumatic murine osteoarthritis. *Osteoarthr Cartil* [Internet]. 2015;23(4):616–28. Available from: <http://dx.doi.org/10.1016/j.joca.2014.12.014>
290. Burleigh A, Chanalaris A, Gardiner MD, Driscoll C, Boruc O, Saklatvala J, et al. Joint immobilization prevents murine osteoarthritis and reveals the highly mechanosensitive nature of protease expression in vivo. *Arthritis Rheum*. 2012;64(7):2278–88.
291. Hamburger V, Hamilton H. A series of normal stages in the development of the chick embryo. *J Morphol*. 1951;88(1):49–92.
292. Zhang H, Guan M, Townsend KL, Huang TL, An D, Yan X, et al. MicroRNA-455 regulates brown adipogenesis via a novel HIF1 α -AMPK-PGC1 α signaling network. *EMBO Rep*. 2015;16(10):1378–93.
293. Yu L, Xia K, Cen X, Huang X, Sun W, Zhao Z, et al. DNA methylation of noncoding RNAs: New insights into osteogenesis and common bone diseases. *Stem Cell Res Ther*. 2020;11(1):1–8.
294. Palencia-Campos A, Ullah A, Nevado J, Yildirim R, Unal E, Ciorraga M, et al. GLI1 inactivation is associated with developmental phenotypes overlapping with Ellis-van Creveld syndrome. *Hum Mol Genet*. 2017;26(23):4556–71.
295. Yousaf M, Ullah A, Azeem Z, Isani Majeed A, Memon MI, Ghous T, et al. Novel heterozygous sequence variant in the GLI1 underlies postaxial polydactyly. *Congenit Anom (Kyoto)*. 2020;60(4):115–9.
296. Xiang Y, Li X, Zhan Z, Feng J, Cai H, Li Y, et al. A Novel Nonsense GLI3 Variant Is Associated With Polydactyly and Syndactyly in a Family by Blocking the Sonic Hedgehog Signaling Pathway. *Front Genet*. 2020;11(November):1–10.
297. Baas M, Burger EB, Van Den Ouweland AMW, Hovius SER, De Klein A, Van Nieuwenhoven CA, et al. Variant type and position predict two distinct limb phenotypes in patients with GLI3-mediated polydactyly syndromes. *J Med Genet*.

- 2020;1–7.
298. Ruiz-Perez VL, Blair HJ, Rodrigues-Andres ME, Blanco MJ, Wilson A, Liu YN, et al. Evc is a positive mediator of Ihh-regulated bone growth that localises at the base of chondrocyte cilia. *Development*. 2007;134(16):2903–12.
 299. Pacheco M, Valencia M, Caparrós-Martín JA, Mulero F, Goodship JA, Ruiz-Perez VL. Evc works in chondrocytes and osteoblasts to regulate multiple aspects of growth plate development in the appendicular skeleton and cranial base. *Bone* [Internet]. 2012;50(1):28–41. Available from: <http://dx.doi.org/10.1016/j.bone.2011.08.025>
 300. Wu M, Chen G, Li YP. TGF- β and BMP signaling in osteoblast, skeletal development, and bone formation, homeostasis and disease. *Bone Res*. 2016;4(December 2015).
 301. Rosen V. BMP2 signaling in bone development and repair. *Cytokine Growth Factor Rev*. 2009;20(5–6):475–80.
 302. Salazar VS, Gamer LW, Rosen V. BMP signalling in skeletal development, disease and repair. *Nat Rev Endocrinol*. 2016;12(4):203–21.
 303. Xu J, E XQ, Wang NX, Wang MN, Xie HX, Cao YH, et al. BMP7 enhances the effect of BMSCs on extracellular matrix remodeling in a rabbit model of intervertebral disc degeneration. *FEBS J*. 2016;283(9):1689–700.
 304. Ornitz DM, Marie PJ. Fibroblast growth factor signaling in skeletal development and disease. *Genes Dev*. 2015;29(14):1463–86.
 305. Boilly B, Vercoutter-edouart AS, Hondermarck H, Nurcombe V, Le Bourhis X. FGF signals for cell proliferation and migration through different pathways. *Cytokine Growth Factor Rev*. 2000;11:295–302.
 306. Sassone-Corsi P. The Cyclic AMP pathway. *Cold Spring Harb Perspect Biol*. 2012;4(12):3–5.
 307. Montemurro C, Vadrevu S, Gurlo T, Butler AE, Vongbunyong KE, Petcherski A, et al. Cell cycle-related metabolism and mitochondrial dynamics in a replication-competent pancreatic beta-cell line. *Cell Cycle*. 2017;16(21):2086–99.
 308. Qian W, Choi S, Gibson GA, Watkins SC, Bakkenist CJ, Van Houten B. Mitochondrial hyperfusion induced by loss of the fission protein Drp1 causes ATM-dependent G2/M arrest and aneuploidy through DNA replication stress. *J Cell Sci*. 2012;125(23):5745–57.
 309. Schipani E, Ryan HE, Didrickson S, Kobayashi T, Knight M, Johnson RS. Hypoxia in cartilage: HIF-1 α is essential for chondrocyte growth arrest and survival. *Genes Dev*. 2001;15(21):2865–76.
 310. Michaels Y, Wu Q, Fulga T. Interrogation of Functional miRNA–Target Interactions by CRISPR/Cas9 Genome Engineering. In: *MicroRNA Detection and Target Identification*. 2017. p. 79–97.
 311. Zhang X, Odom DT, Koo SH, Conkright MD, Canettieri G, Best J, et al. Genome-wide analysis of cAMP-response element binding protein occupancy, phosphorylation, and target gene activation in human tissues. *Proc Natl Acad Sci U S A*. 2005;102(12):4459–64.
 312. Montminy M, Bilezikjian L. Binding of a nuclear protein to the cyclic-AMP response element of the somatostatin gene. *Nature*. 1987;328:175–8.
 313. Steven A, Friedrich M, Jank P, Heimer N, Budczies J, Denkert C, et al. What turns CREB on? And off? And why does it matter? *Cell Mol Life Sci* [Internet]. 2020;77(20):4049–67. Available from: <https://doi.org/10.1007/s00018-020-03525-8>

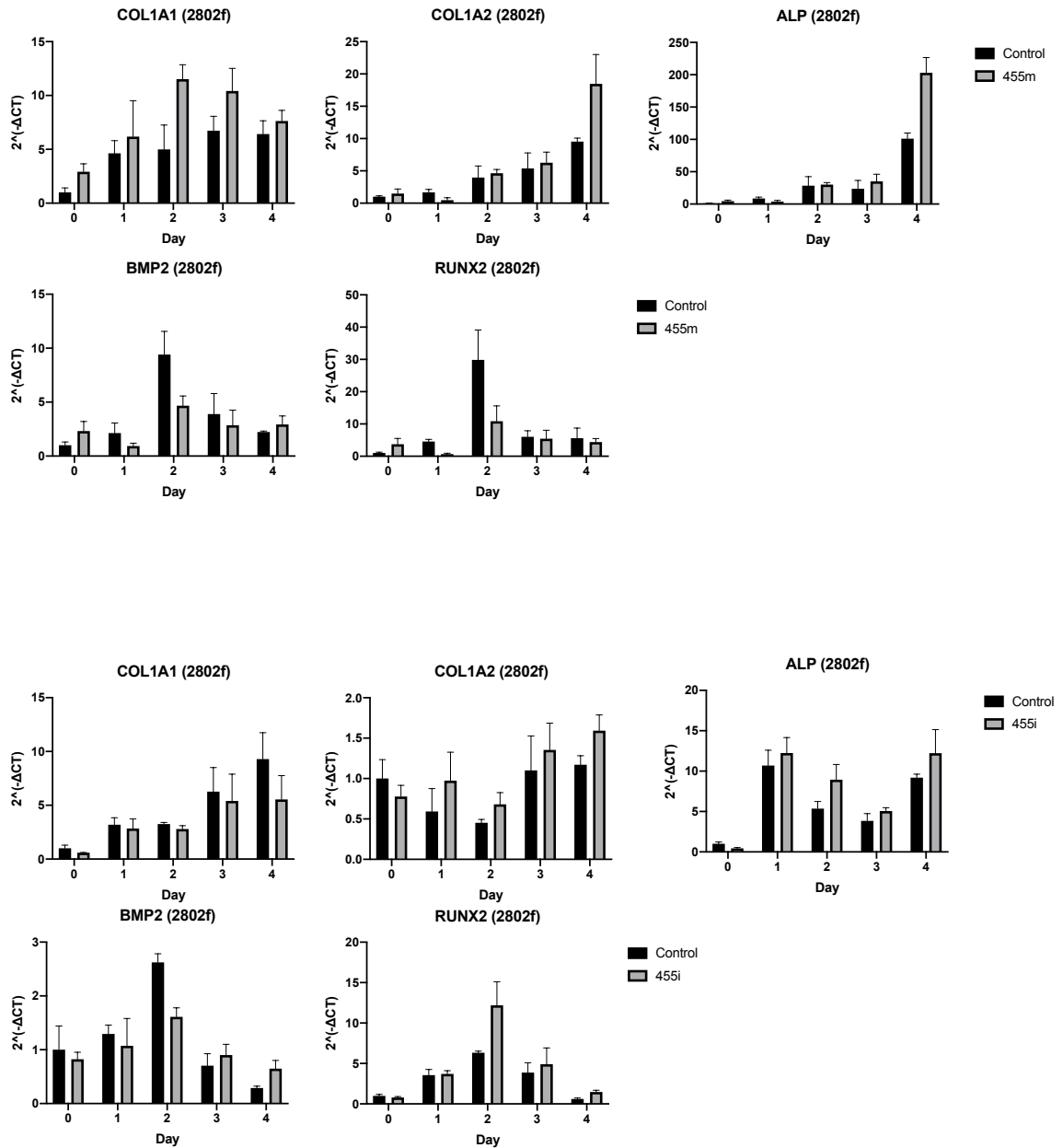
314. Zhang H, Kong Q, Wang J, Jiang Y, Hua H. Complex roles of cAMP–PKA–CREB signaling in cancer. *Exp Hematol Oncol* [Internet]. 2020;9(1):1–13. Available from: <https://doi.org/10.1186/s40164-020-00191-1>
315. Rudolph D, Tafuri A, Gass P, Hämmerling GJ, Arnold B, Schütz G. Impaired fetal T cell development and perinatal lethality in mice lacking the cAMP response element binding protein. *Proc Natl Acad Sci U S A*. 1998;95(8):4481–6.
316. Beier F. Cell-cycle control and the cartilage growth plate. *J Cell Physiol*. 2004;202(1):1–8.
317. Beier F, LuValle P. The cyclin D1 and cyclin A genes are targets of activated PTH/PTHrP receptors in Jansen’s metaphyseal chondrodysplasia. *Mol Endocrinol*. 2002;16(9):2163–73.
318. Ionescu AM, Schwarz EM, Vinson C, Puzas JE, Rosier R, Reynolds PR, et al. PTHrP Modulates Chondrocyte Differentiation through AP-1 and CREB Signaling. *J Biol Chem* [Internet]. 2001;276(15):11639–47. Available from: <http://dx.doi.org/10.1074/jbc.M006564200>
319. Bui C, Barter MJ, Scott JL, Xu Y, Galler M, Reynard LN, et al. cAMP response element-binding (CREB) recruitment following a specific CpG demethylation leads to the elevated expression of the matrix metalloproteinase 13 in human articular chondrocytes and osteoarthritis. *FASEB J*. 2012;26(7):3000–11.
320. Kim KH, Lee YS. Activation of creb by pka promotes the chondrogenic differentiation of chick limb bud mesenchymal cells. *Animal Cells Syst (Seoul)*. 2009;13(3):289–95.
321. Piera-Velazquez S, Hawkins DF, Whitecavage MK, Colter DC, Stokes DG, Jimenez SA. Regulation of the human SOX9 promoter by Sp1 and CREB. *Exp Cell Res*. 2007;313(6):1069–79.
322. Long F, Schipani E, Asahara H, Kronenberg H, Montminy M. The CREB family of activators is required for endochondral bone development. *Development*. 2001;128(4):541–50.
323. Ahn S, Olive M, Aggarwal S, Krylov D, Ginty DD, Vinson C. A Dominant-Negative Inhibitor of CREB Reveals that It Is a General Mediator of Stimulus-Dependent Transcription of c- fos . *Mol Cell Biol*. 1998;18(2):967–77.
324. Reimold A, Grusby M, Kosaras B, Fries J, Mori R, Maniwa S, et al. Chondrodysplasia and neurological abnormalities in ATF-2-deficient mice. *Nature*. 1996;379:262–5.
325. JM K, Choi J, Kim Y, Jin S, Lim S, Jang H, et al. An activator of the cAMP/PKA/CREB pathway promotes osteogenesis from human mesenchymal stem cells. *J Cell Physiol*. 2013;228(3):617–26.
326. Siddappa R, Martens A, Doorn J, Leusink A, Olivo C, Licht R, et al. cAMP/PKA pathway activation in human mesenchymal stem cells in vitro results in robust bone formation in vivo. *Proc Natl Acad Sci U S A*. 2008;105(20):7281–6.
327. Zhao L, Li G, Zhou GQ. SOX9 directly binds CREB as a novel synergism with the PKA pathway in BMP-2-induced osteochondrogenic differentiation. *J Bone Miner Res*. 2009;24(5):826–36.
328. De Cesare D, Sassone-Corsi P. Transcriptional regulation by cyclic AMP-responsive factors. *Prog Nucleic Acid Res Mol Biol*. 2000;64:343–69.
329. Montminy M. Transcriptional regulation by cyclic AMP. *Annu Rev Biochem*. 1997;66(807–22).
330. Yang S, Li L, Zhu L, Zhang C, Li Z, Guo Y, et al. Aucubin inhibits IL-1 β - or TNF- α -

- induced extracellular matrix degradation in nucleus pulposus cell through blocking the miR-140-5p/CREB1 axis. *J Cell Physiol*. 2019;234(8):13639–48.
331. Yamamoto K, Kawai M, Yamazaki M, Tachikawa K, Kubota T, Ozono K, et al. CREB activation in hypertrophic chondrocytes is involved in the skeletal overgrowth in epiphyseal chondrodysplasia Miura type caused by activating mutations of natriuretic peptide receptor B. *Hum Mol Genet*. 2019;28(7):1183–98.
 332. Yokoyama K, Ikeya M, Umeda K, Oda H, Nodomi S, Nasu A, et al. Enhanced chondrogenesis of induced pluripotent stem cells from patients with neonatal-onset multisystem inflammatory disease occurs via the caspase 1-independent cAMP/protein kinase A/CREB pathway. *Arthritis Rheumatol*. 2015;67(1):302–14.
 333. Ji B, Ma Y, Wang H, Fang X, Shi P. Activation of the P38/CREB/MMP13 axis is associated with osteoarthritis. *Drug Des Devel Ther*. 2019;13:2195–204.
 334. Wang Z, Ni S, Zhang H, Fan Y, Xia L, Li N. Silencing SGK1 alleviates osteoarthritis through epigenetic regulation of CREB1 and ABCA1 expression. *Life Sci [Internet]*. 2021;268(October 2020):118733. Available from: <https://doi.org/10.1016/j.lfs.2020.118733>
 335. Zhang L, Gan X, He Y, Zhu Z, Zhu J, Yu H. Drp1-dependent mitochondrial fission mediates osteogenic dysfunction in inflammation through elevated production of reactive oxygen species. 2017;1–12.
 336. *Mitochondrial fission and fusion: A dynamic role in aging and potential target for age-related disease.pdf.
 337. Blanco F, June R. Cartilage Metabolism, Mitochondria, and Osteoarthritis. *J Am Acad Orthop Surg*. 2020;28:242–4.
 338. Spurlock B, Tullet JMA, Iv JLH, Mitra K. Interplay of mitochondrial fission-fusion with cell cycle regulation : Possible impacts on stem cell and organismal aging. *Exp Gerontol [Internet]*. 2020;135(March):110919. Available from: <https://doi.org/10.1016/j.exger.2020.110919>
 339. *Mitochondrial Dynamics in Stem Cells and Differentiation.pdf.
 340. Lee J, Kim C, Simon DK, Aminova L, Kushnareva Y, Murphy AA, et al. MITOCHONDRIAL CREB MEDIATES MITOCHONDRIAL GENE EXPRESSION AND NEURONAL SURVIVAL *. 2005;1–26.
 341. Hu S, Zhang C, Ni L, Huang C, Chen D, Shi K, et al. Stabilization of HIF-1 α alleviates osteoarthritis via enhancing mitophagy. *Cell Death Dis [Internet]*. 2020;11(6). Available from: <http://dx.doi.org/10.1038/s41419-020-2680-0>
 342. Li J, Dong S. The signaling pathways involved in chondrocyte differentiation and hypertrophic differentiation. *Stem Cells Int*. 2016;2016:1–13.
 343. Kvietikova I, Wenger RH, Marti HH, Gassmann M. The transcription factors ATF-1 and CREB-1 bind constitutively to the hypoxia-inducible factor-1 (HIF-1)DNA recognition site. *Nucleic Acids Res*. 1995;23(22):4542–50.
 344. Markway BD, Cho H, Johnstone B. Hypoxia promotes redifferentiation and suppresses markers of hypertrophy and degeneration in both healthy and osteoarthritic chondrocytes. *Arthritis Res Ther*. 2013;15(4).
 345. Qing L, Lei P, Liu H, Xie J, Wang L, Wen T, et al. Expression of hypoxia-inducible factor-1 α in synovial fluid and articular cartilage is associated with disease severity in knee osteoarthritis. *Exp Ther Med*. 2017;13(1):63–8.
 346. Rucci N, Rufo A, Alamanou M, Capulli M, Del Fattore A, Åhrman E, et al. The glycosaminoglycan-binding domain of PRELP acts as a cell type-specific NF- κ B

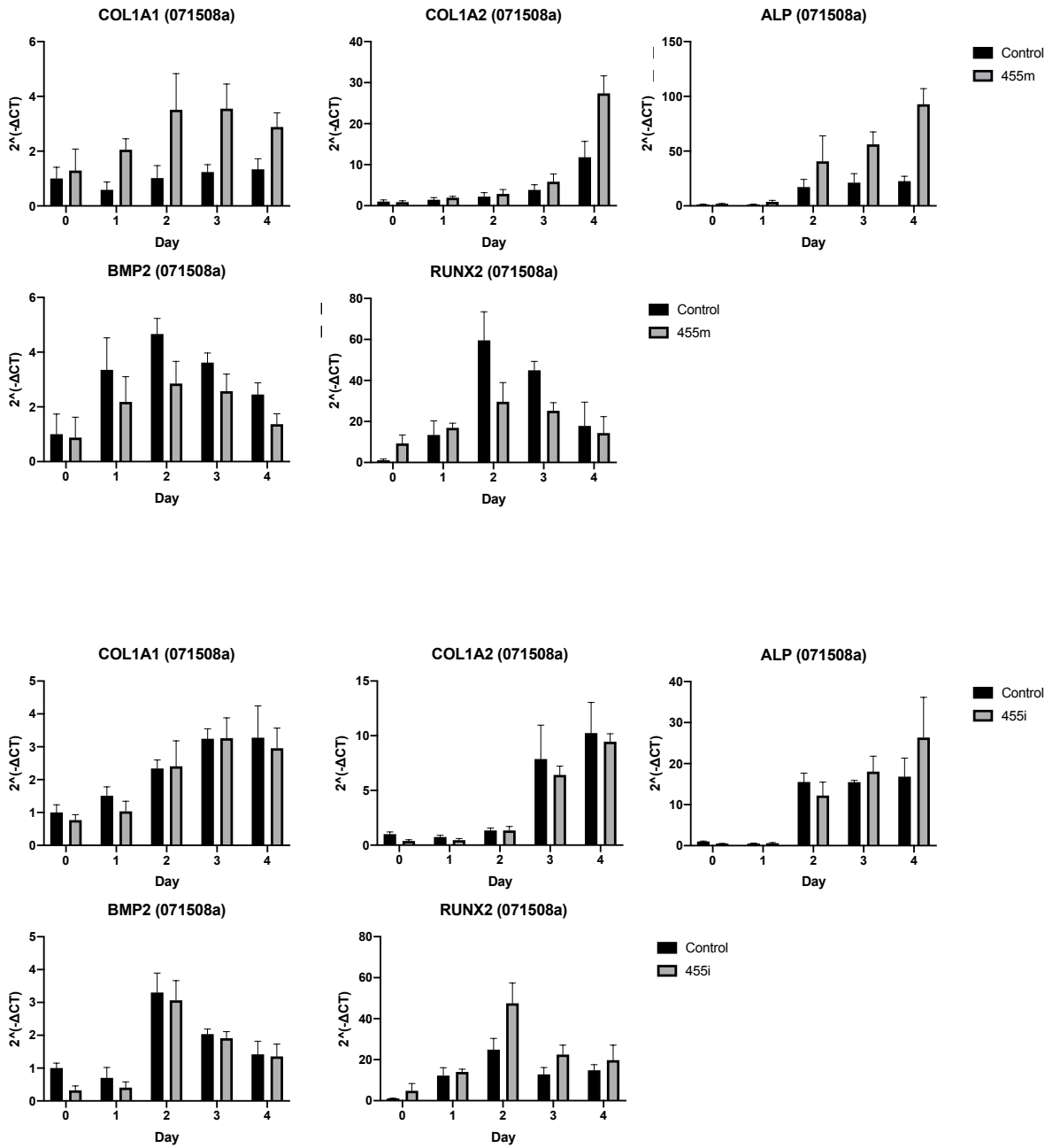
- inhibitor that impairs osteoclastogenesis. *J Cell Biol.* 2009;187(5):669–83.
347. Li H, Cui Y, Luan J, Zhang X, Li C, Zhou X, et al. PRELP (proline/arginine-rich end leucine-rich repeat protein) promotes osteoblastic differentiation of preosteoblastic MC3T3-E1 cells by regulating the β -catenin pathway. *Biochem Biophys Res Commun* [Internet]. 2016;470(3):558–62. Available from: <http://dx.doi.org/10.1016/j.bbrc.2016.01.106>
348. Lewis M. PRELP, collagen, and a theory of Hutchinson-Gilford progeria. *Ageing Res Rev.* 2003;2(1):95–105.
349. Segawa Y, Muneta T, Makino H, Nimura A, Mochizuki T, Ju YJ, et al. Mesenchymal stem cells derived from synovium, meniscus, anterior cruciate ligament, and articular chondrocytes share similar gene expression profiles. *J Orthop Res.* 2009;27(4):435–41.
350. Pelttari K, Winter A, Steck E, Goetzke K, Hennig T, Ochs BG, et al. Premature induction of hypertrophy during in vitro chondrogenesis of human mesenchymal stem cells correlates with calcification and vascular invasion after ectopic transplantation in SCID mice. *Arthritis Rheum.* 2006;54(10):3254–66.
351. Sekiya I, Vuoristo JT, Larson BL, Prockop DJ. In vitro cartilage formation by human adult stem cells from bone marrow stroma defines the sequence of cellular and molecular events during chondrogenesis. *Proc Natl Acad Sci U S A.* 2002;99(7):4397–402.
352. Cescon M, Gattazzo F, Chen P, Bonaldo P. Collagen VI at a glance. *J Cell Sci.* 2015;128(19):3525–31.
353. Fitzgerald J, Rich C, Zhou FH, Hansen U. Three novel collagen VI chains, $\alpha 4(VI)$, $\alpha 5(VI)$, and $\alpha 6(VI)$. *J Biol Chem.* 2008;283(29):20170–80.
354. Smeriglio P, Dhulipala L, Lai J, Goodman S, Dragoo J, Smith R, et al. Collagen VI enhances cartilage tissue generation by stimulating chondrocyte proliferation. *Tissue Eng A.* 2015;21:840–9.
355. Christensen SE, Coles JM, Zelenski NA, Furman BD, Leddy HA, Zauscher S, et al. Altered trabecular bone structure and delayed cartilage degeneration in the knees of collagen vi null mice. *PLoS One.* 2012;7(3).
356. Alexopoulos L, Youn I, Bonaldo P, Giulak F. DEVELOPMENTAL AND OSTEOARTHRITIC CHANGES IN Col6a1 KNOCKOUT MICE: THE BIOMECHANICS OF COLLAGEN VI IN THE CARTILAGE PERICELLULAR MATRIX. *Bone.* 2008;23(1):1–7.
357. Izu Y, Ezura Y, Mizoguchi F, Kawamata A, Nakamoto T, Nakashima K, et al. Type VI collagen deficiency induces osteopenia with distortion of osteoblastic cell morphology. *Tissue Cell* [Internet]. 2012;44(1):1–6. Available from: <http://dx.doi.org/10.1016/j.tice.2011.08.002>
358. Uccelli A, Moretta L, Pistoia V. Mesenchymal stem cells in health and disease. *Nat Rev Immunol.* 2008;8:726–36.

Appendices

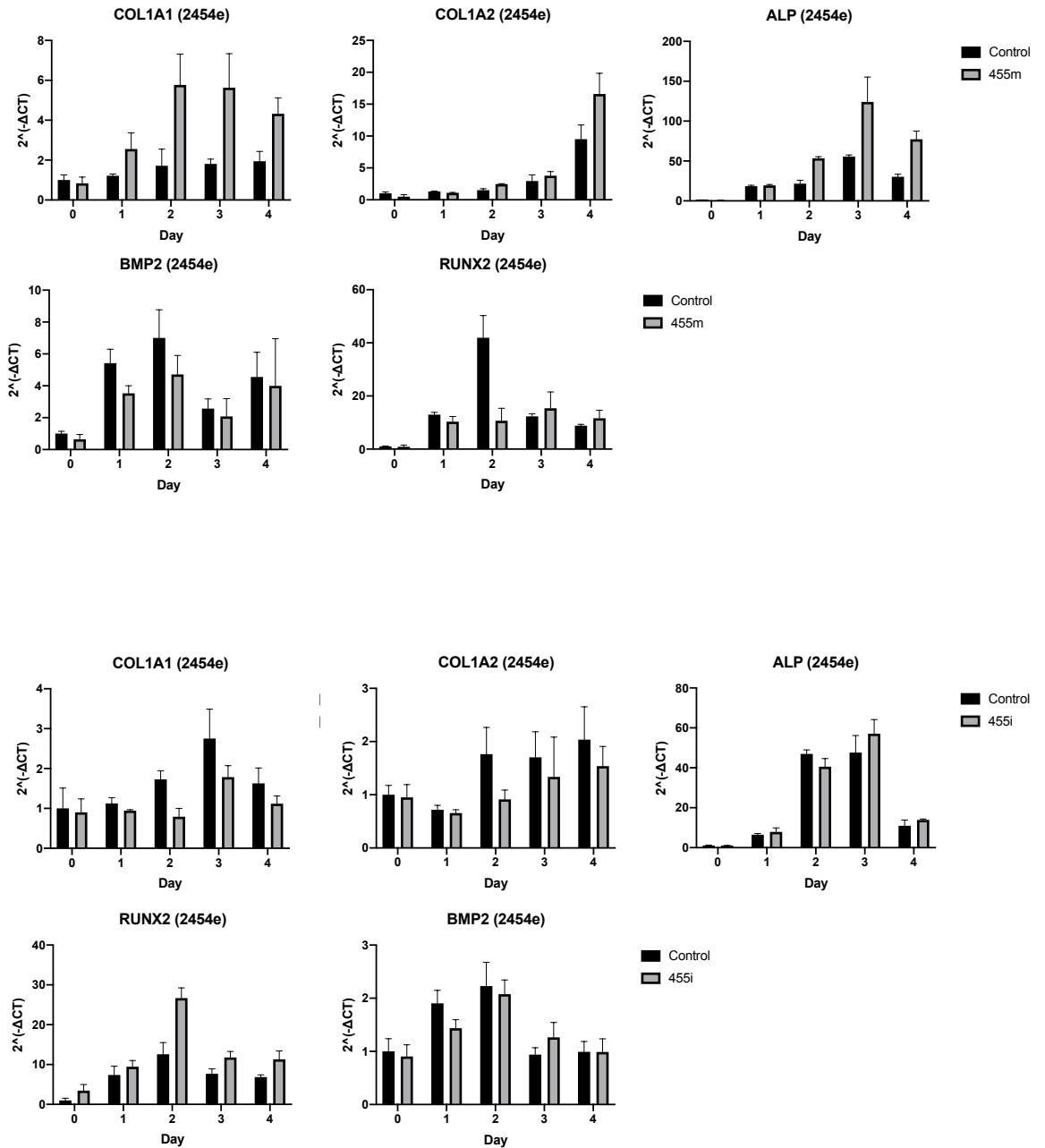
Appendices



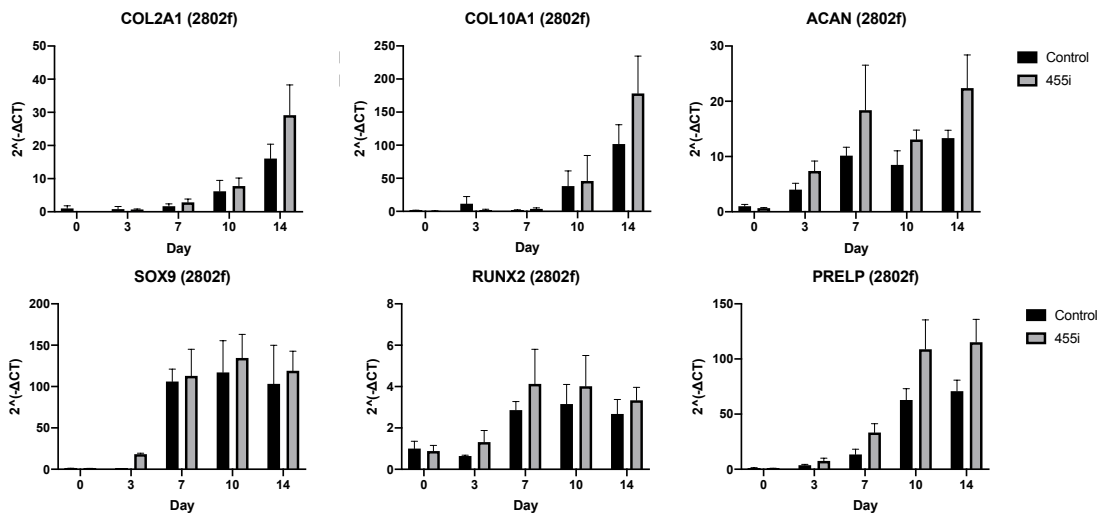
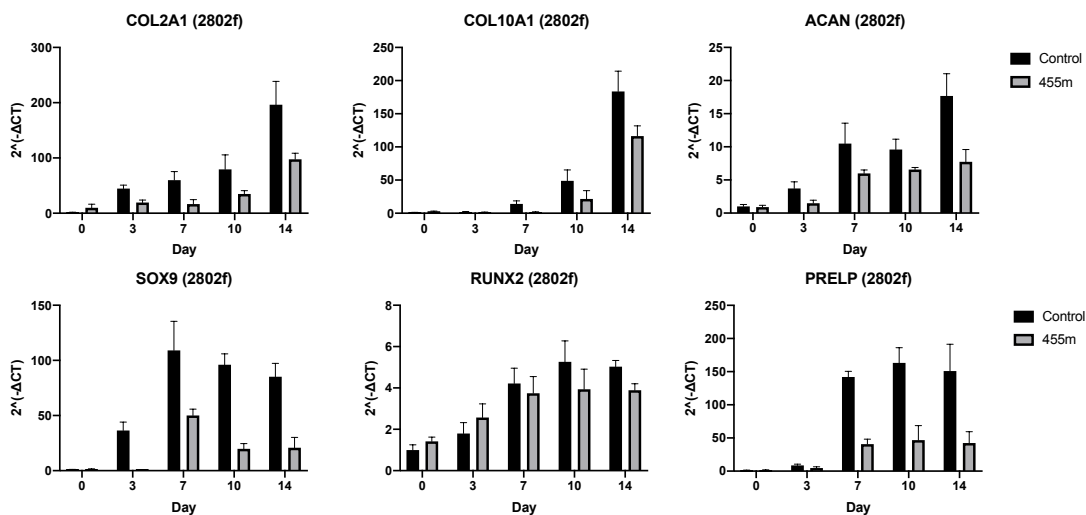
Appendix 1: Osteogenic marker genes, 2802f hMSC donor line. hMSC were transfected with either Cel-39 control or miR-455 mimic, and Neg Ctrl A control or miR-455 inhibitor. Gene expression was measured for COL1A1, COL1A2, BMP2, ALP, and RUNX2 by qPCR.



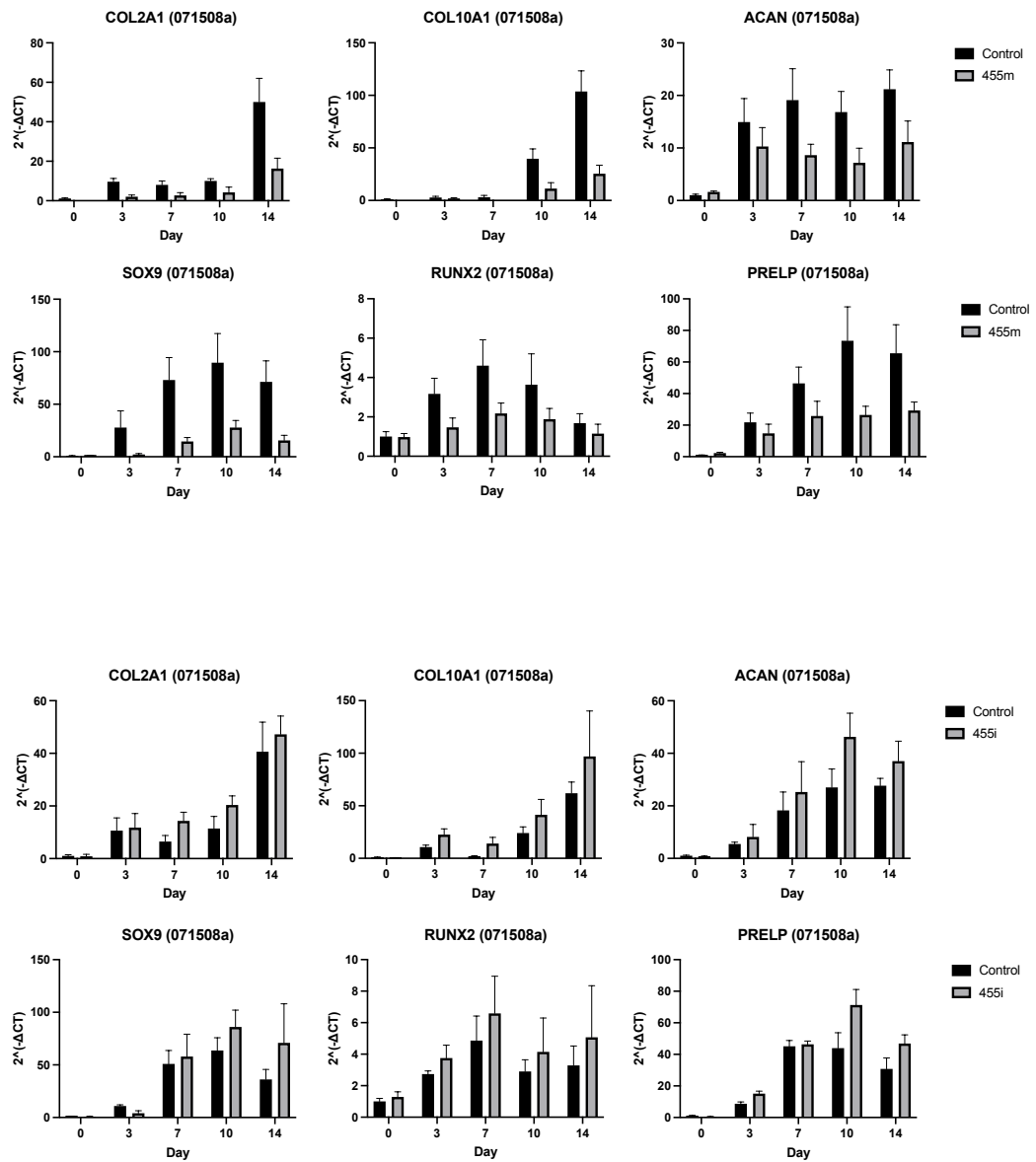
Appendix 2: Osteogenic marker genes, 0715081 hMSC donor line. hMSC were transfected with either Cel-39 control or miR-455 mimic, and Neg Ctrl A control or miR-455 inhibitor. Gene expression was measured for COL1A1, COL1A2, BMP2, ALP, and RUNX2 by qPCR.



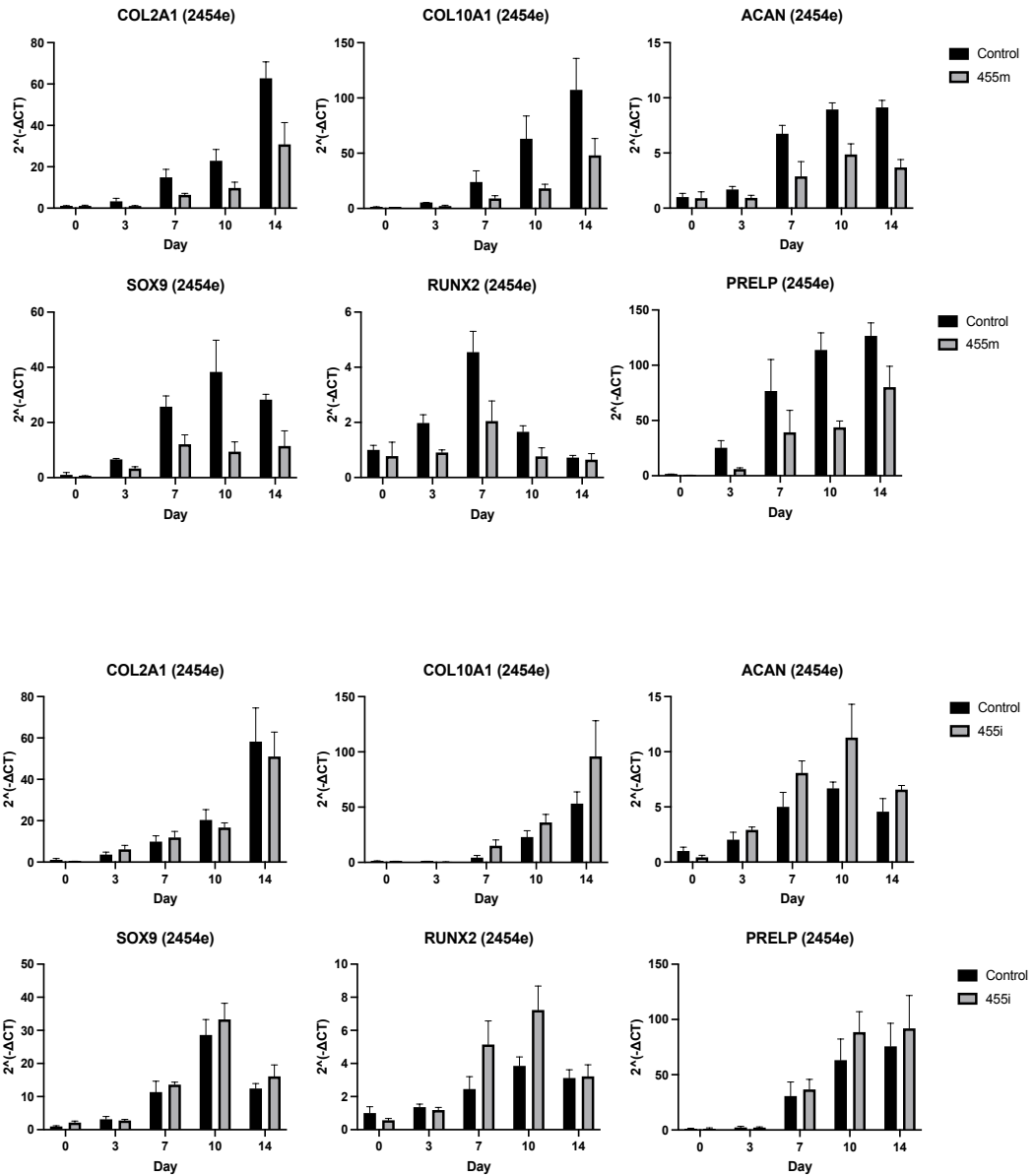
Appendix 3: Osteogenic marker genes, 2454e hMSC donor line. hMSC were transfected with either Cel-39 control or miR-455 mimic, and Neg Ctrl A control or miR-455 inhibitor. Gene expression was measured for COL1A1, COL1A2, BMP2, ALP, and RUNX2 by qPCR.



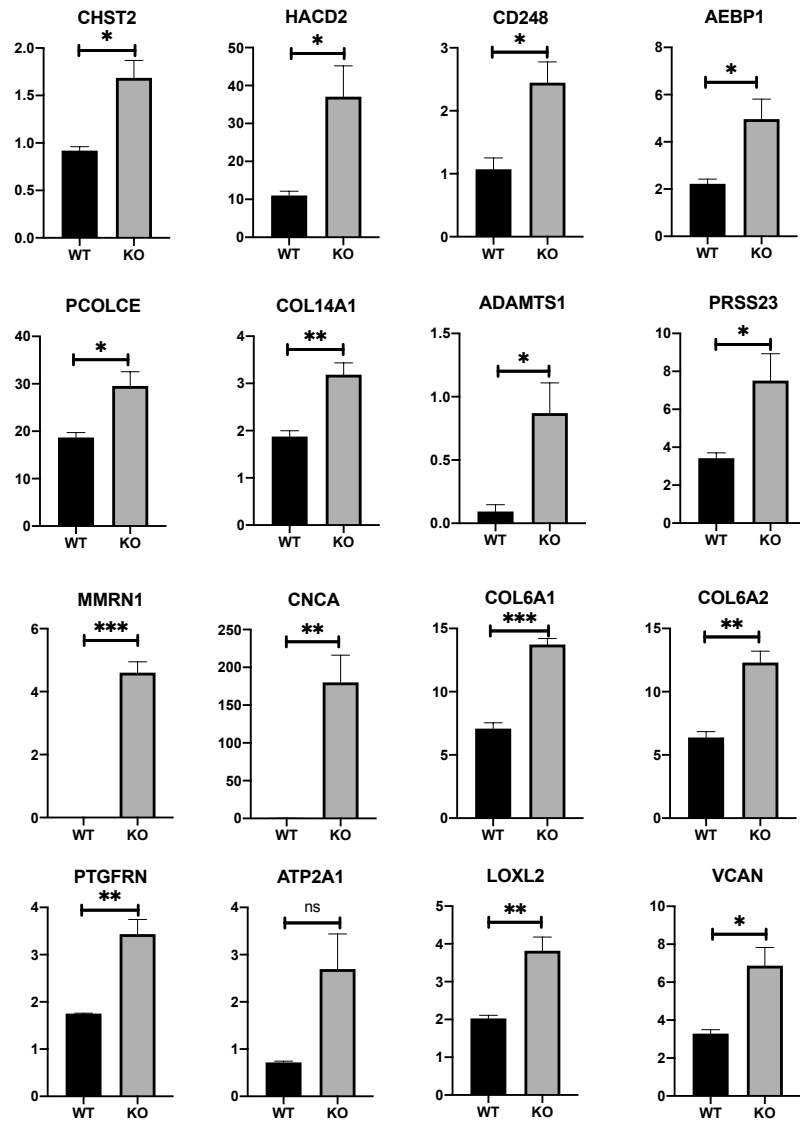
Appendix 4: Chondrogenic marker genes, 2802f hMSC donor line. hMSC were transfected with either Cel-39 control or miR-455 mimic, and Neg Ctrl A control or miR-455 inhibitor. Gene expression was measured for COL1A1, COL10A1, SOX9, ACAN, RUNX2 and PRELP by qPCR.



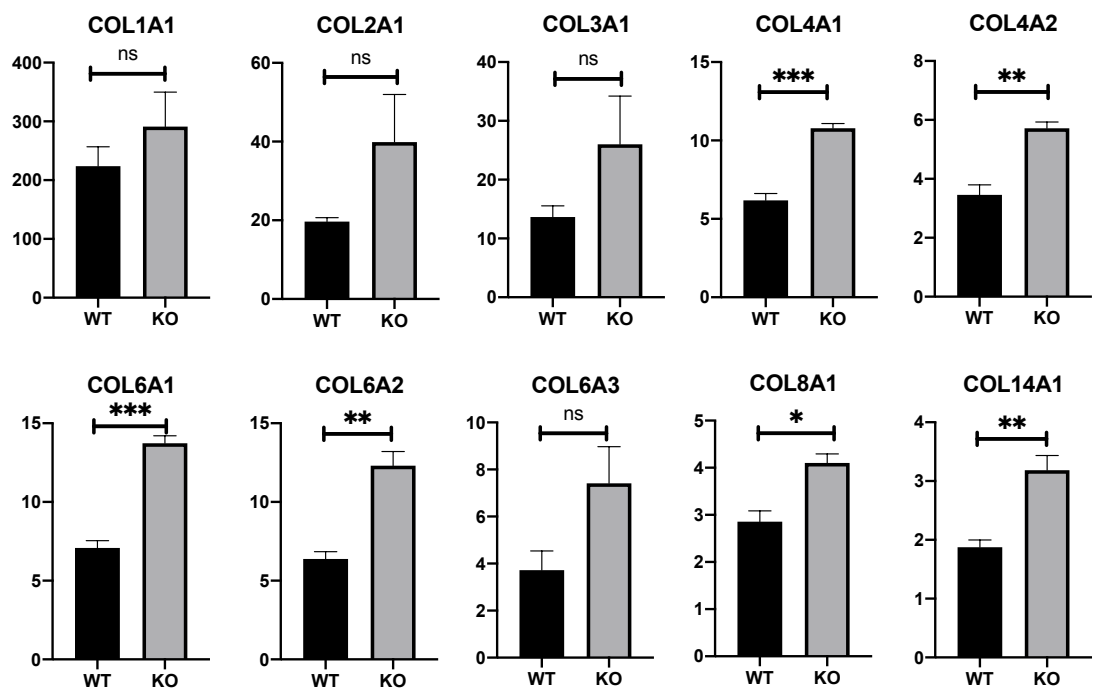
Appendix 5: Chondrogenic marker genes, 071508a hMSC donor line. hMSC were transfected with either Cel-39 control or miR-455 mimic, and Neg Ctrl A control or miR-455 inhibitor. Gene expression was measured for COL1A1, COL10A1, SOX9, ACAN, RUNX2 and PRELP by qPCR.



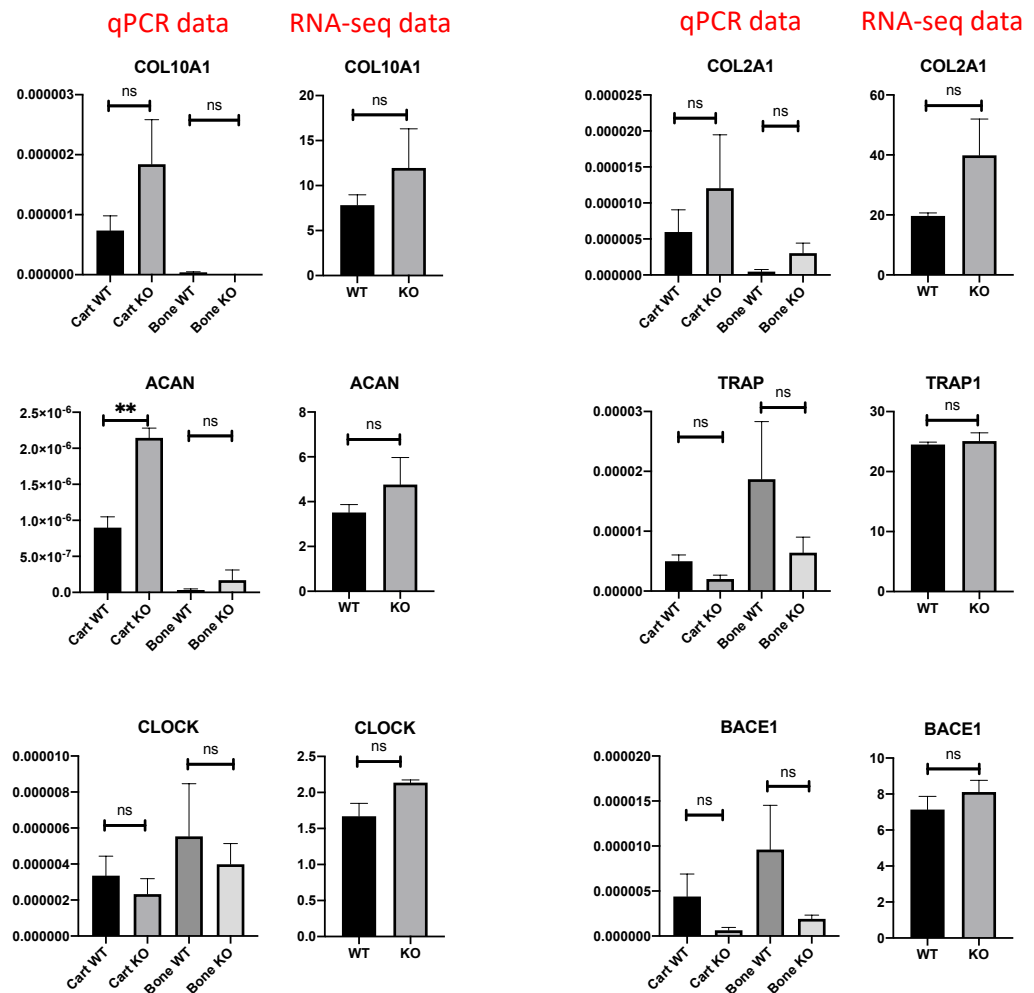
Appendix 6: Chondrogenic marker genes, 2454e hMSC donor line. hMSC were transfected with either Cel-39 control or miR-455 mimic, and Neg Ctrl A control or miR-455 inhibitor. Gene expression was measured for COL1A1, COL10A1, SOX9, ACAN, RUNX2 and PRELP by qPCR.



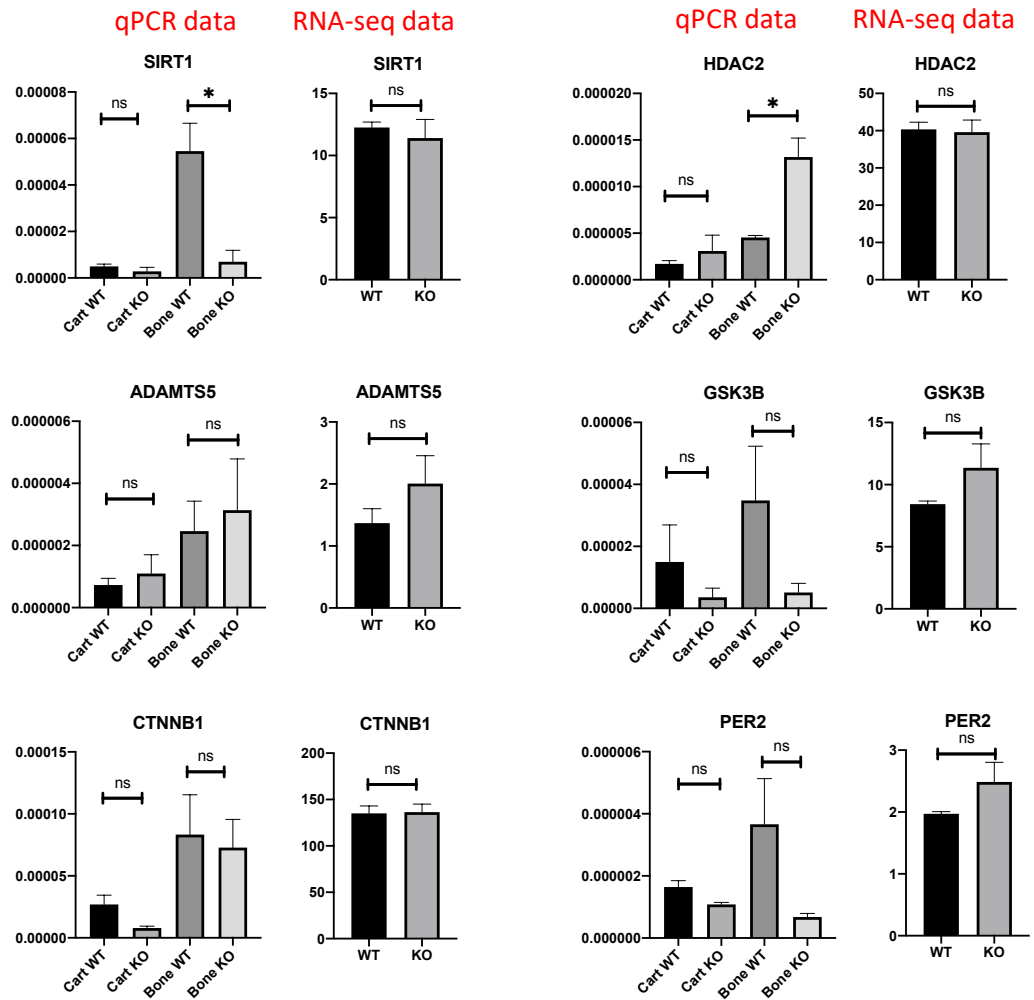
Appendix 7: RNA-seq data from WT and miR-455 null mouse articular cartilage. Genes significantly ($q \leq 0.05$) upregulated in null samples compared with WT control.



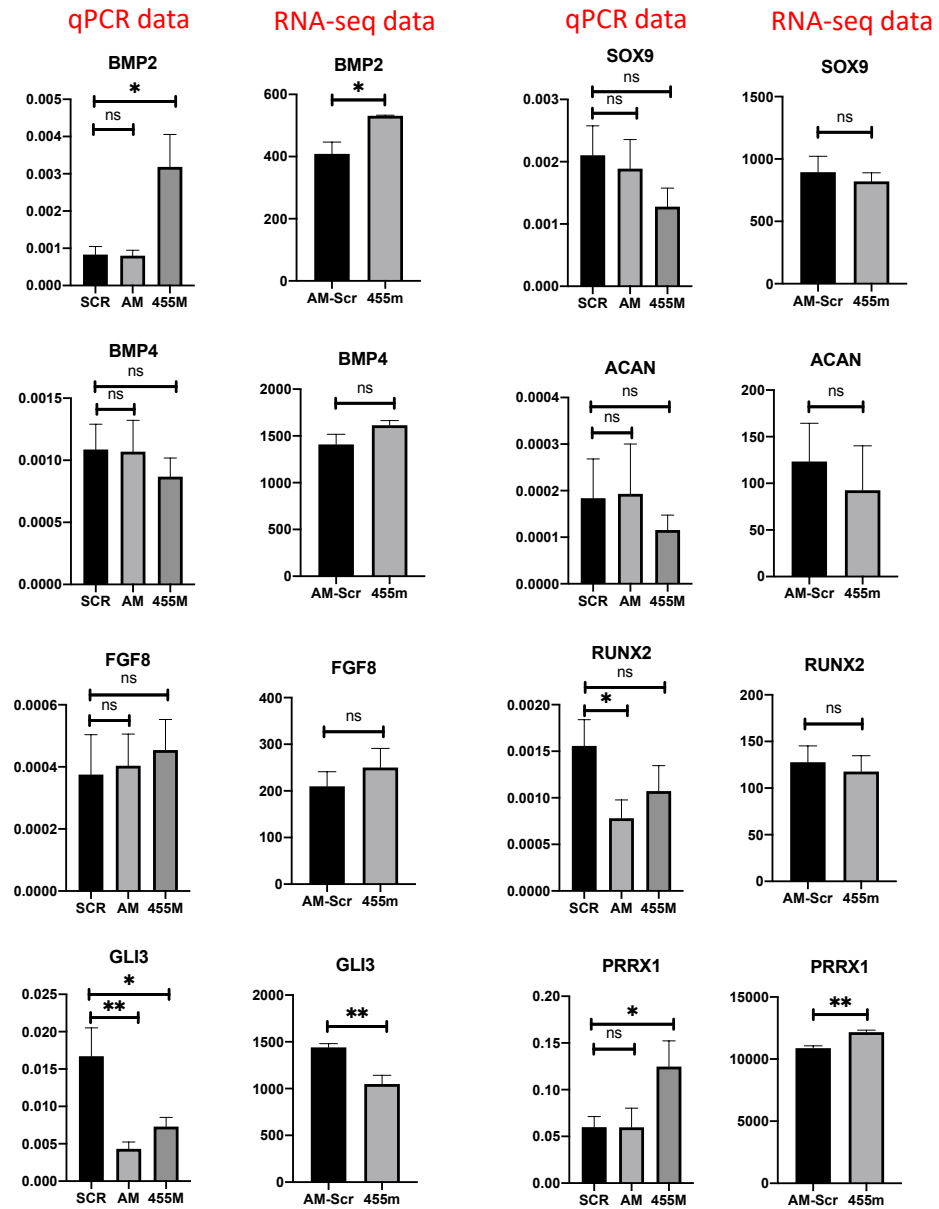
Appendix 8: Collagen expression in WT and miR-455 null mouse articular cartilage. RNA-seq data showing upregulation of Collagen expression in miR-455 null articular cartilage.



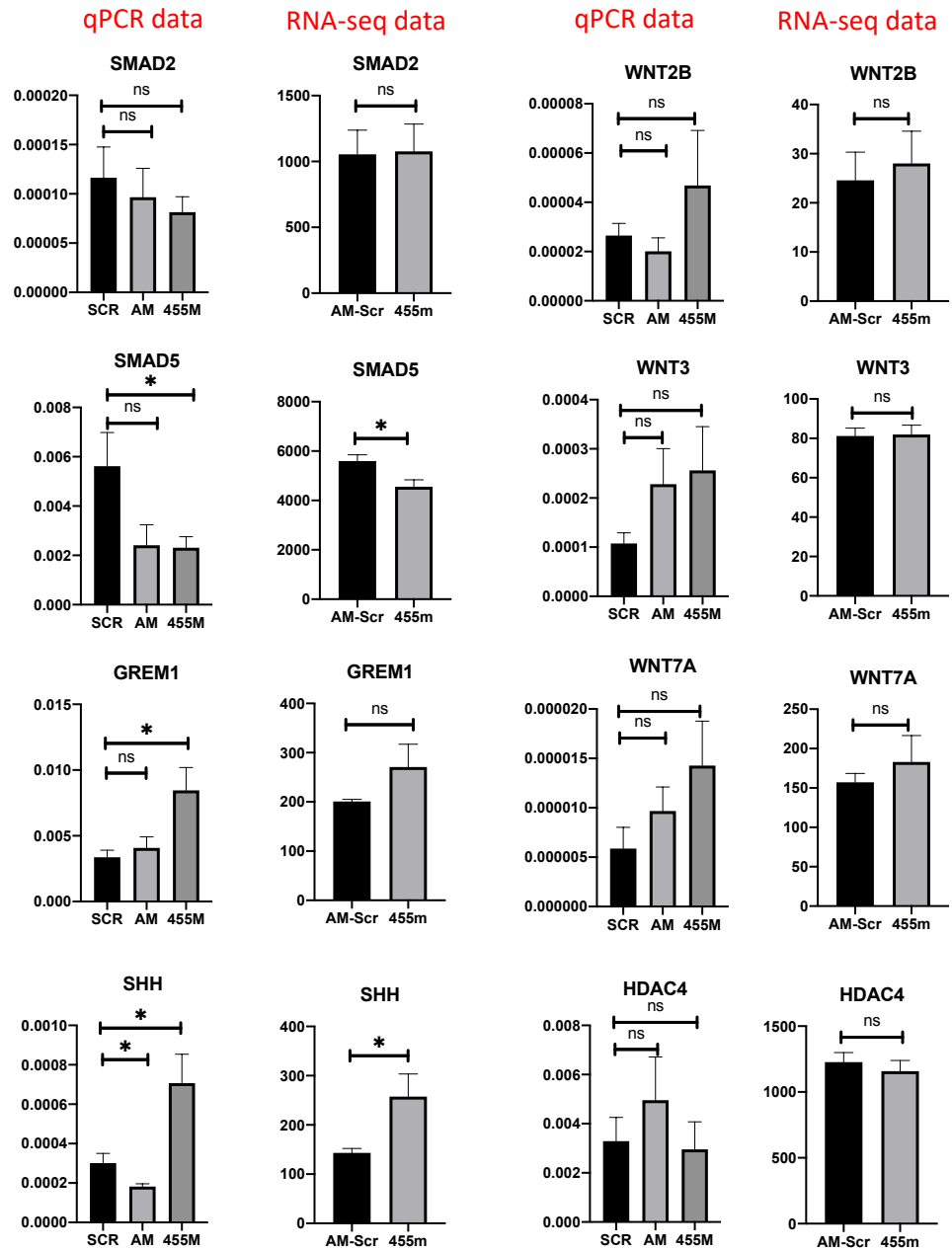
Appendix 9: RNA-seq and qPCR data from WT and miR-455 null mouse articular cartilage. Genes COL10A1, COL2A1, ACAN, TRAP, CLOCK, and BACE were analyzed using qPCR assays to validate RNA-seq data.



Appendix 10: RNA-seq and qPCR data from WT and miR-455 null mouse articular cartilage. Genes SIRT1, HDAC2, ADAMTS5, GSK3B, CTNNB1, and PER2 were analyzed using qPCR assays to validate RNA-seq data.



Appendix 11: RNA-seq and qPCR data from chick limb buds injected with AM-Scr control, miR-455 mimic, and miR-455 AM. Genes were analyzed using qPCR assays to validate RNA-seq data.



Appendix 12: RNA-seq and qPCR data from chick limb buds injected with AM-Scr control, miR-455 mimic, and miR-455 AM. Genes were analyzed using qPCR assays to validate RNA-seq data.

Appendix 13: Chick primers. Oligo name and forward/reverse sequence of primers used for

| Oligo name | Forward seq 5'-3' | Reverse seq 5'-3' |
|------------|--------------------------|------------------------|
| BMP4 | GGAGATCAGCCTGCAGTAC | TGCTGAGGTTGAAGACGAAG |
| BMP2 | GCTGTTTTGAGGTGGATTGC | AGGCACTGTTCTCTTTGTCC |
| SMAD2 | GAGAGGTTGGTGTGCTACG | TGGAGTGAATGGCAGAATGG |
| SMAD5 | TCCCTATCCACCTTCTCCAG | AGAGTTATCCTGCCCCATTTG |
| SOX9 | CTGGGCAAGCTGTGGAG | GGTTGGTACTTGTAGTCGGG |
| CTNNB1 | CTTGGACTTGACATTGGTGC | CAGAGTGGAAAGAACGGTAGC |
| SHH | ACCCCAAATTACAACCCTGAC | CATTCAGCTTGTCTTGCAG |
| FGF8 | AAGAAAATCAATGCGATGGCC | ACTCTTGCCGATCAGTTTCC |
| WNT2B | TGAGTGCCAGTACCAATTCC | GAGATGGCGTAGACGAAGG |
| WNT3 | CATCTTCGGACCTGTGCTAG | GAGATCCCTTGTGACGAGTG |
| WNT7A | AGTGCCAGTTCCAGTTTCG | AATGATGGCGTAGGTGAAGG |
| GREM1 | GTGAAGGAGTGTGCGGTGTATATC | TTCAGTTTCATCCAGCCCC |
| ACAN | GACTTAGATTCTCCGAGCACTG | CAGGTATCTTCACTTCCAGGC |
| RUNX2 | ACCTAGTTTGTTCCTGAACG | GTAATCTGACTCTGCTTGTGG |
| RUNX3 | AAAGCTTCACCCTGACCATC | TTCTAACTTCTGCTGTGCC |
| HDAC4 | AGTGTGAGAATGAAGAGGCTG | CTCGAAGATGAATGCTACAGGG |
| PRRX1 | CCTTTGTACGGGAAGACCTTG | CCTGAGTAGGATTTGAGCAGAG |
| GLI3 | TCCAAGATAAAGCCGGATGAG | AATGGCAGTTCGTCTCGTAG |

Appendix 14: Mouse primers. Oligo name and forward/reverse sequence of primers used for

| Oligo name | Forward seq 5'-3' | Reverse seq 5'-3' |
|-------------|-----------------------|------------------------|
| COL2A1 #3 | AGCTCCTGGGAAGGATGG | CAGGAGGTCCGACTTCTCC |
| ACAN #34 | TGAAGCAGAAGGTCTGGACA | CCAGAAGGAATCCCACTAACA |
| COL1A1 #15 | AGACATGTTTCTGTTGTGGAC | GCAGCTGACTTCAGGGATG |
| TRAP #3 | GGTCAGCAGCTCCCTAGAAG | GGAGTGGGAGCCATATGATTT |
| COL10A1 #84 | GCATCTCCCAGCACCAGA | CCATGAACCAGGGTCAAGAA |
| CLOCK #83 | CAGCTTCCTTCAGTTCAGCA | CCGTGGAGCAACCTAGATGT |
| BACE1 #34 | CCCTTTCCTGCATCGCTAC | TACACACCCTTTCGGAGGTC |
| SIRT1 #68 | CAGTGAGAAAATGCTGGCCTA | TTACCCTCAAGCCGCTTACTA |
| ADAMTS5 #41 | TATAAGCCCTGGTCCAAATG | TCGTGGTAGGTCCAGCAAA |
| GSK3B #10 | CAAGAAGAGCCATCATGTCG | TGGTTACCTTGCTGCCATCT |
| CTNNB1 #21 | GCTTTCAGTTGAGCTGACCA | CAAGTCCAAGATCAGCAGTCTC |
| PER2 #17 | TGACTGCGACGACAATGG | TCATCATGAGTCTGAAGGCA |
| CREB1 #50 | GGAGAAGCGGAGTGTTGGTA | GGAGAAGCGGAGTGTTGGTA |

Appendix 15: Human primers. Oligo name and forward/reverse sequence of primers used for

| Oligo name | Forward seq 5'-3' | Reverse seq 5'-3' |
|--------------|-----------------------------|---------------------------|
| PPARG #1 | TTGCTGTCATTATTCTCAGTGGA | GAGGACTCAGGGTGGTTCAG |
| CEPBA #28 | GGAGCTGAGATCCCGACA | TTCTAAGGACAGGCGTGGAG |
| ACAN #1 | AAGCACTGGAGTTCTGTGAATCT | CGGCATAGCACTTGTGTCCAG |
| COL2A1 #65 | CCCTGGTCTTGGTGAAAC | TCCTTGCATTACTCCCAACTG |
| COL10A1 #6 | CACCTTCTGCACTGCTCATC | GGCAGCATATTCTCAGATGGA |
| SOX9 #61 | GTACCCGCACTTGCACAAC | TCTCGCTCTCGTTTCCAGAGCT |
| RUNX2 #41 | CAGTGACACCATGTCAGCAA | GCTCACGTCGCTCATTTTG |
| PRELP #34 | GGGTGGAAGAGGAGGACTAAA | AGCAGAGGGGTGACCTCAT |
| COL1A1 #1 | CCCAAGGCTTCCAAGGTC | GGACGACCAGGTTTTCCAG |
| COL1A2 #54 | GAGTCCGAGGACCTAATGGA | AGGGGAACCAGGAAGACCT |
| ALP #58 | AACACCACCCAGGGGAC | GGTCACAATGCCACAGATT |
| BMP2 #49 | GACTGCGGTCTCCTAAAGGTC | GGAAGCAGCAACGCTAGAAG |
| NDUFA5 #20 | GTGAGCTGCCTGAGAAAAGAG | TTTACTGAGGGCGTTTCCTC |
| ND4 #14 | CCTCGCTAACCTCGCTTA | GGAGAACGTGGTTACTAGCACA |
| ND6 #77 | ATTGGTGTGTGGGTGAAA | CCTGACCCCTCTCCTTCATA |
| FOEXRED1 #41 | TTGGCTTGTCTGTGGCCTA | AGTGGAGGCTGTGAATACG |
| COX15 #7 | GATCCCGGAGGACCTCTTT | ATGGCAGTGACTGAAGTGATTC |
| TOMM40 #3 | GGACAACAGTGGCAGTCTCA | CACCTGCCAGTTCACAACTT |
| TIMM50 #65 | ACCGTGCTGGAGCACTATG | TGCTTGTTGGACTTGGAGAG |
| E2F8 #33 | GATGCAGACTTGTACCCAGTTACTT | CCGATGGTTCAAGTAGTCCAA |
| TFDP1 #50 | CTGCTCTGCCGAAGACCTTA | GCCGTTAGACGTGGAACCT |
| POLE3 #6 | AACCTGCTTAATACTCCAAAGTGTG | CAAAACGTGAGATTAGAATAAGGAA |
| BCL2 #6 | TTGACAGAGGATCATGCTGTACTT | ATCTTTATTTTATGAGGCACGTT |
| ORC5 #42 | TCATCAGAGCTATTGCAAGGAC | CCTCTCCTTGCCAGCTA |
| CUL4B #40 | CCTTGTTTCAGAAGTGTACAACCA | CCATGTAGTCCCGGTCAATTA |
| CREB1 #34 | TTAGTGCCAGCAACCAAGT | GCTGTGCGAATCTGGTATGTT |
| CREM #76 | CATGTCCAGGGAGTAATTCAGAC | TCTCTGCAATTGCTGCTACC |
| ATF1 #53 | TTTCTAAATAACCAATAGTTGCCAATC | AAACCTGTAGGGTAAATGGATTTTT |

Appendix 16: CRISPR/Cas9 genome engineering qPCR design. Forward (F) and reverse (R) oligo name and sequence used for qPCR.

| Oligo name | Oligo 5'-3' |
|--------------|-------------------------|
| T3 barcode_R | TCCCTTTAGTGAGGGTTAATT |
| T7 barcode_R | CCCTATAGTGAGTCGTATTA |
| CLOCK_F | GGTGATAACTCACCATCTTGAAG |
| DKK3_F | GAAGACAATTATCAACCACGTG |
| ACAN_F | GTCATATAAGGAATCCCATTAAG |
| PRELP_F | GATGCTCCTCTGAGGTCC |
| RUNX2_F | CTTAGACGGTCTCACTGC |

Appendix 17: CRISPR/Cas9 genome engineering sgRNA design. Gene, CRISPR target sequence, PAM, and forward/reverse oligo sequences.

| Gene | CRISPR target sequence | PAM | Forward oligo (5'-3') | Reverse oligo (5'-3') |
|-------|--------------------------|-----|-------------------------------|--------------------------------|
| CLOCK | CTATCAGTCTCTT GGACTGG | AGG | CACCGCTATCAGTCTCTTG GACTGG | AAACCCAAGTCCAAGAGACT GATAGC |
| DKK3 | CAAATGATGTTTT CAGGTGT | TGG | CACCGACACCTGAAAACA TCATTTG | AAACCAAATGATGTTTTCAG GTGTC |
| ACAN | TGGACTGAGTTTA GAGACAT | AGG | CACCGATGTCTCTAAACTC AGTCCA | AAACTGGACTGAGTTTAGA GACATC |
| PRELP | ATGGACTGTCCCT CCCCAG | AGG | CACCGATGGACTGTCCCTC CCCCAG | AAACCTGGGGGAGGGACAG TCCATC |
| RUNX2 | AGGAAAGGGACT GGCCAGA | CGG | CACCGTCTGGGCCAGTCC CTTTCT | AAACAGGAAAGGGACTGGC CCAGAC |

Appendix 18: CRISPR/Cas9 genome engineering ssODN design. Gene, ssODN wt-MRE and mut-MRE sequences. MRE highlighted in grey, red indicates T3 barcode and green T7 barcode.

| Gene | ssODN wt-MRE | ssODN mut-MRE |
|-------|--|--|
| CLOCK | GGTGTCAAGTGCATTATTAGTCTCCTAATAA GTTCTCTGAAGACTGCTATCAGTCTCTCTT GGACTG AATTAACCCTCACTAAAGGG AGAG CTACAAATAATTTAGAAATAAAAGATGATA ACCTAACACTATCATAGTTAT | GGTGTCAAGTGCATTATTAGTCTCCTAATAAG TTCCTCTGAAGACTGCTATCAGTCTCTT TAAT ACGACTCACTATAGGG GAGCTACAAATAATT TAGAAATAAAAGATGATAACCTAACACTATC ATAGTTATTAATGT |
| DKK3 | ATATGCGACTGCGAACACTGAACTCTACGC CACTGCACAAATGATGTTTTCAGGTGTCAT GGACTG AATTAACCCTCACTAAAGGG ATTG CCACCATGTATTCATCCAGAGTTCTTAAAGT TTAAAGTTGCACATGATTGTATAAGC | ATATGCGACTGCGAACACTGAACTCTACGCC ACTGCACAAATGATGTTTTCAGGTGTCAT TAA TACGACTCACTATAGGG TTGCCACCATGTATT CATCCAGAGTTCTTAAAGTTTAAAGTTGCACA TGATTGTATAAGC |
| ACAN | CAAAACCGCATCTAATTTGTCCGCCGAATG CCAAAGCAAAGCAAACCTATTATAACGCTT GGACTG AATTAACCCTCACTAAAGGG AAGT TTAGAGACATTTCTTCAATTTCCCATCGTGC CTTCCAGGGACCAGTGCAGGGACAG | CAAAACCGCATCTAATTTGTCCGCCGAATGCC AAAGCAAAGCAAACCTATTATAACGCTT TAAT ACGACTCACTATAGGG AGTTTAGAGACATTT CTTCAATTTCCCATCGTGCCTTTCCAGGGACC AGTGCAGGGACAG |
| PRELP | CGAATGCAGGACAAGTCTAAATATTTGCC CCTTCCCTTGCAGTAATTTATTTCTGTATG GACTG AATTAACCCTCACTAAAGGG ATCCC TCCCCAGAGCCTTCCCCACCCTCCATTGCC TGGCCCAGGTGAGCAGCTTGGCAGG | CGAATGCAGGACAAGTCTAAATATTTGCC CCTTCCCTTGCAGTAATTTATTTCTGTAT TAAT ACGACTCACTATAGGG TCCCTCCCCAGAGC CTTCCCCACCCTCCATTGCCTGGCCAGGTGA GCAGCTTGGCAGG |
| RUNX2 | AAATTCAGAAGGGAGGAGATGTGTGTACA GCTTTAAGGATTCCCTCAATTGCGAGGAAA GGGACTG AATTAACCCTCACTAAAGGG AGC CCAGAATCCAGTTAATACATGGAAACACG AAGCATTAGCAAAAAGTAATAATTATACC | AAATTCAGAAGGGAGGAGATGTGTGTACAG CTTTAAGGATTCCCTCAATTGCGAGGAAAG T AATACGACTCACTATAGGG GCCAGAATCCA GGTTAATACATGGAAACACGAAGCATTAGCA AAAGTAATAATTATACC |